

DOCTOR OF PHILOSOPHY

Past and future hydroclimatic variability over West and Central Africa and their teleconnections

Sidibe, Moussa

Award date:
2019

Awarding institution:
Coventry University

[Link to publication](#)

General rights

Copyright and moral rights for the publications made accessible in the public portal are retained by the authors and/or other copyright owners and it is a condition of accessing publications that users recognise and abide by the legal requirements associated with these rights.

- Users may download and print one copy of this thesis for personal non-commercial research or study
- This thesis cannot be reproduced or quoted extensively from without first obtaining permission from the copyright holder(s)
- You may not further distribute the material or use it for any profit-making activity or commercial gain
- You may freely distribute the URL identifying the publication in the public portal

Take down policy

If you believe that this document breaches copyright please contact us providing details, and we will remove access to the work immediately and investigate your claim.

**Past and future hydroclimatic variability over West and
Central Africa and their teleconnections**

By

Moussa SIDIBE

May 2019

*A thesis submitted in fulfilment of the University's requirements for
the Degree of Doctor of Philosophy*



Content removed due to data protection considerations.



Certificate of Ethical Approval

Applicant:

Moussa Sidibe

Project Title:

Past and future fluctuations in West and Central African hydroclimatic variability, and their teleconnections

This is to certify that the above named applicant has completed the Coventry University Ethical Approval process and their project has been confirmed and approved as Low Risk

Date of approval:

04 October 2016

Project Reference Number:

P46036

RESEARCH DECLARATION

I declare that this thesis is entirely my own work and that any use of the work of others has been appropriately acknowledged as in-text citations and compiled in the bibliography. I also confirm that the project has been conducted in compliance with Coventry University research ethics policy.

Signed: Date: **07/05/2019**

ACKNOWLEDGEMENTS

It takes a great team to complete a thesis, and I have had one!

First and foremost, I acknowledge and thank my supervisory team for shepherding me through the PhD journey: **Bastien Dieppois**, my director of studies, for his friendship and tireless input into my research. His vision and overall management of the project facilitated my progress. **Damian Lawler**, my second supervisor for his experience and advice. **Jonathan Eden**, my third supervisor for his thoroughness and help with understanding key concepts in climatology.

I also specifically thank my external advisors from HydroSciences Montpellier, France: **Gil Mahé** and **Jean-Emmanuel Paturel** who shared with me their great experience and knowledge of hydrological systems in West Africa. Most importantly, with **Nathalie Rouché**, they provided access to the useful streamflow datasets used in this thesis. I am grateful to **Babatunde Anifowose** and **Ernest Amoussou** for the streamflow datasets they provided and their contributions into my research. I am indebted to **Marco Van de Wiel** for his comments on my manuscripts. Thanks go to all the colleagues from the Centre for Agroecology Water and Resilience and to the dynamic Operations Team.

DEDICATION

I thank the Almighty for granting me faith and stamina to believe in myself.

I would like to dedicate this thesis to my parents who have always been a source of inspiration.

This work is also dedicated to my dear wife for her support and patience.

LIST OF PUBLICATIONS

This thesis by artefact consists of the following research articles:

Peer-reviewed publications

Sidibe, M., Dieppois, B., Mahé, G., Paturel, J. E., Amoussou, E., Anifowose, B., Lawler, D. (2018). Trend and variability in a new, reconstructed streamflow dataset for West and Central Africa, and climatic interactions, 1950–2005. *Journal of hydrology*, 561, 478-493. **(Chapter 2)**

Sidibe, M., Dieppois, B., Eden, J., Mahé, G., Paturel, J. E., Amoussou, E., Anifowose, B., Lawler, D. (2019). Interannual to Multi-decadal streamflow variability in West and Central Africa: interactions with catchment properties and large-scale climate variability. *Global and Planetary Change*, 177, 141-156. **(Chapter 3)**

Manuscript submitted for peer-review

Sidibe, M., Dieppois, B., Eden, J., Mahé, G., Paturel, J. E., Amoussou, E., Anifowose, B., Van De Wiel, M., Lawler, D. (In review). Impacts of near-term climate change on hydrological systems in West and Central Africa. *Climate Dynamics* **(Chapter 4)**

ABSTRACT

This thesis examined past hydroclimatic trends and variability across West and Central Africa from 1950 to 2005, and their interactions with both catchment properties and large-scale climate patterns. The understanding gained from this study was then used to assess the impact of near-term climate change on hydrological regimes. Two imputation methods were successfully applied to assemble a new reconstructed streamflow dataset and time series analyses revealed high non-stationarity in annual streamflow, with two step-changes occurring at the regional scale in 1970 and 1993 respectively. The results also indicated good agreement between precipitation and streamflow fluctuations from one decade to another. Moreover, detailed analysis of streamflow variability modes highlighted significant interannual to multi-decadal fluctuations which were found to be associated with large-scale climate variability and modulated by catchment physical properties. Building upon the detected streamflow-sea surface temperature teleconnections, a multi-timescale linear regression model was built and applied in combination with two hydrological models (GR2M and IHACRES) to examine the potential impacts of climate change on hydrological systems by the mid-21st century. The results highlighted a zonal contrast in future precipitation between western (dry) and eastern (wet) Sahel, and a robust signal in rising temperature, suggesting an increase in potential evapotranspiration, which are likely to induce a slight significant increase in discharge (~+5%) at the regional scale. More importantly, the findings indicated that uncertainties in streamflow predictions inherent to models and gridded observational datasets quality in Central Africa, could be narrowed by the teleconnections-based regression model.

Keywords: *data imputation, hydroclimatic trends and variability, teleconnections, hydrological regimes, climate change, bias-correction, West and Central Africa.*

TABLE OF CONTENTS

RESEARCH DECLARATION.....	i
ACKNOWLEDGEMENTS	ii
DEDICATION	iii
LIST OF PUBLICATIONS	iv
ABSTRACT	v
TABLE OF CONTENTS	vi
LIST OF FIGURES.....	ix
LIST OF TABLES.....	xiii
ABBREVIATIONS & ACRONYMS.....	xiv
CHAPTER 1: General introduction to the research.....	1
1. Introduction.....	2
1.1. Background.....	2
1.2. Literature review.....	3
1.2.1. Hydroclimatic variability in West and Central Africa.....	3
1.2.2. Major drivers of hydroclimatic variability	7
1.2.3. Climate change and hydroclimatic projections.....	14
1.3. Research objectives and methods	19
1.4. Thesis outline	22
CHAPTER 2: Trend and variability in a new, reconstructed streamflow dataset for West and Central Africa, and climatic interactions, 1950-2005.....	23
2. Trend and variability in a new, reconstructed streamflow dataset for West and Central Africa, and climatic interactions, 1950 – 2005.....	24
Abstract	24
2.1. INTRODUCTION.....	25
2.2. STUDY AREA AND DATASETS	27
2.2.1. Research Area.....	27
2.2.2. Data.....	30
2.3. METHODOLOGY.....	32
2.3.1. Gap filling Methods.....	32
2.3.2. Step change detection and trend analysis	36
2.4. RESULTS AND DISCUSSIONS	38
2.4.1. Reconstruction outputs	38
2.4.2. Streamflow changes between 1950 and 2005.....	40
2.4.3. Observed climatic trends between 1950 and 2005	45
2.4.4. Precipitation and streamflow variability.....	49
2.5. CONCLUSION.....	55
2.6. Appendix A: List of reconstructed streamflow time series.....	59
2.7. Supplementary materials.....	63

CHAPTER 3: Interannual to Multi-decadal streamflow variability in West and Central Africa: interactions with catchment properties and large-scale climate variability	64
3. Interannual to Multi-decadal streamflow variability in West and Central Africa: interactions with catchment properties and large-scale climate variability	65
Abstract	65
3.1. INTRODUCTION	66
3.2. Data and Methods	69
3.2.1. Data.....	69
3.2.2. METHODOLOGY	71
3.3. Streamflow variability	74
3.3.1. Modes of streamflow variability and regionalization	74
3.3.2. Importance of streamflow modes of variability	77
3.3.3. Modes of streamflow variability and interactions with catchment properties	79
3.4. Streamflow-climate teleconnections	82
3.4.1. Regional atmospheric circulations	82
3.4.2. Global SST streamflow teleconnections	93
3.4.3. Large-scale convection patterns	96
3.5. CONCLUSIONS	100
3.6. Supplementary materials	104
CHAPTER 4: Impacts of near-term climate change on hydrological systems in West and Central Africa	109
4. Impacts of near-term climate change on hydrological systems in West and Central Africa	110
Abstract	110
4.1. INTRODUCTION	111
4.2. Data and Methods	114
4.2.1. Data.....	114
4.2.2. Methods	117
4.3. Results	121
4.3.1. Climate scenarios: evaluation and bias-correction	121
4.3.2. Hydrological modelling: calibration and validation	131
4.3.3. Linear regression-based streamflow SST model	134
4.3.4. Future hydroclimatic variability in West and Central Africa by mid-21st century	135
4.4. CONCLUSIONS	145
4.5. Appendix A	148
4.6. Supplementary materials	153
CHAPTER 5: General Discussions	160
5. General Discussions	161
5.1. Past hydroclimatic variability in West and Central Africa	161
5.2. Drivers of streamflow variability: from catchment properties to large-scale climate patterns	163
5.3. Impact of near-term climate change on hydrological systems in West and Central Africa	165

5.4. Conclusions and envisaged future work.....	167
Bibliography.....	171
Co-authors declaration.....	188

LIST OF FIGURES

Figure 1.1: (a) Location of the research area: red boxes highlight the Sahel and different sub-regions (adapted from Monerie *et al.*, 2016); (b) Rainfall anomalies from the long term mean for meteorological stations in the Sahel. Red line shows the 7-year running mean, blue line shows the number of stations (Data source: Climatic Research Unit, University of East Anglia, and Global Historical Climatology Network, Oak Ridge National Laboratory) (Image source: http://www.eoearth.org/article/Greening_of_the_Sahel)5

Figure 1.2: Runoff variability over four large regions of West and Central Africa (1901-2000). Equatorial rivers: Ogooué, Kouilou, Ntem, Nyong, Nyanga, in Gabon, Cameroon, Congo. Humid tropical rivers in West Africa: Senegal, Niger, Bandama, Sassandra, comoe, Volta and in Central Africa: Sanaga, Logone-Chari. Sahelian rivers from Mauritania, Niger, Burkina Faso and Cameroon (source: Mahé *et al.*, 2005).7

Figure 1.3: Schematic of the main features of the West African monsoon system during the boreal summer: meridional circulations and zonal means (adapted from Peyrillé, 2006). Below are given the corresponding meridional variations in atmospheric boundary layer potential temperature (θ) and moist static energy (θ_e).....10

Figure 1.4: (Left) Observed anomalous rainfall response and (right) flux diagrams explaining the WAM–SST teleconnection mechanisms associated with the (a) Mediterranean, (b) tropical Atlantic, (c) tropical Pacific, and (d) global tropical SST forcings (source: Rodríguez-Fonseca *et al.*, 2011).....11

Figure 1.5: Anomalous precipitation (mm/day, left column) simulated by the LMDZ model in response to the anomalous pattern of SST (K, right column) for:(a) GW, (b) AMO, and (c) IPO. The precipitation is the averaged response over the ten-member ensemble simulations. Grey contours mark 95% significant anomalies according to at-test (source: Mohino *et al.*, 2011).....13

Figure 1.6: Projected changes in JAS (a–d) precipitation (mm day⁻¹), (e–h) evaporation (mm day⁻¹) and (i–l) P–E budget (mm day⁻¹) for the four groups of models (one group per column) identified by the clustering. The present climatology (HIST) is displayed with red contours and the RCP85-HIST differences by colour shading. Hatching represents the grid-points where at least 80 % of the models agree with the sign of the intra-group ensemble mean within each group (5 for GR1; 7 for GR2; 13 for GR3; 5 for GR4) (Source: Monerie *et al.*, 2016).....16

Figure 1.7: Schematic on approaches to explicitly characterize and reduce the myriad uncertainties in assessments of the hydrologic impacts of climate change and the development of representative quantitative hydrologic storylines for specific applications (source: Clark *et al.*, 2016).....18

Figure 1.8: Schematic on datasets and implemented methodologies.....21

Figure 2.1: Study area with locations of the main catchments (grey shaded), the river network (blue) and streamflow gauges collected from the SIEM database (light blue dots).....29

Figure 2.2: Large dams (Capacity > 10⁶ .m³) in the study area and their start of operation (purple: 1920-1950; blue: 1950-1970; green:1970-1990; red: 1990-2006). Data source: Global Reservoir and Dam database (GRaND; Lehner *et al.*, 2011).....30

Figure 2.3: A) River network (blue lines) and spatial distribution of stream gauges over the study area, and with their percentage of missing data (purple=0-25%, blue=25-50%, green=50-75% and red=>75%. Major catchments are displayed in grey shaded. B) Time-evolution of missing values for the 152 selected stream gauges. Missing values are in red, while observations are in grey. Stations are ordered by country (BF: Burkina Faso, BJ: Benin, CF: Central African Republic, CG: Democratic Republic of Congo, CI: Cote d'Ivoire, CM: Cameroon, GA: Gabon, GH: Ghana, GN: Guinea Conakry, ML: Mali, NG: Nigeria, SN: Senegal, TD: Chad, TO: Togo). The black line represents the number of records per month over the study area for the 1950–2005 period.....31

Figure 2.4: Validation of gap filling methods: boxplot of validation efficiencies for all the reconstructed stations; upper panels for randomly removed values and lower ones for cases of randomly missing data segments. A red line is drawn at KGE=0.75. Outliers are represented in blue dots.....39

Figure 2.5: Reconstructed time series for five streamflow stations representative of different climatic conditions: Wayen (Sahelian), Bonou (Tropical humid), Mbasso (Tropical humid), Niamey (Tropical humid, Sudanian and Sahelian), Bangui (Tropical humid). Blue lines represent observations; black dotted lines represent MICE estimates and Red dotted lines represent Random Forest estimates. Red Boxes highlight time windows of interest.....40

Figure 2.6: Locations of step changes in random-forest based streamflow reconstructions: positive shift in the mean (blue), negative shift in the mean (red). Stations are ordered by country (BF: Burkina Faso, BJ: Benin, CF: Central African Republic, CG: Democratic Republic of Congo, CI: Cote d'Ivoire, CM: Cameroon, GA: Gabon, GH: Ghana, GN: Guinea Conakry, ML: Mali, NG: Nigeria, SN: Senegal, TD: Chad, TO: Togo). The black curve on top presents the temporal distribution of change-points over the study area.....42

Figure 2.7: Spatial correlation between normalized trends calculated using both reconstructed datasets, for the three periods of investigation: 1950-1970 (red), 1970-1993 (green) and 1993-2005 (blue).....43

Figure 2.8: Streamflow trends estimated for both reconstructed datasets, upward triangles for positive trends and downward triangles for negative trends, filling highlights the significance of trend at 10% (negative trends in red and positive trends in blue). River basins are greyed and the river network in blue.44

Figure 2.9: Hydroclimatic trends over the study area for three different time intervals (1950-1970, 1970-1993 and 1993-2005) according to the CRU.TS. V4.00 dataset: a-c) Annual precipitation trends d-f) Minimum annual temperature trends g-i) Maximum annual temperature trends j-l) Annual potential evapotranspiration trends m-o) Annual effective rainfall trends. Sen's slope values are displayed through a red-white-blue colour scale. Solid red lines highlight trend significance at $p \leq 0.1$ according to a modified MK trend test accounting for serial correlation in the time series.....49

Figure 2.10: Spatial distribution of streamflow variability (1950–2005) clusters based on multi-temporal trend analysis superimposed on the river network (blue) and major river basins (grey shaded). All the clusters are highly significant at $p \leq 0.1$ according to the multiscale bootstrapping test. Different colours displayed the location of the different clusters.....50

Figure 2.11: Multi-temporal diagrams of the different cluster centroids: trends in m^3/s are presented in red (negative) – white (null) – blue (positive) colour scale, contours lines represent trend significance at $p \leq 0.1$52

Figure 2.12: Clusters of rainfall variability generated using CRU TS V4.00 ($2.5^\circ \times 2.5^\circ$) on the period 1950-2005: colours and numbers from 1 to 12 refer to the grid points within the 12 initial clusters at $p \leq 0.1$. Red boxes represent grid points which did not fall within the clusters. All the clusters are highly significant at $p \leq 0.1$ according to the multiscale bootstrapping test.....52

Figure 2.13: Multi-temporal diagrams of the 12 rainfall variability clusters derived from the multi-scale bootstrap clustering: trends (mm) are presented in red (negative) – white (null) - blue (positive) colour scale, contours lines represent trend significance at $p \leq 0.1$55

Figure 3.1: Study area: selected streamflow gauging stations (red dots) on top of long term (1950–2005) mean annual rainfall (mm yr⁻¹; grey shaded) and isohyets (250, 500, 900, 1100 and 1800; blue contours) from CRU TS v4.00 precipitation dataset.....70

Figure 3.2: Clusters of streamflow variability significant at $p \leq 0.1$ defined based on multi-scale hierarchical clustering applied to Continuous Wavelet diagrams. Significance is estimated using 1000 bootstrap simulations.....74

Figure 3.3: Top three panels show time series (grey colour) of different clusters and their centroids (blue-green-red). The bottom panels present wavelet spectra of streamflow times series (Cluster centroids).

Significant fluctuations ($p \leq 0.1$) are highlighted with thin black contours. Thick black lines underline the cone of influence.....76

Figure 3.4: Five components of annual streamflow (a-e) and basin averaged precipitation (f-j) extracted using the Maximum Overlap Discrete Wavelet Transform (MODWT), their contribution to total variance (%) and rainfall-runoff relationships (Pearson correlation) using basin averaged precipitation (k-o). Significance level ($p \leq 0.1$) estimated using 1000 Monte Carlo simulations of autoregressive processes are presented with black crosses. C1, C2, C3, C4, C5 correspond to component 1, component 2, component 3, component 4 and component 5 respectively.....78

Figure 3.5: First and second components (~50% explained variance) of the PCA performed on long term average indices of streamflow variability and catchment properties. Streamflow stations are represented by coloured dots. Blue for stations below 4°N (Central Africa), green for stations in Sudanian and Guinean regions (between 4°N-10°N) and red for stations above 10°N. Original variables are superimposed as black vectors (refer to table 1 for variable names): two vectors forming a small angle represent positively correlated variables; if the angle is around 90° variables are not likely to be correlated and an angle close to 180° suggests negatively correlated variables. The importance of each variable on a PC is given by its project value on that PC.....81

Figure 3.6: 20CR.v2 average annual regional atmospheric circulation patterns (1950-2005). (a) average annual moisture fluxes at 950 hPa pressure level, represented in vectors ($\text{g.kg}^{-1}.\text{m.s}^{-1}$) on top of convergence/divergence ($10^{-5}.\text{g.kg}^{-1}.\text{s}^{-1}$). (b) average annual zonal wind speed (m.s^{-1}) unit at 600 hPa pressure level. (c) average annual zonal wind speed (m.s^{-1}) at 200 hPa pressure level.....83

Figure 3.7: Low level winds and their interactions with streamflow modes of variability (five components of decomposition). Cluster 1 (a-e), Cluster 2 (f-j) and Cluster 3 (k-o). Only wind vectors significant at $p \leq 0.1$ in their zonal or meridional components are represented. Divergence calculated for the layer is displayed in shaded colours from dark blue (negative anomalies) to dark red (positive anomalies). EQ is Equator. C1, C2, C3, C4, C5 correspond to component 1, component 2, component 3, component 4 and component 5 respectively.....86

Figure 3.8: Zonal wind circulations in the mid-troposphere (600 hPa) and their interactions with streamflow modes of variability (five components of decomposition). Cluster 1 (a-e), Cluster 2 (f-j) and Cluster 3 (k-o). Composites are presented in shaded colours from dark blue (negative anomalies) to dark red (positive anomalies). Negative anomalies refer to easterly winds, and positive anomalies refer to westerly winds. Red contours highlight significance level $p \leq 0.1$. C1, C2, C3, C4, C5 correspond to component 1, component 2, component 3, component 4 and component 5 respectively.....90

Figure 3.9: Zonal wind circulations in the upper troposphere (200 hPa) and their interactions with modes of streamflow variability (five components of decomposition). Cluster 1 (a-e), Cluster 2 (f-j) and Cluster 3 (k-o). Composites are presented in shaded colours from dark blue (negative anomalies) to dark red (positive anomalies). Negative anomalies refer to easterly winds, and positive anomalies refer to westerly winds. Red contours highlight significance level $p \leq 0.1$. C1, C2, C3, C4, C5 correspond to component 1, component 2, component 3, component 4 and component 5 respectively.....92

Figure 3.10: Global SST patterns and their interactions with streamflow modes of variability (five components of decomposition). Cluster 1 (a-e), Cluster 2 (f-j) and Cluster 3 (k-o). Composites are presented in shaded colours from dark blue (negative anomalies) to dark red (positive anomalies). Red contours highlight significance level $p \leq 0.1$. C1, C2, C3, C4, C5 correspond to component 1, component 2, component 3, component 4 and component 5 respectively.....95

Figure 3.11: Large-scale convection patterns (Outgoing Longwave Radiation at the nominal top of atmosphere) and their interactions with streamflow modes of variability (five components of decomposition). Cluster 1 (a-e), Cluster 2 (f-j) and Cluster 3 (k-o). Composites are presented in shaded colours from dark blue (negative anomalies) to dark red (positive anomalies). Red contours highlight significance level $p \leq 0.1$. C1, C2, C3, C4, C5 correspond to component 1, component 2, component 3, component 4 and component 5 respectively.....99

Figure 4.1: Hydrological model structures a) GR2M hydrological model (adapted from Mouelhi et al., 2006) b) IHACRES-CWI hydrological model (adapted from Jakeman and Hornberger, 1993).....119

Figure 4.2: Long-term mean monthly historical precipitation (1951-2005) in (a) CRU observation (b) Multi-model mean. Long-term historical percentage bias between models and CRU precipitation fields (1951-2005) (c) CanESM2 (d) CNRM (e) CSIRO (f) HadGEM2 (g) IPSL (h) MIROC5 (i) MPI (j) NCC (k) GFDL. Grey contours highlight regions of significant difference between observations and simulations at $p \leq 0.1$ based on a t test.....123

Figure 4.3: Distributional biases between models and CRU precipitation fields (1951-2005) (a) Multi-model mean dissimilarity statistic (b) Models agreement on CDFs similarity at $p \leq 0.1$ significance level based on the KS-test: darker colours correspond to higher model agreement on the similarity in CDFs.....124

Figure 4.4: Long-term mean monthly historical maximum temperatures (1951-2005) (a) CRU observation (b) Multi-model mean. Long-term historical absolute bias between models and CRU maximum temperature (c) CanESM2 (d) CNRM (e) CSIRO (f) HadGEM2 (g) IPSL (h) MIROC5 (i) MPI (j) NCC (k) GFDL. Grey contours highlight regions of significant difference between observations and simulations ($p \leq 0.1$) based on a t test.....126

Figure 4.5: Long-term mean monthly historical minimum temperatures (1951-2005) (a) CRU observation (b) Multi-model mean. Long-term historical absolute bias between models and CRU minimum temperature (c) CanESM2 (d) CNRM (e) CSIRO (f) HadGEM2 (g) IPSL (h) MIROC5 (i) MPI (j) NCC (k) GFDL. Grey contours highlight regions of significant difference between observations and simulations ($p \leq 0.1$) based on a t test.....127

Figure 4.6: Distributional biases between models and CRU observations (1951-2005) (a-b) Maximum temperatures: (a) Maximum temperature multi-model mean dissimilarity statistic (b) Models agreement on CDFs similarity at $p \leq 0.1$ significance level based on the KS-test: darker colours correspond to higher model agreement on the similarity in CDFs (c-d) Minimum temperatures: (c) minimum temperature multi-model mean dissimilarity statistic (d) Models agreement on CDFs similarity at $p \leq 0.1$ significance level based on the KS-test: darker colours correspond to higher model agreement on the similarity in CDFs.....128

Figure 4.7: Distributional biases between bias-corrected model simulations and CRU observations (a-c) Precipitation fields: (a) Precipitation multi-model mean dissimilarity static (b) Models agreement on CDFs similarity at $p \leq 0.1$ significance level based on the KS-test: darker colours correspond to higher model agreement on the similarity in CDFs (c) Summary of bias correction performances: white histograms refer to the average dissimilarity statistics (D); Grey histograms refer to the percentage of area with significantly similar CDFs (%Area) (d-f) Maximum temperature fields: (d) Maximum temperature multi-model mean dissimilarity static (e) Models agreement on CDFs similarity at $p \leq 0.1$ significance level based on the KS-test: darker colours correspond to higher model agreement on the similarity in CDFs (f) Summary of bias correction performances: white histograms refer to the average dissimilarity statistics (D); Grey histograms refer to the percentage of area with significantly similar CDFs (%Area) (g-i) Minimum temperature fields: (g) Minimum temperature multi-model mean dissimilarity static (h) Models agreement on CDFs similarity at $p \leq 0.1$ significance level based on the KS-test: darker colours correspond to higher model agreement on the similarity in CDFs (i) Summary of bias correction performances: white histograms refer to the average dissimilarity statistics (D); Grey histograms refer to the percentage of area with significantly similar CDFs (%Area).....130

Figure 4.8: Hydrological model performances for different calibration and validation periods. a) Kling-Gupta Efficiency; b) Nash-Sutcliffe Efficiency. Blue refers to GR2M and red to IHACRES-CWI.....132

Figure 4.9: Spatial distribution of hydrological model performances (KGE average for all periods) for calibration and validation periods. Overall average performances for GR2M calibration (a) validation (b). Overall average performances for IHACRES-CWI calibration (c) validation (d). Blue values indicate good performances, while red values indicate poor performances. Grey polygons display the geographic boundaries of the major river basins.....134

Figure 4.10: Performance of multi-timescale linear regression models based on K-fold cross-validation, as determined using KGE criterion. Blue values indicate good performances, while red values indicate poor performances. Grey polygons display the geographic boundaries of the major river basins.....135

Figure 4.11: Near-term (2020-2050) relative change in precipitation under RCP4.5 emission scenario (a) CanESM2 (b) CNRM (c) CSIRO (d) HadGEM2 (e) IPSL (f) MIROC5 (g) MPI (h) NCC (i) GFDL. White colour corresponds to relative changes of ± 0.05 . Grey contours highlight regions of significant changes ($p \leq 0.1$) based on a t test.....136

Figure 4.12: Near-term (2020-2050) absolute changes in maximum temperatures under RCP4.5 emission scenario (a) CanESM2 (b) CNRM (c) CSIRO (d) HadGEM2 (e) IPSL (f) MIROC5 (g) MPI (h) NCC (i) GFDL. Grey contours highlight regions of significant changes ($p < 0.1$) based on a t test.....138

Figure 4.13: Near-term (2020-2050) absolute changes in minimum temperatures under RCP4.5 emission scenario (a) CanESM2 (b) CNRM (c) CSIRO (d) HadGEM2 (e) IPSL (f) MIROC5 (g) MPI (h) NCC (i) GFDL. Grey contours highlight regions of significant changes ($p < 0.1$) based on a t test.....139

Figure 4.14: Near-term (2020-2050) relative change in discharge for the GR2M model under RCP4.5 emission scenario (a) CanESM2 (b) CNRM (c) CSIRO (d) HadGEM2 (e) IPSL (f) MIROC5 (g) MPI (h) NCC (i) GFDL. Black crosses highlight regions of significant changes ($p \leq 0.1$) based on a t test.....141

Figure 4.15: Near-term (2020-2050) relative change in discharge for the IHACRES model under RCP4.5 emission scenario (a) CanESM2 (b) CNRM (c) CSIRO (d) HadGEM2 (e) IPSL (f) MIROC5 (g) MPI (h) NCC (i) GFDL. Black crosses highlight regions of significant changes ($p \leq 0.1$) based on a t test.....142

Figure 4.16: Near-term (2020-2050) relative changes in discharge for the teleconnections-based linear regression model under RCP4.5 emission scenario (a) CanESM2 (b) CNRM (c) CSIRO (d) HadGEM2 (e) IPSL (f) MIROC5 (g) MPI (h) NCC (i) GFDL. Black crosses highlight regions of significant changes ($p \leq 0.1$) based on a t test.....144

LIST OF TABLES

Table 3.1: List of variables considered for the PCA. Catchment properties (Area, WHC, slope) datasets are collected from the SIEREM database and groundwater datasets are collected from the BGS database (MacDonald *et al.*, 2012).....73

Table 3.2: Periods in years of MOWDT components for each cluster centroid. Explained variance associated with each component is given in parentheses. CGQ2000 (Congo at Brazzaville), CFQ0025 (Oubangui at Zinga) and MLQ0137 (Faleme at Fadougou).....83

Table 4.1: List of datasets and climatic variables used in the study.....116

ABBREVIATIONS & ACRONYMS

20CR.v2: 20th Century Reanalysis version 2

AEJ: African Easterly Jet

AEW: African Easterly waves

ALMIP: AMMA Land Surface Model Intercomparison Project

AMMA: African Monsoon Multidisciplinary Analysis

AMO: Atlantic Multi-decadal Oscillation

AMOC: Atlantic Meridional Overturning Circulation

ARMAX: Auto-Regressive Moving Average with exogenous inputs

AU: African Union

CEA: Central Equatorial Africa

CMIP: Coupled Model Intercomparison Project

CORDEX: Coordinated Regional Climate Downscaling Experiment

CRU: Climate Research Unit

CWT: Continuous Wavelet Transform

EM: Atlantic Niño Equatorial Mode

eMED: eastern Mediterranean

ENSO: El Niño Southern Oscillation

EOF: Empirical Orthogonal Function

EOT: Empirical Orthogonal Teleconnection

ERSST.v5: Extended Reconstructed Sea Surface Temperature version 5

FAO: Food and Agriculture Organisation

GCM: Global Climate Model

GPCC: Global Precipitation Climatology Centre

GR2M: Modèle du Génie Rural à 2 paramètres Mensuel

GRanD: Global Reservoir and Dam Database

GW: Global Warming

ICOADS: International Comprehensive Ocean-Atmosphere Data Set

ICOLD: International Commission on Large Dams

IHACRES: Identification of unit Hydrographs and Component flows from Rainfall, Evapotranspiration and Streamflow

IPCC: Intergovernmental Panel on Climate Change

IPO: Inter-Decadal Pacific Oscillation

IRD: Institut de Recherche pour le Développement

IRSTEA: Institut National de Recherche en Sciences et Technologies pour l'Environnement et l'Agriculture

ITD: Intertropical discontinuity

ITCZ: Intertropical Convergence Zone

KGE: Kling-Gupta Efficiency

LLW: Low-level Westerlies

MCS: Mesoscale Convective System

MICE: Multiple Imputations by Chained Equations

MODWT: Maximum Overlap Discrete Wavelet Transform

NCEP/NCAR: National Centres for Environmental Prediction and the National Centre for Atmospheric Research

NRMSE: Normalized Root Mean Squared Error

NSE: Nash-Sutcliffe Efficiency

OLR: Out-going Longwave Radiation

P : Precipitation

PBIAS: Percent Bias

PC: Principal Component

PCA: Principal Component Analysis

PDO: Pacific Decadal Oscillation

PET: Potential Evapotranspiration

QDM: Quantile Delta Mapping

RCM: Regional Climate Model

RCP: Representative Concentration Pathway

R_{et}: Extra-terrestrial radiation

RF: Random Forest

SDGs: Sustainable Development Goals

SHL: Saharan Heat Low

SIEREM: Système d'Informations Environnementales sur les ressources en Eau et leur Modélisation

SMHI: Swedish Meteorological and Hydrological Institute

SST: Sea Surface Temperature
T_{avg}: Average Temperature
T_d: Temperature diurnal range
TEJ: Tropical Easterly Jet
TFPW: Trend-free Pre-whitening procedure
T_{max}: Maximum temperature
T_{min}: Minimum temperature
TSA: Theil-Sen approach
UDEL: University of Delaware
WAM: West African Monsoon
WMO: World Meteorological Organization

**CHAPTER 1: GENERAL INTRODUCTION TO THE
RESEARCH**

1. Introduction

1.1. Background

Sub-Saharan Africa is one of the poorest regions in the world (*e.g.* World Bank 2015b; Serdeczny *et al.*, 2017). Populations, mostly relying on rain-fed agriculture and animal husbandry to sustain their livelihoods, are highly vulnerable to climate variability and change (*e.g.* Mortimore, 2010; Roudier *et al.*, 2011; IPCC, 2014). Such a vulnerability to climate change, combined with low levels of adaptive capacity inherent to economic, demographic and natural factors among others, point out to urgent adaptation needs (Niang *et al.*, 2014).

Development of sound adaptation strategies, based on a better understanding of hydrological systems, is particularly important in the current context of climate and environmental changes (*e.g.* Niang *et al.*, 2014), whose impacts are already being felt across Sub-Saharan Africa. In fact, since the 1950s, this region has experienced unprecedented changes in the hydrological system, especially marked by the prolonged droughts of the 1970s and 1980s (*e.g.* Dai *et al.*, 2004; Held *et al.*, 2005; Nicholson, 2013; Sheen *et al.*, 2017), as well as more recent changes in extreme events (*i.e.* droughts, floods; Ringard *et al.*, 2016; Taylor *et al.*, 2017; Panthou *et al.*, 2018). These changes, mainly driven by human induced warming of the climate system have significantly impacted hydrological regimes (Descroix *et al.*, 2009, 2018). While the drought episodes of the 1970/80s increased interest and research activity investigating the potential climatic drivers (Nicholson, 2013 and the references therein), the impacts of these unprecedented changes on hydrological regimes at the regional scale, remained relatively less documented.

Due to the dearth of observational data, researchers often limited their investigations to local scales with a focus on testing standard statistical applications and hydrological models forced with climate change scenarios to characterize the hydroclimatic variability (*e.g.* Amoussou *et al.*, 2010; Ibrahim *et al.*, 2015). Different study areas and spatial scales considered, together

with inhomogeneity in datasets thus often resulted in different findings (Ali and Lebel, 2009; Nicholson, 2013). In addition, understanding of the erratic internal variability is often constrained by the basic assumptions considered in time series analysis (randomness, non-persistence and stationarity) which are rarely observed in natural processes (Wilcox *et al.*, 2018). Even though recent advances make it possible to account for non-stationarity, very few of these new techniques have been implemented to characterize hydroclimatic variability and unravel the driving mechanisms of this variability in sub-Saharan Africa. Notwithstanding the achievements of meteorological field experiments [*e.g.* African monsoon multidisciplinary analysis (AMMA), the associated Land Surface Model Intercomparison Project (ALMIP)], hydroclimatic variability across West and Central Africa, especially processes occurring at decadal to multi-decadal timescales, associated teleconnections with large-scale climate, as well as the potential influence of catchment properties on these fluctuations are not fully understood (Washington *et al.*, 2013; Roudier *et al.*, 2014).

The high internal hydroclimatic variability combined with scarce long-term hydrological records, as well as the uncertainties of climate projections in this part of the world, challenge the scientific community to improve understanding of hydrological processes and provide more robust predictions to inform adaptation strategies (Clark *et al.*, 2016; Wilcox *et al.*, 2018).

1.2. Literature review

1.2.1. Hydroclimatic variability in West and Central Africa

Precipitation over West and Central Africa is controlled by the South-North-South migration of the Intertropical Convergence Zone (ITCZ; cf. Section 1.2.2), leading to a meridional gradient in precipitation amount (*e.g.* L'Hôte *et al.*, 1996; Roudier *et al.*, 2014). In the South, annual precipitation is abundant, and occurs mostly during two rainy seasons (September-November and March-July) without a marked dry season. Further North, precipitation amounts decrease, and the seasonal cycle is characterized by a single rainy season with a maximum

occurring in August (the Sahelian rainy season; Le Barbé *et al.*, 2002; Sultan and Janicot, 2003; Nicholson, 2013).

Precipitation variability over this region is governed by several factors, which interact in a complex way and present strong interannual to multi-decadal fluctuations (Nicholson *et al.*, 2013; Dieppois *et al.*, 2013, 2015). For instance, the wet period of the 1950s and the early 1960s was followed by unprecedented droughts in the 1970s and 1980s (*e.g.* Dai *et al.*, 2004; Held *et al.*, 2005; Panthou *et al.*, 2014; Figure 1.1), which triggered several studies in the region. The focus was mainly on the so-called “Sahel” zone, which appeared to be more vulnerable to climate fluctuations (Nicholson, 2013). Described as a transitional zone between the Sahara Desert in the North and the Sudanian savanna in the South, the Sahel spans approximately 5400 km from the Atlantic Ocean in the west to the Red sea in the East (Figure 1.1a). While there is unanimity among the scientific community about the humid periods of the 1950s and early 1960s and the severity of droughts that occurred in the 1970s and 1980s, difficulties inherent to declining meteorological observation networks (Figure 1.1b) have resulted in poor description of the post-1990 period. Analyses of recent rainfall conditions indicate a partial recovery in the late 1990s (Nicholson, 2005; Ali and Lebel, 2009; Lebel and Ali 2009; Mahé and Paturel, 2009; Jury, 2013).

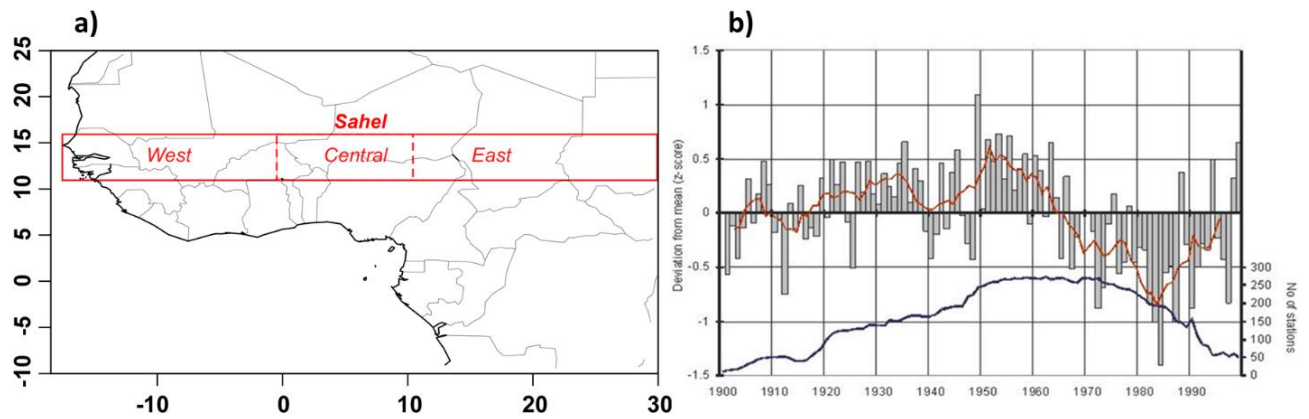


Figure 1.1: (a) Location of the research area: red boxes highlight the Sahel and different sub-regions (adapted from Monerie *et al.*, 2016); (b) Rainfall anomalies from the long term mean for meteorological stations in the Sahel. Red line shows the 7-year running mean, blue line shows the number of stations (Data source: Climatic Research Unit, University of East Anglia, and Global Historical Climatology Network, Oak Ridge National Laboratory) (Image source: http://www.eoearth.org/article/Greening_of_the_Sahel).

Furthermore, superimposed to the very well-known meridional gradient in West African precipitation amount and variability, zonal contrasts between eastern and western regions have recently been identified over the Sahelian regions (Dai *et al.*, 2004; Nicholson, 2005; Lebel and Ali, 2009; Fontaine *et al.*, 2011). Lebel and Ali (2009) for instance, reported ~10% increase in Central Sahel annual precipitation and a constant deficit over western Sahel, for the period 1990-2007 compared to the period 1970-1989. Interestingly, while 2006 was considered a significantly dry year over the entire Sahel, Ali and Lebel (2009) found that, working at the $0.5^{\circ} \times 0.5^{\circ}$ resolution, only 28% of the area was significantly dry, while 15% of the region was significantly wet. This study revealed the high spatial variability of precipitation patterns, which explains to some extent the divergence between studies, and raises the important issue of the appropriate spatial scales in precipitation variability studies. Another key issue is the inhomogeneity resulting from the integration of different data sources. For instance, Nicholson (2005) assessed rainfall conditions from 1998 to 2003 using satellite data, while the previous conditions were assessed using gauge data. Discrepancies might therefore potentially emerge from the bias between satellite and gauge data.

Even though rainfall variability and trend have been deeply investigated over Africa during the last decades (Giannini *et al.*, 2008, Maidment *et al.*, 2015), the prevailing conditions over

Central Equatorial Africa remain poorly documented. Mahé *et al.* (2001) indicated that no discontinuity was apparent in precipitation over Central Africa for the 1950-1989 period. Few studies however report a long-term drying trend from the 1970s (Yin and Gruber, 2010; Asefi-Najafabady and Saatchi, 2013; Diem *et al.*, 2014). According to previous studies (McCabe and Wolock, 2002; Liebmann *et al.*, 2010; IPCC, 2014), due to high level of natural variability, hydroclimatic trends can thus be very sensitive to beginning and end dates of study periods.

Hydrological systems across West and Central Africa were substantially impacted by these fluctuations in climate (Figure 1.2). Conway *et al.* (2009) documented strong rainfall-river flow relationships in West Africa (*i.e.* rainfall accounts for around 60%-70% of streamflow variability) and robust, but slightly weaker, relationships in Central Africa (around 50% of explained variance). These relationships are however non-linear due to the combined influence of different factors, such as land use changes, water withdrawals at the basin scale and carbon effect on plant water efficiency (Sterling *et al.*, 2013). In the Sahel region for instance, a rainfall deficit of 20% was found to result in approximately 60% decrease in streamflow (Mahé *et al.*, 2013) during the 1970s and 1980s. Similarly, opposite results were found in response to an increase of annual rainfall amount in the Niger basin (Aich *et al.*, 2014).

At the regional scale, large rivers experienced important decline in streamflow, which was proportionally greater than the decrease in precipitation (Mahé and Paturel, 2009). This finds its explanation in the long-lasting depletion of groundwater, reducing baseflow contribution to river discharge (Mahé *et al.*, 2013). At the sub-regional scale, several basins in Central Africa presented negative trends in streamflow (Servat *et al.*, 1997; Mahé and Olivry, 1999; Conway *et al.*, 2009). Over West Africa, two contrasting hydrological behaviours were observed. While Sudano-Guinean (South of 12°N) regions witnessed negative trends, for the 1960-2010 period (Mahé *et al.*, 2005; Descroix *et al.*, 2009, 2018), river basins located further North (between 12°N and 16°N) experienced increased runoff conditions despite drought conditions (Figure

1.2). This phenomenon – *the so-called “Sahelian paradox”* – was primarily driven by changes in surface conditions, resulting in superficial crusting and reduced infiltration (Leblanc *et al.*, 2008; Descroix *et al.*, 2009, 2018; Figure 1.2).

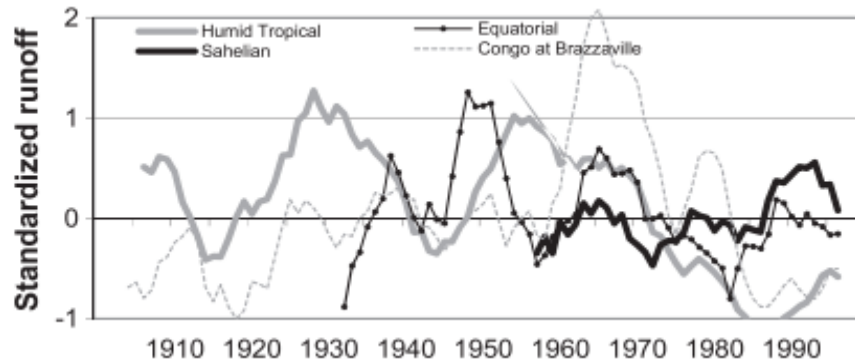


Figure 1.2: Runoff variability over four large regions of West and Central Africa (1901-2000). Equatorial rivers: Ogooué, Kouilou, Ntem, Nyong, Nyanga, in Gabon, Cameroon, Congo. Humid tropical rivers in West Africa: Senegal, Niger, Bandama, Sassandra, comoe, Volta and in Central Africa: Sanaga, Logone-Chari. Sahelian rivers from Mauritania, Niger, Burkina Faso and Cameroon (source: Mahé *et al.*, 2005).

It is also important to mention that these findings were mainly derived using stations with the most complete hydrological records over selected periods. Missing information in time series is often addressed with linear interpolation techniques (*e.g.* Nka *et al.*, 2015), and the potential impact of shorter-term fluctuations on long-term trends is not very well understood. Several studies were conducted at basin scale to estimate the impact of climate change on hydrological regimes. The results, however, are diverse and vary depending on hydrological models, climate models and the complexity of hydrological processes taking place at the catchment scale (Roudier *et al.*, 2014).

1.2.2. Major drivers of hydroclimatic variability

Over West and Central Africa, studies have pointed out the important role of sea surface temperature (SST) (*e.g.* Fontaine *et al.*, 1998; Ward, 1998; Rowell, 2001), land surface conditions (*e.g.* Eltahir and Gong, 1996) and atmospheric circulations (*e.g.* Burpee, 1972; Thorncroft and Blackburn, 1999; Nicholson, 2013) in driving hydroclimatic variability.

1.2.2.1. The West African Monsoon (WAM) system

The West African monsoon (WAM) is a coupled atmosphere-ocean-land system, which impacts precipitation, leading to wet summer and dry winter over the continent (Figure 1.3). The WAM is characterized by several key approximately zonal flows that are established in association with meridional heating contrasts and associated direct circulations (Parker *et al.*, 2005).

At low-levels (*i.e.* near-surface), south-westerlies (or monsoon flux) from the Atlantic provide most of the moisture for the WAM, while, poleward, northeasterlies (or Harmattan flux) advect relatively drier Saharan air into the region. These two fluxes then converge into the ITCZ, which is the primary factor controlling precipitation over West Africa (Figure 1.3). The mean seasonal cycle of precipitation is determined by a stepwise South-North-South displacement of the ITCZ (Louvet *et al.*, 2003). In winter, the ITCZ is located around 5°S on the Tropical Atlantic, and the continent is dry. The ITCZ then moves to the North, and it coincides with the first rainy season along the Gulf of Guinea coastal regions. In late June, an abrupt northward shift of the ITCZ from 5°N to 10°N, which is referred to as the “monsoon onset” occurs (Sultan and Janicot, 2003). Some researchers also emphasize the role of the Saharan Heat Low (SHL; Lavaysse *et al.*, 2010), which increases in intensity at the time of the onset, probably as a result of interactions with the North Africa orography (Sultan and Janicot, 2003; Drobinski *et al.* 2005), together with effects of albedo and net shortwave radiative budget (Ramel, 2004). However, mechanisms linked to the annual cycle of the West African monsoon remain unclear (*e.g.* Sultan and Janicot, 2003; Janicot *et al.*, 2011).

In the mid to upper-troposphere, the WAM is also characterized by two predominant jets: the African Easterly Jet (AEJ) and the Tropical Easterly Jet (TEJ) (Figure 1.3). The AEJ is located in the mid-troposphere (*i.e.* 600-700 hPa) between 15°W and 15°E, and results from a combination of temperature, humidity gradients and feedback mechanisms associated with

land cover (Thorncroft and Blackburn, 1999). This jet is marked by intra-seasonal shifts induced by Mesoscale Convective Systems (MCSs), which are crucial in rainfall production over the region. For instance, over the Sahel, Lebel *et al.* (2003) found that ~90% of rainfall during the peak period is produced by ~12% of the total number of MCSs. The TEJ is located in the upper-troposphere between 100 and 200 hPa, and originates from the thermal gradient between the Indian Ocean and the Tibetan highlands (Fontaine and Janicot, 1993). From end of June to beginning of September, the TEJ is located around 5°N and 15°N. Compared to the AEJ, the TEJ has received less interest. It exhibits a more stable latitudinal position from year to year, but is quite unstable in terms of speed and East-West extent (Grist and Nicholson, 2001; Nicholson, 2009). Several studies highlighted the importance of the TEJ in modulating Sahel precipitation variability. For instance, a stronger (weaker) flux was associated with wetter (drier) Sahel (Mahé and Citeau, 1993; Nicholson and Grist, 2001; Nicholson, 2009). The strong ascending mass lying between the AEJ and the TEJ is the most important component in rain production over West Africa. Even though, the TEJ significantly affects Sahel rainfall variability, the phenomena behind its change in intensity are not yet understood.

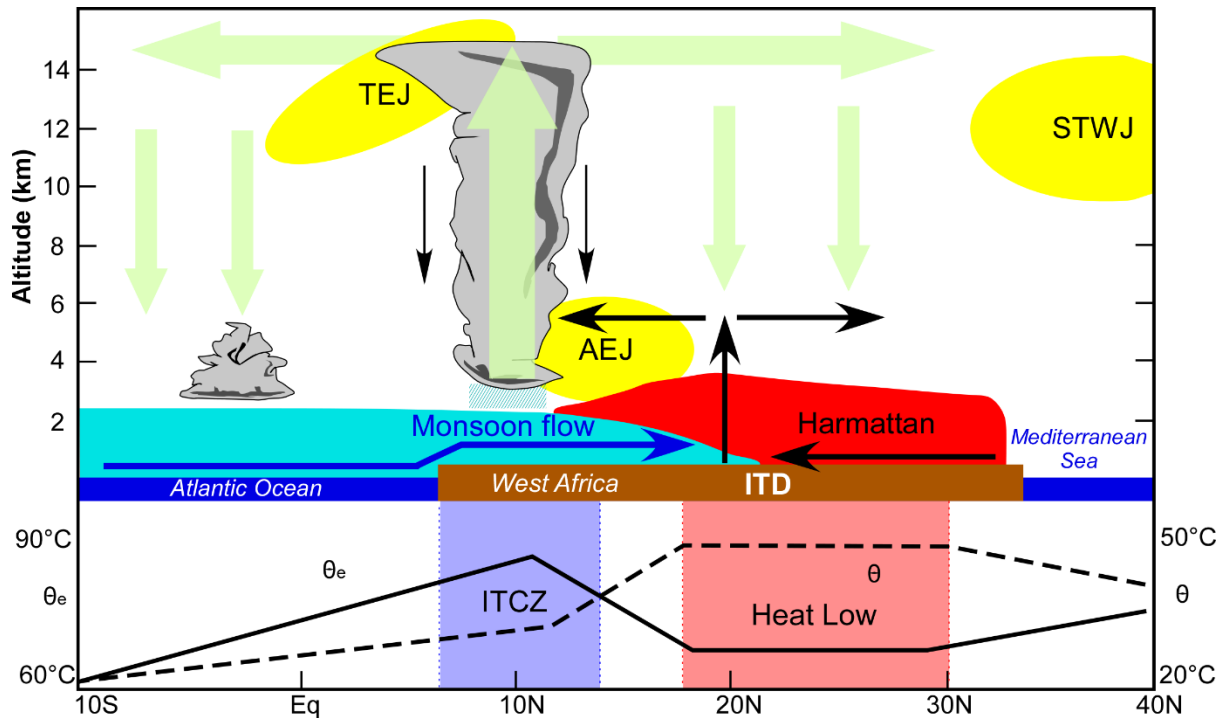


Figure 1.3: Schematic of the main features of the West African monsoon system during the boreal summer: meridional circulations and zonal means (adapted from Peyrillé, 2006). Below are given the corresponding meridional variations in atmospheric boundary layer potential temperature (θ) and moist static energy (θ_e).

All this system is marked by fluctuations at the interannual to multi-decadal timescales (Dieppoiss *et al.*, 2013, 2015), which result in different precipitation anomaly patterns (Janicot, 1992; Nicholson, 2008, 2013): North/South dipole (*i.e.* +/- or -/+) and monopole (*i.e.* +/+, -/-).

1.2.2.2. Sea Surface temperatures and precipitation variability

Previous studies suggested that different patterns of precipitation variability over West and Central Africa primarily result from fluctuations in global and regional SST at interannual to multi-decadal timescales (*e.g.* Fontaine *et al.*, 1998; Ward, 1998; Rowell, 2001; Mohino *et al.*, 2011; Rodriguez-Fonseca *et al.*, 2011, Dieppoiss *et al.*, 2013, 2015; Suarez-Moreno *et al.*, 2018).

At interannual timescales, West African precipitation is strongly linked to two co-variability modes of SST in the tropics (Figure 1.4). In the first one, a warming of the tropical Pacific, which is associated with El Niño Southern Oscillation (ENSO), relates to reduced Sahelian precipitation (*e.g.* Giannini *et al.*, 2003; Joly *et al.*, 2007). The second mode associates the

WAM to the Atlantic Niño Equatorial Mode (EM), with a warm summer EM resulting in a southward displacement of the ITCZ/monsoon. In addition, after 1979, a warming over the Eastern Mediterranean (eMED) was found to result in increased precipitation over the Sahel (Rowell, 2003; Polo *et al.*, 2008; Figure 1.4).

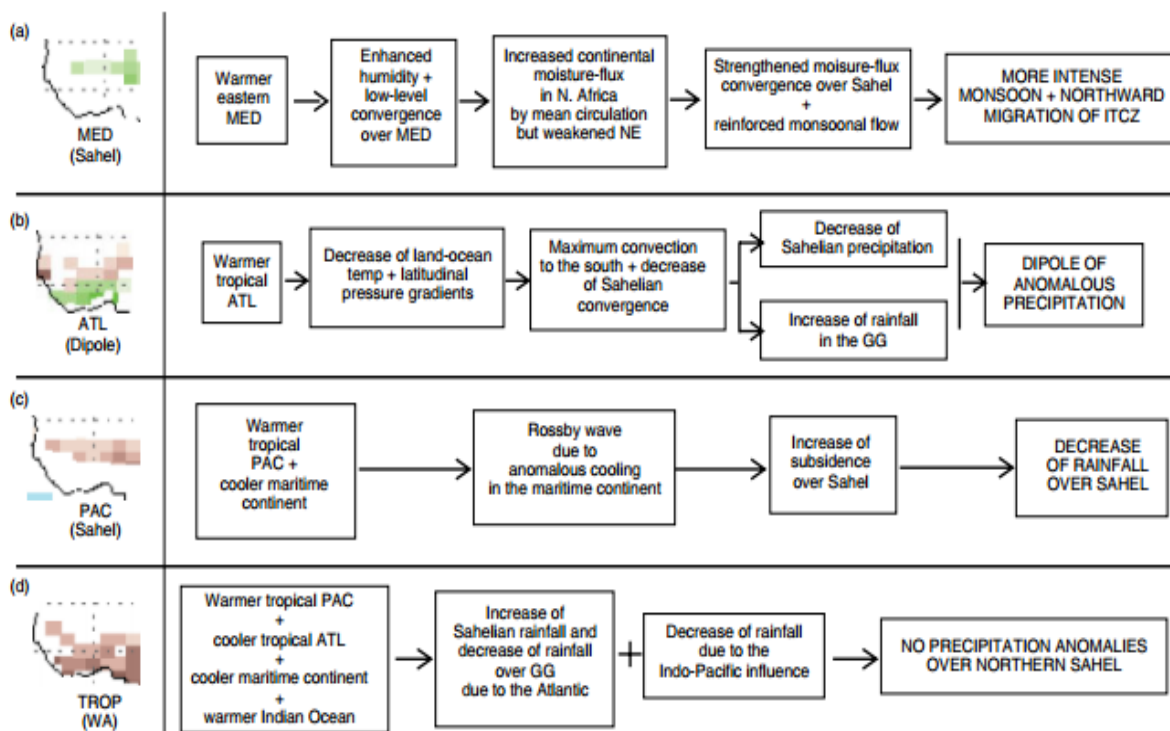


Figure 1.4: (Left) Observed anomalous rainfall response and (right) flux diagrams explaining the WAM–SST teleconnection mechanisms associated with the (a) Mediterranean, (b) tropical Atlantic, (c) tropical Pacific, and (d) global tropical SST forcings (source: Rodríguez-Fonseca *et al.*, 2011).

Concerning Central Equatorial Africa, very few studies exist in the literature due to the lack of high-quality gridded datasets (New *et al.*, 2000; Camberlin *et al.*, 2001; Nikulin *et al.*, 2012). Climate over this region is characterized by complex interactions between atmospheric, oceanic and static geographical features occurring at different spatio-temporal scales (Dezfuli, 2017). For instance, Balas *et al.* (2007) found that precipitation interannual variability over the region is driven seasonally by SST anomalies along the Benguela Coast, the thermal gradient between the Atlantic, the Indian Ocean and ENSO (in particular during the winter-months). Early in the year the effects of Pacific El Niño and the Western Indian Ocean on Central Africa

rainfall are predominant during the winter-months, while the influence of the Atlantic is more pronounced during the summer-months (Dezfuli, 2017).

At the decadal time scale, the WAM is mainly linked to a global SST inter-hemispheric pattern, which partly explains the transition between the wet (1950-60s) and dry (1970-80s) periods over West Africa (Mohino *et al.*, 2011; Rodriguez-Fonseca *et al.*, 2011; Dieppois *et al.*, 2013; Villamayor and Mohino, 2015). Dry conditions over the Sahel are linked to a warmer tropical region together with positive Inter-decadal Pacific Oscillation (IPO) and Atlantic Multi-decadal Oscillation (AMO) patterns (Figure 1.5). In addition, these decadal oscillations, as well as their impact, are interacting with the current warming of the global ocean (GW). Mohino *et al.* (2011) thus found that decadal Sahel precipitation variability can be explained by the competing effect between the AMO, GW and IPO (Figure 1.5). In fact, according to the latter study, half of the 1980s drought would be related to a negative shift of the AMO, and to the GW pattern to a lesser extent. Such decadal fluctuations also seem to drive zonal contrasts in precipitation variability over the Sahel (Dieppois *et al.*, 2013, 2015), consistently with the recent trend over this region (Dai *et al.*, 2004; Nicholson, 2005; Lebel and Ali, 2009; Fontaine *et al.*, 2011).

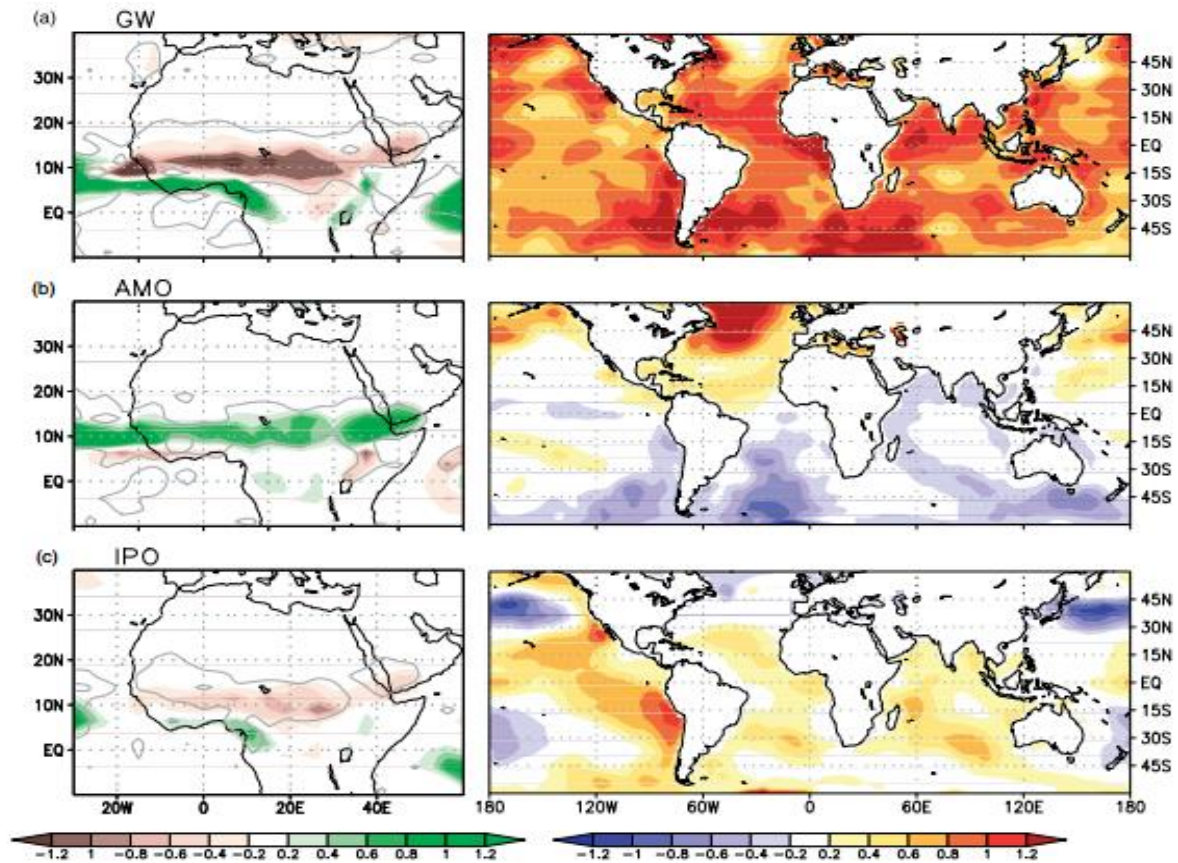


Figure 1.5: Anomalous precipitation (mm/day, left column) simulated by the LMDZ model in response to the anomalous pattern of SST (K, right column) for:(a) GW, (b) AMO, and (c) IPO. The precipitation is the averaged response over the ten-member ensemble simulations. Grey contours mark 95% significant anomalies according to at-test (source: Mohino *et al.*, 2011).

The prevailing conditions over Central Africa, *i.e.* climate drivers of decadal rainfall variability, remain relatively less documented. Investigating the possible causes of the long-term drought over the same region, Hua *et al.* (2016) proposed a link to SST dynamics over the Indo-Pacific related to westward tropical Walker circulation, similarly to what was proposed at the interannual scale (Balas *et al.*, 2007).

1.2.2.3. Feedback mechanisms, land use and change in precipitation

Studies based on global circulation model (GCM) simulations concluded that vegetation changes in the study area can result in dramatic precipitation reduction. Eltahir and Gong (1996) indicated a tight connection between West African precipitation and changes in vegetation. For most GCM simulations, their results show an obvious tendency of decreasing precipitation and evaporation associated with increasing vegetation loss. Taylor (2002) tested

the hypothesis that land use change over the Sahel was significant enough to cause the observed drought episodes. His findings suggest that climate over the Sahel was quite sensitive to small changes in vegetation cover, but historical changes in land use were not pronounced enough to trigger the drought episodes. These could however have a substantial impact on surface hydrology (Mahé *et al.*, 2013; Gerbaux *et al.*, 2009; Descroix *et al.*, 2009; 2018).

1.2.3. Climate change and hydroclimatic projections

In Sub-Saharan Africa, population lives, and livelihoods are highly impacted by seasonal and interannual climate variability, which will likely worsen with climate change. Different tools have been implemented to evaluate the future climate over this region, and in general researchers are more confident in the projections of temperature changes than the changes in precipitation (IPCC, 2013; Roehrig *et al.*, 2013; Aloysius *et al.*, 2016; Sylla *et al.*, 2016). Over Central Africa, Aloysius *et al.* (2016) detected a robust warming trend (2-4°C) consistent across CMIP5 models by the end of the 21st Century. In West Africa, average temperatures over the region are already rising with a reported increase of about 1°C since 1950 (Morice *et al.*, 2012). The change however is more exacerbated over the Sahelian region, and ranges from 1.5 to 2°C. This tendency to warming conditions is persistent in both Coupled Model Intercomparison Project – phase 3 (CMIP3) and phase 5 (CMIP5) simulations, with a robust projection of about 4°C on average under the Representative Concentration Pathways (RCP) 8.5 scenario over the Sahel (Roehrig *et al.*, 2013). Over West Africa, the spread of model projections remains large. For instance, by the mid-21st century, temperatures are projected to increase between 1.5 and 4°C relative to the 1986-2005 period (Niang *et al.*, 2014), with larger increases expected in the Sahel and the Sahara Desert compared to the Gulf of Guinea regions. Changes are also expected in the regime of extreme temperatures, with faster increase of night time (minimum daily) temperatures compared to day time (maximum daily; Funk *et al.*, 2012; Ringard *et al.*, 2016).

In addition, more heatwave days (*i.e.* a sequence of days in excess of a certain temperature) are predicted over the western Sahel (Vizy and Cook, 2012).

As mentioned earlier, the level of confidence decreases when it comes to precipitation predictions. State-of-the-art climate models do not agree on whether precipitation will increase or decrease. Over vast regions of Africa, there is no consensus on the sign of the future trends (Roehrig *et al.*, 2013; Niang *et al.*, 2014; Aloysius *et al.*, 2016; Monerie *et al.*, 2016; Sylla *et al.*, 2016). In Central Africa, precipitation projections, present dissimilarities across models regarding the sign and amplitude of changes (-9% to 27%; Aloysius *et al.*, 2016). Considering the baseline period 1986-2005, rainfall projections for July-August-September (JAS) range between -40% and 20% in the Western Sahel (15°-5°W), and between -20% and 40% in the Central and Eastern (between 0° and 30°E) Sahel (Rowell *et al.*, 2016). Nonetheless, in their assessment of the West African Monsoon based on CMIP5 simulations, Roehrig *et al.* (2013) found that approximately 80% of models agree on drying of about 20% over the western part of the Sahel, while 75% of models predict a wetter eastern Sahel with, however, a wider spread of amplitude. These findings are consistent with the recent assessment of CMIP5 models conducted by Monerie *et al.* (2016), which defined four groups of models based on the sign of the projected Sahel precipitation (Figure 1.6).

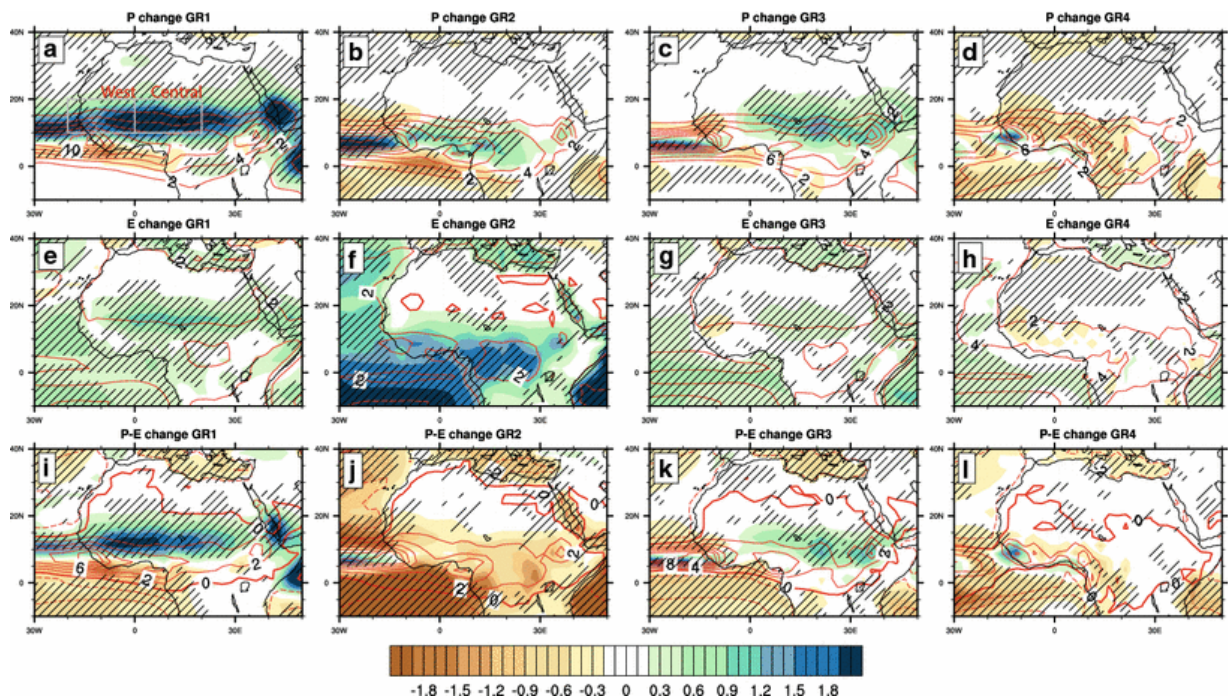


Figure 1.6: Projected changes in JAS: (a–d) precipitation (mm day⁻¹), (e–h) evaporation (mm day⁻¹) and (i–l) P–E budget (mm day⁻¹) for the four groups of models (one group per column) identified by the clustering. The present climatology (HIST) is displayed with red contours and the RCP85–HIST differences by colour shading. Hatching represents the grid-points where at least 80 % of the models agree with the sign of the intra-group ensemble mean within each group (5 for GR1; 7 for GR2; 13 for GR3; 5 for GR4) (source: Monerie *et al.*, 2016).

The spread in projections brings to question the mechanisms considered in precipitation projections, as some equally credible models predict neither a dry westernmost Sahel nor a wetter easternmost Sahel (Figure 1.6). Recent findings attribute these uncertainties in predictions to the deficiencies coupled models have in characterizing the Atlantic SST (Richter and Xie, 2008; Patricola *et al.*, 2012; Roehrig *et al.*, 2013; Monerie *et al.*, 2016). In Central Africa for instance, this bias in the Atlantic SST leads to the so-called “double ITCZ problem” characterized by precipitation overestimation off the equator, and underestimation along the equator resulting in important bias (Lin, 2007). Moreover, state-of-the-art GCMs often underestimate decadal to multi-decadal fluctuations (Ault *et al.*, 2014; Martin *et al.*, 2014; Dieppois *et al.*, 2019), suggesting that future climate projections could poorly represent decadal variability, and offer a limited view of long-term hydro-meteorological risks (*i.e.* prolonged droughts/floods). Underlying drivers of such model uncertainties however remain unclear,

especially at decadal timescales, and might be region-dependant (Hawkins and Sutton, 2009; Deser *et al.*, 2012).

These projected changes in precipitation and temperature will significantly impact hydrological regimes. So far, few studies have investigated the future trends of streamflow in Sub-Saharan Africa (Washington *et al.*, 2013; Roudier *et al.*, 2014; Stanzel *et al.*, 2018).

Often, climate change impacts on hydrological systems are estimated within a modelling chain, whereby climate model projections are used to drive different hydrological models under different greenhouse gas emission scenarios (Clark *et al.*, 2016; Hattermann *et al.*, 2018; Figure 1.7). The process is however not straightforward as climate model outputs are generally available on coarse spatial resolutions and, therefore, post-processing is often required prior to their use in hydrological models (*e.g.* Kundzewicz *et al.*, 2007; Maraun *et al.*, 2010). So-called downscaling approaches have been used extensively during the past two decades to address this spatial resolution mismatch through either dynamical or statistical means (*e.g.* Maraun *et al.*, 2010; Cannon *et al.*, 2015; Yira *et al.*, 2017). Dynamical downscaling uses high-resolution models to solve process-based dynamics related to the climate system at smaller scales (*e.g.* Giorgi and Mearns, 1991; Giorgi *et al.*, 2009; Eden *et al.*, 2012; Nikulin *et al.*, 2012). Statistical downscaling seeks to derive relationships between local-scale observation time series and large-scale climate predictors (*e.g.* Wilby and Wigley, 1997; Maraun *et al.*, 2010). In addition, climate simulations generally present systematic biases, which ought to be reduced through bias-correction algorithms to achieve realistic hydrological simulations (*e.g.* Teutschbein and Seibert, 2012; Yira *et al.*, 2017).

In a comprehensive review, Clark *et al.* (2016) present the limitations in climate change impact studies and the range of uncertainties associated with the modelling process (Figure 1.7). The authors advocate for future hydrological scenarios, which encompass the full spectrum of

uncertainties associated with global climate modelling, climate downscaling, hydrological modelling and natural climate variability through adequate models/methods selection.

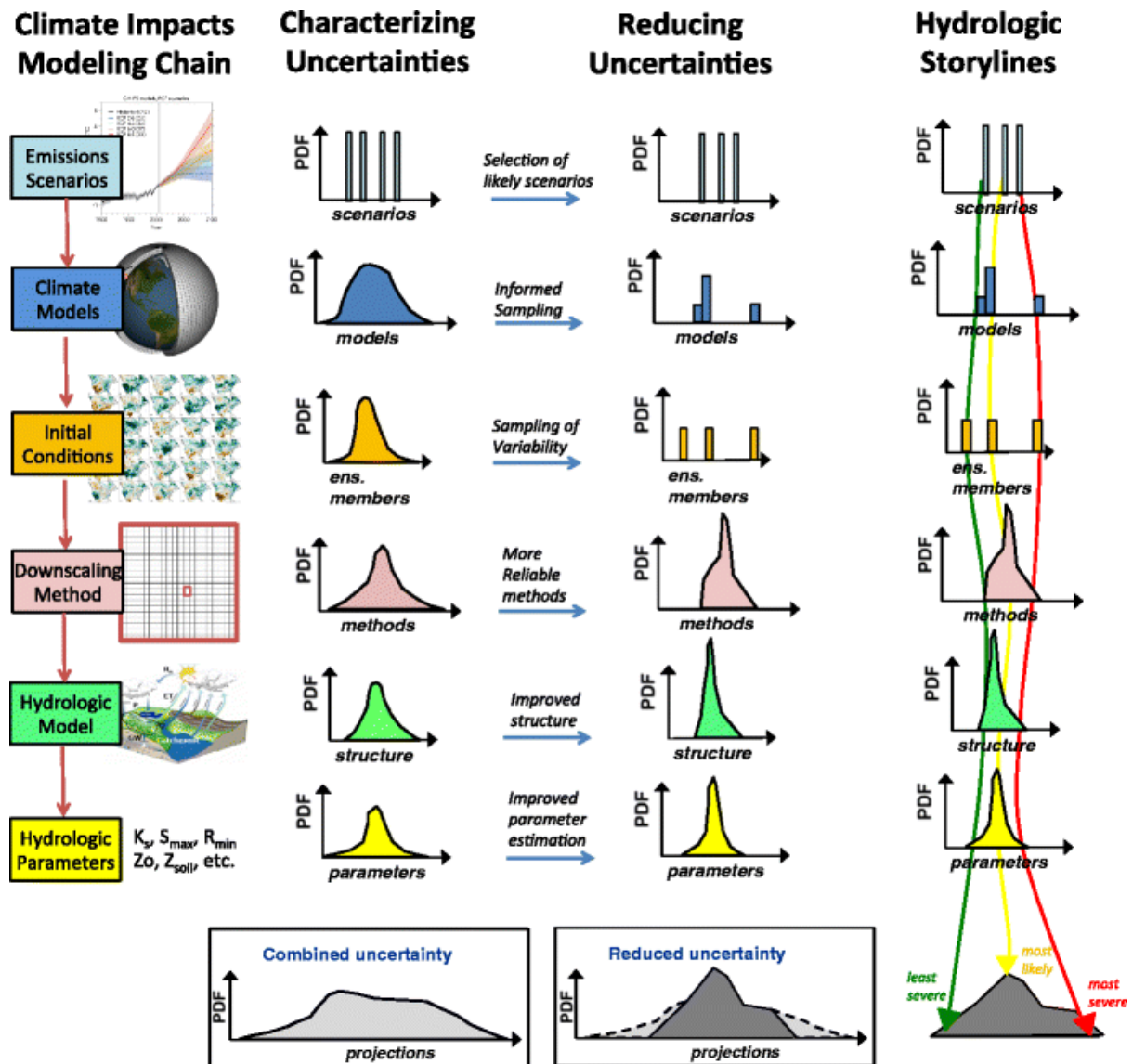


Figure 1.7: Schematic on approaches to explicitly characterize and reduce the myriad uncertainties in assessments of the hydrologic impacts of climate change and the development of representative quantitative hydrologic storylines for specific applications (source: Clark *et al.*, 2016).

The proposed framework underlines the importance of appropriate models and methods, as well as future greenhouse gas emission scenarios selection in reducing uncertainties in hydroclimatic predictions (Figure 1.7). Previous findings also advocate for streamlined streamflow prediction techniques using teleconnections-based linear regression models. In fact, researchers were able to detect robust teleconnections between streamflow series and

large-scale climate drivers (*e.g.* Yarnal, 1993; Chiew and McMahon, 2002; Sen, 2012; Kingston *et al.*, 2013; Nalley *et al.*, 2016; Massei *et al.*, 2017), which could be used to assess the impact of climate change on hydrological systems. Although, limited by weak predictor-predictand relationships and external factors, such as land use and urbanization, these techniques, due to the high signal-to-noise ratio in streamflow time series, can potentially improve projections in regions with poor quality gridded observational datasets (*e.g.* precipitation, temperature).

1.3. Research objectives and methods

The present thesis aims to understand past and future hydroclimatic variability across West and Central Africa, and their teleconnections.

More specifically, analyses are performed to provide a global picture of hydroclimatic trends and variability and their interactions with large-scale climate patterns, to unravel the complex processes driving streamflow variability beyond the catchment scale perspective and assess the impact of near-term climate change on hydrological systems in West and Central Africa.

The main research objectives of this thesis are as stated:

- To assemble a new, robust reconstructed streamflow dataset for West and Central Africa and examine hydroclimatic trends and variability over the region between 1950 and 2005.
- To unravel the complex processes associated with streamflow variability beyond the catchment scale perspective in data scarce environments.
- To provide further insights into the response of hydrological systems to a changing climate across West and Central Africa by the mid-21st century.

In Figure 1.8, the different datasets used and the applied methods to address the research objectives in this thesis by artefact, are summarised. The linkages between the research papers

are also highlighted. Data imputation techniques are implemented to tackle limitations related to data-scarcity. The important issue of non-stationarity in times series is accounted for through spectral analysis and multi-temporal trend analysis. In addition, building upon the recommendations by Clark *et al.* (2016; Figure 1.7), hydroclimatic predictions are provided within a modelling framework combining hydrological models, and a multi-timescale teleconnections-based regression model. The main assumption here is that reducing the steps in the modelling chain has the potential to reduce uncertainties in data-scarce regions. This approach, which has never been applied to Sub-Saharan Africa covers the broad spectrum of uncertainties in climate change impact studies.

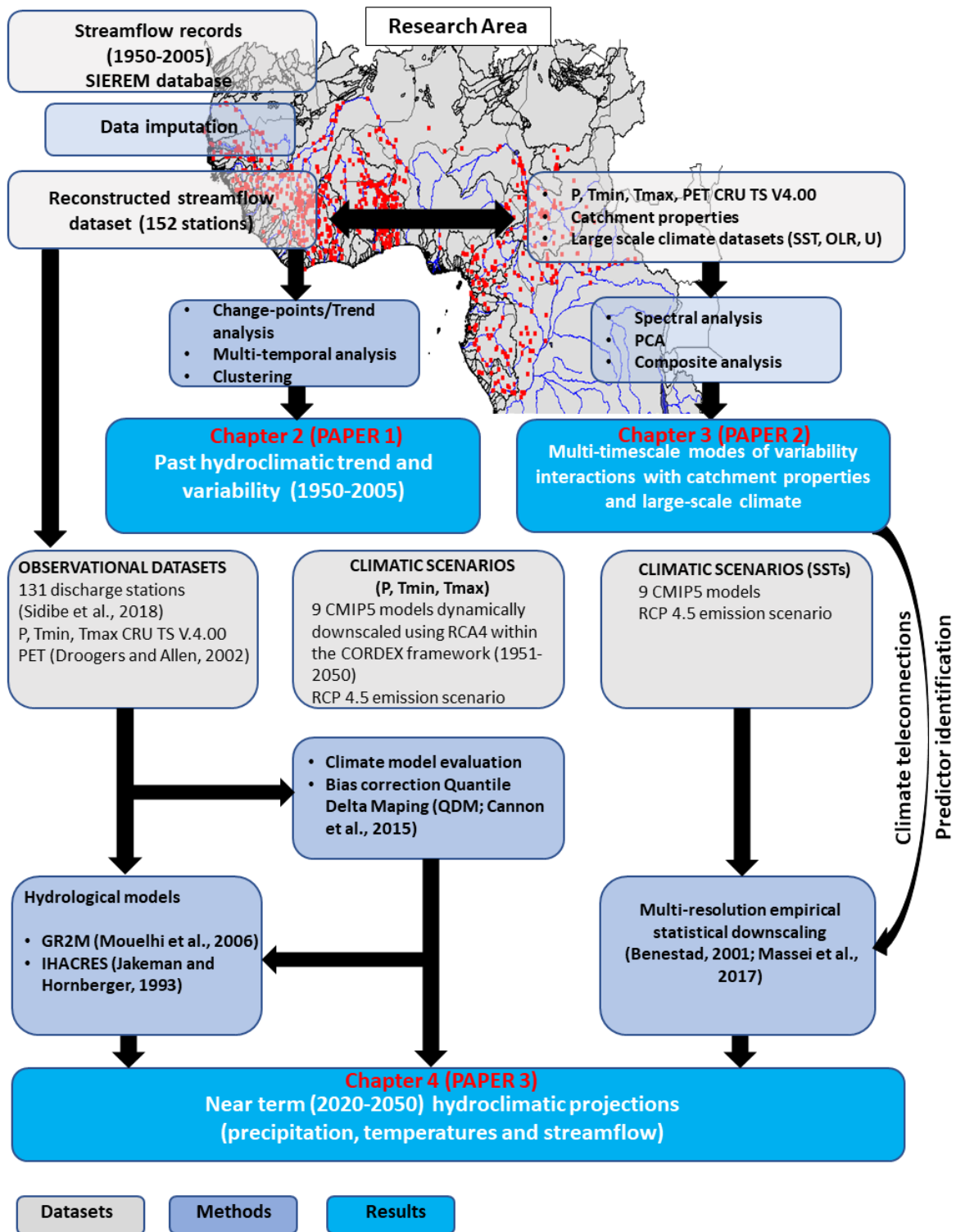


Figure 1.8: Schematic on datasets and implemented methodologies.

1.4. Thesis outline

This thesis by artefact, built upon three research papers is organized as follows:

Chapter 1 provided a general introduction and a review of the current understanding of hydroclimatic variability in West and Central Africa. In **Chapter 2**, a complete streamflow dataset for West and Central Africa is built using two imputation approaches. Hydroclimatic trends and variability from 1950 to 2005 are then investigated to understand past climatic fluctuations at the sub-continental scale. Further investigations are undertaken in **Chapter 3**, to provide a better understanding of internal variability in streamflow, and highlight the major modes of variability using spectral analysis. Interactions between these modes of streamflow variability, catchment properties and large-scale climate patterns are also examined, and a first assessment of multi-timescale predictability skills for streamflow over the region is provided. Building upon the previous findings, **Chapter 4**, presents an eclectic approach, combining hydrological models and a teleconnections-based linear regression model to provide reliable hydro-climatic predictions, and to assess the impact of near-term climate change (*i.e.* by the mid-21st century) impacts on hydrological regimes in West and Central Africa. The significance of these findings, their limitations and potential areas of further developments are discussed in **Chapter 5**.

CHAPTER 2: Trend and variability in a new, reconstructed streamflow dataset for West and Central Africa, and climatic interactions, 1950 – 2005

“It is a capital mistake to theorise before one has data.”
Sherlock Holmes

Some materials have been removed from this thesis due to Third Party Copyright and confidentiality considerations. Pages where material has been removed are clearly marked in the electronic version. The unabridged version of the thesis can be viewed at the Lanchester Library, Coventry University.

This chapter appears as the following published paper in Journal of Hydrology

Sidibe, M., Dieppois, B., Mahé, G., Paturel, J. E., Amoussou, E., Anifowose, B., Lawler, D., 2018. Trend and variability in a new, reconstructed streamflow dataset for West and Central Africa, and climatic interactions, 1950–2005. *Journal of Hydrology*, 561, 478-493.

2. Trend and variability in a new, reconstructed streamflow dataset for West and Central Africa, and climatic interactions, 1950 – 2005

Abstract – Over recent decades, regions of West and Central Africa have experienced different and significant changes in climatic patterns, which have significantly impacted hydrological regimes. Such impacts, however, are not fully understood at the regional scale, largely because of scarce hydroclimatic data. Therefore, the aim of this study is to (a) assemble a new, robust, reconstructed streamflow dataset of 152 gauging stations; (b) quantify changes in streamflow over 1950 – 2005 period, using these newly reconstructed datasets; (c) significantly reveal trends and variability in streamflow over West and Central Africa based on new reconstructions; and (d) assess the robustness of this dataset by comparing the results with those identified in key climatic drivers (*e.g.* precipitation and temperature) over the region. Gap filling methods applied to monthly time series (1950-2005) yielded robust results (median Kling-Gupta Efficiency >0.75). The study underlines a good agreement between precipitation and streamflow trends and reveals contrasts between western Africa (negative trends) and Central Africa (positive trends) in the 1950s and 1960s. Homogenous dry conditions of the 1970s and 1980s, characterized by reduced significant negative trends resulting from quasi-decadal modulations of the trend, are replaced by wetter conditions in the recent period (1993-2005). The effect of this rainfall recovery (which extends to West and Central Africa) on increased river flows are further amplified by land use change in some Sahelian basins. This is partially offset, however, by higher potential evapotranspiration rates over parts of Niger and Nigeria. Crucially, the new reconstructed streamflow datasets presented here will be available for both the scientific community and water resource managers.

Keywords: *West and Central Africa, streamflow trend and variability, hydroclimate variability, multi-temporal trend identification, gap filling methods.*

2.1. INTRODUCTION

Rainfall in Africa during the 20th century was characterized by decreasing annual trends over the continent except regions in Cameroon, Sierra Leone and southern equatorial Africa (Hulme *et al.*, 2001). Since 1950, most of the extreme climatic conditions occurred in the Sahel region, which has experienced several drought events from the end of the 1960s to the 1990s (Dai *et al.*, 2004; Lebel, 2003; Nicholson, 2013). For the 1968–1997 period, rainfall in August in the West African Sahel showed a decrease of up to 37% compared to the 1931–1960 period (Nicholson *et al.*, 2000). Rainfall patterns in the post-1990 period are, however, less well documented, given data scarcity: this has led to controversial findings regarding the end of Sahel drought. For example, Ozer *et al.* (2003) claimed that the Sahel drought ended in the 1990s, whereas L'Hôte *et al.* (2002) suggested that the drought continued beyond the 1990s. These contradictions partly reflect the significant changes in the spatial distribution of precipitation, which make findings highly dependent on the specific region, and the years and even months considered. This underlines the need for studies covering larger spatial scales. However, there is agreement on an increase in annual rainfall over the West African Sahel since the 1990s (*e.g.* Ali and Lebel, 2009; Jury, 2013; Lebel and Ali, 2009; Mahé and Paturel, 2009). See also Maidment *et al.* (2015), who described rainfall trends over Africa during the period 1983–2010, using different observational datasets and simulations from the current state-of-the-art global climate models.

Interestingly, while rainfall variability has been investigated at the continental scale in Africa, its effects on runoff regimes have mostly been investigated at catchment scales, using different statistical approaches and hydrological models (*e.g.* Ibrahim *et al.*, 2015). This is mainly due to restricted data, and several factors (*e.g.* Gyau-Boakye and Schultz, 1994) resulted in missing values in streamflow records. Such data restrictions have limited attempts to systematically assess streamflow trend, variability and changes at the regional scales. Descroix *et al.* (2009)

reported a negative trend (more than 15% decrease) in streamflow for the 1960-2010 period in Sudanian regions (receiving approximately 700 - 1300 mm yr⁻¹ annual rainfall) as a response to changes in rainfall regimes. Also, Mahé *et al.* (2013) found that a decrease in annual rainfall of around 20% since 1970 has resulted in a streamflow decrease of up to 60% for some rivers in West Africa (*e.g.* Niger and Senegal rivers). Amogu *et al.* (2010), in their attempt to regionalize runoff evolution over western Africa (1950-2010), found a clear difference between the Sahelian zone (where, curiously, runoff increases despite reduction in rainfall) and Sudanian and Guinean areas (where runoff decreases logically with rainfall). While major rivers of West Africa show a distinct runoff decrease since 1970, river flows in Central Africa do not show any long-term trend (Mahé *et al.*, 2013). However, these results are restricted to a few long and gap-free time series, making it difficult to describe regional streamflow variability.

Changes in the observational networks (*e.g.* station locations, gauge maintenance and data collection methods) have limited attempts to study streamflow trends and variability at regional scales. Different gap filling methods have been used (*e.g.* regression analysis, time series analysis, artificial neural network and interpolation). Multiple imputations approaches, such as proposed by Rubin (1987), were recently implemented to construct a complete rainfall-runoff database in Iran (Kalteh and Hjorth, 2009). More complex methods such as artificial neural networks (Kim and Pachepsky, 2010) and random forest-based approaches (Stekhoven and Bühlmann, 2012) have also been implemented for gap filling problems with satisfactory results. Despite many hydrological data gap filling studies, few African examples exist. Most African studies focus on gap-free stations (*e.g.* Nka *et al.*, 2015) or reconstructions using linear interpolation techniques. A decision support system based on length of data-gaps, seasons, climatic zones, model performances and data availability has been provided by Gyau-Boakye and Schultz (1994), but such a system would be difficult to implement at the regional scale due

to substantial input data requirement and it may result in: i) spatially non-homogenous reconstructions, and ii) non-statistically independent reconstructions from climate variables. The development of regional climate models (RCM) also open new prospects for hydrological data reconstruction. For instance, Moalafhi *et al.* (2017), testing such approaches over the Limpopo basin, in southern Africa, found that dynamical downscaling of reanalysis products can be very useful for semi-arid, data-scarce environments. However, important biases in RCM physics combined with uncertainties in hydrological modelling could substantially impact the quality of streamflow estimates. The present study aims at (1) providing a new, robust reconstructed streamflow dataset, using only streamflow records as predictands, over West and Central Africa, and (2) using the new dataset, together with gridded climatic data, to examine and assess flow changes and variability over the region between 1950 and 2005. This paper is organized as follows. After introducing the study area and the different datasets in section 2.2, we present the methods in section 2.3. In section 2.4.1, two gap filling methods are used to generate a robust and complete streamflow dataset for West and Central Africa. Then, we examine changes (abrupt and gradual) and variability in streamflow, and we compare these results to those observed in climatic variables from section 2.4.2 to section 2.4.4. Results are interpreted, and their wider implications discussed in Section 2.5.

2.2. STUDY AREA AND DATASETS

2.2.1. Research Area

The study area covers West and Central Africa, from -10°N to 25°N and -20°E to 30°E . The selection of the research area was motivated by the key importance of climate change and variability in this region, which also has a dense streamflow gauging network (Figure 2.1). Some records were short or incomplete, mainly due to equipment failure, instrumentation maintenance issues and sometimes political instability. Most hydrological studies in the region primarily refer to four eco-climatic zones, which are based on both annual rainfall amounts and

agricultural properties (FAO, 2004; Roudier *et al.*, 2014): (a) the Sahelian zone (mean annual precipitation ranges between 250 and 500 mm yr⁻¹), (b) the Sudano-sahelian zone (mean annual precipitation ranges between 500 to 900 mm yr⁻¹), (c) the Sudanian zone (mean annual precipitation ranges from 900 to 1100 mm yr⁻¹) and (d) the Guinean zone (mean annual precipitation exceeds 1100 mm yr⁻¹). However, more complex classifications based on seasonal to interannual variability of rainfall can be found (Badr *et al.*, 2016; Hermann and Mohr, 2011; Janicot, 1992; L'Hôte *et al.*, 1996; Mahé *et al.*, 2001).

West African rainfall is primarily related to the displacement of the Intertropical Convergence Zone (ITCZ), which results in two major seasonal cycles. Regions with less than ~1100 mm yr⁻¹ annual rainfall are characterized by a single rainy season with a maximum in August, while, further south, the rainfall seasonal cycle is characterized by two rainy seasons (September-November and March-July) (*e.g.* L'Hôte *et al.*, 1996; Roudier *et al.*, 2014). The boundary between these two zones is however not very clear, with areas experiencing both cycles from year to year because of high rainfall variability (*e.g.* Le Barbé *et al.*, 2002).

These different rainfall patterns result in different streamflow regimes. If the characteristics of the flow hydrographs coincide with the rainfall seasonal cycle, aspects such as the timing of the peak and the shape of hydrographs are mainly related to the size and physical properties of drainage basins (Roudier *et al.*, 2014). For example, headwater catchments in the Niger river basin (*e.g.* Mopti, Koulikoro), are characterized by hydrographs with shorter lag times compared to their downstream counterparts (*e.g.* Niamey, Malanville).

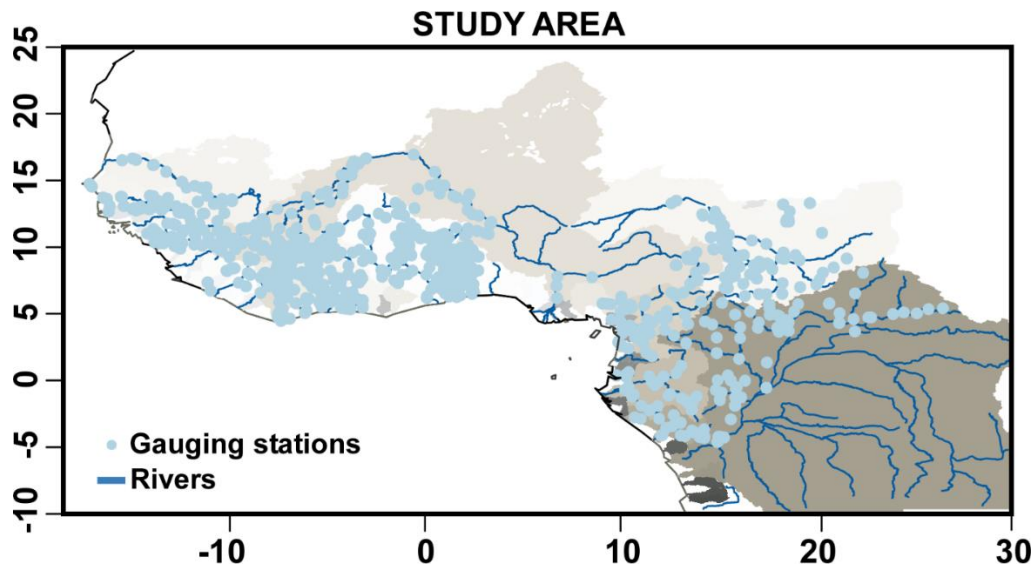


Figure 2.1: Study area with locations of the main catchments (grey shaded), the river network (blue) and streamflow gauges collected from the SIEREM database (light blue dots).

Furthermore, water related issues have led to the construction of several hydraulic structures, which can have significant impacts on hydrological regimes in some basins. According to the Global Reservoir and Dam database (GRanD; Lehner *et al.*, 2011), large dams (capacity $>10^6$.m³), as defined by the International Commission on Large Dams (ICOLD; <http://www.icold-cigb.net/GB/Dictionary/dictionary.asp>), are primarily located in the Volta basin (53.5%) and in the Niger River basin (35.2%; Figure 2.2). The other large dams are distributed within the Lake Chad basin (9.4%), the Senegal River basin (1.2%) and the Congo basin ($<1\%$; Figure 2.2). This corroborates the study by Adeaga *et al.* (2012) who found that the Volta River and the lower Niger River are the most impacted rivers in western Africa. A summary of the key characteristics of the existing major water resource schemes (hydropower, irrigation) in the Volta basin is provided by McCartney *et al.* (2012).

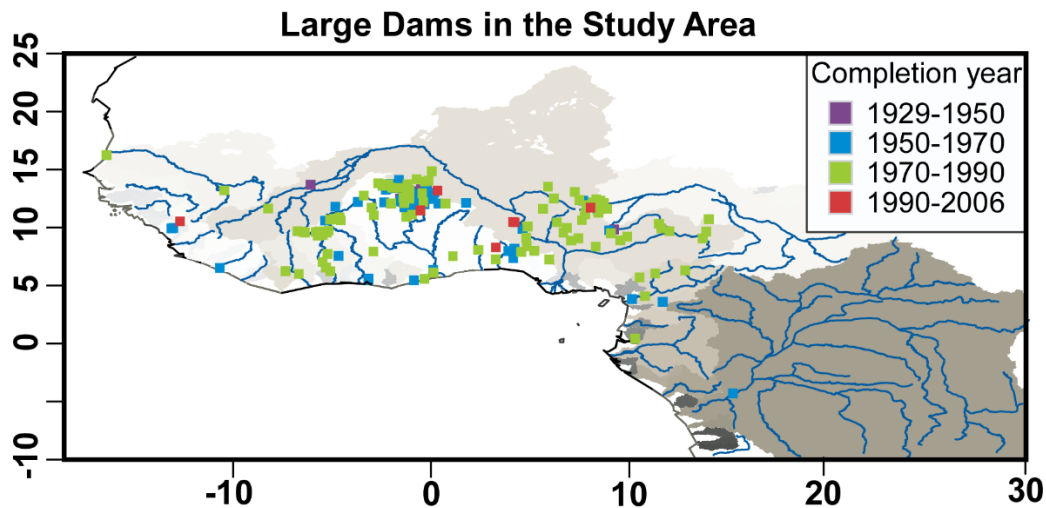


Figure 2.2: Large dams (Capacity > 10⁶ .m³) in the study area and their start of operation (purple: 1920-1950; blue: 1950-1970; green:1970-1990; red: 1990-2006). Data source: Global Reservoir and Dam database (GRanD; Lehner *et al.*, 2011).

2.2.2. Data

2.2.2.1. Streamflow data

Mean daily streamflow data were collected from the SIEREM (“Système d’Informations Environnementales sur les Ressources en Eaux et leur Modélisation”) database, which initially consisted of data collected by the “Institut de Recherche pour le Développement” (IRD). Further developments include data quality assessment and a coupling to gridded environmental data over West and Central Africa (Boyer *et al.*, 2006). Station metadata and GIS format files (basin contours, hydrological network, soil water holding capacity, vegetation, and geology) can freely be retrieved from <http://www.hydrosciences.org/sierem>. Additional streamflow data for the Niger River (Idah, Lokoja, Makurdi and Onitsha) were collected from the National Inland Waterways Authority of Nigeria.

Over the study area, 863 daily streamflow datasets were collected, and monthly time series were generated but only for the complete months. The percentage of missing data was then calculated for the entire region (Figure 2.3A), and only stations with less than 50% missing records were selected for analysis. This approach covered most of the study area, and rigorously minimized reconstruction errors. (see Appendix A for the list of reconstructed stations). Figure 2.3B shows that most gaps are in the 1950s and 2000s for the 152 selected

stations. This is due, in some countries, to the absence of gauging stations (*e.g.* Burkina Faso) and lack of updated records for the recent period (*e.g.* Central African Republic).

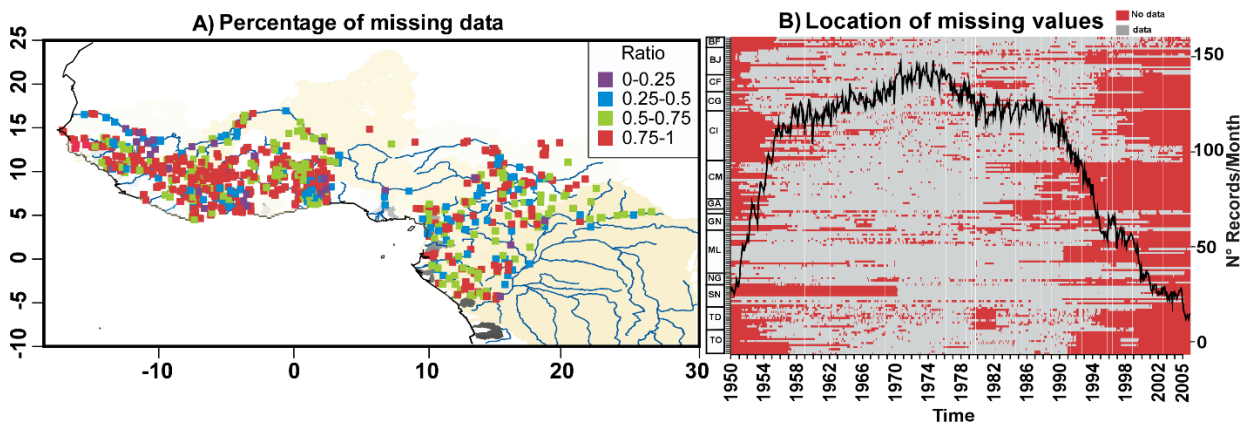


Figure 2.3: A) River network (blue lines) and spatial distribution of stream gauges over the study area, and with their percentage of missing data (purple=0-25%, blue=25-50%, green=50-75% and red= >75%). Major catchments are displayed in grey shaded. B) Time-evolution of missing values for the 152 selected stream gauges. Missing values are in red, while observations are in grey. Stations are ordered by country (BF: Burkina Faso, BJ: Benin, CF: Central African Republic, CG: Democratic Republic of Congo, CI: Cote d'Ivoire, CM: Cameroon, GA: Gabon, GH: Ghana, GN: Guinea Conakry, ML: Mali, NG: Nigeria, SN: Senegal, TD: Chad, TO: Togo). The black line represents the number of records per month over the study area for the 1950–2005 period.

2.2.2.2. Gridded climate data

To investigate climate variability and its impact on streamflow regimes over West and Central Africa, gridded monthly climatic datasets (P, T, PET) from the Climatic Research Unit (Mitchel and Jones, 2005) were used. The dataset consists of monthly climatic data for the entire world (generated with more than 4000 weather stations at the global scale) at half a degree resolution. The development of this database required seven data sources, the most important being: the Global Historical Climatology Network (GHCN; Peterson and Vose, 1997), Jones Surface Temperature Anomaly dataset (Jones, 1994; Jones and Moberg, 2003) and Hulme Historical Monthly Precipitation (Hulme *et al.*, 1998). The latest release (CRU TS v.4.00) was preferred as it was built using a new gridding technique (Angular Distance Weighting), which provides more robust results due to a better selection of observation stations for gridding (Harris and Jones, 2017). Unlike precipitation and temperature, which are observed variables, potential evapotranspiration was derived based on a variant of the Penman-Monteith formula, *i.e.* the FAO (Food and Agriculture Organisation) grass reference

evapotranspiration equation (Ekström *et al.*, 2007), which assumes a homogenous grass surface (0.12 m height) with no moisture stress, surface albedo of 0.23 and bulk surface resistance of 0.70 s/m. All climate variables are measured at 2m AGL (Above Ground Level), except for wind speed (commonly recorded at 10m AGL) which has been reduced to 2m AGL using a conversion coefficient. Absolute values of the different variables were computed using the baseline values (*i.e.* 1961–1990 long-term average) (see Harris *et al.*, 2014; Appendix 1).

Even though the high spatial resolution of the dataset makes it very convenient for investigating local processes, limited number of operational stations over West and Central Africa before 1940 could have resulted in inconsistencies in the CRU dataset (Mitchell and Jones, 2005). Therefore, analyses in this study will be performed from 1950 to 2005. In addition, Harris *et al.* (2014) compared the CRU dataset to datasets developed by the University of Delaware (UDEL) and the Global Precipitation Climatology Centre (GPCC), which both used different observation datasets, interpolation and quality control techniques than the CRU dataset and found good agreement. For instance, for the period considered in this study, mean annual precipitation values from the CRU dataset and the GPCC dataset have a correlation coefficient of 0.9885 significant at $p \leq 0.1$.

2.3. METHODOLOGY

Methods have been implemented using R, a free software environment for statistical computing and graphics (<https://www.R-project.org/>).

2.3.1. Gap filling Methods

Although parametric gap-filling methods are more commonly used (*e.g.* Gyau-Boakye and Schultz, 1994; Kalteh and Hjorth, 2009), non-parametric tests are more suitable for hydroclimate variables, as there is no assumption regarding the distribution of the data. Both parametric and non-parametric gap filling methods are therefore tested in this study to generate robust streamflow reconstructions.

2.3.1.1. Multiple Imputation by Chained Equations (MICE)

Based on a set of imputation models defined for individual variables with missing values, Multiple Imputation by Chained Equations (MICE; Van Buuren and Oudshoorn, 1999) is a practical approach for handling missing data. The method has been successfully tested for both continuous and categorical variables in hydrology (*e.g.* Kalteh and Hjorth, 2009).

In this study, for each incomplete streamflow record, the first step consists of imputing missing values by randomly sampling with replacement from the distribution of observed values. The observed values of each streamflow station are then regressed to other streamflow stations, and missing values are completed by simulated draws from the corresponding posterior predictive distribution of the considered variable (*e.g.* observed values of x_1 are regressed on all other variables $x_2 \dots x_k$, and the missing values of x_1 are sampled from its posterior predictive distribution). Several simulations are required to generate a stable single reconstructed streamflow dataset, and the process is repeated several times to generate multiple complete streamflow datasets. In most applications, linear regression models are used for imputing normally distributed continuous variables. The different steps are summarized below:

Considering an incomplete variable z (with n_{obs} observed values) to be reconstructed using other complete variables $X = (x_1 \dots x_k)$ the following linear model is used:

$$z|x; \beta \sim N(\beta x, \sigma^2) \quad (\text{eq. 1})$$

Let $\hat{\beta}$ be a row vector of length k , a realization of the estimated parameters from fitting the model with the observed z . V represents the covariance matrix of $\hat{\beta}$, and $\hat{\sigma}$ the estimated root mean-squared error. Imputation parameters σ^* and β^* are drawn from the exact joint distribution of σ, β such that:

$$\sigma^* = \hat{\sigma} \sqrt{(n_{obs} - k)/g} \quad (\text{eq. 2})$$

$$\beta^* = \hat{\beta} + \frac{\sigma^*}{\sigma} u_1 V^{1/2} \quad (\text{eq. 3})$$

with g , a random draw from a χ^2 distribution on $n_{obs} - k$ degrees of freedom, u_1 a row vector of k independent random draws from a standard Normal distribution and $V^{1/2}$ the Cholesky decomposition of V .

For each missing observation z_i estimates are calculated:

$$z_i^* = \beta^* x_i + u_{2i} \sigma^* \quad (\text{eq. 4})$$

where u_{2i} is a random draw from a standard normal distribution.

As the normal assumption is not often valid for streamflow data (*e.g.* Kundzewicz and Radziejewski, 2006), missing values were estimated using the Predictive Mean Matching (PMM) approach, which samples estimates from the observed values of the variable z . Instead of estimating missing values of z as in eq. 4, PMM identifies α elements with the smallest error $|\hat{\beta} x_h - \beta^* x_i|$ ($h=1, \dots, n_{obs}$). One of these elements is randomly selected and the imputed value of z_i is z_i' . The method was implemented using 50 iterations and 100 multiple imputations, which produce a standard deviation only 0.25% wider than a case of infinite multiple imputations according to Rubin (1987). The median was taken as the better estimate to combine the multiple reconstructed datasets.

2.3.1.2. Random forest-based reconstruction

The method is based on the random forest (RF) technique (Breiman, 2001), and involves iteratively training a RF on observed values for predicting the missing values. This method was chosen for its ability to perform under high dimensions, complex interactions and non-linearity (Stekhoven and Bühlmann, 2012). Furthermore, compared to other gap filling methods (*e.g.* KNNimpute: Troyanskaya *et al.*, 2001; MICE: Van Buuren and Oudshoorn, 1999), it does not require tuning parameters and prior knowledge of the data, making it computationally

attractive. The main limitation, however, is the lack of understanding around the construction of the different trees. The different steps are presented below:

Assuming $X = (X_1, X_2, \dots, X_p)$ a $n \times p$ -dimensional dataset (in our case n observations and p streamflow gauges), the missing values are estimated based on a RF trained on the observed parts of the dataset. For a given gauging station X_s with missing values at the indices $i_{mis}^{(s)}$, the dataset is separated in four parts:

- The observed streamflow values at the station X_s , denoted by $Y^{(s)}_{obs}$;
- The missing values at the station X_s , denoted by $Y^{(s)}_{mis}$;
- The other gauging stations with streamflow records at the indices $i^{(s)}_{obs} = \{1, \dots, n\} \setminus i^{(s)}_{mis}$ denoted $X^{(s)}_{obs}$
- The other gauging stations with streamflow records at $i^{(s)}_{mis}$ denoted by $X^{(s)}_{mis}$.

The initial step consists of an initial guess of missing values using mean values. The data frame is then sorted and gauging stations are placed in increasing order, based on the proportion of missing data. For each gauging station X_s , the missing data is imputed by first fitting a RF taking $Y^{(s)}_{obs}$ as response variable and $X^{(s)}_{obs}$ as predictors; then estimating missing values $Y^{(s)}_{mis}$ by applying the trained RF to $X^{(s)}_{mis}$. The procedure is repeated until the difference between the newly filled data matrix and the previous one increases for the first time. The stopping criteria is defined as follows:

$$\Delta = \frac{\sum_{j \in N} (X_{new}^{imp} - X_{old}^{imp})^2}{\sum_{j \in N} (X_{new}^{imp})^2} \quad (\text{eq. 5})$$

The simulations were performed using 1000 trees with the maximum number of iterations set to 100.

2.3.1.3. Validation of gap filling methods

The validation method used to assess the performance of the implemented reconstruction techniques involves generating artificial gaps in the time series, performing the reconstructions on the new dataset and estimating agreements between predictions and observations. Over the study area, the assumption of data missing completely at random was considered. First, observed values (12, 24, 36, 48, 60 and 120 months) over the entire period, 1950–2005, were randomly removed in each of the stations and later compared to the predictions. Secondly, we randomly removed entire segments of observed data to assess the ability of the gap filling methods to reconstruct contiguous missing data. The modified Kling-Gupta Efficiency (KGE) was used as an indicator of agreement between observations and predictions. This efficiency criterion ensures that the temporal dynamics (measured by the correlation coefficient) as well as the distribution of flows (measured by both the bias and variability ratio) are well represented (Kling *et al.*, 2012).

2.3.2. Step change detection and trend analysis

Changes (natural or artificial) in hydro-climatic time series can occur abruptly (step change) or gradually (trend) or in more complex forms (Machiwal and Jha, 2006). Step-like changes, induced by reservoir construction and changes of gauging structures, for example, might also result from gradual changes since nonlinear system dynamics may show cumulative effects and thresholds (Kundzewicz and Radziejewski, 2006). In this study, step-like changes in the mean are investigated in reconstructed mean annual streamflow time series using a multiple change-points detection analysis (Killick and Eckley, 2014). This technique, which is similar to the method proposed by Hubert *et al.* (1989), is based on the segment neighborhood algorithm (Auger and Lawrence, 1989). The non-parametric cumulative sum test statistic (Page, 1954) is used to assess the optimal position of change-points.

Linear trends are then investigated for periods defined based on the results of the multiple change-points analysis at the regional scale. The significance of the Mann-Kendall (MK) test

(Kendall, 1975; Mann, 1945) is highly sensitive to positive serial correlation (Von Storch, 1995), so its variant (Yue *et al.*, 2002) was preferred for linear trend detection here. The Yue *et al.* (2002) method assumes trends are linear; datasets are first detrended before extracting the lag-1 serial correlation from the detrended series (i.e. a trend-free pre-whitening procedure (TFPW) which should generate independent residuals series). The detected trend and the residuals are combined, before the MK test for significance is applied. The Theil Sen Approach (TSA) is used to estimate the slope of the trend in a dataset. This approach is less sensitive to outliers and therefore provides a better estimate of slope for skewed data, compared to regression methods.

In addition, as trend values are highly dependent on start and end dates, a multitemporal trend analysis approach has been implemented here (Liebmann *et al.*, 2010; McCabe and Wolock, 2002). Trends here are calculated for all possible segments (minimal length of 5 years) from 1950 to 2005 to explore and define the time series internal variability. For each time series, the multitemporal trend analysis generates a diagram in which each possible pair of start and end dates is associated with a trend value. To investigate the spatial extent and zonal coherence of the different variability patterns in precipitation and streamflow, the multi-temporal trend analysis results were grouped using hierarchical clustering, using the Euclidean distance as the metric of dissimilarity. Different approaches exist to determine the optimal number of clusters (Charrad *et al.*, 2014), but we used the multiscale bootstrapping approach of Suzuki and Shimodaira (2006), which allows uncertainty estimation for each cluster. This is achieved through thousands of bootstraps resampling and used to estimate the probability that a cluster appears in the replicates.

2.4. RESULTS AND DISCUSSIONS

2.4.1. Reconstruction outputs

Two reconstruction methods were applied to the subset of streamflow stations with less than 50% missing data (*i.e.* 152 streamflow gauges here). All 152 stations were reconstructed with satisfactory results as illustrated in Figures 2.4 and 2.5.

The validation shows that gap filling methods perform well for both cases of randomly removed observations and contiguous missing segments. Figure 2.4 shows that the median of the KGE is always greater than 0.75, which indicates that for half of the stations, the worst component (*e.g.* correlation, bias ratio or variability ratio) is higher or equal to 0.75: this suggests good reconstruction performance. Very similar results were achieved using the Nash-Sutcliffe Efficiency and the normalized Root Mean Squared Error (not shown). Also, both methods are reasonably stable when artificially increasing the number of missing observations and when artificially increasing the length of missing segments, despite an artefact suggesting better performances with increasing missing data, which is in fact caused by the sensitivity of efficiency criteria to sample size (*e.g.* Schönbrodt and Perugini, 2013). However, MICE seem to perform better than RF when increasing the number and the length of missing data (Figure 2.4).

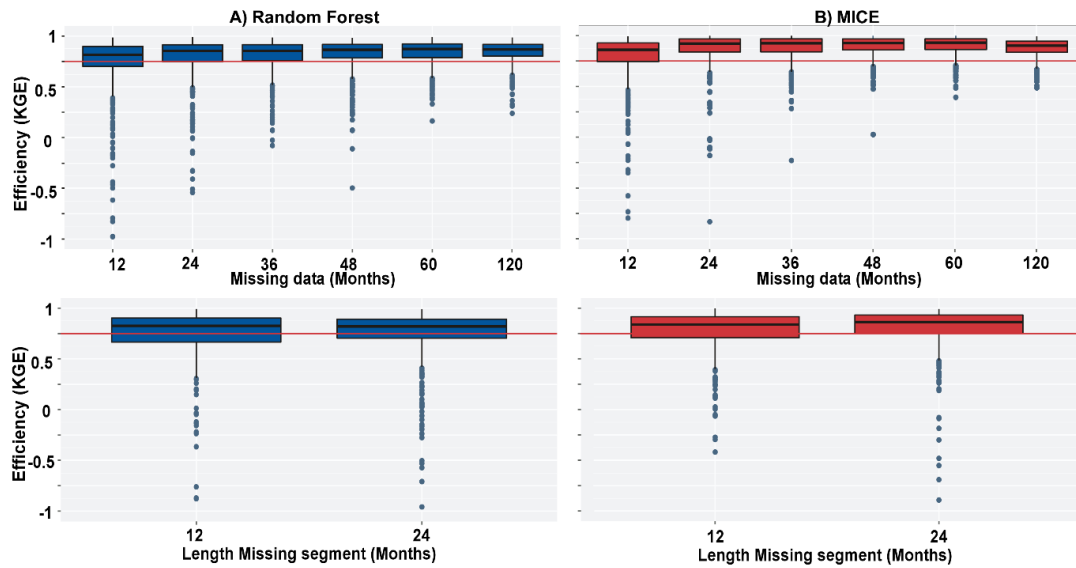


Figure 2.4: Validation of gap filling methods: boxplot of validation efficiencies for all the reconstructed stations; upper panels for randomly removed values and lower ones for cases of randomly missing data segments. A red line is drawn at $KGE=0.75$. Outliers are represented in blue dots.

To compare both gap filling methods, results from five stations from different climatic zones and hydrological regimes are presented in Figure 2.5. While both methods show similar results overall, significant dissimilarity appears in some cases, such as in the Niger River at Niamey, where MICE show an abrupt increase in minimum flow, and decrease in peak flow from 1999 (Figure 2.5). This pattern, which is similar to those induced by large dams (higher low flows and lower peak flows in downstream reaches), is not consistent with recent studies in the region (*e.g.* Amogu *et al.*, 2010; Mahé *et al.*, 2013), highlighting increased runoff coefficients at Niamey from the 1990s. MICE generate estimates of missing values by sampling from the observed values and might therefore fail at reconstructing flows beyond observed ranges. Thus, even though MICE often seem to provide better estimates than the RF based method, the latter appears to be more appropriate in the context of changing hydrological regimes, because of its ability to capture complex nonlinear relations between predictors and predictands.

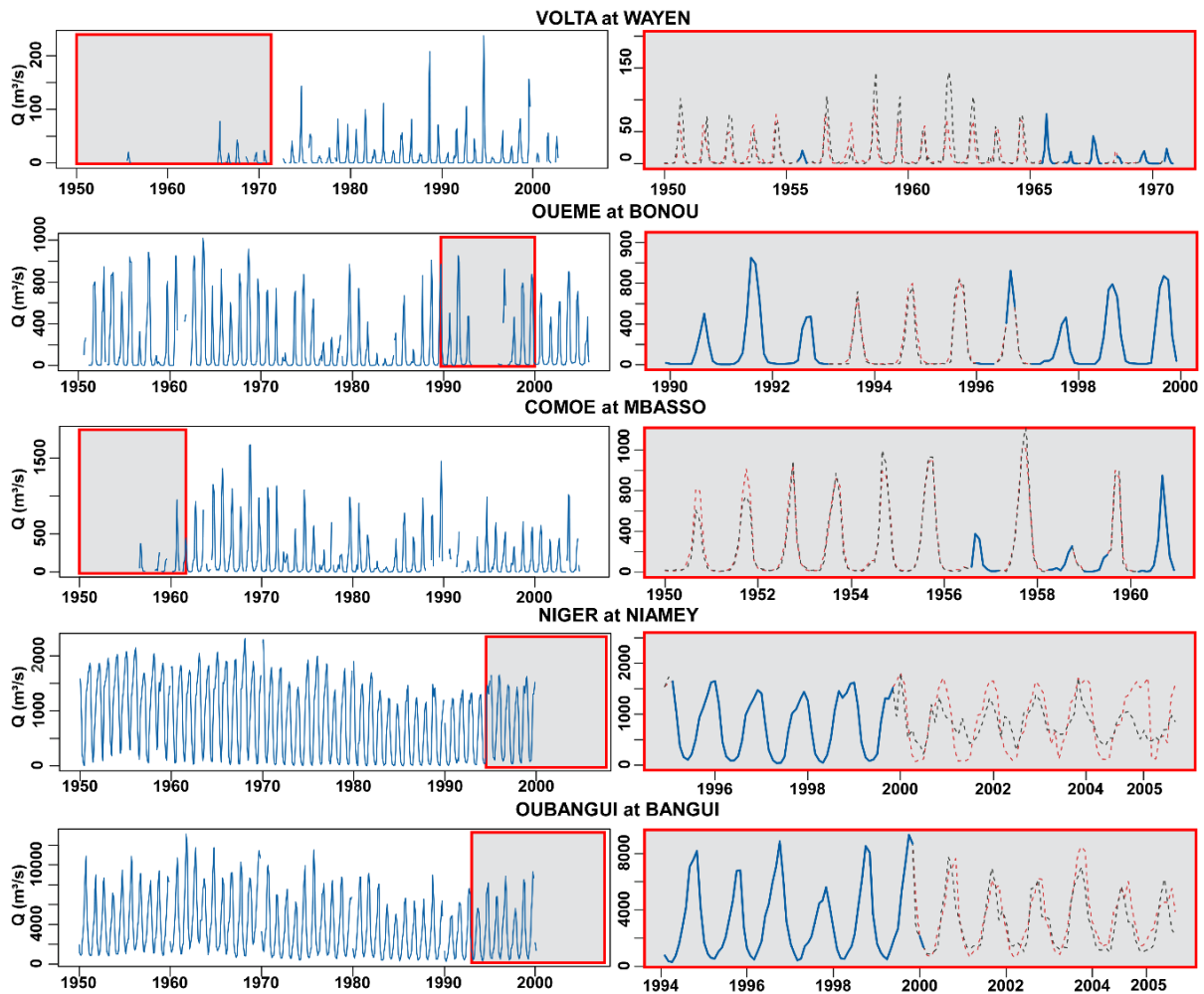


Figure 2.5: Reconstructed time series for five streamflow stations representative of different climatic conditions: Wayen (Sahelian), Bonou (Tropical humid), Mbasso (Tropical humid), Niamey (Tropical humid, Sudanian and Sahelian), Bangui (Tropical humid). Blue lines represent observations; black dotted lines represent MICE estimates and Red dotted lines represent Random Forest estimates. Red Boxes highlight time windows of interest.

2.4.2. Streamflow changes between 1950 and 2005

With the assumption that two major break points occurred in the streamflow time series, the step change analysis detected changes in 147 stations over the study area. Both reconstruction methods presented similar results and only those of random-forest based reconstructions are presented. At the regional scale, the first discontinuity in mean annual streamflow occurred in 1970 (Figure 2.6), with a marked negative shift in the mean (up to -60%). Similar results were found by Hubert *et al.* (1989), for the Niger and Senegal rivers. The second discontinuity at the regional scale occurred around 1993 and is characterized by a positive shift for more than 70%

of the stations (with an average increase of about +23%, Figure 2.6). Despite this positive shift in mean streamflow, recent conditions are still below the 1950s and 1960s wet periods.

Some sub-regional differences, however, emerge along the Gulf of Guinea and regions in Central Africa, where a discontinuity in the mean annual streamflow occurred in the 1950s and early 1960s, with an average positive shift of around 18% (Figure 2.6). These results are consistent with the findings of Mahé *et al.* (2001), underlining differences in rainfall variability between West and Central Africa from 1951 to 1989. Also, some discontinuities are revealed before the 1990s in some stations (Figure 2.6), probably induced by the wet episodes observed at the end of the 1980s. Based on the data collected from the Global Reservoir and Dam database (GRanD; Lehner *et al.*, 2011), presented in Figure 2.2, regional scale discontinuities in streamflow were more likely induced by climate variability and land use change rather than reservoirs as only 4% of the large dams in the region were completed between 1968 and 1970 and 14% between 1985 and 1993.

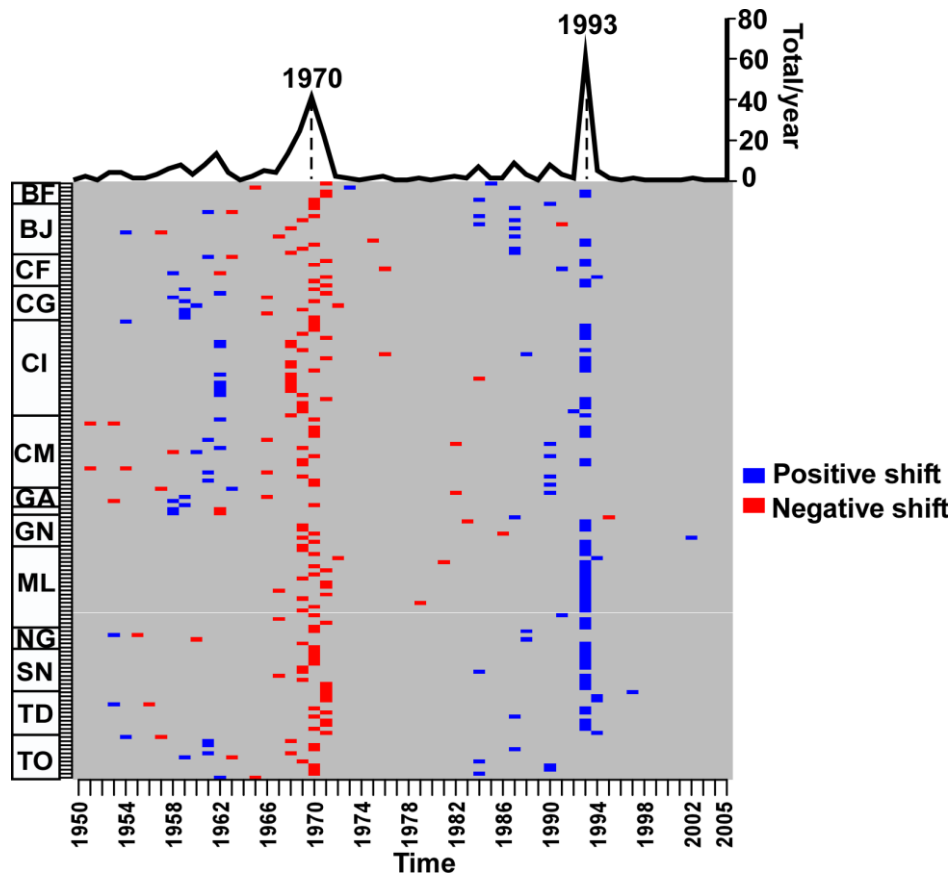


Figure 2.6: Locations of step changes in random-forest based streamflow reconstructions: positive shift in the mean (blue), negative shift in the mean (red). Stations are ordered by country (BF: Burkina Faso, BJ: Benin, CF: Central African Republic, CG: Democratic Republic of Congo, CI: Cote d'Ivoire, CM: Cameroon, GA: Gabon, GH: Ghana, GN: Guinea Conakry, ML: Mali, NG: Nigeria, SN: Senegal, TD: Chad, TO: Togo). The black curve on top presents the temporal distribution of change-points over the study area.

Gradual changes (trends) are investigated in mean annual reconstructed streamflow time series (MICE and RF) over the periods defined by the change-points analysis, which highlights two major discontinuities at the regional scale (1970 and 1993): 1950-1970 (wet conditions), 1970-1993 (drought conditions), 1993-2005 (partial recovery). Figure 2.7 presents the correlation between the results from both reconstruction methods for the different time intervals. Both reconstruction methods show similar streamflow trends at the regional scale (Figure 2.7). However, although the results from both methods remain significantly correlated ($p \leq 0.1$), trends differ slightly in the post-1990 period, mainly due to the limited ability of MICE to extrapolate beyond the range of observed values, highlighting that hydrological regimes may have changed in the 1993–2005 period.

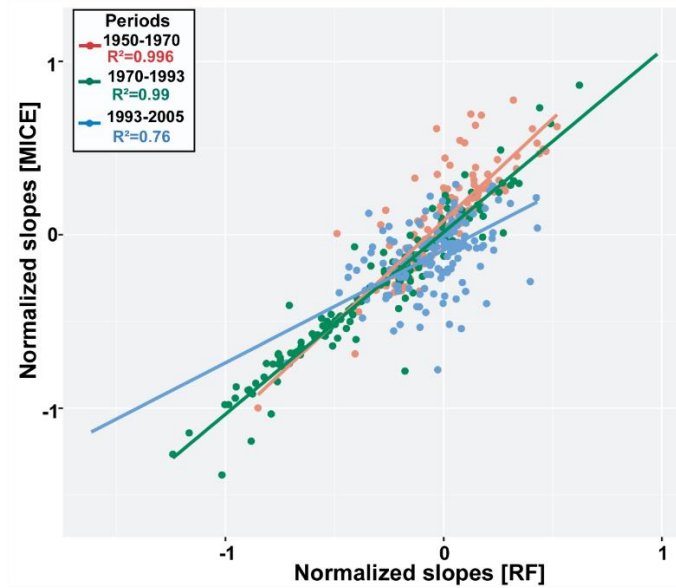


Figure 2.7: Spatial correlation between normalized trends calculated using both reconstructed datasets, for the three periods of investigation: 1950-1970 (red), 1970-1993 (green) and 1993-2005 (blue).

Trend analysis over the three different time intervals revealed that, during the 1950–1970 period, even though mean annual streamflow values are at the highest, streamflow trends are significantly negative (up to -4% per year) over the Sahelian and Sudanian regions of West Africa (Figure 2.8a-b): this suggests that the step change observed around 1970 in this region was mainly induced by a gradual aridification pattern. During the same period, significant positive trends are identified over Central Africa (up to +2.5% per year) (Figure 2.8a-b). At the regional scale, 35% and 30% of trends are significant for MICE and RF respectively. Among those significant trends, 52% and 40% are positive mainly in Sudanian and coastal regions (Figure 2.8a-b) for MICE and RF respectively. Most of the significant negative trends are in the Sahelian region, driven by dryer conditions in the end of the 1960s compared to the 1950s (Figure 2.8a-b).

These negative streamflow trends along the Sahelian band spread toward the Gulf of Guinea and over Central Africa during the well-known drought period of the 1970s and 1980s (Dai *et al.*, 2004; Lebel, 2003; Nicholson, 2013; Figure 2.8c-d), marking a stronger spatial coherence. During this dry period, mean annual streamflow values decrease by up to 69% compared to the

1950s and 1960s. Also, more than 90% of all significant trends (40% and 38% using MICE and RF, respectively) are negative (up to -5% per year), as a result of intensified dry conditions from the end of the 1960s (Figure 2.8c-d).

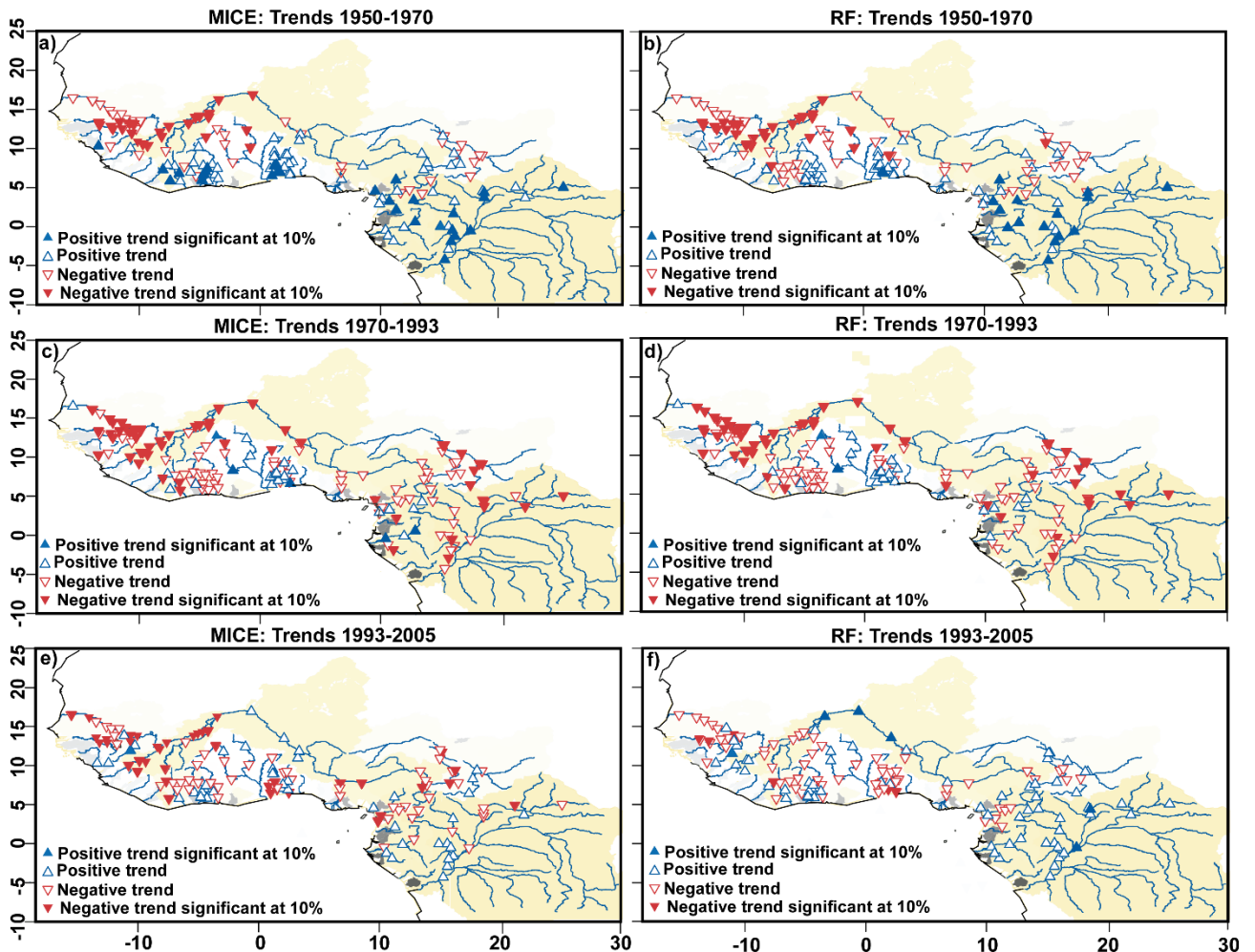


Figure 2.8: Streamflow trends estimated for both reconstructed datasets, upward triangles for positive trends and downward triangles for negative trends, filling highlights the significance of trend at 10% (negative trends in red and positive trends in blue). River basins are greyed and the river network in blue.

The last period (1993-2005) is characterized by a reduction in significant trends [MICE (26%) and RF (8%)] and contrasting patterns mainly due to the limited ability of MICE to fully capture complex streamflow interactions (Figure 2.8e-f). Compared to the previous period (1970-1993) mean annual streamflow values mark an increase of at least 15% over more than half of the study area and a decrease of around 7% in some regions (Figure 2.8c-f). Significant positive trends on the Niger River, as shown using RF, would however be consistent with the “Sahelian

paradox” (Descroix *et al.*, 2013; Mahé *et al.*, 2005), with a higher flow contribution from the Sahelian tributaries. Despite positive rainfall trends in some Sudanian areas (Northern Ghana and Ivory Coast), which are detected using both MICE and RF, streamflow trends remain negative (Figure 2.8e-f). This might have resulted from severe groundwater depletion during the dry periods 1970s and 1980s (Mahé *et al.*, 2005), but this needs further research.

2.4.3. Observed climatic trends between 1950 and 2005

2.4.3.1. Trends in annual precipitations

Annual rainfall trends for the 1950–1970 period decline by ~ 10 mm yr⁻¹ (significant for around 34% of the study area) along the entire Sahelian band, but locally increase in parts of the Central African Republic and Democratic Republic of Congo (Figure 2.9a). This suggests that the drying trends might have started earlier than hitherto recognized. The negative trends observed along the Sahelian band then spread towards the Gulf of Guinea during the 1970–1993 period (Figure 2.9b), similarly to the pattern observed in streamflow (Figure 2.8c-d).

However, although this period is widely recognized to be extremely dry from comparisons of mean values, we find here that only 11.5% of the study area show significantly negative precipitation trends. Interestingly, however, significant positive trends are identified in the Congo River basin (Figure 2.9b). This highlights a potential hiatus in the regional drying trend during the 1970s and 1980s, supporting earlier studies (Le Barbé and Lebel, 1997; D’Amato and Lebel, 1998). These could result from increasing quasi-decadal rainfall variability as suggested in Dieppois *et al.* (2013, 2015). In the post-1993 period, we note an increase of annual precipitation compared to the previous period (trends significant for 11% of the study area), corroborating previous findings (Biasutti, 2013; Lebel and Ali, 2009; Nicholson *et al.*, 2000). This potential annual rainfall recovery ($\sim +11.5$ mm yr⁻¹) is particularly pronounced in western and eastern Sahel and Liberia (Figure 2.9c), which agrees with the findings of Ogungbenro and Morakinyo (2014) in northern Nigeria. At the same time, regions in northern

Cameroon and in the Democratic Republic of Congo, are characterized by significant negative trends (~ -7 mm yr⁻¹, to ~ -30 mm yr⁻¹), in agreement with the recent study of central African rainfall by Maidment *et al.* (2015).

The same analysis, conducted using the GPCC V7 datasets, show similar patterns. The relationships are, however, slightly more significant over the study area for the three periods (35%, 11.43%, and 14.65% for the 1950-1970, 1970-1993 and post-1993 periods, respectively; not shown). In addition, during the post-1993 period, the GPCC V7 dataset underlines a significant decreasing trend in Guinea (which, interestingly, does not appear in the CRU dataset) and a wider spatial extent of negative trends in Cameroon and Central African Republic. Despite these slight differences probably resulting from the greater number of observation stations used to generate the GPCC V7 dataset, agreement between precipitation and streamflow trends remains strong.

Overall, there is a good agreement between annual streamflow and precipitation trends over the entire study area highlighting the importance of precipitation in driving hydrological systems. However, quantifying runoff response to increasing precipitation is likely to be a complex task since rising temperatures and potential evapotranspiration could offset increasing precipitation. This issue is addressed in the following section by investigating trends in temperatures and potential evapotranspiration and their impact on runoff responses.

2.4.3.2. Trends in mean annual minimum and maximum temperatures, and potential evapotranspiration

As widely accepted, temperatures over the African continent have been increasing during the 20th century (since 1950), and this is primarily associated with anthropogenic causes (*e.g.* IPCC, 2014; Stott *et al.*, 2010). However, here we aim to discuss temperature trends in term of impact on water resources, through its impact on evapotranspiration and effective rainfall.

Trends in annual minimum and maximum temperatures over the study area show different amplitude and spatial extents. For instance, in West and Central Africa, the 1950–1970 period is characterized by positive trends (+0.5 to +1.5°C) in minimum annual temperatures (significant for 32.5% of the study area). However, weaker and spatially less coherent trends are detected for annual maximum temperatures (~ +0.5°C; significant for 9.5% of the study area). Maximum values are reported only in the western Sahel (Figure 2.9d, g). The rest of the study area shows few significant trends, apart from some significant negative trends in both minimum and maximum annual temperatures (Figure 2.9d, g). According to the CRU potential evapotranspiration estimates, the patterns in both minimum and maximum temperatures could have resulted in significant positive evapotranspiration trends (~ +2.5 mm yr⁻¹) in western and central Sahel, and significant decreasing trends (~ -3.75 mm yr⁻¹) over the Gulf of Guinea and Central Africa regions (Figure 2.9j).

The 1970–1993 period is marked by a homogeneous increase in annual minimum temperatures, which is significant over 63% of the study area (including regions in the Congo River basin, where significant cooling is identified; Figure 2.9e). These trends contrast with annual maximum trends, which are negative in the Sahelian region (~ -1°C), but positive in the Gulf of Guinea coastal regions and Central Africa (Figure 2.9h). This configuration is, however, consistent with a weaker meridional thermal gradient, which characterizes a southward shift of the ITCZ and dry conditions in the Sahel (Chiang and Friedman, 2012; Webster *et al.*, 1998). The fluctuation of temperature range during this period has driven a uniform decrease in potential evapotranspiration over the Sahelian band but increased significant positive trends in the Gulf of Guinea and Central Africa (Figure 2.9k).

Since 1993, greater spatial coherence emerges, with increasing trends of both annual minimum temperatures (significant for 65% of the study area) and maximum temperatures (significant for 85% of the study area; Figure 2.9f, i). Trends in annual maximum temperatures, however,

are more pronounced ($\sim 0.1^\circ\text{C}$ higher in average) than in annual minimal temperature (Figure 2.9i). This could be an artefact of the baseline period used in our study, as this result contrasts with those revealed in some other studies (*e.g.* Funk *et al.*, 2012; Ringard *et al.*, 2016), which suggested that minimum temperatures have risen faster compared to maximum temperatures in the post-1990 period. Nonetheless, temperature trends are consistent with trends in potential evapotranspiration (Figure 2.9l), which highlight a uniformly significant (for around 46.8% of the study area) and positive trend ($\sim < +3.8 \text{ mm yr}^{-1}$) over almost the entire eastern part of the study region. Regions in western, eastern Sahel and part of the Gulf of Guinea, however, show non-significant negative trends (Figure 2.9l), which may result from the spurious trends (above) in minimum temperatures and errors resulting from the use of the same monthly wind speed values (1961-1990) for each year.

Trends in effective rainfall, approximated here as the difference between rainfall totals and potential evapotranspiration are presented in Figure 2.9m-o. Over the two first periods (1950-1970 and 1970-1993), these trends are similar to precipitation trends: this suggests the limited effect of potential evapotranspiration on the relationship between rainfall and streamflow (Figure 2.9m-n). However, from 1993, the situation is reversed, mainly in the eastern part of the Sahel (eastern Niger, Chad and northern Nigeria), where high potential evapotranspiration rates significantly subdue the potential impact of the rainfall recovery (Figure 2.9o) on streamflow. This might help explain, at least partially, why the rainfall recovery over these regions is not associated with significant positive streamflow trends (Figure 2.8c-d). Over Central Africa (areas in the Congo basin), it also appears from trends in effective rainfall that during recent decades, the decrease in rainfall is exacerbated by increased evapotranspiration (Figure 2.9c, i, o). This suggests enhanced climatic stress on Central African streamflow in relation to warming temperatures.

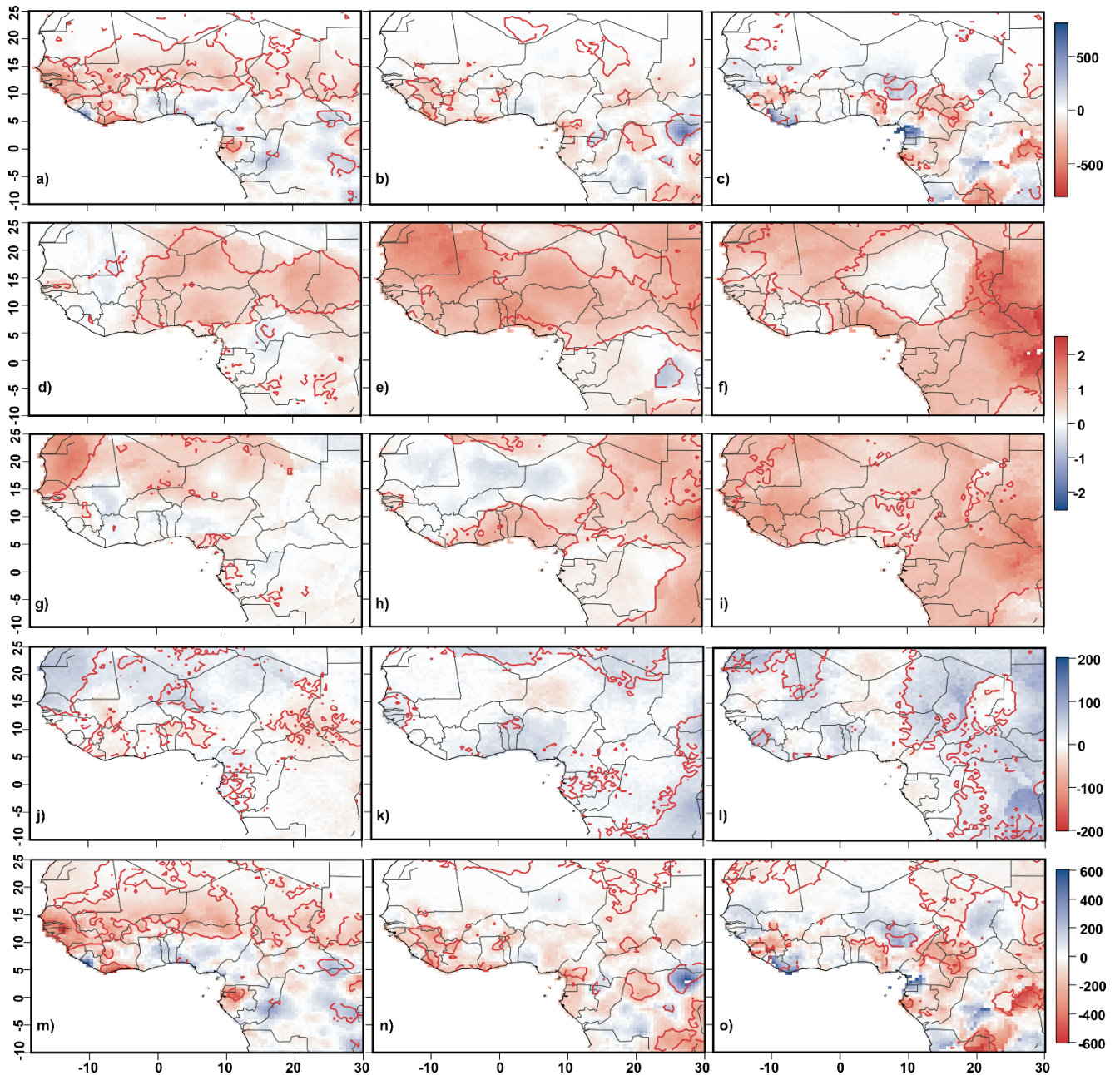


Figure 2.9: Hydroclimatic trends over the study area for three different time intervals (1950-1970, 1970-1993 and 1993-2005) according to the CRU.TS. V4.00 dataset: (a-c) Annual precipitation trends (d-f) Minimum annual temperature trends (g-i) Maximum annual temperature trends (j-l) Annual potential evapotranspiration trends (m-o) Annual effective rainfall trends. Sen's slope values are displayed through a red-white-blue colour scale. Solid red lines highlight trend significance at $p \leq 0.1$ according to a modified MK trend test accounting for serial correlation in the time series.

2.4.4. Precipitation and streamflow variability

Standard trend analysis methods assess the slope of the considered variables over the period of investigation. The value of the slope is, however, highly dependent on the selected time window and changes significantly for different start and end dates, mainly because of internal variability. Such limitations are tackled in the multitemporal trend analysis method (Liebmann

et al., 2010; McCabe and Wolock, 2002). We used the Liebmann *et al.* (2010) approach, to calculate precipitation and streamflow trends for all possible segments of 5 to 56 years between 1950 and 2005. The results are stored in two-dimensional diagrams (*e.g.* Figure 2.11), which have been analysed using multiscale bootstrapped agglomerative hierarchical clustering.

Clustering streamflow variability diagrams resulted in three main clusters, which are highly significant ($p \leq 0.1$) based on the multiscale bootstrapping test, with associated spatial distributions presented in Figure 2.10, identified using hierarchical clustering.

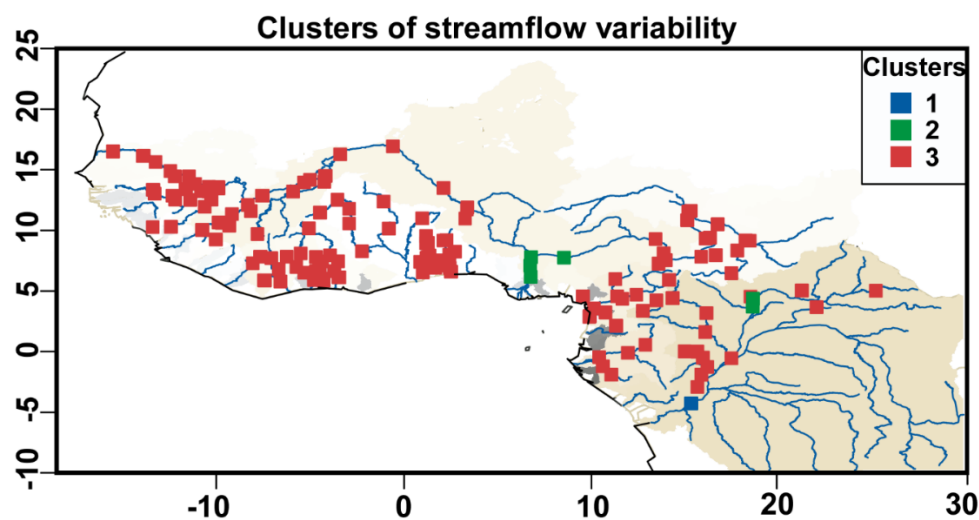


Figure 2.10: Spatial distribution of streamflow variability (1950–2005) clusters based on multi-temporal trend analysis superimposed on the river network (blue) and major river basins (grey shaded). All the clusters are highly significant at $p \leq 0.1$ according to the multiscale bootstrapping test. Different colours displayed the location of the different clusters.

Overall, these three clusters show decreasing flow trends over the entire period (1950–2005), but we also identify decadal periods of alternating positive and negative trends with different amplitudes, modulating the general trend, according to the three clusters (Figure 2.11). For instance, a pronounced positive trend in the mid-1970s during the drought period emerges in cluster 1 (Congo Basin at Brazzaville), which progressively disappears in cluster 2 (lower Niger River, Benue and stations in the upper Congo basin) and cluster 3 (all the other stations; Figure 2.11). This emphasizes the importance of decadal variability in modulating streamflow

trends (which has hitherto been little studied) and provides a new picture of the behaviour of hydrological systems in West and Central Africa.

These differences in the contribution of interannual to decadal variability could, however, arise from differences in the large-scale climate drivers. According to Mahé *et al.* (2013), Cluster 1, which is located at the outlet of the Congo Basin at Brazzaville, could be more sensitive to changes in the thermal gradient between the Atlantic and Indian oceans resulting in a unique runoff variability. Such decadal fluctuations have also been reported for eastern Sahel rainfall in Dieppois *et al.* (2013, 2015), suggesting that differences between clusters should at least partly be related to different interactions with catchment properties (*e.g.* reduction in soil water holding capacity) and water management. In addition, while trend amplitude is a distinctive element between clusters, the sign and temporal scale during the humid period (1950-1960) and the recovery period (post-1990) are also very important. For instance, stations in clusters 1 and 2 are characterized by wet conditions in the 1950s-1960s, whereas most of the stations in cluster 3 show decreasing trends during the same period (Figure 2.11). Furthermore, cluster 3 highlights less intense dry conditions in the 1980s and a more pronounced recovery in the recent years compared to the first two clusters (Figure 2.11). A further classification of the stations in cluster 3 is provided as supplementary materials (see Figure S2.1-S2.2). The significant negative trend (observed in the 1980s) in stations of cluster 2, for instance might have been partly accentuated by large dams in Nigeria (*e.g.* the Dadin Kowa Dam and the Kiri dam, on a main tributary of the Benue river).

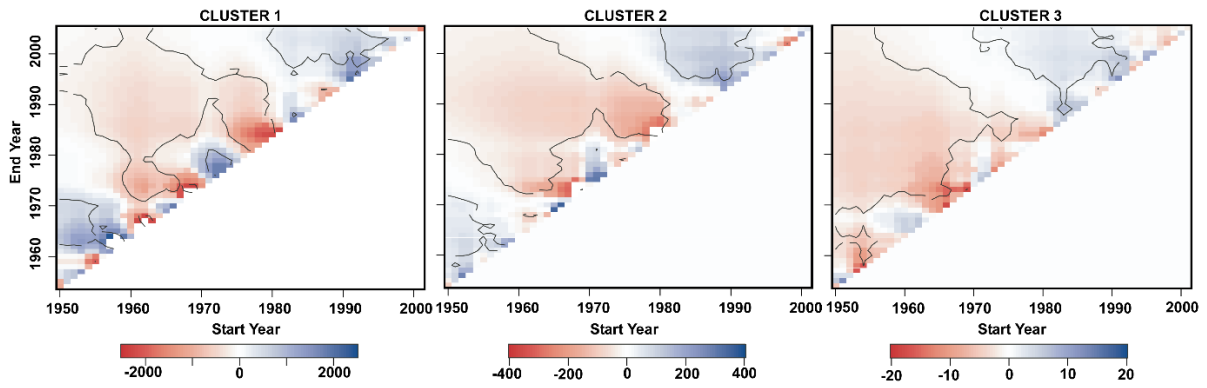


Figure 2.11: Multi-temporal diagrams of the different cluster centroids: trends in m^3/s are presented in red (negative) – white (null) – blue (positive) colour scale, contours lines represent trend significance at $p \leq 0.1$.

Applying the same clustering method to gridded annual rainfall, variability diagrams resulted in 12 major clusters ($p \leq 0.1$) and few grid points with lower probabilities ($p \leq 0.2$) and therefore unclassified (Figure 2.12).

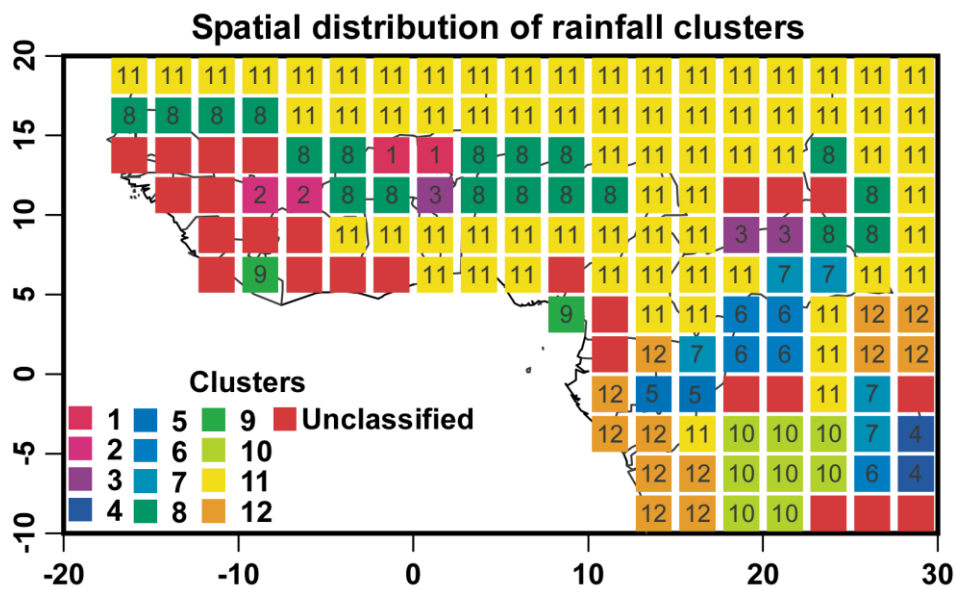


Figure 2.12: Clusters of rainfall variability generated using CRU TS V4.00 ($2.5^\circ \times 2.5^\circ$) on the period 1950-2005: colours and numbers from 1 to 12 refer to the grid points within the 12 initial clusters at $p \leq 0.1$. Red boxes represent grid points which did not fall within the clusters. All the clusters are highly significant at $p \leq 0.1$ according to the multiscale bootstrapping test.

West African regions predominantly fall within clusters 11, 8, 2 and 1 (Figures 2.12, 2.13) which are mainly characterized by persistent dry conditions from the end of the 1960s, and positive trends starting earlier in clusters 2 and 8 (1970s) compared to clusters 1 and 11 (end of 1980s). Comparing, for instance, patterns observed in streamflow cluster 3 and rainfall

cluster 11, it appears that the significant negative rainfall trend in the 1980s is attenuated in the streamflow signal and, furthermore, the observed streamflow recovery is more widespread compared to the recovery observed in rainfall. This suggests a combination of drivers which might have enhanced the runoff response, described by some authors as the “Sahelian paradox” (Descroix *et al.*, 2013; Mahé *et al.*, 2005) which refers to a counterintuitive increase in runoff coefficient despite decreasing rainfall. In fact, parts of this region are known to have experienced drastic changes in land cover resulting from several coupled interactions between increasing cultivated areas (Cappelaere *et al.*, 2009), and natural vegetation changes after the 1970s and 1980s major drought periods (Gal *et al.*, 2017).

The clustering underlines a high variability in rainfall over the western part of West Africa, where some grid points are left outside the clusters. Some parts of this region are characterized by the pattern observed in cluster 9 (Figures 2.12-2.13). After the humid period of the 1960s, rainfall is characterized by decreasing trends until the 1990s (Figure 2.13). From the end of the 1990s rainfalls largely returned to their level of the 1960s as a result of a recovery which started in the 1980s (Figure 2.13). From these different clusters, it appears that most regions over western Africa have experienced improved streamflow conditions because of the recent rainfall recovery even though long-term trends remain negative.

Over Central Africa, rainfall shows high decadal variability (succession of wet and dry periods) with no clear long-term trends (clusters 4, 5, 6, 10 and 12; Figure 2.13). This region is characterized by a humid period from the mid-1950s to the 1970s, with dry episodes around 1980 (Figure 2.13). In cluster 4, for instance, recent conditions (1990s-2000s) are almost as wet as the humid period, which is not the case for cluster 6 where recent conditions remain relatively drier (Figure 2.13). The streamflow variability displayed in cluster 1 (Congo basin at Brazzaville) appears to have resulted from a combination of rainfall clusters 6, 10 and 12, highlighting the diverse climatic influences in this basin (Figure 2.11-2.13). Rainfall-runoff

relations over this region suggest that rainfall is the main driving factor, with no, or limited, effect from other moderating factors (*e.g.* land use change, intensification of agriculture, deforestation, and warming temperatures). The change in seasonal rainfall distribution may likely be the major factor related to climatic change in this area to have an impact on discharges' seasonal regimes. This can be observed at the scale of small basins like the Kienke at Kribi in the South coastal Cameroon, where the small dry season disappeared during the last decades (Lienou *et al.*, 2008), and at the larger scale for the Ogooue river in Gabon, where the Spring flood lost 30% of discharge value after the rainfall regimes slightly changed over past decades (Mahé *et al.*, 2013), the same being observed to a lesser extent for the whole Congo basin (Alsdorf *et al.*, 2016; Tshimanga *et al.*, 2016).

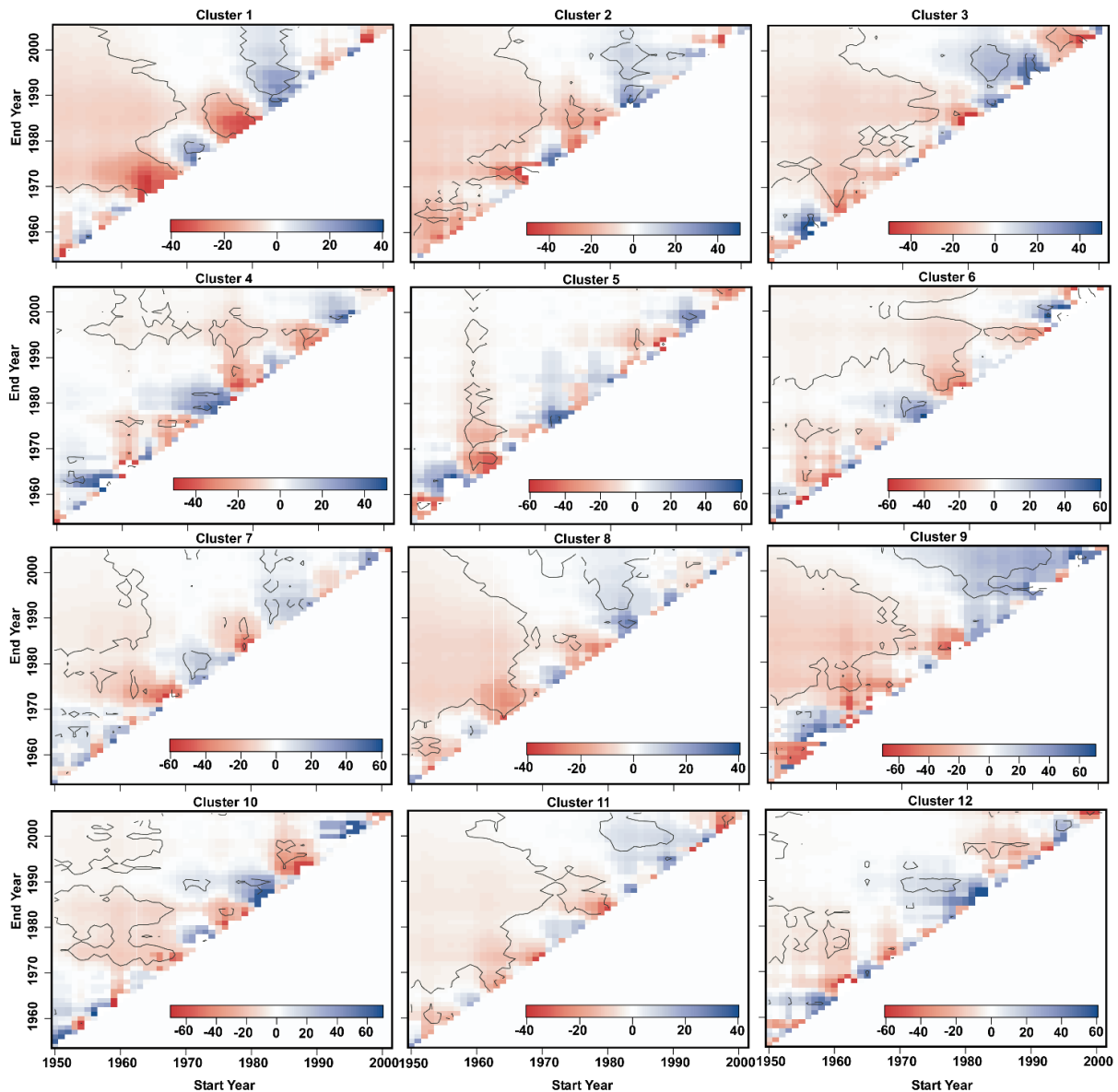


Figure 2.13: Multi-temporal diagrams of the 12 rainfall variability clusters derived from the multi-scale bootstrap clustering: trends (mm) are presented in red (negative) – white (null) - blue (positive) colour scale, contours lines represent trend significance at $p \leq 0.1$.

2.5. CONCLUSION

Using parametric (MICE) and non-parametric (RF) gap filling methods, a new and complete streamflow dataset, spatially distributed over West and Central Africa and encompassing different climatic zones and hydrological regimes has been generated. Gap filling results highlighted that both methods performed well, though, in general, MICE was slightly outperforming RF. However, due to its parametric nature, MICE analyses, in some cases, failed to capture changes in streamflow conditions (case of Niamey on the Niger River). The complete streamflow dataset (RF method) was then used to investigate streamflow changes and

variability and their interactions with key climatic variables (P, T, PET) over West and Central Africa between 1950 and 2005.

Majority of streamflow stations over the study area present a step change in 1970 mainly induced by a gradual aridification pattern. In the 1990s a positive shift in mean discharge is observed, but it is difficult to conclude whether this change is led by positive rainfall trends or single wet episodes amplified by land use change, warming temperature and evapotranspiration reduction. In general, there is a good agreement between streamflow and precipitation trends, with an offsetting effect of potential evapotranspiration observed in some regions. Over the study area, the period 1950–1970 was characterized by negative streamflow trends in Sahelian and Sudanian regions of West Africa, which seems counterintuitive considering that this period was the wettest on record. The opposite is observed over Central Africa where significant positive streamflow trends emerge. The following period (1970–1993), is marked mostly by negative trends due to dryer conditions. This pattern is reversed during the 13-year period 1993–2005, with mainly positive trends resulting from increased rainfall and changes in land use in Sahelian regions. Annual streamflow trends reflect annual precipitation trends which decrease from the 1950s to 1980s and increase from the 1990s. More importantly, the study showed that, even though the 1950s and 1960s were the wettest decades in terms of total rainfall amounts, decreasing annual rainfall trends were more prominent, suggesting an earlier start of the drought. The drought peaked during the 1970s/80s, over most of western Africa, but the reduced negative trends in precipitation suggest a hiatus, which have resulted from quasi-decadal variability.

Furthermore, over most of the study area, hydrological regimes during the recent period have been impacted by the rainfall recovery which is not limited to the west African Sahel. Even though other climatic variables such as wind speed and vapor pressure deficit might have played an important role, temperature trends appeared to be highly related to trends in potential

evapotranspiration, which seem to have hampered the effect of the rainfall recovery on hydrological regimes in some areas over the eastern Sahel (eastern Niger, Chad and northern Nigeria).

Building significantly on previous studies, which generally provide trend estimates over a certain period, we have provided novel information and analyses of the impact of internal variability using the multitemporal trend analysis method. The results highlight strong interannual to decadal signals which clearly modulate streamflow and precipitation trends. In West Africa, for instance, the 1970-1989 period is characterized by two main dry events (1972-1973 and 1983-1984) separated by a wet period (Nicholson *et al.*, 2000; Dai *et al.*, 2004). This probably resulted in increased runoff coefficients in Sahelian catchments, as observed by Albergel (1987) in Burkina Faso over the period (1969-1984) and later in larger Sahelian catchments (Descroix *et al.*, 2013; Mahé *et al.*, 2005). Such a rainfall-runoff response (referred to as the Sahelian paradox) indeed seems paradoxical when considering long-term trends but becomes less counterintuitive when investigating variability in precipitation and streamflow time series. Therefore, rather than describing the “Sahelian paradox” as an increase in runoff despite reduced rainfall since 1970, it should be considered as enhancing runoff response to positive rainfall anomalies, as a result of changes in land-surface properties.

If flow trends can be largely explained by decadal variability in rainfall (Dieppois *et al.*, 2013), influence of other driving factors should also be considered at the catchment level (such as geology, soils, agricultural land use change, water consumption and urbanization). For instance, large dams constructed in the 1980s in Nigeria (*e.g.* the Dadin Kowa Dam and the Kiri dam, on a main tributary of the Benue river), might have affected to some extent the variability of the lower Niger river, but this is beyond the scope of the present paper.

This study has shed light on hydroclimatic variability and its associated impact on streamflow regimes over large, key parts of West and Central Africa over recent decades, and also provides

water practitioners with reconstructed streamflow time series which can be used as input for water balance models to develop sound water and agricultural management policies. These useful time series here can form the basis of future developments, to include updating of the streamflow datasets through national water offices. This should further improve the quality of the reconstructions and open up investigations of more recent conditions. In addition, future in-depth studies are required of climate processes (*e.g.* sea surface temperature, atmospheric circulation), catchment land use properties, and water management policies, all of which can drive streamflow variability at interannual to decadal timescales. As these potentially modulate the climate signal, such work is required to further improve our understanding of hydrological variability in West and Central Africa, and our ability to model hydrological changes in this region.

Acknowledgements

We acknowledge the HydroSciences Montpellier Laboratory, particularly Nathalie Rouché for providing us with streamflow datasets used in this study. Moussa gratefully acknowledges the funding received towards his PhD studies from Coventry University, UK, and resources provided by the Centre for Agroecology, Water and Resilience (CAWR). We thank the anonymous reviewers for their insightful comments and suggestions.

2.6. Appendix A: List of reconstructed streamflow time series

ID	Basin	Station name	latitude	Longitude
BFQ0010	LERABA	YENDERE au pont	10.1667	-5.0683
BFQ0060	VOLTA	WAYEN	12.3789	-1.08
BFQ0064	VOLTA	BOROMO	11.7833	-2.9167
BFQ0065	VOLTA	DAPOLA	10.5667	-2.9167
BFQ0072	VOLTA	NWOKUY	12.5278	-3.55
BFQ0074	VOLTA	SAMANDENI	11.4667	-4.4667
BJQ0009	SOTA	COUBERI	11.74	3.3333
BJQ0022	COUFFO	LANHOUNTA - LANTA	7.1	1.8833
BJQ0028	MONO	ATHIEME	6.9167	1.6667
BJQ0033	OUEME	BONOU	6.9	2.45
BJQ0036	OUEME	HETIN SOTA	6.6	2.5
BJQ0047	OKPARA	KABOUA	8.25	2.7167
BJQ0050	SOTA	RTE KANDI-SEGBANA AMONT	10.9833	3.25
BJQ0075	WE-WE	WE-WE	9.1667	2.1083
BJQ1000	PENDJARI	PORGA	10.99401	0.9773
BJQ2000	NIGER	MALANVILLE	11.888	3.383
BJQ2004	OUEME	PONT DE BETEROU	9.199179	2.267582
BJQ2005	OUEME	PONT DE SAVE	8	2.4167
BJQ2006	ZOU	ATCHERIGBE	7.5333	2.0333
CFQ0005	OUHAM	BOSSANGOA	6.4667	17.45
CFQ0025	OUBANGUI	ZINGA TRANSIT	3.713833	18.58716
CFQ0027	MBOMOU	ZEMIO	5.028726	25.1471
CFQ0028	BANGUI-KETTE	ALINDAO	5.04457	21.20172
CFQ0034	LOBAYE	M'BATA	3.666296	21.98114
CFQ0040	M'POKO	BOSSELE-BALI	4.530737	18.46878
CFQ0057	SANGHA	SALO	3.181621	16.11362
CFQ2000	OUBANGUI	BANGUI	4.364275	18.59487
CGQ0003	ALIMA	TCHIKAPIKA	-1.26385	16.16937
CGQ0013	LEFINI	BWEMBE	-2.9167	15.6308
CGQ0014	LIKOUALA	ETOUMBI	0.0167	14.95
CGQ0015	LIKOUALA	MAKOUA	0.00167	15.633
CGQ0017	N'KENI	GAMBOMA	-1.9	15.85
CGQ0020	KOUYOU	LINNEGUE	-0.5	15.9333
CGQ0026	LIKOUALA	BOTOUALI	-0.55	17.45
CGQ2000	CONGO	BEACH - V.N. Brazzaville	-4.27285	15.29392
CGQ2001	SANGHA	OUESSO	1.6167	16.05
CIQ0007	BANDAMA	MBRIMBO	6.0125	-4.425
CIQ0013	BANDAMA	KIMOUKRO BALISE 10201	6.5056	-5.3053
CIQ0032	MARAOUE	RTE BEOUMI-SEGUELA - KONGASSO 10145	7.8319	-6.2542
CIQ0033	MARAOUE	BOUAFLE 10147	6.979988	-5.75437
CIQ0058	NZI	BOCANDA	7.0442	-4.52
CIQ0061	NZI	DIMBOKRO 10141	6.6358	-4.71

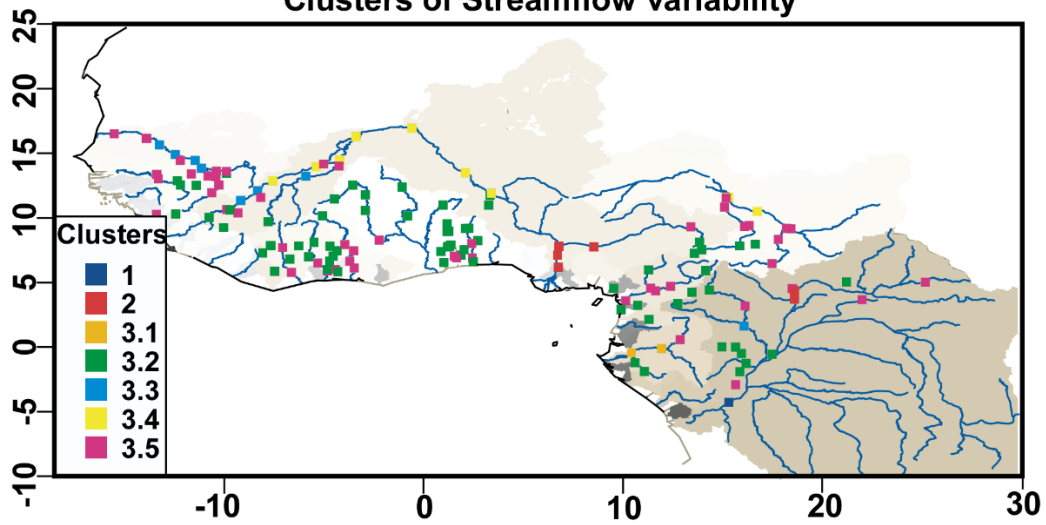
CIQ0154	KOUROUKELE	IRADOUGOU	9.7069	-7.8028
CIQ0292	KAVI	MBESSE	5.8386	-4.2961
CIQ0312	CAVALLY	FLAMPLEU	7.2833	-8.0583
CIQ0314	CAVALLY	TAI	5.86	-7.45
CIQ0319	NSE	TAI 1 (TAI PONT)	5.875	-7.4583
CIQ4020	BANDAMA	BADA	8.1069	-5.4972
CIQ4022	BANDAMA	TIASSALE 10144	5.8947	-4.8178
CIQ4025	NZI	FETEKRO	7.8106	-4.6875
CIQ4026	NZI	MBAHIAKRO 10133	7.4458	-4.3556
CIQ4027	NZI	NZIENOA 10136	5.9964	-4.8125
CIQ4028	COMOE	ANIASSUE PONT 10138	6.6375	-3.7126
CIQ4029	COMOE	MBASSO	6.125	-3.48
CIQ4030	COMOE	SEREBOU	7.9383	-3.9419
CIQ4031	SASSANDRA	SEMIEN 10130	7.7083	-7.0669
CIQ4032	SASSANDRA	SOUBRE	5.7833	-6.6131
CIQ4033	BAFING	BAFINGDALA (BADALA) BIANKOUMA 10162	7.841611	-7.66658
CIQ4034	LOBO	NIBEHIBE (NIBEIGBEU)	6.8003	-6.7
CIQ4035	COMOE	AKAKOMOEKRO 10149	7.447418	-3.5094
CMQ0008	DOUME	DOUME	4.2333	13.45
CMQ0029	SANAGA	NACHTIGAL	4.35	11.6333
CMQ0030	SANAGA	NANGA EBOKO	4.7	12.3833
CMQ0038	MBAM	BAC DE GOURA	4.5667	11.3667
CMQ0071	NYONG	DEHANE	3.5667	10.1167
CMQ5001	VINA NORD	PONT DE BEREM	7.55	13.95
CMQ5005	DJA	SOMALOMO	3.3667	12.7333
CMQ5006	BENOUE	BUFFLE NOIR	8.1167	13.8333
CMQ5007	BENOUE	GAROUA	9.294019	13.4041
CMQ5015	MAPE	AU PONT DE MAGBA AMONT	5.9833	11.2667
CMQ5016	VINA DU SUD	LAHORE	7.25	13.5667
CMQ5018	LOBE	BAC KRIBI-CAMPO	2.8667	9.8833
CMQ5019	LOKOUNDJE	LOLODORF	3.2333	10.7333
CMQ5038	MUNGO	MUNDAME	4.5667	9.5333
CMQ5040	NTEM	BAC DE NGOAZIK	2.1333	11.3
CMQ5044	LOM	BETARE OYA	5.9167	14.1333
CMQ5047	KIENKE	KRIBI SCIERIE	2.9333	9.9
CMQ5050	KADEI	BATOURI	4.4167	14.3167
GAQ0006	OGOOUE	BOOUE (LMNG)	-0.1025	11.9367
GAQ0015	OGOOUE	NDJOLE OPERATIONNEL	-0.455	10.4025
GAQ0028	IVINDO	MAKOKOU (LMNG)	0.5689	12.8611
GAQ0041	NGOUNIE	FOUGAMOU S H O (LMNG)	-1.2156	10.5908
GAQ0046	NGOUNIE	MOUILA VAL MARIE	-1.8869	11.0558
GHQ0045	NASIA	NASIA	10.15	-0.8
GHQ1005	VOLTA NOIRE	BUI AMONT	8.2833	-2.2333
GNQ0015	NIGER	FARANAH	10.03744	-10.7495

GNQ0016	NIGER	KOUROUSSA	10.65169	-9.87096
GNQ0018	NIGER	TIGUIBERY (Siguiriri)	11.3545	-9.16459
GNQ0026	MILO	KANKAN	10.3833	-9.3
GNQ0030	NIANDAN	BARO	10.6167	-9.7
GNQ0034	NIANDAN	KISSIDOUYOU (NIANDAN SCIERIE)	9.25	-10.0167
GNQ0200	BADI	BAC DE BADI	10.2833	-13.4
GNQ0204	KONKOURE	PONT DE LINSAN	10.3	-12.4167
MLQ0009	NIGER	DIRE	16.27595	-3.395
MLQ0012	NIGER	KE MACINA	13.95831	-5.35896
MLQ0019	NIGER	KOULIKORO	12.85727	-7.55811
MLQ0022	NIGER	MOPTI	14.49605	-4.20127
MLQ0036	NIGER	TOSSAYE	16.9333	-0.5833
MLQ0052	DIKA	KARA	14.1667	-5.0167
MLQ0091	BANI	SOFARA	14.01393	-4.2429
MLQ0123	SENEGAL	GALOUGO	13.8333	-11.1333
MLQ0130	SENEGAL	BAFING MAKANA	12.55	-10.2667
MLQ0131	SENEGAL	SOUKOUTALI	13.2	-10.4167
MLQ0134	BAKOYE	OUALIA	13.6	-10.3833
MLQ0135	BAKOYE	TOUKOTO	13.45	-9.8833
MLQ0137	FALEME	FADOUYOU	12.5167	-11.3833
MLQ0145	BAOULE	SIRAMAKANA (Balenda)	13.5833	-9.8833
MLQ2003	NIGER	KENIEROBA	12.1	-8.3167
MLQ2007	SANKARANI	SELINGUE	11.5833	-8.1667
MLQ2008	BANI	DOUNA	13.21385	-5.90311
MLQ2064	SENEGAL	DAKA SAIDOU	11.95	-10.6167
MLQ2066	SENEGAL	DIBIA	13.2333	-10.8
MLQ2069	FALEME	GOURBASSY	13.4	-11.6333
MLQ2070	SENEGAL	KAYES	14.45	-11.45
NEQ2000	NIGER	NIAMEY	13.5016	2.105
NGQ0001	BENUE	MAKURDI	7.75	8.5333
NGQ0002	NIGER	ONITSHA	6.166667	6.75
NGQ2000	NIGER	LOKOJA	7.8	6.7667
NGQ2004	NIGER	IDAH	7.1	6.716667
SNQ2039	GAMBIE	KEDOUYOU	12.55	-12.1833
SNQ2045	GAMBIE	MAKO	12.8667	-12.35
SNQ2055	GAMBIE	SIMENTI	13.0333	-13.3
SNQ2060	GAMBIE	WASSADOU-AMONT	13.35	-13.3667
SNQ2062	GAMBIE	WASSADOU-AVAL	13.35	-13.3833
SNQ2063	SENEGAL	BAKEL	14.9	-12.45
SNQ2064	SENEGAL	DAGANA	16.5167	-15.5
SNQ2065	FALEME	KIDIRA UHEA	14.45466	-12.205
SNQ2066	SENEGAL	MATAM	15.65	-13.25
SNQ2067	DOUE	NGOUI	16.15	-13.9167
SNQ2068	SENEGAL	SALDE	16.16325	-13.8795

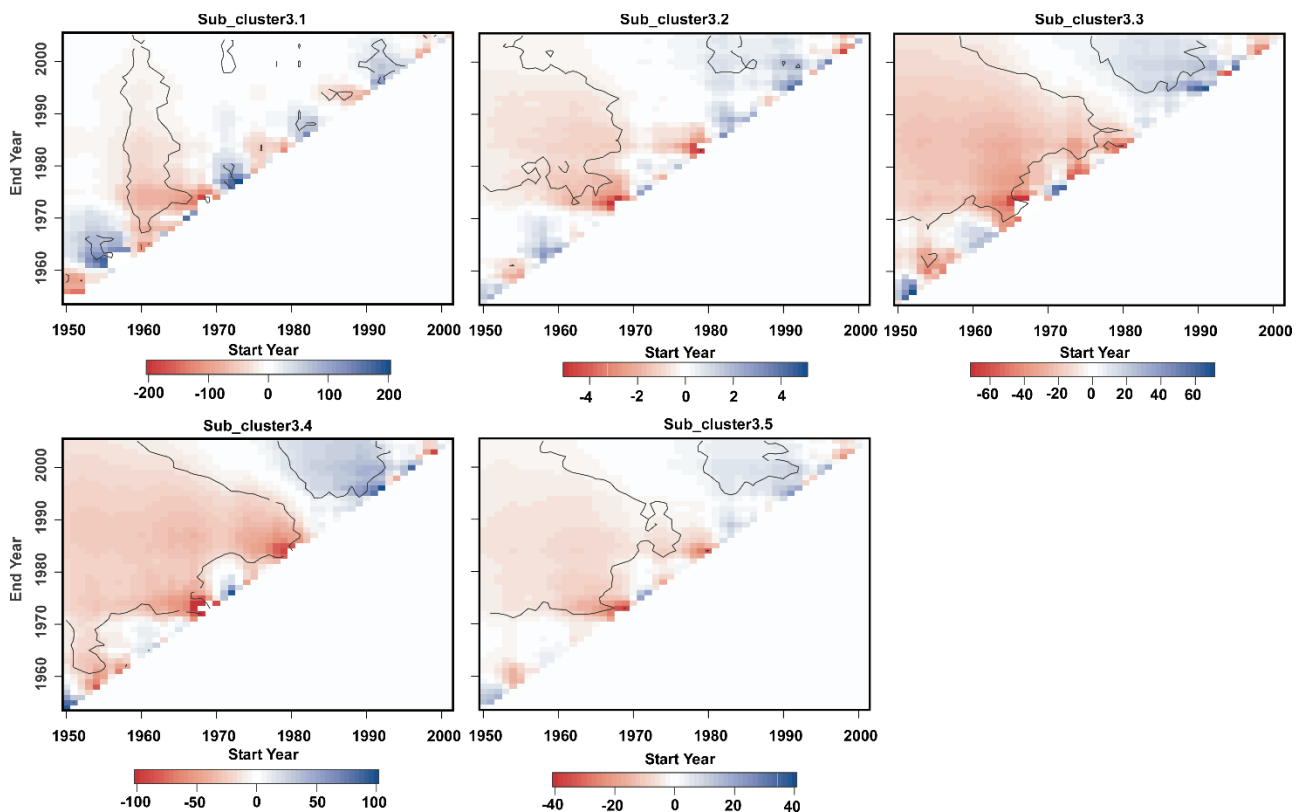
TDQ0004	CHARI	SARH (EX.FORT-ARCHAMBAULT)	9.15	18.4167
TDQ0009	CHARI	MAILAO	11.6	15.2833
TDQ0013	BAHR-SARA	MANDA	9.1833	18.2
TDQ0014	BAHR-SARA	MOISSALA	8.3333	17.7667
TDQ0036	LIM	OULI BANGALA	7.8333	15.8333
TDQ0041	PENDE	GORE	7.95	16.6167
TDQ0043	TANDJILE	TCHOA	9.3333	16.0833
TDQ2011	CHARI	BOUSSO	10.5	16.7167
TDQ5004	LOGONE	KATOA	10.8333	15.0833
TDQ5005	LOGONE	LAI (MISSION)	9.4	16.3
TDQ5006	LOGONE	LOGONE-GANA	11.55	15.15
TOQ0006	KARA	LAMA KARA 1	9.5333	1.1833
TOQ0037	SIO	KPEDJI	6.5317	1.0083
TOQ0042	MONO	CORREKOPE	7.8	1.3
TOQ0043	MONO	DOTAIKOPE	7.8167	1.2667
TOQ0046	MONO	TETETOU	7.0167	1.5333
TOQ0048	AMOU	AMOU OBLO	7.4	0.8667
TOQ0053	ANIE	PONT C F T	7.7333	1.2
TOQ0056	KOLOWARE	KOLOWARE	8.9667	1.2833
TOQ0057	NA	PARATAO	8.95	1.1833
TOQ0059	OGOU	SIRKA	7.9167	1.3667

2.7. Supplementary materials

Clusters of Streamflow variability



S2.1: Spatial distribution of streamflow variability (1950-2005) clusters based on multi-temporal trend analysis displayed on the river network (blue) and major river basins (grey shaded). Numbers 3.1-3.5 refer to the five sub-clusters derived from stations in cluster 3. All the clusters are highly significant at $p \leq 0.1$ according to the multiscale bootstrapping test. Different colours displayed the location of the different clusters.



S2.2 : Multi-temporal diagrams of the 5 sub-clusters derived from the clustering of streamflow stations within cluster 3: trends in m^3/s are presented in red to blue color scale, contours lines represent trend significance at $p \leq 0.1$.

CHAPTER 3: Interannual to Multi-decadal streamflow variability in West and Central Africa: interactions with catchment properties and large-scale climate variability

“Study the past if you would define the future.”
Confucius

Some materials have been removed from this thesis due to Third Party Copyright and confidentiality considerations. Pages where material has been removed are clearly marked in the electronic version. The unabridged version of the thesis can be viewed at the Lanchester Library, Coventry University.

This chapter appears as the following published paper in *Global and Planetary Change*

Sidibe, M., Dieppois, B., Eden, J., Mahé, G., Paturel, J. E., Amoussou, E., Anifowose, B., Lawler, D., 2019. Interannual to Multi-decadal streamflow variability in West and Central Africa: interactions with catchment properties and large-scale climate variability. *Global and Planetary Change*, 177, 141-156.

3. Interannual to Multi-decadal streamflow variability in West and Central Africa: interactions with catchment properties and large-scale climate variability

Abstract - Droughts and floods are responsible for ~ 80% of fatalities, and ~70% of economic losses related to natural hazards in Sub-Saharan Africa. Rainfall variability which is driven by interannual to multi-decadal climate fluctuations, here underpins these issues but is also crucial to agriculture and livelihoods. However, due to data scarcity, little is known about the impact of these climatic fluctuations and catchment properties on streamflow variability. Therefore, in this study, using a newly reconstructed streamflow dataset, we aim to extend understanding of hydrological variability through investigation of key large-scale controls which modulate climate-river flows relationships at the subcontinental scale. Modes of variability are extracted using continuous wavelet transform and maximum overlap discrete wavelet transform. We first assess the relative importance of catchment properties in modulating streamflow and modes of variability, before examining teleconnections with climate variables from different datasets (ERSST.v5 and 20CR.v2). The results underline the importance of interannual components of river flow along the Gulf of Guinea and the coastal regions of Central Africa where annual rainfall amounts are higher, and runoff is mostly generated from surface and sub-surface processes. In contrast, river flows along the Sahelian band show stronger multi-decadal components: this partly reflects the prominent role of geological formations in modulating high frequency rainfall signals. These modes of variability (also significantly detected in rainfall) are likely related to anomalies in sea-surface temperature (SST) anomaly patterns and associated atmospheric circulations, which together modulate the West African monsoon. Clarifying the picture of streamflow variability in western and Central Africa thus opens up the prospect for improved future predictions for streamflow and water resources in data scarce environments.

Keywords: *Streamflow, Rainfall, Spectral analysis, interannual to multi-decadal variability, catchment properties, large-scale climate teleconnections*

3.1. INTRODUCTION

Rainfall and river flow variability in West and Central Africa exacerbate challenges of water resource management which drive a range of socio-economic issues (*e.g.* Goulden *et al.*, 2009). Droughts and floods are responsible for approximately 80% of fatalities, and around 70% of economic losses that are related to natural hazards in Sub-Saharan Africa (World Bank, 2010; Vicente-Serrano *et al.*, 2012). Since the 1950s, many unprecedented changes have occurred, driven mainly by the human induced warming of the climate system (IPCC, 2014). West Africa has experienced several drought events, especially from the end of the 1960s to the 1990s (Lebel, 2003; Dai *et al.*, 2004; Dezfuli and Nicholson, 2013), leading to key decreases in river flows. In contrast, regions in Central Africa witnessed prolonged periods of high flows in the 1960s and 1970s (Conway, 2002). These extreme conditions raised key concerns, and triggered several studies investigating water resource variability in these regions.

While some researchers focused on catchment scale interactions (*e.g.* Mahé *et al.*, 2005; Amogu *et al.*, 2010), others approached the problem more globally and considered large-scale climate drivers (Roudier *et al.*, 2014; Sidibe *et al.*, 2018). These different approaches contribute to a better understanding of hydrological variability in West and Central Africa (although Central Africa has received less attention). At the catchment scale, findings highlighted that land-use changes over Sahelian regions combined with local wet periods in the 1970/80s, paradoxically resulted in increasing river flows despite decreasing mean annual rainfall amounts (Mahé *et al.*, 2005; Descroix *et al.*, 2009; Amogu *et al.*, 2010). In their comprehensive review of the evolution of hydrological regimes over the Sahelo-Sudanian regions of West Africa, Descroix *et al.* (2018) point out the significant role of land use/land cover changes and the intensification of the hydro-climatic system (*i.e.* higher frequency of extreme rainfall events; Panthou *et al.*, 2018). Although catchment properties (*e.g.* land cover, vegetation and geology) play key roles in shaping complex rainfall-runoff relationships, rainfall is the main

driver of streamflow variability (Conway *et al.*, 2009; Roudier *et al.*, 2014).

Over West and Central Africa, rainfall variability is dominated by the West Africa Monsoon (WAM) system, which strongly depends on fluctuations in global sea surface temperature (SST) and regional land surface conditions at different timescales (*e.g.* Nicholson *et al.*, 2000; Giannini *et al.*, 2005; Lu and Delworth 2005; Balas *et al.*, 2007; Dezfuli and Nicholson, 2013; Dieppois *et al.*, 2013, 2015). These linkages between global SST and West and Central African rainfall are mainly established through modulations of regional atmospheric circulation features, namely the upper-level Tropical Easterly Jet (TEJ), the mid-level African Easterly Jet (AEJ), low-level westerlies (LLW) and the Inter-Tropical Convergence Zone (Nicholson and Grist, 2001; Nicholson, 2013; Dezfuli, 2017). At the interannual timescale, for instance, the WAM dynamics are mainly driven by the El-Nino-Southern Oscillation (ENSO) (*e.g.* Giannini *et al.*, 2005; Rodriguez-Fonseca *et al.*, 2015), the Atlantic Equatorial Mode (also referred to as Atlantic Nino) (*e.g.* Losada *et al.*, 2010) and SST anomalies in the Mediterranean Sea (*e.g.* Gaetani *et al.*, 2010). In Central Equatorial Africa (CEA), SST-rainfall relationships underline the importance of SST anomalies along the Benguela Coast, as well as the changes in the Pacific Ocean and associated anomalies in the Walker circulation (Dezfuli, 2017). Hua *et al.* (2016) found that drought conditions in CEA (between April and June) were primarily related to SST variability over the Indian and Pacific oceans resulting in a westward shift in the Walker circulation: this underlines the significant heterogeneity of the region. At decadal to multi-decadal timescales, West African rainfall variability is mainly driven by the Inter-decadal Pacific Oscillation (IPO) and the Atlantic Multi-decadal Oscillation (AMO) patterns (*e.g.* Biasutti *et al.*, 2008; Mohino *et al.*, 2011; Dieppois *et al.*, 2013). Central African rainfall variability and associated SST teleconnections remain relatively less understood at these timescales. While the interactions between rainfall and large-scale climatic conditions have been relatively well documented, very few studies have investigated modes of streamflow

variability and associated climatic teleconnections over West and Central Africa. In most cases, streamflow variability is investigated through hydrological modelling using different climatic variables (*e.g.* rainfall and temperature) as input. Such an approach, despite reasonably strong streamflow predictions, is however limited by uncertainties in both input data quality and hydrological modelling steps (*e.g.* Steinschneider *et al.*, 2015; Kauffeldt *et al.*, 2016). Alternative approaches using observed streamflow and large-scale climate datasets were able to detect robust teleconnections, providing predictability skills (*e.g.* Yarnal, 1993; Chiew and McMahon, 2002; Sen, 2012; Kingston *et al.*, 2013; Nalley *et al.*, 2016; Massei *et al.*, 2017). For instance, Chiew and McMahon (2002) investigated ENSO-streamflow teleconnections in 581 catchments worldwide (59 catchments in Africa) using the harmonic analysis. In general, such techniques are likely to detect more robust teleconnections due to the reduced noise-signal ratio in streamflow series and the fact that river flow integrates information spatially (Chiew *et al.*, 1998). However most existing studies focus on specific timescales (*e.g.* interannual) and are mainly concentrated in regions with hydrological datasets of sufficient length and completeness (*e.g.* McGregor, 2017). Where data are scarce and the variability high, however, understanding of major multi-timescale climatic teleconnections driving streamflow variability can be constrained.

To fill these gaps, we use, in this study, a newly reconstructed streamflow dataset (Sidibe *et al.*, 2018) to better understand drivers of streamflow variability beyond the catchment scale perspective in data scarce environments. This will enable information from climatology and hydrological sciences to be better integrated into disaster mitigation planning *e.g.* for food security / agriculture, floods, drought and general water resource management in these developing nations. Therefore, using spectral analysis, we examine modes of streamflow variability and their teleconnections with climate variables (SST, Outgoing Longwave Radiation [OLR], zonal winds and moisture fluxes) from interannual to multi-decadal

timescales to provide a better understanding of streamflow-climate interactions and identify suitable predictors for streamflow prediction models. The relative importance of catchment properties in modulating streamflow modes of variability is also assessed.

In section 3.2, datasets and methods are presented. In section 3.3, rainfall-runoff relationships and modes of streamflow variability are quantified. The effect of catchment properties is discussed in section 3.4, and the main streamflow climate teleconnections are investigated in section 3.5. Finally, the results are summarized and discussed in section 3.6.

3.2. Data and Methods

3.2.1. Data

Streamflow and catchment properties (*e.g.* area, elevation, water holding capacity) datasets were collected from the SIEREM (“*Système d’Informations Environnementales sur les Ressources en Eaux et leur Modélisation*”) database (Boyer *et al.*, 2006) over the study area (Figure 3.1). Information related to groundwater resources (groundwater productivity, storage and depth to groundwater at 5 km resolution) was collected from the British Geological Survey (BGS) database (MacDonald *et al.*, 2012). Missing records in streamflow times series were reconstructed using a random forest-based approach (Stekhoven and Bühlmann, 2012) for a subset of 152 gauging stations with less than 50% missing data (Sidibe *et al.*, 2018). Catchment sizes range from 197 to 3,700,000 km² (median of 20,492 km²).

The Climatic Research Unit (CRU) dataset was used to investigate multi-scale rainfall-runoff relationships from 1950 to 2005. The CRU TS v4.00 rainfall field is produced on a 0.5°×0.5° grid and is derived from monthly rainfall provided by about 4,000 weather stations distributed around the world over the last century (Harris *et al.*, 2014; Table 1).

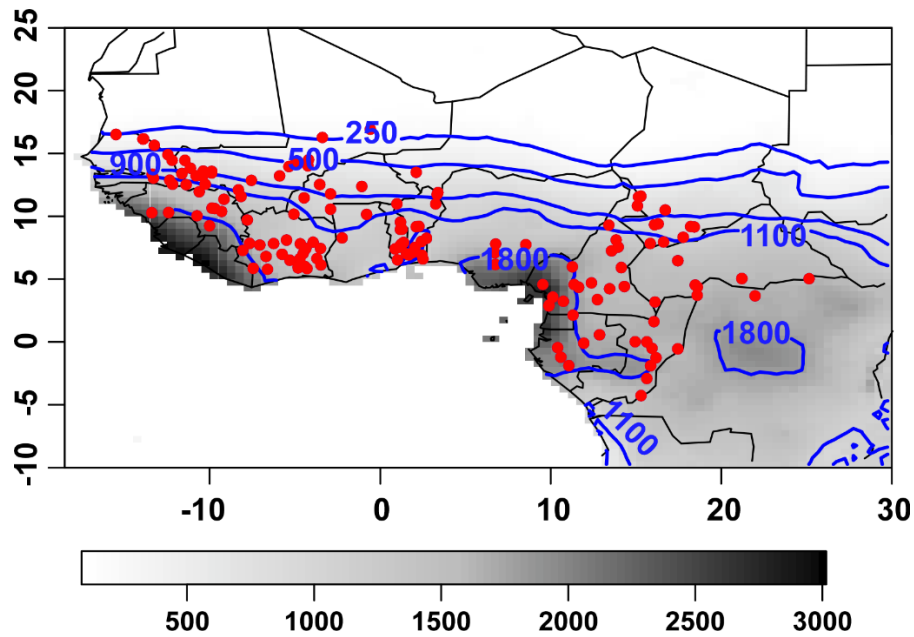


Figure 3.1 : Study area: selected streamflow gauging stations (red dots) on top of long term (1950–2005) mean annual rainfall (mm yr⁻¹; grey shaded) and isohyets (250, 500, 900, 1100 and 1800; blue contours) from CRU TS v4.00 precipitation dataset.

We make use of a global monthly gridded SST dataset, the Extended Reconstructed SST version 5 (ERSST.v5, Huang *et al.*, 2017), which is derived from the International Comprehensive Ocean–Atmosphere Dataset (ICOADS) Release 3.0, to understand SST-streamflow teleconnections. This dataset spans from January 1854 to present at a 2°×2° grid resolution and has improved SST spatial and temporal variability through new reconstruction methods, especially related to the use of Empirical Orthogonal Teleconnections (EOTs). More importantly, the dataset is not affected by cold SST biases resulting from satellite data assimilation at the end of the 20th century, which can sometimes induce a modest decrease in the global warming trend, and possibly for decadal signals (Reynolds *et al.*, 2002).

To investigate regional to global atmospheric anomalies associated with streamflow variability, the Twentieth Century Reanalysis version 2 (20CR.v2; Compo *et al.*, 2011), a 56-member ensemble global reanalysis (from 1871 to present) dataset at a 2°×2° grid resolution, was preferred. This reanalysis product assimilates only surface pressure with monthly SST and sea-ice distributions as boundary conditions. This modelling and data assimilation strategy remain

constant over the entire period to allow spectral decompositions in analyses of atmospheric circulation across different timescales with a reduced sensitivity to artificial shifts induced by assimilation of new datasets – *as is the case for NCEP/NCAR-1 reanalysis as shown in Pocard et al. (2000)*. The density of the observational network required for assimilation, as well as the quality of the SST field used as boundary conditions, remain nevertheless difficult issues. These are likely to impact upon the realistic representation of large-scale atmospheric states in the reanalysis and the consistency between its different members for the first decades of the period (He *et al.*, 2016; Pohl *et al.*, 2018). In addition to OLR at the nominal top of the atmosphere, moisture flux convergence/divergence was calculated at 950 hPa (*i.e.* monsoon layer) and winds were extracted at two pressure levels: 600 hPa (approximate location of the African Easterly Jet [AEJ] core) and 200 hPa (approximate location of the Tropical Easterly Jet [TEJ] core).

3.2.2. METHODOLOGY

In section 3.3, to investigate streamflow variability over West and Central Africa from 1950 to 2005, each streamflow time series is decomposed into a time-frequency domain using the continuous wavelet transform (CWT; Torrence and Compo, 1998). This approach uses a set of non-orthogonal wavelets (Morlet wavelet, order 6) to produce local wavelet spectra, highlighting the dominant timescales of streamflow variability and their time evolution. The significance test of the wavelet spectra, following Torrence and Compo (1998), assumes a red noise background spectrum for the null hypothesis, which is tested by Monte-Carlo simulations of first-order autoregressive (AR[1]) process. To summarize the results, wavelet spectra were classified using multi-scale bootstrap hierarchical clustering (Suzuki and Shimodaira, 2006) to define homogenous regions of streamflow variability. Through thousands of bootstraps resampling, this clustering technique provides the probability associated with each cluster enabling a more robust selection of homogenous regions (more details about probability

estimation of each cluster are provided in Dieppois *et al.*, 2019). Only clusters with a probability greater or equal to 0.9 were selected. Clusters centroids (based on distance matrices: stations with minimum average distance within each cluster) are then used to investigate streamflow variability and associated climate teleconnections.

Hydroclimatic (streamflow and rainfall) modes of variability are then extracted using the multi-resolution analysis based on Maximum Overlap Discrete Wavelet Transform (MODWT; Percival and Walden, 2000). We used a least asymmetric (LA 8) wavelet filter, which is better suited for decomposition of turbulent signals (Cornish *et al.*, 2006). In our study, for time series of length N , the largest component of decomposition J_0 was selected such that $J_0 \leq \log_2(N)$ (e.g. $J_0 = 5$ hereafter). The five components correspond to fluctuations of 2.5, 5, 12.5, 20 and >20-year periods respectively.

In section 3.4, we first describe precipitation and streamflow variability in terms of the contribution of each timescale to the overall variance to highlight the relative importance of the dominant modes of variability over the region. Then, rainfall-runoff relationships from 1950 to 2005 are estimated using correlations between catchment averaged annual precipitation and streamflow. Finally, underlying relationships between modes of streamflow variability and catchment properties are assessed through a principal component analysis (PCA), using the singular value decomposition (SVD) method for 129 catchments (variables used are presented in Table 3.1). We focus on three different timescales of streamflow variability: interannual (components 1 and 2; ~2.5 and 5 years), quasi-decadal (component 3; ~12.5 years) and multi-decadal timescales (components 4 and 5; ≥ 20 years).

Table 3.1: List of variables considered for the PCA. Catchment properties (Area, WHC, slope) datasets are collected from the SIEM database and groundwater datasets are collected from the BGS database (MacDonald *et al.*, 2012).

Variables	Code
Interannual scale contribution to total streamflow variance (MODWT components 1 and 2) (%)	Q_int
Decadal scale contribution to total streamflow variance (MODWT component 3) (%)	Q_dec
Multi-decadal scale contribution to total streamflow variance (MODWT components 4 and 5) (%)	Q_mlt
Catchment Area (km ²)	Area
Latitude of streamflow gauging station (°)	Lat
Altitude of the streamflow gauging station (m)	Alt
Catchment average slope (°)	Slp
Gravelius Compactness Index (no unit)	GCI
Catchment average water holding capacity (mm)	WHC
Catchment average Long term (1980-2005) Normalized Difference Vegetation Index (NDVI) (no unit)	NDVI
Catchment average depth to groundwater (m)	DGW

In section 3.5, similarly to Dieppois *et al.* (2013, 2016, 2019), composite analyses are performed to investigate teleconnections between streamflow and large-scale climate variability at multiple timescales. Two sets of large-scale climate variables, *i.e.* SST, OLR, moisture fluxes (950 hPa) and wind fields (at 600 and 200 hPa), are produced for each timescale, where streamflow fluctuations exceed ± 1 standard deviation (*i.e.* wet and dry anomalies); the resulting composites thus describe the difference in large-scale climate variables between wet and dry conditions. Such an approach is implemented without any prior assumption about the link between the variables, and therefore favours a good representation of both linear and non-linear relationships (Von Storch and Zwiers, 1999). Statistical significance is estimated by testing the difference in mean between wet and dry anomalies using a two-sided Student's *t* test at $p = 0.05$. In addition, when time series are serially

correlated, the degree of freedom is adjusted by recalculating the “effective sample size” (N^{eff}).

This is given by the following approximation (Yue and Wang, 2004):

$$\frac{N}{N^{\text{eff}}} = 1 + \frac{2}{N(N-1)(N-2)} \sum_{i=1}^t (N-i-1)(N-i-2)ts(i) \quad (\text{eq.1})$$

where N is the number of observations in the sample, $ts(i)$ is the serial correlation between ranks of the observations for lag i , and t is the maximum time lag considered.

3.3. Streamflow variability

3.3.1. Modes of streamflow variability and regionalization

Applying the CWT to runoff records over West and Central Africa allows simultaneous assessment of spatial and temporal variability of streamflow data. Over the study area, three different regions of streamflow variability were highlighted (significant at $p \leq 0.1$; Figure 3.2), using the multi-scale bootstrap hierarchical clustering method applied to all the CWT diagrams. Identical regions of streamflow variability were found by applying the same procedure to multi-temporal trend analysis (Sidibe *et al.*, 2018).

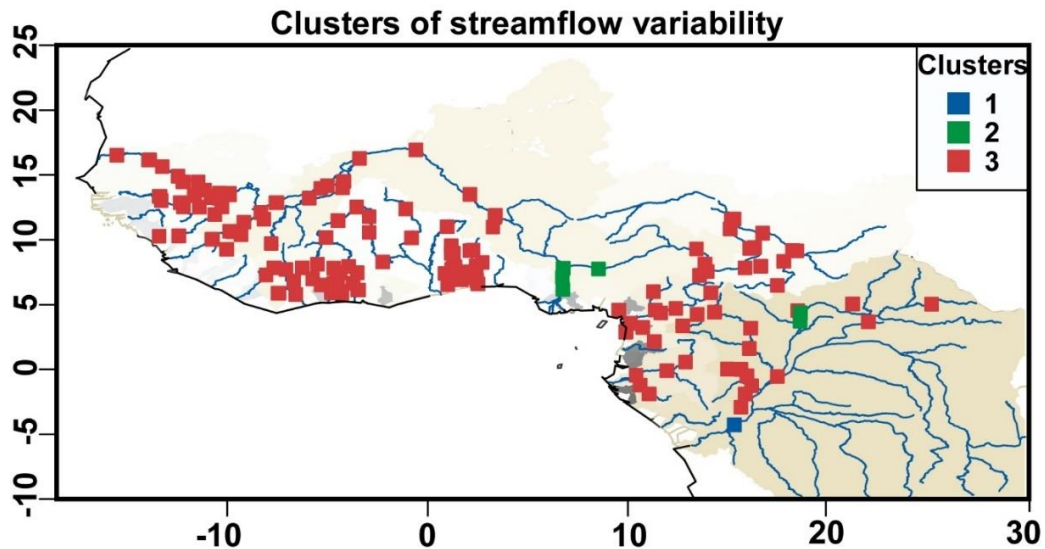


Figure 3.2: Clusters of streamflow variability significant at $p \leq 0.1$ defined based on multi-scale hierarchical clustering applied to Continuous Wavelet diagrams. Significance is estimated using 1000 bootstrap simulations.

The first cluster (Congo Basin at Brazzaville) is characterized by high flows in the 1950s and 1960s and relatively lower flows between the 1970s and the 2000s (Figure 3.3a). The CWT

highlights significant interannual variability (2-8 years) between 1950 and 1980, which is superimposed with significant quasi-decadal fluctuations (8-16 years) between 1960 and 1970 (Figure 3.3d). These results suggest that the positive streamflow trends observed in this region in the 1950s and 1960s might have been induced by concurrent positive interannual and quasi-decadal streamflow anomalies.

The second cluster, which describes stations from the lower Niger River, the Benue and parts of the upper Congo basin, presents two decades (1950s and 1960s) of high flow with a maximum around 1970 (Figure 3.3b). Dry conditions are observed between 1970 and 2005, with a recovery around the end of the 1980s. This cluster shows significant interannual fluctuations between 1960 and 1980 (Figure 3.3e). A significant quasi-decadal signal is also observed between 1970 and 1990 (Figure 3.3e). During the wet period, interannual components are prominent, whereas quasi-decadal signals are more pronounced during the dry period (1970-1990).

The third cluster covers a wider spatial extent and reveals pronounced decrease in streamflow trends between 1950 and 1970 compared to clusters 1 and 2 (Figure 3.3c). From 1970 to 1990, high streamflow variability is detected, with two major dry episodes (1972-1973 and 1983-1984) separated by wet episodes (1974-1982). In addition, a partial recovery in streamflow is identified in the post 1990s. These results are consistent with previous studies describing rainfall variability over West Africa (*e.g.* Nicholson *et al.*, 2000; Dai *et al.*, 2004; Lebel and Ali, 2009; Masih *et al.*, 2014). For this cluster, CWT displays significant interannual fluctuations (2-6 years) from the late 1960s to the mid-1970s (Figure 3.3f). These interannual fluctuations are combined with quasi-decadal fluctuations from the mid-1950s to the mid-1970s, and multi-decadal fluctuations from the mid-1960s to the 1980s (Figure 3.3f). Such findings underline that streamflow variability over this region results from interannual to multi-decadal fluctuations, comparable to those detected in Sahel rainfall by Dieppois *et al.* (2015).

Interestingly, the drought episode of 1972-1973 is associated with significant interannual to multi-decadal fluctuations, whereas the drought episode of 1983-1984 is primarily associated with multi-decadal fluctuations only (Figure 3.3f).

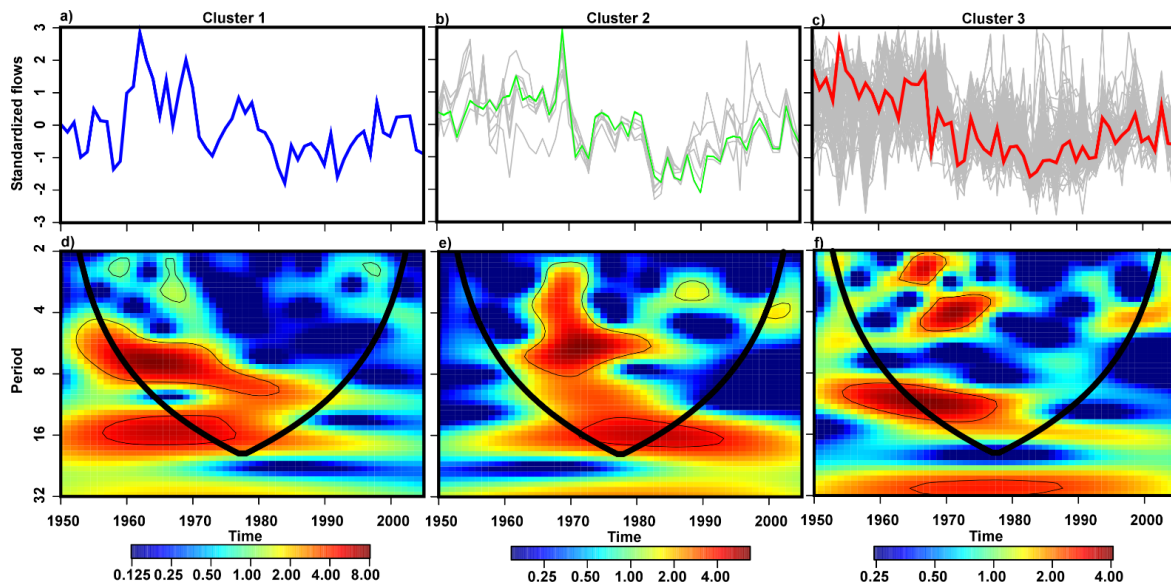


Figure 3.3: Top three panels show time series (grey colour) of different clusters and their centroids (blue-green-red). The bottom panels present wavelet spectra of streamflow times series (Cluster centroids). Significant fluctuations ($p \leq 0.1$) are highlighted with thin black contours. Thick black lines underline the cone of influence.

The main modes of streamflow variability over the study area are overall similar despite different contributions to total variance. Some dissimilarities in streamflow variability between parts of West and Central Africa are consistent with the findings of Mahé *et al.* (2001), underlining differences in rainfall variability between the two regions for the 1951-1989 period. Moreover, the fact that Cluster 3 includes catchments with different hydrological behaviours suggests that the detected modes of variability from interannual to multi-decadal timescales are primarily driven by climatic fluctuations. The relative contribution of the different modes of variability to the total variance, as well as the rainfall-runoff relationships across different timescales, are assessed in the following section.

3.3.2. Importance of streamflow modes of variability

Multi-resolution analysis based on MODWT was applied to annual streamflow and basin-averaged precipitation time series to extract the different modes of variability. Five different MODWT components are extracted, and the contribution of each component to the total variance is quantified. Correlations between rainfall and runoff are also calculated for each component of decomposition (Figure 3.4).

Over the study area, at the interannual timescale, a meridional gradient is identified over West Africa in both streamflow and rainfall (Figure 3.4a, f), although interannual variability is higher in rainfall compared to streamflow. Streamflow stations located along the Gulf of Guinea, and most of Central Africa, are characterized by high contributions (20-60%) of the interannual timescale to the total variance. Meanwhile, interannual variability was responsible for less than 20% of the total variance above 10°N (Figure 3.4a). These results underline that streamflow stations located in regions with higher annual precipitation amounts (Figure 3.1) present a higher interannual component (Figures 3.1, 3.4a). Local differences can however be identified. For instance, the Wayen station (1.08°W, 12.3789°N) in the Upper Volta basin shows high interannual streamflow variability (more than 50%). This is consistent with previous studies highlighting increased runoff coefficients in Sahelian basins linked to high rainfall variability and land use changes (Mahé and Paturel, 2009; Ibrahim *et al.*, 2015). Over the study area, significant rainfall-runoff relationships ($p \leq 0.1$) are highlighted at this timescale, except for the Niger River in its middle reach (Figure 3.4k). Low correlations over this region are mainly induced by the Inner Niger Delta (Figure 3.4k), which significantly delays the peak runoff (*e.g.* Aich *et al.*, 2014).

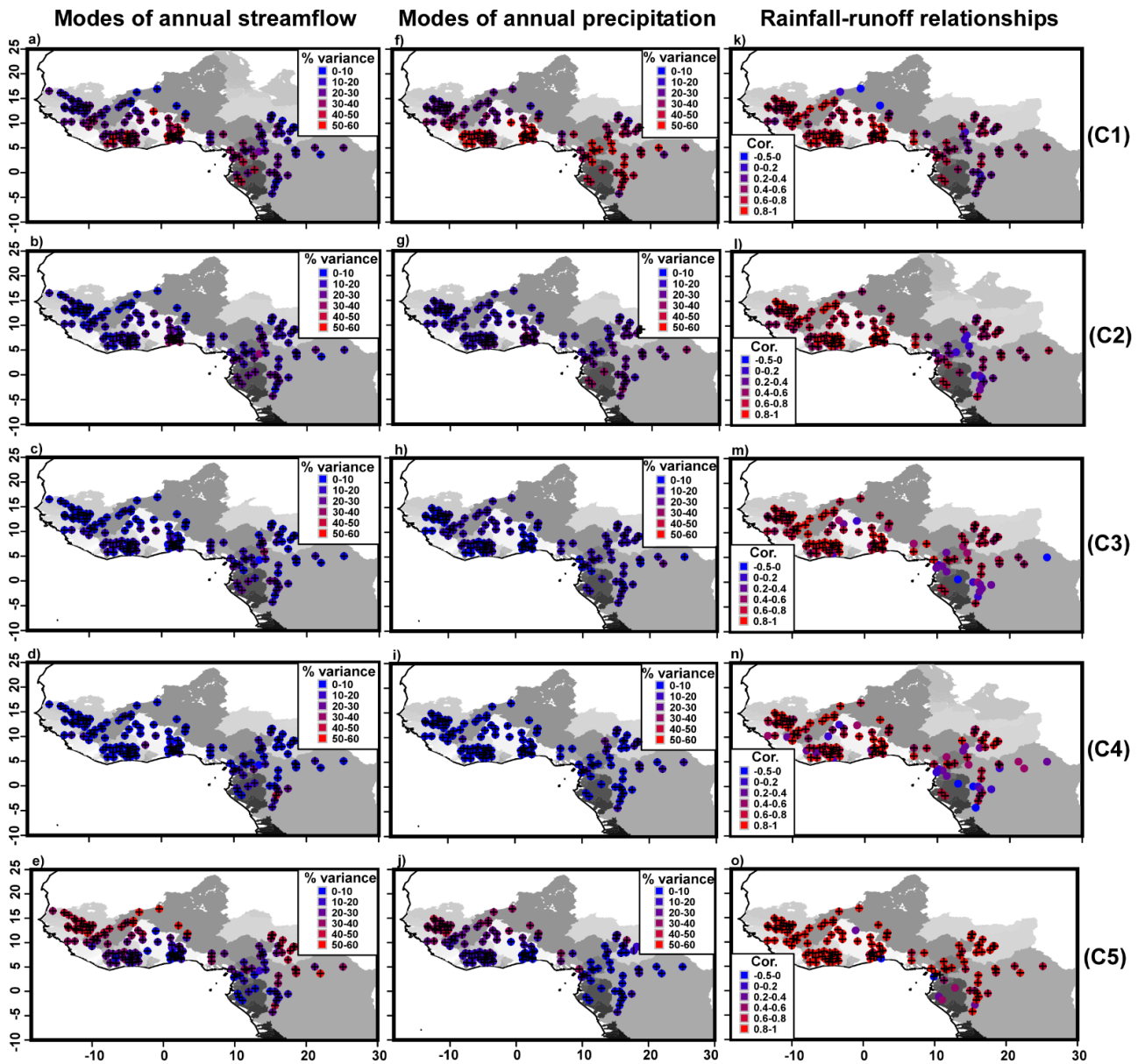


Figure 3.4: Five components of annual streamflow (a-e) and basin averaged precipitation (f-j) extracted using the Maximum Overlap Discrete Wavelet Transform (MODWT), their contribution to total variance (%) and rainfall-runoff relationships (Pearson correlation) using basin averaged precipitation (k-o). Significance level ($p \leq 0.1$) estimated using 1000 Monte Carlo simulations of autoregressive processes are presented with black crosses. C1, C2, C3, C4, C5 correspond to component 1, component 2, component 3, component 4 and component 5 respectively.

The meridional gradient is less pronounced for the second, third and fourth MODWT components (*i.e.* 5, 12.5 and 20-year periods, respectively). These different modes of variability represent less than 20% of the total variance for most of the stations (Figure 3.4b-d), except in some regions over the Gulf of Guinea and Central Africa, where the contribution is higher (20-40%). Weak rainfall runoff relationships are observed over parts of Central Africa

(Figure 3.4l-n), consistently with changes in discharges' seasonal regimes documented by Mahé *et al.* (2013). The fifth MODWT component, which corresponds to the multi-decadal timescale (> 20 years period; Figure 3.4e), highlights an opposite pattern to the one depicted at the interannual timescale (Figure 3.4a). The contribution of the multi-decadal timescale to the total variance is higher (40-60%) for streamflow stations located above 10°N (Figure 3.4e). This suggests that streamflow variability in Sahelo-Sudanian regions is primarily related to multi-decadal fluctuations. At this timescale, rainfall-runoff relationships are very strong (> 0.8 significant at $p \leq 0.1$) in most of West and Central Africa (Figure 3.4o). High correlations should however be interpreted with caution, as the multi-decadal signal is strongly autocorrelated, and the degree of freedom very low, possibly leading to artificially increasing correlation coefficients. Interestingly, however, the contribution of multi-decadal variability to total rainfall variance is comparatively lower than in streamflow (Figure 3.4j).

These findings suggest that streamflow variability is mainly driven by fluctuations in annual precipitation, which was found to exhibit interannual to multi-decadal components (Dieppois *et al.*, 2013, 2015). From the regional to local scales, however, weak rainfall-runoff relationships, as well as discrepancies in the contribution of the different timescales between rainfall and streamflow, suggest potential contributions of catchment properties (*e.g.* natural vegetation, agricultural land-use, soil permeability and geology) in modulating rainfall input signals to river flow signals.

3.3.3. Modes of streamflow variability and interactions with catchment properties

Interactions between modes of streamflow variability (interannual, decadal and multi-decadal) and catchment properties are investigated using PCA. The first two components of the PCA (~50% described variance) are presented for data exploration (Figure 3.5). The first component is determined by the variables **Q_mlt**, **Lat**, **GCI**, **DGW** and **Area** which are negatively

associated with **Q_int, Q_dec, WHC and NDVI**. The second component is determined by the variables **Lat, Q_int and Slp** which are negatively correlated to **Alt, NDVI, WHC, Q_dec, Q_mlt and Area** (see Table 3.1 for variable names).

The first two components of the PCA (~ 50% described variance) (Figure 3.5), suggest that large contributions of interannual timescales are often observed in steep, round catchments with shallow groundwater, whereas greater contributions on multi-decadal timescales are more likely in large elongated catchments with deep groundwater. For instance, catchments along the Gulf of Guinea and some Sudanian regions, where interannual components are stronger, often present shallow groundwater and a “Hewlett type” hydrological behaviour characterized by presence of an impervious underlying layer limiting infiltration, and therefore presenting a faster response to runoff (Hewlett, 1974; MacDonald *et al.*, 2012).

Also, predominant contribution of multi-decadal timescales to total variance are observed for stations along the Sahelian band (Figure 3.5). This behaviour seems counterintuitive, regarding the predominance of Hortonian (Horton, 1933) hydrological processes exacerbated by land cover changes (*e.g.* more cultivated areas and less natural bushes). At the regional scale, however, it is difficult to limit modes of streamflow variability to catchment hydrological behaviour, as Hortonian runoff can be observed in Sudanian (mean annual precipitation ranges from 900 to 1100 mm yr⁻¹) regions and inversely “Hewlett-type” runoff processes are observable in the Sahelian (mean annual precipitation ranges between 250 and 500 mm yr⁻¹) regions (Descroix *et al.*, 2009). The large contribution of multi-decadal timescales could be explained to some extent by the impact of the Inner Niger delta (Figure 3.5), deep groundwater tables (MacDonald *et al.*, 2012) and the Iullemenden sedimentary basin (which covers western Niger, Mali, Benin, Nigeria; Favreau *et al.*, 2012). For instance, the Inner Niger delta plays a significant role in modulating high frequency rainfall signals (Figure 3.5). Furthermore, the Iullemenden sedimentary basin, with its relatively coarse sediments, encourages high

infiltration capacities and remains the main source of groundwater in the region. The importance of groundwater over this region is discussed by Descroix *et al.* (2009), who found that high runoff rates drive rising groundwater tables due to the appearance of recharge ponds. Interactions between the Iullemeden aquifer system and the Niger River underlines the potential impact of groundwater abstraction on streamflow variability.

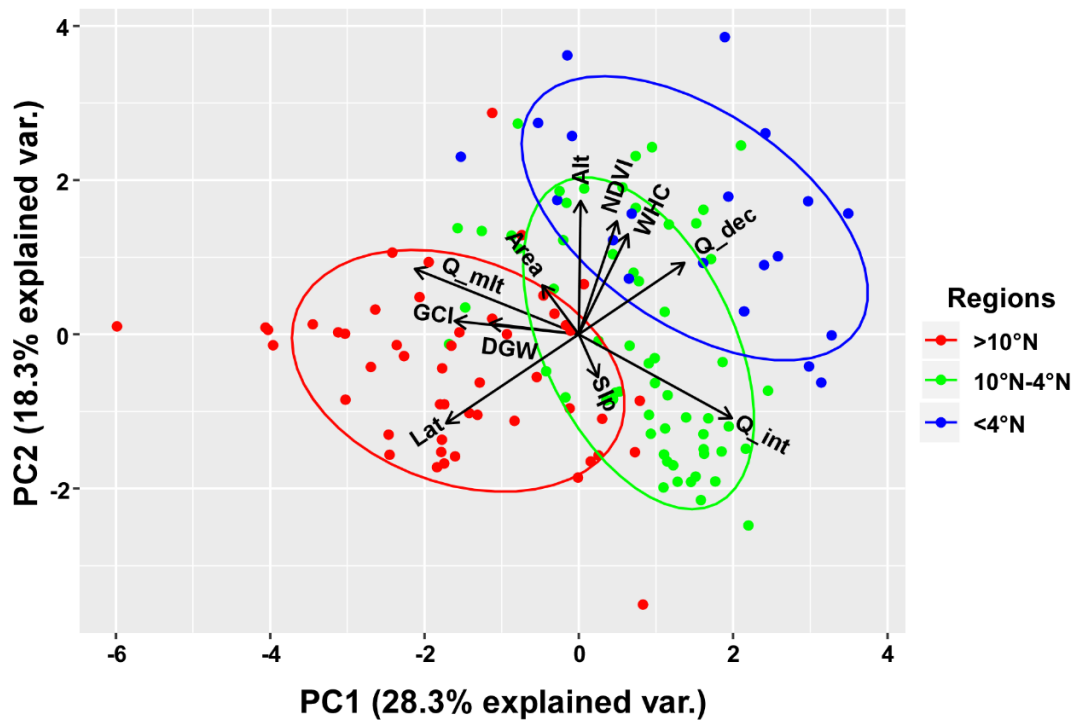


Figure 3.5: First and second components (~50% explained variance) of the PCA performed on long term average indices of streamflow variability and catchment properties. Streamflow stations are represented by coloured dots. Blue for stations below 4°N (Central Africa), green for stations in Sudanian and Guinean regions (between 4°N-10°N) and red for stations above 10°N. Original variables are superimposed as black vectors (refer to table 1 for variable names): two vectors forming a small angle represent positively correlated variables; if the angle is around 90° variables are not likely to be correlated and an angle close to 180° suggests negatively correlated variables. The importance of each variable on a PC is given by its project value on that PC.

In addition, quasi-decadal fluctuations of river flows appear positively related to vegetation cover and water holding capacity (Figure 3.5). Dense vegetation cover, for instance, enhances soil organic matter content, structural stability and hydraulic conductivity, which all together could contribute to dampen interannual signals (Mahé *et al.*, 2005; Descroix *et al.*, 2009). For instance, Trichon *et al.* (2018), reported that persistent degradation of the woody cover in the

Sahel since the droughts of the 1970s resulted in a shift of surface flow processes from sheet to concentrated runoff. Even though NDVI measurements show good agreement with field observations over the Sahel (Dardel *et al.*, 2014), the role of vegetation should however be interpreted with caution, as the datasets used in this study only cover the 1981-2005 period.

3.4. Streamflow-climate teleconnections

3.4.1. Regional atmospheric circulations

Average annual regional atmospheric circulation patterns over the study area between 1950 and 2005 are presented in Figure 3.6. At the regional scale, the main circulation features impacting the WAM and regional hydroclimatic variability, are the upper-level Tropical Easterly Jet (TEJ), the mid-level African Easterly Jet (AEJ) and the low-level westerly monsoon flow (LLW) (Lambergeon *et al.*, 1981; Mahé and Citeau, 1993; Nicholson *et al.*, 2013; Dezfuli, 2017) (Figure 3.6). LLW highlight convergence on the continent, with a maximum along the Gulf of Guinea and Central Africa at 950 hPa, corresponding to the average annual location of the Intertropical Convergence Zone (ITCZ) (Figure 3.6a). The AEJ is located at 600 hPa over West Africa between the Equator and 15°N, with maximum annual average speeds higher than 6 m.s⁻¹ (Figure 3.6b). Stronger and more widespread, the TEJ is located further East at 200 hPa between 10°S and 15°N (Figure 3.6c), with a core over the Indian Ocean (maximum annual average higher than 10 m.s⁻¹), and a stronger development over West Africa during wet years than dry years (Mahé and Citeau, 1993).

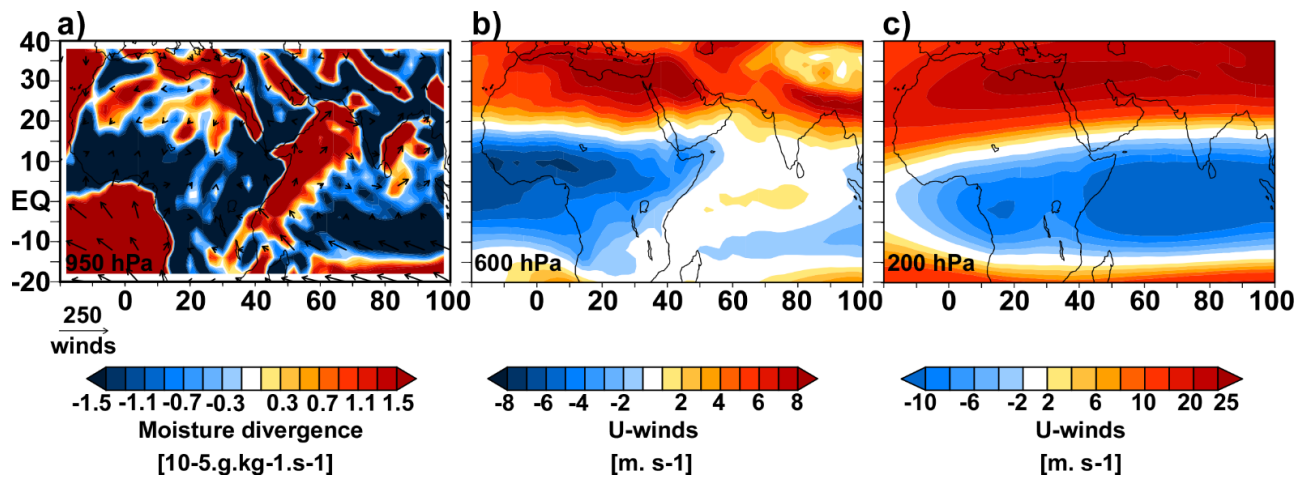


Figure 3.6: 20CR.v2 average annual regional atmospheric circulation patterns (1950-2005). (a) average annual moisture fluxes at 950 hPa pressure level, represented in vectors ($\text{g.kg}^{-1}.\text{m.s}^{-1}$) on top of convergence/divergence ($10^{-5}.\text{g.kg}^{-1}.\text{s}^{-1}$). (b) average annual zonal wind speed (m.s^{-1}) unit at 600 hPa pressure level. (c) average annual zonal wind speed (m.s^{-1}) at 200 hPa pressure level.

In the following sections, interannual to multi-decadal teleconnections between streamflow modes of variability and atmospheric circulations are investigated for centroids (stations presenting the maximum similarity with each cluster member based on distance matrices) of the three clusters presented in section 3.3.1. The results are presented in panels with each column corresponding to a cluster and each row to a component of decomposition.

Table 3.2: Periods in years of MOWDT components for each cluster centroid. Explained variance associated with each component is given in parentheses. CGQ2000 (Congo at Brazzaville), CFQ0025 (Oubangui at Zinga) and MLQ0137 (Faleme at Fadougou).

Centroids	Component 1 (C1)	Component 2 (C2)	Component 3 (C3)	Component 4 (C4)	Component 5 (C5)
Cluster 1: CGQ2000	2 (12%)	6 (13%)	12 (10%)	30 (9.4%)	>30 (16.2%)
Cluster 2: CFQ0025	3 (10%)	6 (10.4%)	15 (4.6%)	20 (3.7%)	>30 (29.1%)
Cluster 3: MLQ0137	2 (13.15%)	5 (3.84%)	15 (5.7%)	30 (1.9%)	>30 (33.2%)

3.4.1.1. Lower-tropospheric regional circulation anomalies

Anomalies of the low-level westerly monsoon flux driving streamflow variability in West and Central Africa are investigated through moisture fluxes and convergence at 950 hPa (Figure 3.7). Negative anomalies of divergence refer to convergence in moisture fluxes, and therefore help highlighting potential anomalies in the intensity and latitudinal position of the ITCZ.

Atmospheric composite anomalies for cluster 1 (Congo Basin at Brazzaville) show different patterns from interannual to multi-decadal timescales. The first component of decomposition (~2 years) is characterized by anomalously high moisture convergence along the western coasts of Central Equatorial Africa and regions in the eastern Sahel (Figure 3.7a). The pattern is slightly modified for component 2 (~ 6 years), with high moisture convergence along the Gulf of Guinea and the northern edge of Central Equatorial Africa (Figure 3.7b). Thus, for cluster 1, interannual variability (component 1 and 2) may relate to a southward shift of the ITCZ. At the quasi-decadal timescale (component 3), higher than normal moisture convergence is detected over the western and eastern Sahel, while lower than normal moisture convergence is identified over the Gulf of Guinea coastal regions (Figure 3.7c). This is also consistent with enhanced westerlies at the equator associated with high moisture convergence in Central Equatorial Africa (Figure 3.7c). At multi-decadal timescales (components 4 and 5), a similar pattern is much more pronounced, with enhanced moisture convergence over the northern edge of Central Africa and anomalous moisture divergence along the Gulf of Guinea (Figure 3.7d-e), inferring a northeastward shift of the ITCZ.

Interannual streamflow variability in cluster 2 is associated with moisture divergence anomalies along the Gulf of Guinea and moisture flux convergence anomalies over the entire Sahelian band (component 1; Figure 3.7f) along 15°N, suggesting a northward shift of the ITCZ. At the quasi-decadal timescale (component 3), streamflow variability is associated with anomalous westerlies and divergence along the Gulf of Guinea, while moisture convergence is identified over the western Sahel and along the northern edge of Central Equatorial Africa (Figure 3.7h). This pattern therefore suggests a northward position of the ITCZ at the quasi-decadal timescale, which shifts eastward and becomes even clearer at multi-decadal timescale (component 5; Figure 3.7j).

Despite its large spatial extent, Cluster 3 presents coherent atmospheric composite anomalies associated with streamflow variability. The first component of decomposition highlights moisture divergence anomalies in the Atlantic near the West African coasts, and high moisture convergence along 10°N (Figure 3.7k). This suggests a northward position of the ITCZ in component 1, which seems to retreat southward for component 2 (Figure 3.7l). These different patterns observed at the interannual timescales might have been induced by the location of the cluster centroid, which reflects influence of wet conditions over both the Gulf of Guinea and the Sahel. A comparison between two stations located in the Gulf of Guinea (Oueme at Bonou) and further North (Senegal at Bakel) is thus provided in supplementary material (S3.1). The main difference between these two zones is more pronounced at the interannual timescale (component 1), where positive streamflow fluctuations over the Sahel are associated with a northward position of the ITCZ, while they are associated with a southward position of the ITCZ over the Gulf of Guinea. At the quasi-decadal timescale (component 3; Figure 3.7m) a northward position of the ITCZ seems to drive positive streamflow phases. High moisture flux convergence is observed around 10°N , while high moisture flux divergence is observed along the Gulf of Guinea (Figure 3.7m). The northward location of the ITCZ is more pronounced, and shifted eastward, at the multi-decadal timescale (component 5), with homogenous high moisture flux convergence along 15°N over the western region of West Africa (Figure 3.7o). Such findings underline the complexity of processes occurring at the regional scale, but more importantly highlight that, for low frequency components, a northeastward shift of the ITCZ is often associated with wet conditions over the entire study area.

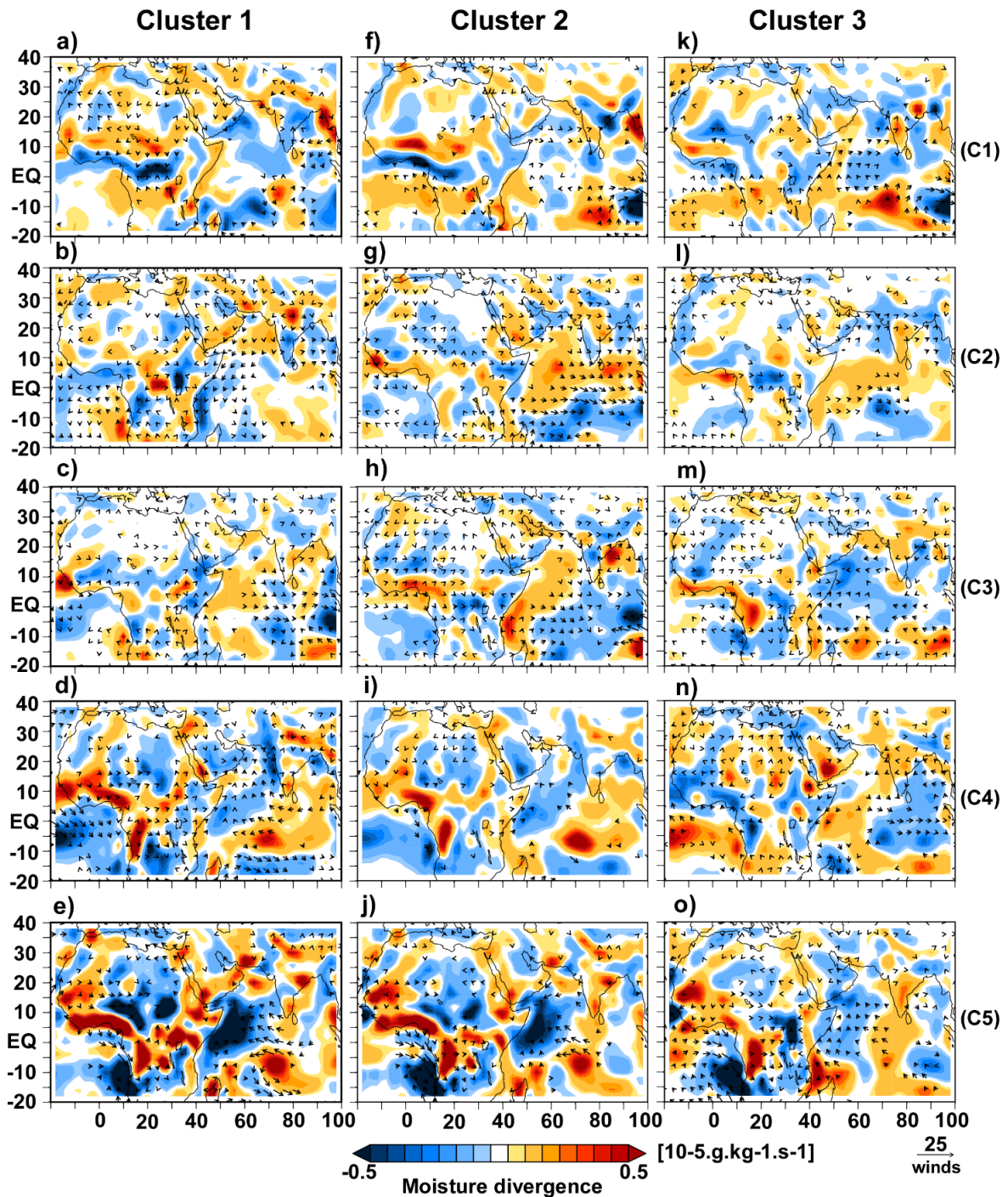


Figure 3.7: Low level winds and their interactions with streamflow modes of variability (five components of decomposition). Cluster 1 (a-e), Cluster 2 (f-j) and Cluster 3 (k-o). Only wind vectors significant at $p \leq 0.1$ in their zonal or meridional components are represented. Divergence calculated for the layer is displayed in shaded colours from dark blue (negative anomalies) to dark red (positive anomalies). EQ is Equator. C1, C2, C3, C4, C5 correspond to component 1, component 2, component 3, component 4 and component 5 respectively.

In summary, streamflow teleconnections with lower-tropospheric circulation anomalies exhibit regional timescale-dependent relationships. At interannual timescales, positive streamflow

phases over the study area are primarily related to high moisture converge over western Central Equatorial Africa for Cluster 1 and northward shifts of the ITCZ for Cluster 2 and Cluster 3. For lower frequency components (decadal to multi-decadal) streamflow variability over the study area is primarily associated with northeastward shifts of the ITCZ in all regions. In addition, Lavaysse *et al.* (2010) found that northeastward shifts of the ITCZ, associated with a strengthening of the monsoon flow over Central and Eastern Sahel, result mainly from strong phases of the Saharan Heat Low (SHL).

However, it has been reported in previous studies (Citeau *et al.*, 1988; Mahé and Citeau, 1993), that the ITCZ northern reach over the Atlantic (according to satellite images) was not significantly different from one year to another whatever the quality of the upcoming rainy season over West Africa.

3.4.1.2. Mid-tropospheric regional circulation anomalies

Teleconnections between mid-tropospheric regional circulations and streamflow over the study area are examined using zonal winds at 600 hPa (Figure 3.8), the average location of the AEJ (Figure 3.6b). Negative zonal wind anomalies refer to easterly winds, while positive anomalies refer to westerly winds.

Mid-tropospheric regional circulation anomalies associated with streamflow variability for Cluster 1 (Congo Basin at Brazzaville) show different patterns from interannual to multi-decadal timescales. At the interannual timescale (component 1), significant negative zonal wind anomalies (*i.e.* easterlies) are detected between 10 and 20°N over the western Sahel, and further North over the eastern regions. Southward of this easterly jet, which resembles the AEJ-N presented by Nicholson and Grist (2003), significant positive zonal wind anomalies (*i.e.* westerlies) are observed along the equator (Figure 3.8a). Such zonal mid-tropospheric circulation anomalies suggest a weakening of the African Easterly Waves (AEWs), which form southward of the AEJ-N and trigger mesoscale rainfall systems (Dezfuli, 2017), in Cluster 1

for component 1. Similarly, the second MODWT component, underlines a southward shift of the AEJ-N, which is now located over West Africa from the Gulf of Guinea to 20°N. Anomalous westerlies previously detected over the equator are now limited to the western part of Central Africa (Figure 3.8b), consistently with a southward position of the ITCZ (Figure 3.7b). At the quasi-decadal timescale (component 3), positive zonal wind anomalies (*i.e.* westerlies) observed over western Central Africa, expand to the Gulf of Guinea up to 10°N (Figure 3.8c). These positive anomalies are bounded by significant negative anomalies (*i.e.* easterlies), which present commonalities with the AEJ-N and AEJ-S described by Nicholson and Grist (2003). At the multi-decadal scale (components 4 and 5), anomalous westerlies describe a weakening of the AEJ over West Africa and parts of Central Africa (Figure 3.8d, e). Significant teleconnections are also detected for Cluster 2 (regions in Central Africa and Lower Niger River). The first component of decomposition is characterized by significant positive zonal wind anomalies (*i.e.* westerlies) over West Africa from the Gulf of Guinea up to 15°N, as well as in the equatorial Atlantic Ocean (Figure 3.8f). Interestingly, enhanced easterlies are observed in eastern Central Africa (Figure 3.8f). The second component of decomposition highlights intensified easterlies over West Africa, and anomalous westerlies in the Atlantic Ocean around western Central Africa (Figure 3.8g). This pattern, like the one highlighted for Cluster 1, at the same timescale (Figure 3.8b), is consistent with a southward position of the ITCZ (Figure 3.7g). At the quasi-decadal timescale (component 3), significant anomalous westerlies are observed from the equator to 15°N. This pattern suggests a weakening of the AEJ, which however intensifies above 15°N (Figure 3.8h). At multi-decadal timescales (components 4 and 5), as for cluster 1, we note a weakening of the AEJ over West Africa and parts of Central Africa, as determined through westerly anomalies over these regions (Figure 3.8i, j).

In Cluster 3, component 1 displays positive zonal wind anomalies (*i.e.* westerlies) over West Africa, above 15°N and anomalous easterlies from East Africa to India (Figure 3.8k). This pattern suggests a weakening and a northward shift of the AEJ, which were found to positively influence rainfall over West Africa (*e.g.* Nicholson, 2009). This is coherent with results found by Lienou *et al.* (2008), showing an increase of rainfall in the Central African area close to the Atlantic coast during the so called small dry season in July-August, which could be associated with a more southern position of the ITCZ from the beginning of the drought years (late 1960s) in West and Central Africa. This pattern is however reversed for the second component, with anomalous easterlies highlighting a clearer position of the AEJ-N above 10°N (Figure 3.8l). Compared to Cluster 1 and Cluster 2, such a pattern is consistent with a northward shift of the ITCZ (Figure 3.8l), which occurs southward of the AEJ-N. At the quasi-decadal timescale (component 3), the negative anomalies observed at the previous timescale are only significant over the western Sahel and parts of the Indian Ocean (Figure 3.8m). Streamflow variability seems to be mainly associated with anomalous westerlies over West Africa between 5 and 10°N (Figure 3.8m). At multi-decadal timescales (components 4 and 5), we note a weakening of AEJ over West and Central Africa (Figure 3.8n-o). Differences between regions over the Gulf of Guinea and the Sahel are presented in supplementary material (S3.2). The main difference between the two regions resides mainly in the latitudinal position of anomalous westerlies, *i.e.* the weakening of the AEJ: southward for Guinean stations and northward for Sahelian stations.

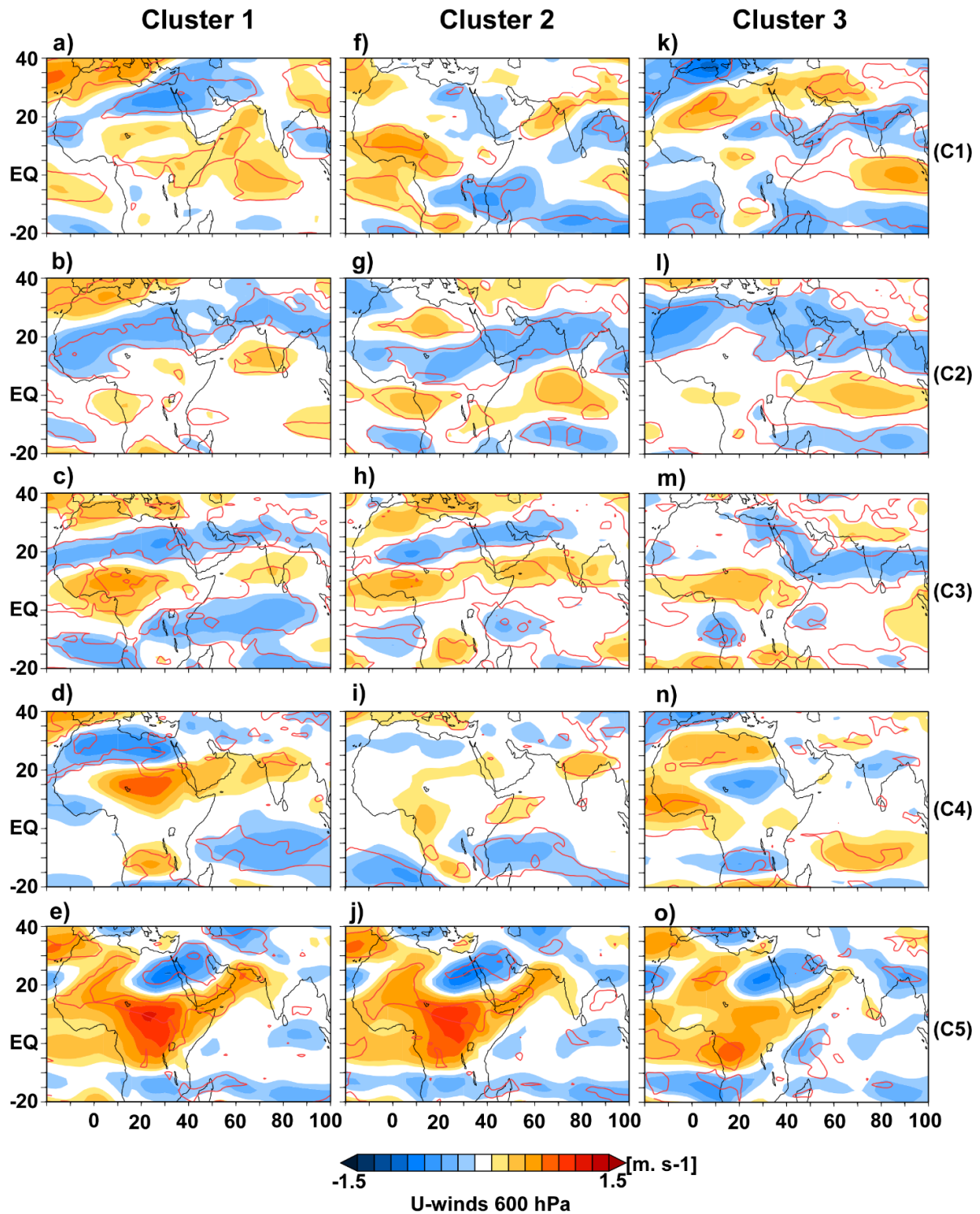


Figure 3.8: Zonal wind circulations in the mid-troposphere (600 hPa) and their interactions with streamflow modes of variability (five components of decomposition). Cluster 1 (a-e), Cluster 2 (f-j) and Cluster 3 (k-o). Composites are presented in shaded colours from dark blue (negative anomalies) to dark red (positive anomalies). Negative anomalies refer to easterly winds, and positive anomalies refer to westerly winds. Red contours highlight significance level $p \leq 0.1$. C1, C2, C3, C4, C5 correspond to component 1, component 2, component 3, component 4 and component 5 respectively.

3.4.1.3. Upper-tropospheric regional circulation anomalies

Upper-tropospheric anomalies, impacting the TEJ, and associated with positive streamflow anomalies, are examined using zonal winds at 200 hPa (Figure 3.9), where is the TEJ located on average (Figure 3.6c). Negative zonal wind anomalies refer to easterly winds, while positive anomalies refer to westerly winds.

Component 1 for the outlet of the Congo basin at Brazzaville (cluster 1) shows positive zonal wind anomalies (*i.e.* westerlies) over most of the study area, except around 20°N where anomalous easterlies are predominant (Figure 3.9a). This pattern suggests a weakening of the jet below 20°N at the interannual timescale (component 1; Figure 3.9a), as westerlies are detected in the average location of the TEJ (Figure 3.6c). This weakening pattern is, however, not stable according to the timescales. Between component 2 and 5 (interannual [6yr] to multi-decadal timescales), positive streamflow anomalies are associated with negative zonal wind anomalies, suggesting a strengthening of the TEJ over the study area (Figure 3.9b-e).

For Cluster 2, at interannual timescales (component 1 and 2), we note significant easterlies over West and Central Africa, which are interspersed by westerlies (Figure 3.9f-g), suggesting regional modulations of the TEJ. At the quasi-decadal timescale (component 3), we note significant westerlies below 15°N (Figure 3.9h), consistently with a weakening of the TEJ. At multi-decadal timescales (component 5), positive streamflow anomalies are mainly associated with anomalous easterlies over the study area (Figure 3.9j), which are consistent with a strengthening of the TEJ.

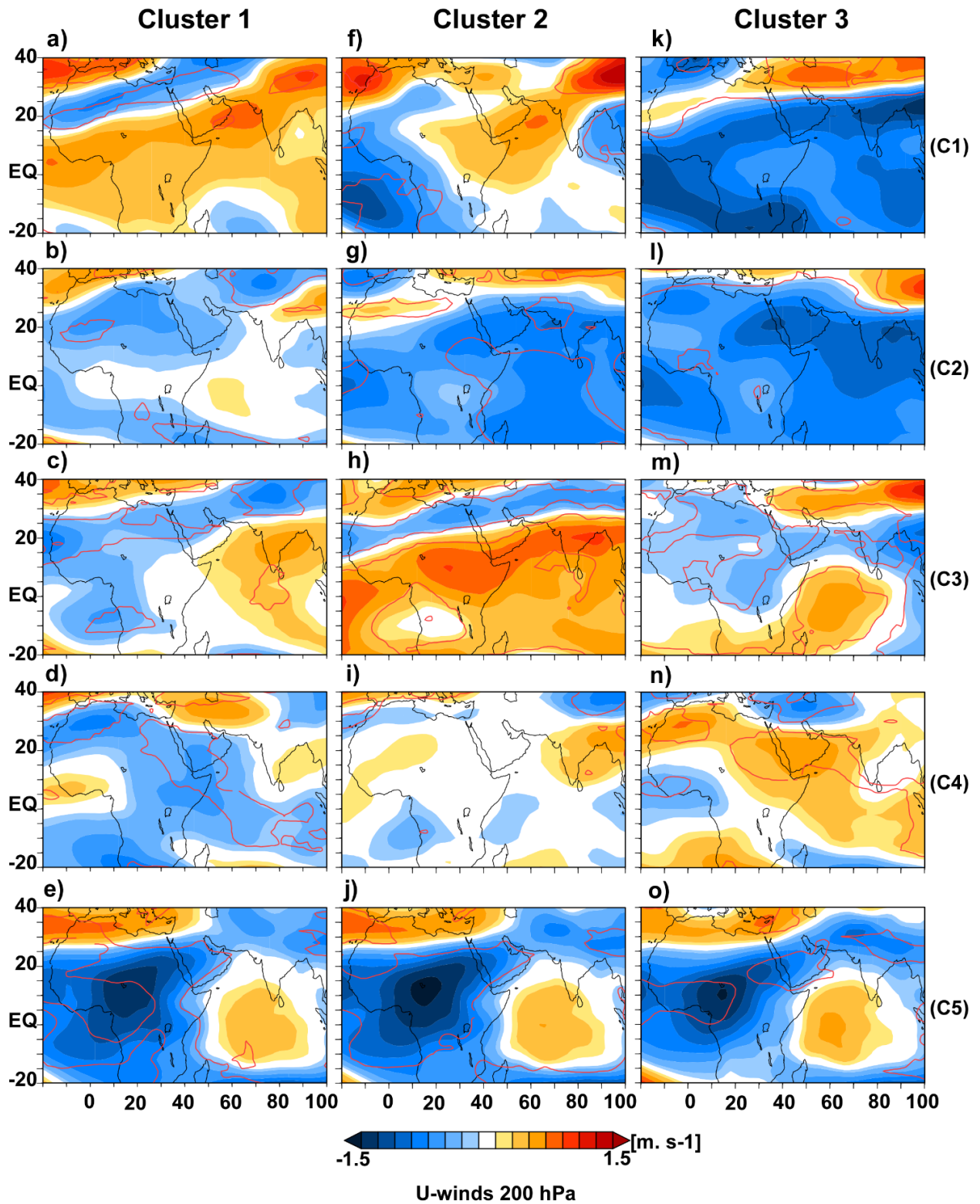


Figure 3.9: Zonal wind circulations in the upper troposphere (200 hPa) and their interactions with modes of streamflow variability (five components of decomposition). Cluster 1 (a-e), Cluster 2 (f-j) and Cluster 3 (k-o). Composites are presented in shaded colours from dark blue (negative anomalies) to dark red (positive anomalies). Negative anomalies refer to easterly winds, and positive anomalies refer to westerly winds. Red contours highlight significance level $p \leq 0.1$. C1, C2, C3, C4, C5 correspond to component 1, component 2, component 3, component 4 and component 5 respectively.

In Cluster 3, interannual timescales (components 1 and 2) are characterized by significant positive anomalies, which extend further North compared to Cluster 1 and Cluster 2 (Figure 3.9k-l), suggesting a strengthening of the TEJ. The importance of strong TEJ in driving positive streamflow phases remains perceptible at decadal timescales, but with regional modulations (Figure 3.9m-n). At multi-decadal timescales (components 5), consistently with cluster 1 and 2, we note a strengthening of the TEJ. Details of contrasts between the Gulf of Guinea and Sahelian regions are provided in supplementary materials (S3.3). While the contrast is obvious for high frequency fluctuations with anomalous easterlies (Sahel) and anomalous westerlies (Gulf of Guinea), low frequency streamflow-TEJ composites are independent of the location.

Over the study area, teleconnections between streamflow and regional atmospheric circulation features (upper and mid-troposphere) display different configurations. Despite dissimilarities observed for high frequency components resulting from the non-stationarity of climatic signals, streamflow variability seems to be mainly driven by a combined effect of TEJ and AEJ: this usefully reinforces previous findings (*e.g.* Nicholson and Grist, 2001; Nicholson, 2009; Dezfuli, 2017). In general, positive streamflow phases are associated with strong TEJ and weak AEJ, resulting in deep convection and high rainfall.

3.4.2. Global SST streamflow teleconnections

For Cluster 1 (Congo basin at Brazzaville), SST-streamflow teleconnections associated with component 1 show significant warm anomalies over the global tropical oceans (Figure 3.10a). This pattern is reversed for the second mode of variability (component 2), *i.e.* significant warm SST in the equatorial Pacific, Tropical South Atlantic and Tropical Indian Ocean (Figure 3.10b). Interestingly, we also note patterns resembling the Atlantic Nino (*e.g.* Rodriguez-Fonseca *et al.*, 2009; Mohino and Losada, 2015) and Indian Ocean dipole (*e.g.* Webster *et al.*, 1999). The contrasts observed between the first two components underline the complexity of processes driving Central African rainfall (*e.g.* Balas *et al.*, 2007) and associated streamflow

variability at interannual timescales. These interannual timescale teleconnections suggest first, a direct impact of local SSTs along the western equatorial coasts. In fact, warm (cold) SSTs in the Atlantic along the Central African coast, result in wet (dry) conditions over the adjacent area (*e.g.* Okumura and Xie, 2006; Dezfuli and Nicholson, 2013). Second, a large-scale forcing from the Pacific and Indian Ocean *via* the so-called “atmospheric bridges” (Dezfuli, 2017). SST teleconnections detected at the quasi-decadal timescale (component 3) present similarities with component 2. In component 3, cold SST anomalies in the equatorial Pacific are however limited to the East, the tropical North Atlantic is warmer, and cold anomalies persist in the tropical South Atlantic (Figure 3.10c). Very similar patterns are then detected in component 4 (Figure 3.10d). At multi-decadal timescale (Figure 3.10e), warm SST anomalies tend to be detected in the northern Hemisphere, while cold SST anomalies are identified in the Southern Hemisphere, describing an inter-hemispheric thermal gradient.

For Cluster 2 (parts of Central Africa and lower Niger River), at the interannual timescale (component 1), we note cold SST anomalies in the equatorial Pacific (La Niña) and warm anomalies both in the tropical Atlantic (Atlantic Nino) and eastern Indian Ocean (Figure 3.10f). These teleconnections (*i.e.* La Niña and Atlantic Nino SST anomalies) prevail and appear more pronounced for the second component (Figure 3.10g). At the quasi-decadal timescale, warm anomalies in the equatorial Pacific may also play an important role (Figure 3.10h). We also observe differences between North Atlantic (warm anomalies), the South Atlantic (cold anomalies) and the Indian Ocean, which is predominantly warm (Figure 3.10h). At quasi-decadal to multi-decadal timescales (Figure 3.10i-j), Cluster 2 presents commonalities with Cluster 1.

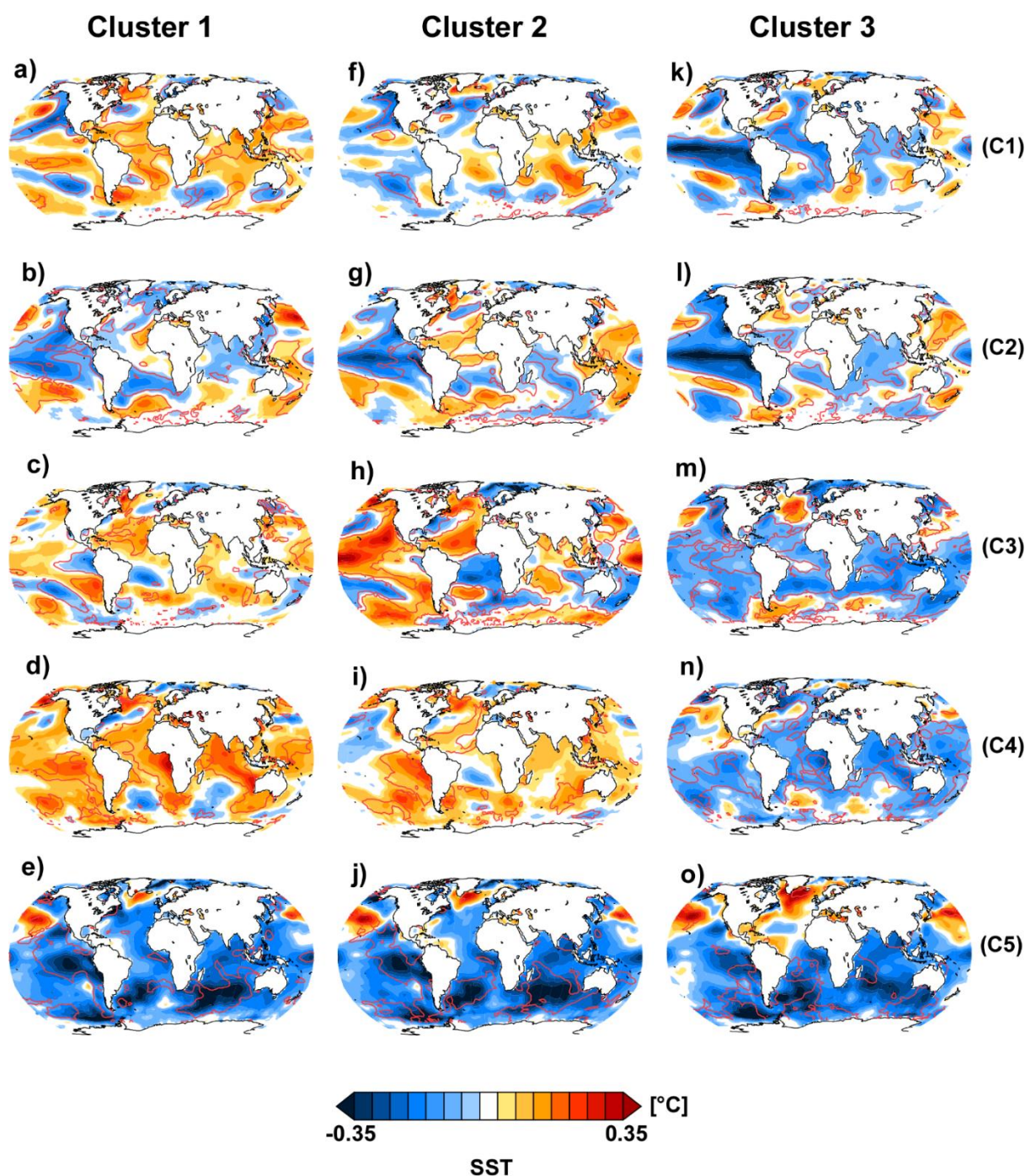


Figure 3.10: Global SST patterns and their interactions with streamflow modes of variability (five components of decomposition). Cluster 1 (a-e), Cluster 2 (f-j) and Cluster 3 (k-o). Composites are presented in shaded colours from dark blue (negative anomalies) to dark red (positive anomalies). Red contours highlight significance level $p \leq 0.1$. C1, C2, C3, C4, C5 correspond to component 1, component 2, component 3, component 4 and component 5 respectively.

For Cluster 3, which covers a larger extent compared to Cluster 1 and Cluster 2, significant streamflow-SST relationships were also detected. As observed in earlier studies (Mahé and Citeau 1993; Fontaine and Philippon, 2000; Losada *et al.*, 2010; Rodriguez-Fonseca *et al.*,

2015; Dieppois *et al.*, 2015), we note cold equatorial Atlantic SSTs at all timescales (Figure 3.10k-o). In addition, at the interannual timescale (component 1 and 2), positive streamflow anomalies are associated with cold SST anomalies in the equatorial Pacific, suggesting strong connections with La Niña events (Figure 3.10k-l). Furthermore, warm anomalies in the eastern Mediterranean consistent with wet conditions over the Sahel due to enhanced moisture flux across the Sahara (Gaetani *et al.*, 2010), are here observed for component 2 (Figure 3.10l). Similarly to Cluster 1 and 2, at multi-decadal timescale (component 4 and, especially, 5), streamflow anomalies are primarily related to interhemispheric SST anomalies, with cold SST in the Southern Hemisphere and warm SST in the northern Hemisphere. This is reminiscent of the Atlantic Multi-decadal Oscillation (AMO), as described in (Mohino *et al.* 2011; Dieppois *et al.*, 2013; Rodriguez-Fonseca *et al.*, 2015), but also the Pacific Decadal Oscillation (PDO; Mantua and Hare, 2002).

Further details regarding streamflow-SST teleconnections for streamflow stations over the Gulf of Guinea and the Sahel are provided in supplementary material (S3.4).

3.4.3. Large-scale convection patterns

Large-scale convection patterns associated with streamflow variability are examined through OLR at the nominal top of the atmosphere in Figure 3.11. In tropical regions, OLR anomalies are used as a proxy for deep-convection processes. Negative OLR anomalies are associated with enhanced deep-convection, while positive OLR anomalies refer to suppressed deep-convection.

For Cluster 1 (Congo basin at Brazzaville), component 1 highlights significant negative OLR anomalies over the equatorial Pacific and western Indian Ocean (Figure 3.11a). This pattern aligns to some extent with SST composites presented in Figure 3.10a. In fact, warm SST anomalies in the Atlantic, Pacific and Indian Oceans are associated with deep convection. In addition, negative anomalies are also detected on the northern fringe on Central Equatorial

Africa. Counterintuitively, positive OLR anomalies, suggesting absence of deep convection, appear over Central Equatorial Africa (Figure 3.11a). This pattern is inherent to the quality of the reanalysis, as similar negative OLR anomalies are observed further South over parts of Central Equatorial Africa in NCEP/NCAR reanalysis 1 (not shown). The second component is characterized by positive OLR anomalies in the equatorial eastern Pacific and negative anomalies in the West, which suggest a westward shift in the Walker circulation (Figure 3.11b). We also note negative OLR anomalies on the continent over Central and eastern Africa, promoting rainfall over this region. The different patterns detected at the interannual timescales (components 1 and 2) thus suggest a link between positive streamflow anomalies over some regions in Central Africa and regional changes in the Walker circulation. At the quasi-decadal timescale (component 3), the Atlantic Nino observed for the same timescale is consistent with deep convection (negative anomalies) over the same region and is associated with a westward shift of the Walker circulation. Negative OLR anomalies are also identified over the western coast of Central Equatorial Africa and eastern Africa, (Figure 3.11c), suggesting regional deep-convection processes and promoting rainfall. At the multi-decadal timescales (components 4 and 5), we note significant negative OLR anomalies over most eastern sub-Saharan Africa, suggesting enhanced deep-convection over the ITCZ region (Figure 3.11d-e). At the same time, western regions of western Africa present significant positive OLR anomalies, *i.e.* damped deep-convection processes, preventing rainfall; this is consistent with a northeastward of the ITCZ, as described in Figure 3.7e. In addition, changes in the western equatorial Pacific also seem to be associated with a large-band of negative OLR anomalies, *i.e.* enhancing deep-convections, over central and eastern Africa (Figure 3.11d-e), hence promoting rainfall.

For Cluster 2, at interannual timescales (components 1 and 2), negative OLR anomalies (*i.e.* enhanced deep-convections) are detected over the Atlantic near the West African coast and over parts of eastern Africa (Figure 3.11f-g). These patterns are consistent with warm SST

anomalies along the Gulf of Guinea and western Indian Ocean (Figure 3.10f-g). Furthermore, cold SST anomalies in the central Pacific are associated with positive OLR anomalies, while warm SST anomalies in the western Pacific are associated with negative OLR anomalies, describing a westward shifted Walker circulation (Figure 3.11f-g). Conversely, for the quasi-decadal timescale (component 3), positive OLR anomalies are detected along the Gulf of Guinea, suggesting a northward position of the ITCZ (Figure 3.11h). Furthermore, we note an eastward (westward) shift of the Walker circulation, associated with cold (warm) SST anomalies and positive (negative) OLR anomalies in the western (central) Pacific (Figure 3.10h, 3.11h). At the multi-decadal timescales, while component 4 highlights a northward shift of the ITCZ over West Africa (Figure 3.11i), component 5 presents deep convection (significant negative anomalies) over most of eastern sub-Saharan Africa, which seem to be embedded in the changes in the Walker circulation (Figure 3.11j).

For Cluster 3, at the interannual timescale, positive streamflow anomalies are associated with a westward shift in the Walker circulation (Figure 3.11k-l), as determined by negative (positive) OLR anomalies in the western (central) Pacific. This is thus consistent with the La Niña-like anomalies detected for this cluster at this timescale (Figure 3.10k-l). Interestingly, a contrast is observed on the continent: component 1 suggests a northward position of the ITCZ, while component 2, highlights a southward shift (Figure 3.11k-l). These patterns, also detected for the moisture flux anomalies (Figure 3.7k-l), result from the wide spatial extent of Cluster 3, which is affected by rainfall conditions over the Sahel and the Gulf of Guinea. Further details regarding differences between these two zones are provided in supplementary material (S3.5). We note that positive streamflow anomalies in Sahelian regions highlight a northward ITCZ position for most timescales, whereas high convective activity is observed along the Gulf of Guinea for Guinean stations. Quasi-decadal to multi-decadal timescales (component 3-5) are

mainly characterized by a northward position of the ITCZ (Figure 3.10m-o) and an eastward shift in the Walker circulation.

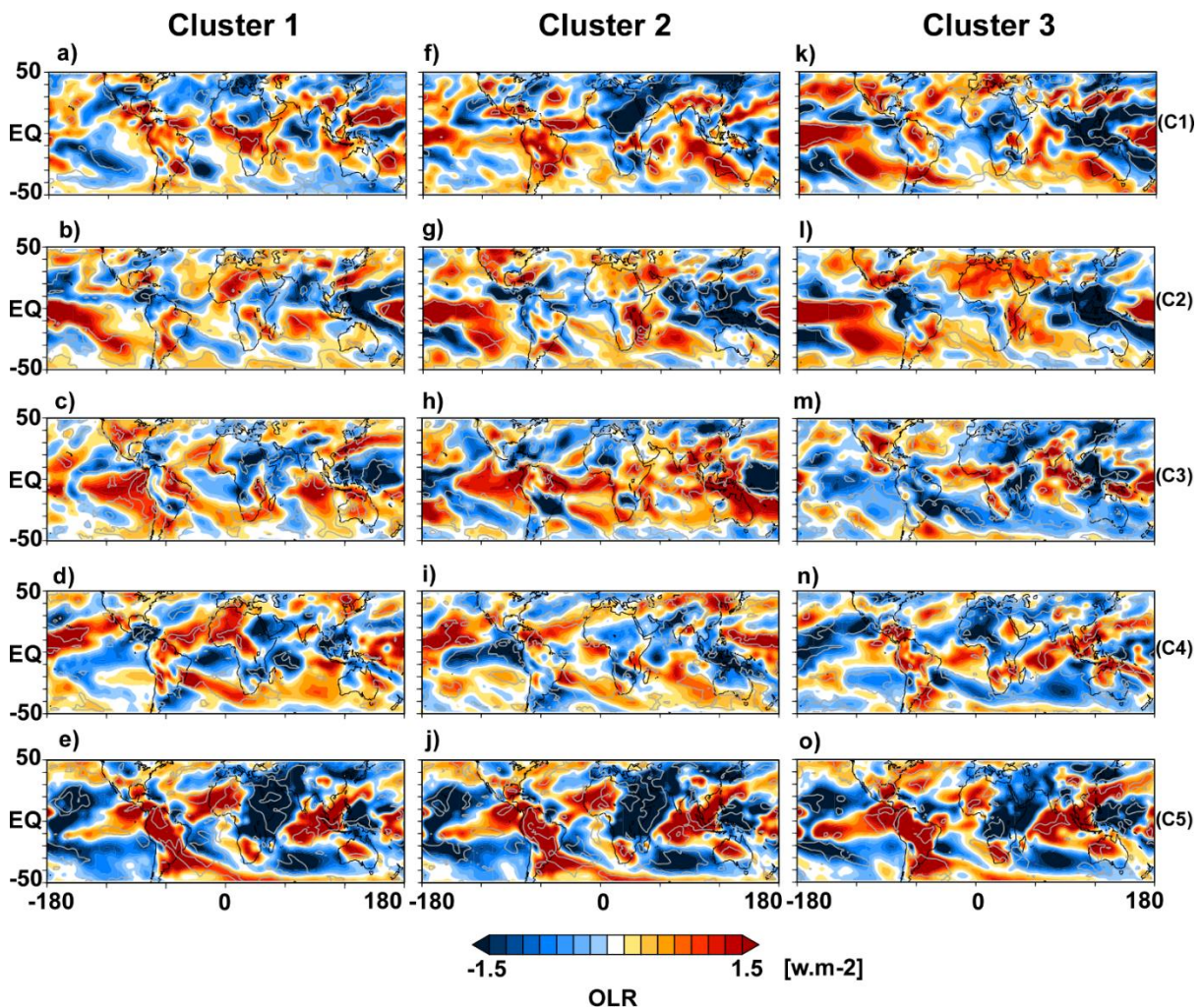


Figure 3.11: Large-scale convection patterns (Outgoing Longwave Radiation at the nominal top of atmosphere) and their interactions with streamflow modes of variability (five components of decomposition). Cluster 1 (a-e), Cluster 2 (f-j) and Cluster 3 (k-o). Composites are presented in shaded colours from dark blue (negative anomalies) to dark red (positive anomalies). Red contours highlight significance level $p \leq 0.1$. C1, C2, C3, C4, C5 correspond to component 1, component 2, component 3, component 4 and component 5 respectively.

Analysis of streamflow and large-scale convection teleconnections over the study area, highlighted the importance of the Walker circulations (for all timescales), mainly induced by SST changes in the Pacific and Indian Oceans (cf. Sect. 3.5.2).

3.5. CONCLUSIONS

Spectral analysis methods applied to reconstructed streamflow time series over West and Central Africa revealed different modes of variability. Over parts of Central Africa and the lower Niger River (Clusters 1&2), streamflow variability is mainly related to interannual and quasi-decadal fluctuations. In most regions of West Africa, however, interannual and quasi-decadal fluctuations are also combined with multi-decadal fluctuations. Dissimilarities in streamflow variability over these two regions are consistent with the findings of Mahé *et al.* (2001), underlining differences in rainfall variability between West and Central Africa between 1951 and 1989. Streamflow variability patterns over West Africa present similarities with rainfall patterns, which were found to exhibit stronger interannual to multi-decadal components (Dieppois *et al.*, 2015).

Decomposition of streamflow modes of variability underlines that, in general, high interannual components are observed along the Gulf of Guinea and the coastal regions of Central Africa, and high multi-decadal components emerge along the Sahelian band. However, local dissimilarities arise in some Sahelian catchments (*e.g.* Wayen in the upper Volta), where interannual components are more important. This high interannual variability is consistent with previous findings, suggesting increased runoff coefficients triggered by land degradation (Mahé *et al.*, 2005; Descroix *et al.*, 2018). Rainfall-runoff relationships investigated at different timescales suggest strong linkages over the study area, except for parts of the Niger River, where the Inner Niger Delta delays peak flows, and in parts of Central Equatorial Africa, where seasonal rainfall distributions have significantly changed over recent decades (Lienou *et al.*, 2008; Mahé *et al.*, 2013). The spatial distribution of streamflow variability modes over the study area suggests that catchment properties serve as a proxy for shaping rainfall-runoff relationships. High interannual variability is generally observed in steep, round catchments with shallow groundwater systems, whereas a greater contribution of multi-decadal timescales

is more likely to occur in large elongated catchments with deep groundwater. At the same time, decadal fluctuations are mainly positively related to vegetation cover and water holding capacity. Such interactions stress the importance of groundwater contributions to streamflow variability in some Sahelo-Sudanian regions as observed by Descroix *et al.* (2018). They highlight the potential harmful effects of vegetation degradation on hydrological regimes in Guinean regions with plutonic geological formations. The role of vegetation is also highlighted in this study through its impact on soil properties (*e.g.* hydraulic conductivity). However, potential feedback of vegetation degradation on climate through increasing CO₂ concentrations, change in surface albedo, evapotranspiration and cloud physics processes (*e.g.* Lawrence and Vandecar, 2015) are beyond the scope of this study.

At the regional scale, streamflow is primarily driven by rainfall and composite analysis revealed significant large-scale teleconnections with rainfall-producing mechanisms. For instance, positive streamflow phases at interannual timescales are associated with a southerly position of the ITCZ for Cluster 1 and Cluster 2 (parts of Central Africa and the lower Niger River) and a northward position for Cluster 3 (mostly West Africa). These teleconnections are different for multi-decadal timescales with a northeastward shift of the ITCZ over the entire study area: this suggests that “the wet Sahel dry Guinean region” paradigm (Nicholson, 2008) mainly holds at interannual timescales only. The relationship between these northeastward ITCZ shifts and, potentially, the Saharan Heat Low (Biasutti *et al.*, 2009; Lavaysse *et al.*, 2010) indicate the important role temperature and pressure fields over the Sahel might also have in driving streamflow variability. Significant teleconnections were also detected for the leading circulation features (AEJ and TEJ). Despite spatial discrepancies, it appears that positive streamflow anomalies over the study area are associated with a stronger TEJ and weaker AEJ. The importance of zonal circulations is also highlighted through shifts in the Walker circulation, as identified using OLR anomalies. Such shifts in the Walker circulation primarily

arise from ocean forcing (Rowell *et al.*, 1995), and especially from zonal gradient in equatorial SST, such as driven by ENSO (*e.g.* Giannini *et al.*, 2005; Rodriguez-Fonseca *et al.*, 2015) at the interannual timescale, and the PDO at decadal timescales (*e.g.* Wang *et al.*, 2014). Interannual streamflow variability is thus associated with warm (Cluster 1 and Cluster 2) and cold (Cluster 3) anomalies in the global tropical oceans, namely the Atlantic Nino, Indian Ocean dipole and ENSO-like patterns in the Pacific Ocean. Meanwhile decadal timescales seem to be dominated by the combined effect of inter-hemispheric SST gradient in the Atlantic and Pacific Ocean: AMO and PDO. Nonetheless, the multi-resolution analysis here has also highlighted divergences between timescales (component 1 and component 2): this underlines the unstable nature of detected teleconnections, consistently with earlier studies of rainfall-SST teleconnections (*e.g.* Rodriguez-Fonseca *et al.*, 2015; Suárez-Moreno *et al.*, 2018).

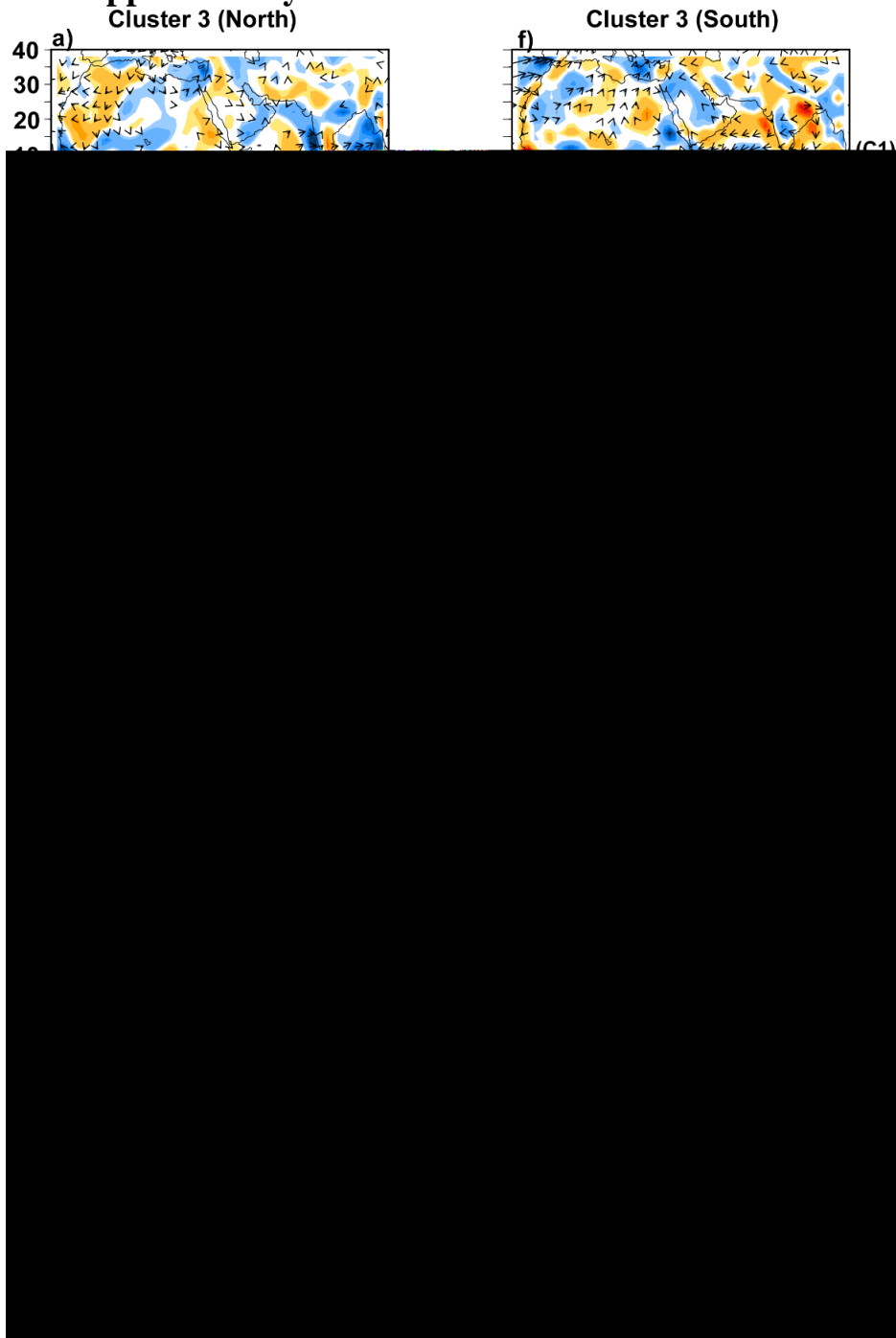
Using multi-timescale analysis approaches which enable the quantification of hydrological fluctuations and associated climatic drivers in modified catchments (Massei *et al.*, 2017), this study sheds light on catchment-scale and climatic drivers of streamflow variability over West and Central Africa. In addition, the teleconnections highlighted herein, present great similarities with those detected for rainfall and therefore open up the potential for robust multi-timescale climate-streamflow prediction in data-scarce environments and better water management strategies. It is crucial, however, to realize that performance of such prediction methods might be constrained over Sahelian regions, given the underestimated multi-decadal climate variability in state-of-the-art GCMs (*e.g.* Ault *et al.*, 2013; Martin *et al.*, 2014) and the shortcomings in the depiction of convective rainfall (Taylor *et al.*, 2017). Although, the focus was on annual averages here, the implemented techniques could be extended to extreme events to unravel the complex processes driving hydrological systems intensification (Taylor *et al.*, 2017; Panthou *et al.*, 2018; Wilcox *et al.*, 2018). Further investigations will include an eclectic approach to reduce uncertainty through comparison of SST-based streamflow predictions and

those resulting from impact studies using climate projections and hydrological models.

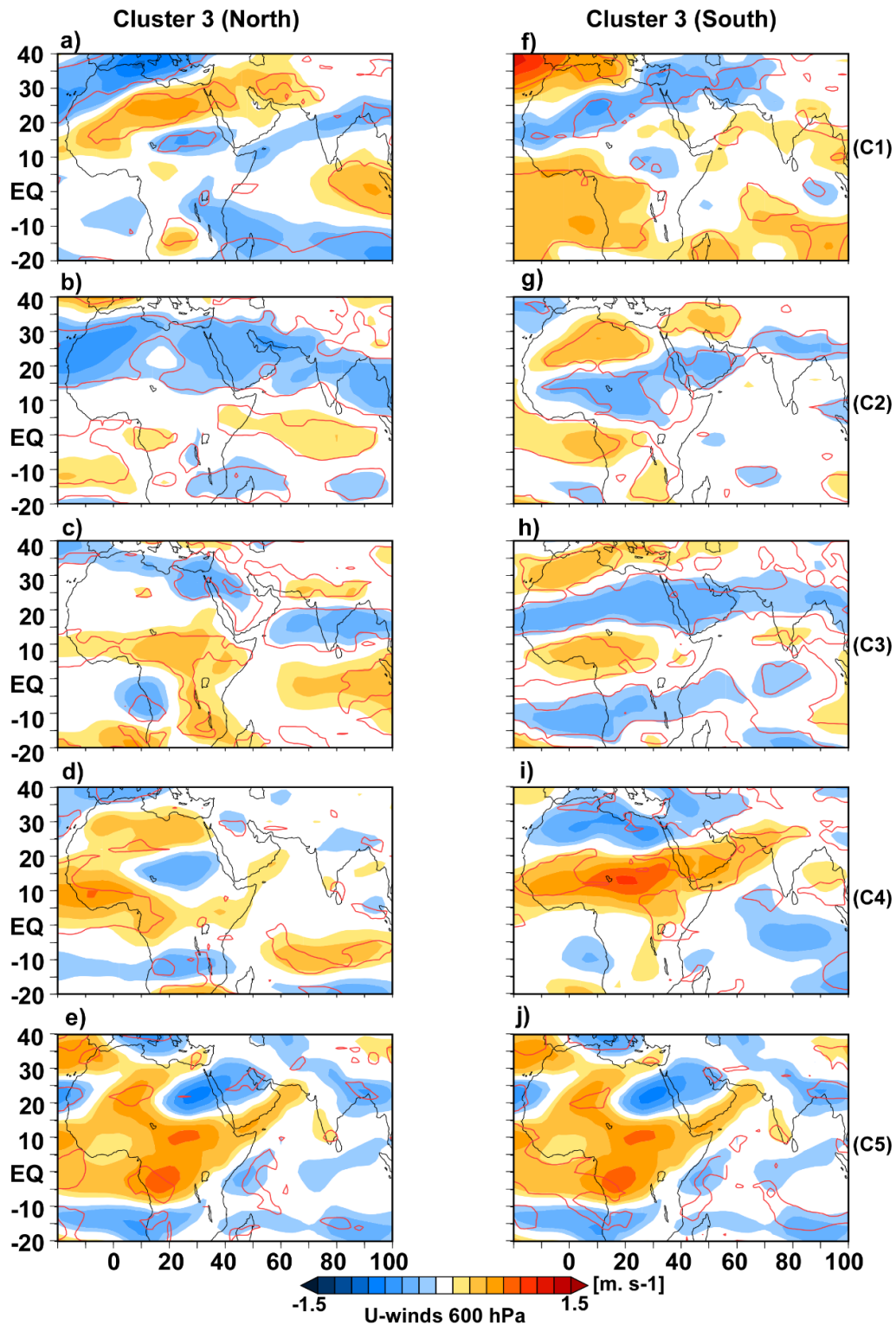
Acknowledgements

Moussa gratefully acknowledges the funding received towards his PhD studies from Coventry University, UK, and resources provided by the Centre for Agroecology Water and Resilience (CAWR). We thank the anonymous reviewers for their insightful comments and suggestions. The authors would like to thank Prof. Nicolas Massei for the helpful discussions.

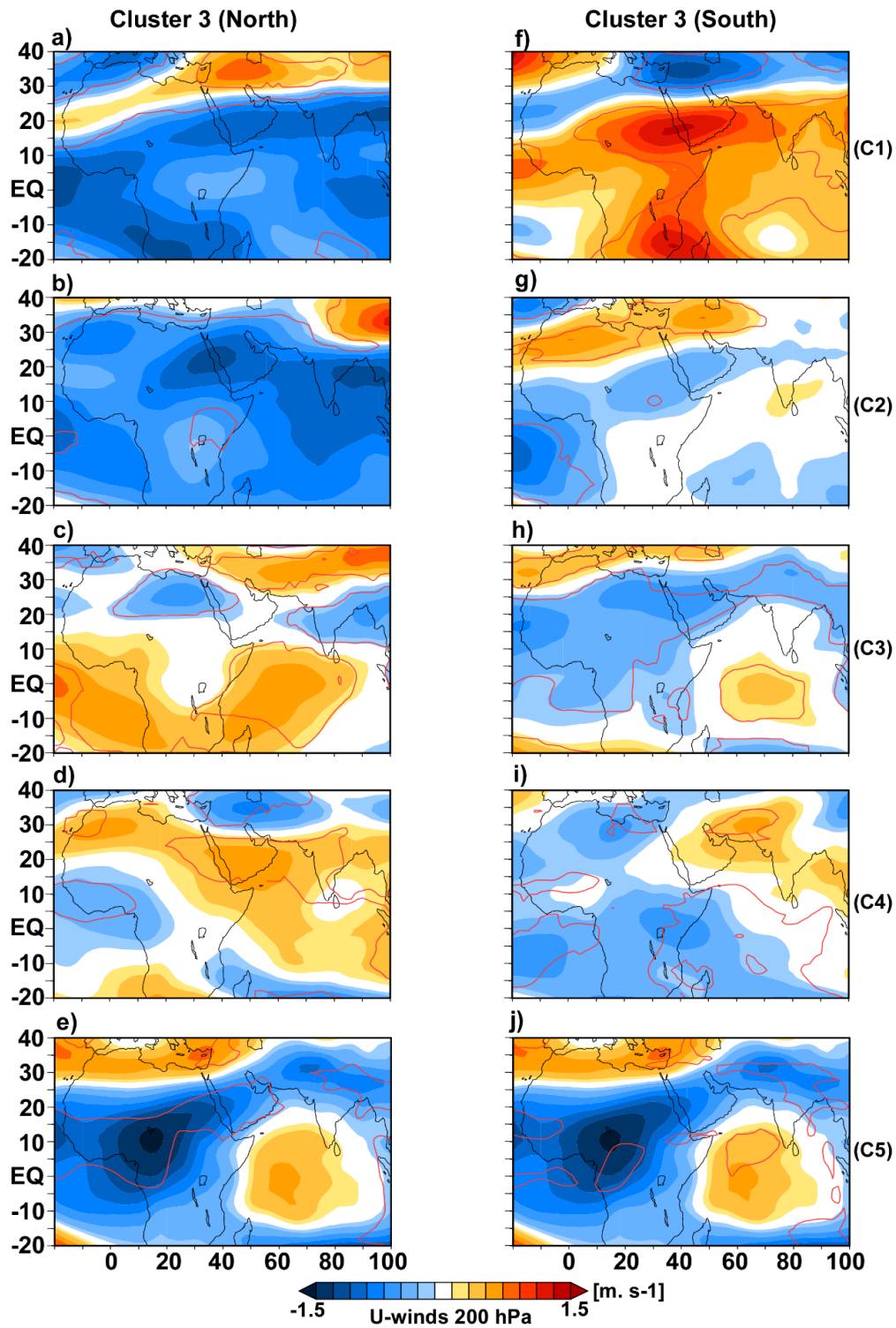
3.6. Supplementary materials



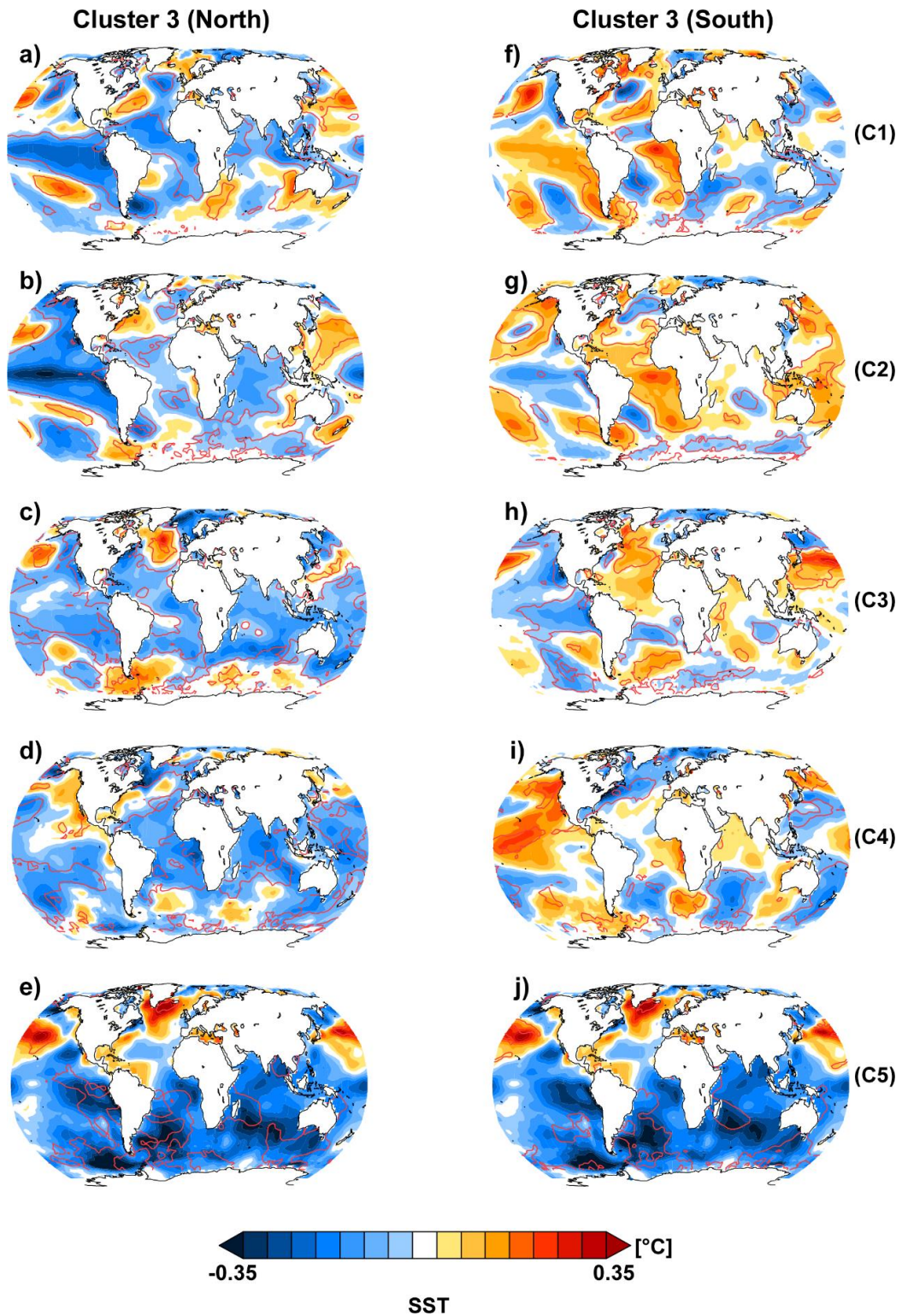
S3.1: Low level winds and their interactions with streamflow modes of variability (five components of decomposition). Sahelian station (a-e), Guinean station (f-j). Only wind vectors significant at $p \leq 0.1$ in their zonal or meridional components are represented. Divergence calculated for the layer is displayed in shaded colours from dark blue (negative anomalies) to dark red (positive anomalies). C1, C2, C3, C4, C5 correspond to component 1, component 2, component 3, component 4 and component 5 respectively.



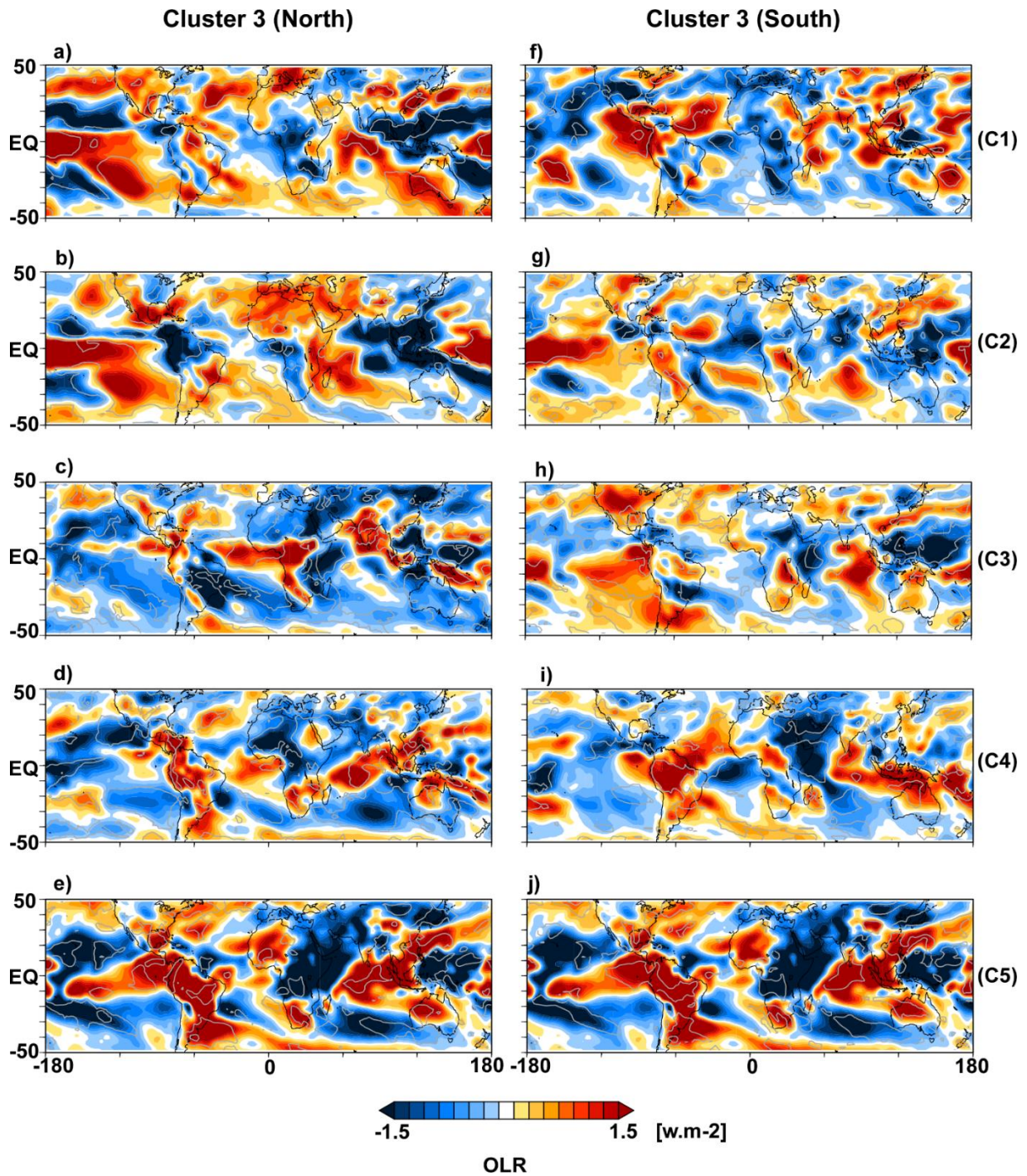
S3.2: Zonal wind circulations in the mid-troposphere (600 hPa) and their interactions with streamflow modes of variability (five components of decomposition). Sahelian station (a-e), Guinean station (f-j). Composites are presented in shaded colours from dark blue (negative anomalies) to dark red (positive anomalies). Negative anomalies refer to easterly winds, and positive anomalies refer to westerly winds. Red contours highlight significance level $p \leq 0.1$. C1, C2, C3, C4, C5 correspond to component 1, component 2, component 3, component 4 and component 5 respectively.



S3.3: Zonal wind circulations in the upper troposphere (200 hPa) and their interactions with modes of streamflow variability (five components of decomposition). Sahelian station (a-e), Guinean station (f-j). Composites are presented in shaded colours from dark blue (negative anomalies) to dark red (positive anomalies). Negative anomalies refer to easterly winds, and positive anomalies refer to westerly winds. Red contours highlight significance level $p \leq 0.1$. C1, C2, C3, C4, C5 correspond to component 1, component 2, component 3, component 4 and component 5 respectively.



S3.4: Global SSTs patterns and their interactions with streamflow modes of variability (five components of decomposition). Sahelian station (a-e), Guinean Station (f-j). Composites are presented in shaded colours from dark blue (negative anomalies) to dark red (positive anomalies). Red contours highlight significance level $p \leq 0.1$. C1, C2, C3, C4, C5 correspond to component 1, component 2, component 3, component 4 and component 5 respectively.



S3.5: Large-scale convection patterns and their interactions with streamflow modes of variability (five components of decomposition). Sahelian station (a-e), Guinean station (f-j). Composites are presented in shaded colours from dark blue (negative anomalies) to dark red (positive anomalies). Red contours highlight significance level $p \leq 0.1$. C1, C2, C3, C4, C5 correspond to component 1, component 2, component 3, component 4 and component 5 respectively.

CHAPTER 4: Impacts of near-term climate change on hydrological systems in West and Central Africa

“There is one issue that will define the contours of this century more dramatically than any other, and that is the urgent threat of a changing climate.”

Barack Obama

Some materials have been removed from this thesis due to Third Party Copyright and confidentiality considerations. Pages where material has been removed are clearly marked in the electronic version. The unabridged version of the thesis can be viewed at the Lanchester Library, Coventry University.

This chapter appears as the following paper submitted for publication

Sidibe, M., Dieppois, B., Eden, J., Mahé, G., Paturel, J. E., Amoussou, E., Anifowose, B., Van De Wiel, M., Lawler, D., (In review). Impacts of near-term climate change on hydrological systems in West and Central Africa. *Climate Dynamics*.

4. Impacts of near-term climate change on hydrological systems in West and Central Africa

Abstract - Climate change is expected to significantly impact on the availability of water resources in West and Central Africa through changes in rainfall, temperature and evapotranspiration. Understanding these changes in this region, where surface water is fundamental for economic activity and ecosystem services, is of paramount importance. In this study, we examine the potential impacts of climate change on hydrological systems by the mid-21st century in West and Central Africa, as well as the uncertainties in the different climate-impact modelling pathways. Simulations from nine global climate models downscaled using the Rossby Centre Regional Climate model (RCA4) are evaluated and subsequently bias-corrected using a nonparametric trend-preserving quantile mapping approach. We then use two conceptual hydrological models (GR2M and IHACRES), and a regression-based model built upon multi-timescale sea surface temperatures and streamflow teleconnections, to understand hydrological processes at the subcontinental scale and provide hydrological predictions for the near-term future (2020-2050) under the RCP4.5 emission scenario.

The results highlight a zonal contrast in future precipitation between western (dry) and eastern (wet) Sahel, and a robust signal in rising temperature, suggesting an increase in potential evapotranspiration, across the multi-model ensemble. Overall, a significant increase in discharge (~+5%) is expected by the mid-21st century over the region, albeit with high uncertainties reported over most of Central Equatorial Africa inherent to climate models and gridded observation data quality. Interestingly, in this region, teleconnections-based regression models tend to be a more reliable alternative to hydrological models.

Keywords: *Climate change, Hydroclimatic variability, rainfall-runoff modelling, streamflow projections, RCP4.5 scenario, West and Central Africa.*

4.1. INTRODUCTION

In Sub-Saharan Africa, more than 60% of the population relies heavily on rainfed agriculture and surface water to sustain a living. This part of the world is identified as one of the most vulnerable to climate change (IPCC, 2014; Serdeczny *et al.*, 2017). In particular, the increased risk of droughts and floods, predicted to result from global warming (*e.g.* Aich *et al.*, 2014), is very likely to have severe implications for both natural and human systems. Development of adaptation strategies to adequately tackle the harmful effects of climate change on water resource availability, food production and ecosystem services is one of the most important challenges faced in Sub-Saharan Africa (*e.g.* Aloysius *et al.*, 2016). Such adaptation strategies depend on reliable climate change scenarios and a good representation of different hydrological processes. Climate impacts on hydrological systems are often investigated through a modelling chain whereby outputs of different climate models under different greenhouse gases emission scenarios are used as inputs for hydrological models (*e.g.* Clark *et al.*, 2016; Hattermann *et al.*, 2018). This process however is limited, particularly by the quality of observational datasets and the uncertainties introduced at both the climate (*e.g.* Yira *et al.*, 2017) and hydrological modelling steps (*e.g.* Steinschneider *et al.*, 2015; Clark *et al.*, 2016; Kauffeldt *et al.*, 2016; Giuntoli *et al.*, 2018).

Despite significant advances in climate modelling, both global climate models (GCMs) and regional climate models (RCMs) exhibit important biases in their characterization of West and Central Africa hydroclimatic variability (*e.g.* Druyan *et al.*, 2010; Nikulin *et al.*, 2012, Salack *et al.*, 2015; Aloysius *et al.*, 2016; Mba *et al.*, 2018). These biases result to some extent from: (1) the influence of climate forcings or unrealistic large-scale variability; (2) poor representation of internal variability and; (3) errors in parameterization schemes and unresolved subgrid-scale orography (Eden *et al.*, 2012). The discrepancies observed in future climate change scenarios over the region, which are more pronounced in precipitation than

temperature trends (*e.g.* Aloysius *et al.*, 2016; Yira *et al.*, 2017), need to be reduced prior to any climate change impact assessment. Some authors demonstrated the importance of multi-model approaches in reducing uncertainties of hydroclimatic scenarios (*e.g.* Déqué *et al.*, 2007). Furthermore, projections for the near-term climate, defined in the fifth assessment report (AR5) of the Intergovernmental Panel on Climate Change (IPCC) as the period from present through mid-century (IPCC, 2013), tend to be less sensitive to Representative Concentration Pathways (RCP) scenarios (Hawkins and Sutton, 2009; IPCC, 2013; Sylla *et al.*, 2016). Relatively few studies have considered multi-model ensembles for impact assessment at the scale of Sub-Saharan Africa (*e.g.* Mbaye *et al.*, 2015; Oyerinde *et al.*, 2016; Yira *et al.*, 2017). Even in the case that this approach successfully accounts for climate model-related uncertainties, realistic hydrological simulations still require a postprocessing step to remove systematic bias from hydroclimate variables. So-called bias correction algorithms (*e.g.* Maraun *et al.*, 2010; Teutschbein and Seibert, 2012; Yira *et al.*, 2017) are often associated with an additional source of uncertainty whose impacts are increasing with the length of the projection lead-time (Hingray and Said, 2014). In the context of hydrological climate change impact studies, nonparametric quantile mapping bias-correction approaches appear more appropriate, as they can be applied without specific assumptions regarding the nature of the underlying statistical distribution (Gudmundsson *et al.*, 2012). However, some of these methods, despite preserving trends in long-term mean states, result in erroneous trends in extreme quantiles (Cannon *et al.*, 2015). It is therefore important that physical consistency and climate model sensitivity are not altered by bias-correction (Hempel *et al.*, 2013).

Hydrological model uncertainty, while in general lesser than climate model uncertainty, ought to be also accounted for in climate change impact studies, at least for near-term regional projections (Giuntoli *et al.*, 2018). Hydrological simulations in natural ecosystems are always limited by simplified representation of complex processes occurring in the real world (Paturel

et al., 2003; Clark *et al.*, 2008; Dezetter *et al.*, 2008). However, complex physically-based models do not necessarily yield better results than simpler models, especially in data-scarce regions, due to the large number of parameters and their inherent uncertainties (Singh and Marcy, 2017). Identifying the most suitable hydrological model for a given purpose remains an outstanding challenge for the hydrological community. Nonetheless, a multi-model approach favouring different model structures provides better characterization of different hydrological processes (*e.g.* Clark *et al.*, 2008, 2016). To address the caveat concerning hydrological model structures and bias-correction methods, some researchers have suggested streamflow predictions using regression models based on large-scale climate teleconnections (*e.g.* Chiew and McMahon, 2002; Kingston *et al.*, 2013). As reported in Sidibe *et al.* (2019), most of these studies focus on specific regions (mainly regions with sufficiently long and complete observation records) and climatic indices, and therefore lack of reproducibility at larger spatial scales.

The comprehensive review of previous studies investigating the impact of climate change on water resources in West Africa by Roudier *et al.* (2014), underlines the fact that existing studies mainly focus on individual basins with climate change scenarios often provided by coarse spatial scale GCMs or early versions of RCMs. At the sub-continental scale, the impacts of climate change on hydrological systems over West and Central Africa are not fully understood (Washington *et al.*, 2013; Roudier *et al.*, 2014). The study by Stanzel *et al.* (2018) bridges this gap over West Africa by applying a multi-model ensemble of 15 RCMs from the CORDEX initiative (Coordinated Regional Climate Downscaling Experiment; Giorgi *et al.*, 2009). However, in the latter, streamflow is estimated using a water balance model (at the annual timescale), which does not fully describe the complexity of hydrological processes. Moreover, climate projections are corrected using the widely applied delta-change approach, which, while stable and robust, does not account for potential future changes in climate fluctuations and

makes no distinction between extreme and normal events (*i.e.* the amount of change is similar for heavy rainfall and drizzle; Teutschbein and Seibert, 2012).

Here, we aim to provide further insights into the response of hydrological systems to a changing climate across West and Central Africa by the mid-21st century. Climate simulations from the Rossby Centre Regional Climate model (RCA4) driven by nine GCMs available within the CORDEX initiative are evaluated and bias-corrected using a nonparametric trend preserving quantile mapping approach (QDM; Cannon *et al.*, 2015). We then use two conceptual hydrological models to understand hydrological processes at the subcontinental scale and provide future hydrological scenarios. For the first time, we also assess uncertainty inherent to hydrological model structures and bias correction algorithms through the implementation of a regression-based model linking streamflow with sea surface temperature (SST).

4.2. Data and Methods

The study area covers West and Central Africa (from 10°S to 25°N and 20°W to 30°E), with different climatic conditions: from arid in the northern fringe to tropical humid in the South. Hydrological regimes are described in Sidibe *et al.* (2018). Over the study area, 131 catchments with sizes ranging from 197 to 3,700,000 km² (median of 20,492 km²) were considered.

4.2.1. Data

Streamflow and catchment properties (*e.g.* area, elevation, shape) datasets were collected from the SIEREM (“*Système d’Informations Environnementales sur les Ressources en Eaux et leur Modélisation*”) database (Boyer *et al.*, 2006; Dieulin *et al.*, 2019). Over the study area, 131 discharge stations from the reconstructed streamflow dataset presented in Sidibe *et al.* (2018) were selected. Information about selected watersheds is provided in Appendix A.

Observed mean monthly precipitation (P), minimum and maximum temperature (T_{min} and T_{max}, respectively) datasets for the historical period (1951-2005) were collected from the Climatic Research Unit (CRU TS v4.00; Harris *et al.*, 2014). Harris *et al.* (2014) found good agreement

between the CRU dataset and other datasets, such as the Global Precipitation Climatology Centre (GPCC; Schneider *et al.*, 2011). Due to the large scale of the study and climatic data availability/quality, evapotranspiration is estimated using relatively few input variables. The method used herein (eq.1), after Droogers and Allen (2002), is a modified version of the Hargreaves approach (Hargreaves and Samani, 1985), which accounts for precipitation as a proxy for insolation and relative levels of humidity. Such an approach is a reliable alternative to the more physically based Penman-Monteith equation for data scarce environments (Allen *et al.*, 1998).

$$PET = 0.0013 * 0.408R_{et} * (T_{avg} + 17.0) * (Td - 0.0123P)^{0.76} \quad (\text{eq.1})$$

With P the monthly precipitation amount (mm), R_{et} the extra-terrestrial radiation (MJ.m^{-2}), T_{avg} the average temperature ($^{\circ}\text{C}$) and Td the temperature range ($^{\circ}\text{C}$). R_{et} is approximated from the latitude and the month of the year.

The Extended Reconstructed SST version 5 (ERSST.v5, Huang *et al.*, 2017) is used to develop multi-timescale linear regression models based on large-scale climate teleconnections. ERSST.v5 is a global monthly $2^{\circ}\times 2^{\circ}$ gridded SST dataset derived from the International Comprehensive Ocean–Atmosphere Dataset (ICOADS) Release 3.0. In addition, climate simulations (P , T_{max} , T_{min}) from nine GCMs of the fifth phase of the Coupled Model Intercomparison Project (CMIP5; Taylor *et al.*, 2012), dynamically downscaled by the latest version of the Rossby Centre Regional Climate Model (RCA4), developed by the Swedish Meteorological and Hydrological Institute (SMHI) and available within the CORDEX framework, were collected via the Earth System Grid Federation (ESGF) data portals (Table 1).

Table 4.1: List of datasets and climatic variables used in the study

		Institution	Name	Variable	Period
Obs.		SIEREM, <i>France</i>	SIEREM	$Q, Area$	1951-2005
		CRU, <i>UK</i>	CRU TS v.4.00	P, T_{max}, T_{min}	1951-2005
		NOAA-NCDC, <i>USA</i>	ERSST.v5	sst	1951-2005
CMIP5 Model outputs	GCM	CCCma, <i>Canada</i>	CanESM2	sst	1951-2050
		CNRM, <i>France</i>	CNRM-CM5		
		CSIRO-QCCCE, <i>Australia</i>	CSIRO-Mk3-6-0		
		MOHC, <i>UK</i>	HadGEM2-ES		
		IPSL, <i>France</i>	IPSL-CM5A-MR		
		MIROC, <i>Japan</i>	MIROC5		
		MPI-M, <i>Germany</i>	MPI-ESM-LR		
		NCC, <i>Norway</i>	NorESM1-M		
		NOAA-GFDL, <i>USA</i>	GFDL-ESM2M		
	RCM	SMHI, <i>Sweden</i>	CanESM2_SMHI-RCA4	P, T_{max}, T_{min}	
			CNRM-CM5_SMHI-RCA4		
			CSIRO-Mk3-6-0_SMHI-RCA4		
			HadGEM2-ES_SMHI-RCA4		
			IPSL-CM5A-MR_SMHI-RCA4		
			MIROC5_SMHI-RCA4		
MPI-ESM-LR_SMHI-RCA4					
NorESM1-M_SMHI-RCA4					
GFDL-ESM2M_SMHI-RCA4					

The multi-model ensemble is downscaled using a single RCM to constrain the uncertainty inherent to process representation within different RCMs. Previous studies highlighted that the SMHI-RCA family of models satisfactorily represents different characteristics of historical precipitation and temperatures over West Africa (Nikulin *et al.*, 2012; Mascaro *et al.*, 2015; Stanzel *et al.*, 2018).

Streamflow near-term projections (2020-2050) are then derived from two hydrological models, and a teleconnection-based regression model using SST fields from the nine aforementioned

GCMs. With a view to reduce the uncertainty in streamflow projections associated with RCP scenarios over the near-term future (Hawkins and Sutton, 2009; IPCC, 2013; Sylla *et al.*, 2016), we only considered a single future scenario, *i.e.* RCP 4.5 (corresponding to a medium range emission and high mitigation with radiative forcings stabilized at 4.5 W.m^{-2} and 650 ppm CO_2 equivalent in the year 2100; Moss *et al.*, 2010).

4.2.2. Methods

4.2.2.1. Bias correction

Climate simulations are compared to corresponding observed fields for the period 1951-2005 with Quantile Delta Mapping (QDM; Cannon *et al.*, 2015) applied as a bias correction algorithm. Standard quantile mapping techniques are limited by the assumption of bias stationarity (*i.e.* future climatic conditions are identical to those observed in the historical period; Cannon *et al.*, 2015). More advanced algorithms tackle this issue by applying quantile mapping on detrended time series (*i.e.* removing trend in the long-term mean) and reintroducing the trend afterwards (detrended quantile mapping). This however preserves only the climate change signal in the mean, while changes in other quantiles (extremes) are not accounted for. QDM preserves changes in simulated quantiles from climate models.

Discrepancies between model simulations and observations over a given period are corrected by: (1) detrending model-projected future quantiles and applying quantile mapping on the detrended series; (2) preserving the climate sensitivity by reintroducing projected trends on bias-corrected results. More details about the different steps are provided in Cannon *et al.* (2015).

The method is applied at each grid point within the study area, and to each month individually for a better representation of seasonal cycles. Biases in future simulations (2006-2050) are corrected using transfer functions derived over the entire historical period (1951-2005) to

mitigate to some extent the so-called “variability related apparent bias changes” (Maraun, 2012).

A K-fold (K=11) cross-validation approach (Geisser, 1975) is separately implemented to assess the performance of bias-correction algorithms. For each grid-point we generate a cross-validated time series consisting of all validation segments. Performance of the bias-correction algorithms is first assessed with respect to the overall deviation between simulations and observations using the percent bias (PBIAS). Second, we investigate biases in cumulative distribution functions (CDFs) using the Kolmogorov-Smirnov (K-S) test, with the null hypothesis being that both samples (observations and simulations) are drawn from the same statistical distribution.

4.2.2.2. Hydrological modelling

Identifying the most appropriate model structure for the characterization of hydrological processes and quantifying associated uncertainties are the main challenges facing the hydrological community (Clark *et al.*, 2008). In this study, two hydrological models (GR2M and IHACRES) are used to investigate the impacts of climate change on streamflow over West and Central Africa. Both models are computationally attractive (due to few calibration parameters), and therefore convenient for data-scarce environments.

GR2M is a two parameter spatially lumped conceptual monthly rainfall-runoff model developed by the IRSTEA (*Institut national de Recherche en Sciences et Technologies pour l'Environnement et l'Agriculture*). In the version used herein (developed by Mouelhi *et al.*, 2006), hydrological processes are described using two reservoirs: a production reservoir with capacity X1 and a routing reservoir (fixed capacity of 60 mm), whose interactions with groundwater systems are governed by the parameter X2 (Figure 4.1a). Due to its robustness and very low input data requirement (precipitation, potential evapotranspiration and

streamflow), the GR2M model has been extensively used in West and Central Africa (e.g. Paturel *et al.*, 1995; Dezetter *et al.*, 2008; Ardoin-Bardin *et al.*, 2009; Ibrahim *et al.*, 2015).

The IHACRES model is a conceptual-metric model built upon a non-linear soil moisture accounting module (Jakeman *et al.*, 1990), which converts total precipitation into effective rainfall and a linear routing module generating stream discharge from effective rainfall. In this study, the non-linear soil moisture accounting module is based on the Catchment Wetness Index (CWI; Jakeman and Hornberger, 1993), where effective rainfall is proportional to an antecedent soil moisture index and a scaling factor used to enforce mass balance. The soil moisture accounting module is built upon three main calibration parameters: the drying rate at reference temperature, the temperature dependence of drying rate and the mass balance term. The linear routing module is represented by two reservoirs (quick flow and baseflow) in parallel. The outflow is then processed using ARMAX-type (auto-regressive moving average with exogenous inputs) linear transfer functions (Jakeman *et al.*, 1990) to generate simulated streamflow (Figure 4.1b).

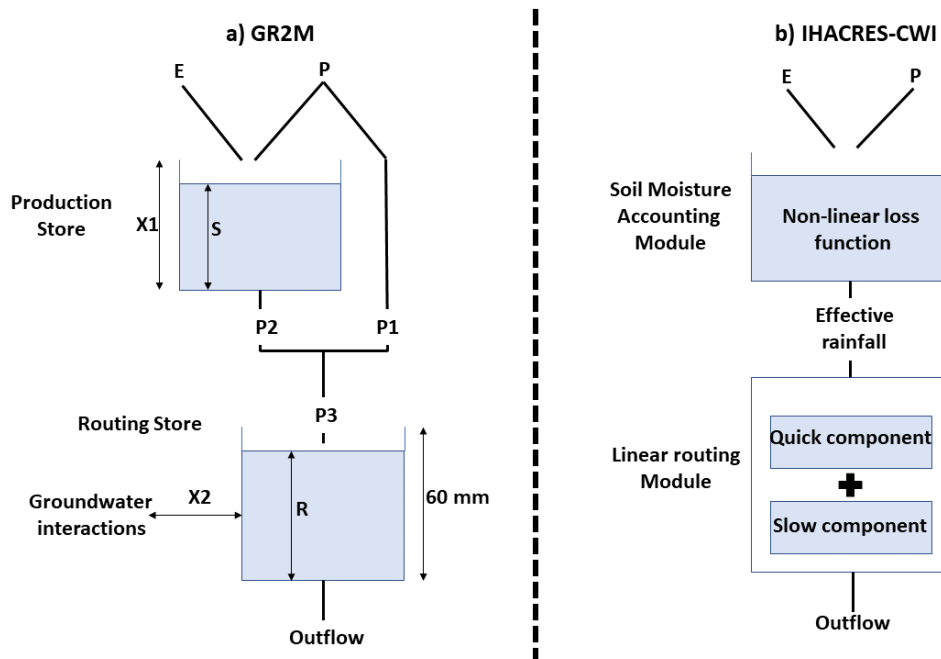


Figure 4.1: Hydrological model structures a) GR2M hydrological model (adapted from Mouelhi et al., 2006) b) IHACRES-CWI hydrological model (adapted from Jakeman and Hornberger, 1993).

Such a formulation reduces parameter uncertainty inherent to hydrological models, while at the same time attempting to characterize internal hydrological processes (Croke and Jakeman, 2004). This model implemented for the Niger River basin by Oyerinde *et al.* (2016) yielded satisfactory results.

4.2.2.3. Regression-based SST-streamflow model

Sidibe *et al.* (2019) found streamflow variability in West and Central Africa to be significantly associated with SST anomalies in the Pacific and Atlantic Oceans at different timescales: interannual (~2-5 years) to multi-decadal (> 20 years). Such relationships are similar to those detected for rainfall over the region (*e.g.* Mohino *et al.*, 2011; Rodriguez-Fonseca *et al.*, 2015; Dieppois *et al.*, 2013, 2015; Sheen *et al.*, 2017). Building upon these teleconnections, we thus use multiple regressions of annual streamflow on empirical orthogonal functions (EOFs) of SST fields following the modelling strategy developed by Benestad (2001). This approach is modified based on the findings of Massei *et al.* (2017) to fully capture the main modes of variability.

In data-scarce regions, this streamflow prediction strategy, due to the lower number of input variables (Streamflow and SST), could potentially help narrowing the uncertainty associated with the quality of gridded observational datasets (*e.g.* rainfall and temperature), which is likely to be poor and substantially impact the robustness of bias correction and hydrological modelling. The main steps are: (1) to generate individual predictor datasets (1951-2050) by combining (along the time axis) observations (ERSST v5) and GCMs SST fields; (2) to extract wavelet details using the Maximum Overlap Discrete Wavelet Transform (MODWT; Percival and Walden, 2000) for both predictors and predictands; (3) to implement one regression model for each wavelet decomposition level of the atmospheric field and local hydrometeorological variables using the common EOF analysis; and (4) to reconstruct the final time series by summing up all models at the end of the process.

Linear step-wise regression models are calibrated using principal components (PCs) of the 20 leading EOFs representing the observation part of the combined dataset. The selected PCs derived from future GCM simulations are then used to generate streamflow projections. Using the common EOF analysis ensures the physical consistency of climate model simulations (Benestad, 2001).

A K-fold cross-validation is also implemented (K=11), and performance is assessed with the Kling Gupta efficiency criteria (Kling *et al.*, 2012).

4.3. Results

4.3.1. Climate scenarios: evaluation and bias-correction

4.3.1.1. Model evaluation

The ability of climate models to reproduce historical (1951-2005) climatic patterns is assessed relatively to the CRU observation datasets.

4.3.1.1.1. Precipitation patterns

The spatial distribution of precipitation (mean climatology) for the period 1951-2005, is characterized by a strong meridional gradient, with highest amounts found in the Southwest and Southeast of West Africa and Central Equatorial Africa (Figure 4.2a), as observed by Mahé *et al.* (2001). Major parts of the study area receive around 61.4 mm.month⁻¹, with maximum reaching 253 mm.month⁻¹ (Figure 4.2a). Most models are able to capture this meridional gradient, but dissimilarities are observed in the representation of the spatial extent and rainfall amounts (figure 4.2b). Over West Africa, most models except CNRM and CSIRO capture relatively well the regions of maximum precipitation, despite overestimations along the Guinean highlands (Figure S4.1), as suggested by Akinsanola *et al.* (2018). In addition, precipitation patterns over the Sahel (between 11°N and 18°N) are generally well-represented, except for CanESM2 and IPSL, where the region of minimum rainfall (<25 mm.month⁻¹) extends southwards to 15°N. This can be attributed to model representation of the ITCZ northward propagation and gradual southward retreat (Nikulin *et al.*, 2012). In fact, all models

fail at representing the pattern observed in Central Equatorial Africa (Figure 4.2a-b), leading to higher biases in total precipitation. More specifically, the magnitude of deviation between RCA4 simulations and CRU observations (assessed using the PBIAS) over the entire historical period (1951-2005) underlines a dry bias (between -20% and -35%) in Central Africa regardless of the driving GCMs (Figure 4.2c-k), consistently with the findings of Aloysius *et al.* (2016). A dry bias is also observed in the Guinean Coastal regions (4°N-8°N) for most models, except MIROC5 (median PBIAS of +6.4%) (Figure 4.2c-k). Further North, the influence of driving GCMs becomes more important. In Sudanian (8°N-11°N) and Sahelian (11°N-18°N) regions for instance, models such as CanESM2, CNRM, HadGEM2, IPSL and NCC present negative biases (reaching -62.9% for IPSL), while others present wet biases (up to +40% for CSIRO over the Sahel). Overall the mean climatology is best represented by MIROC5 (median PBIAS of 0.25%), HadGEM2 (median PBIAS of -2.6%) and NCC (median PBIAS -7.9%) (Figure 4.2h, f, j). Similar results are found for the NRMSE statistic (not shown).

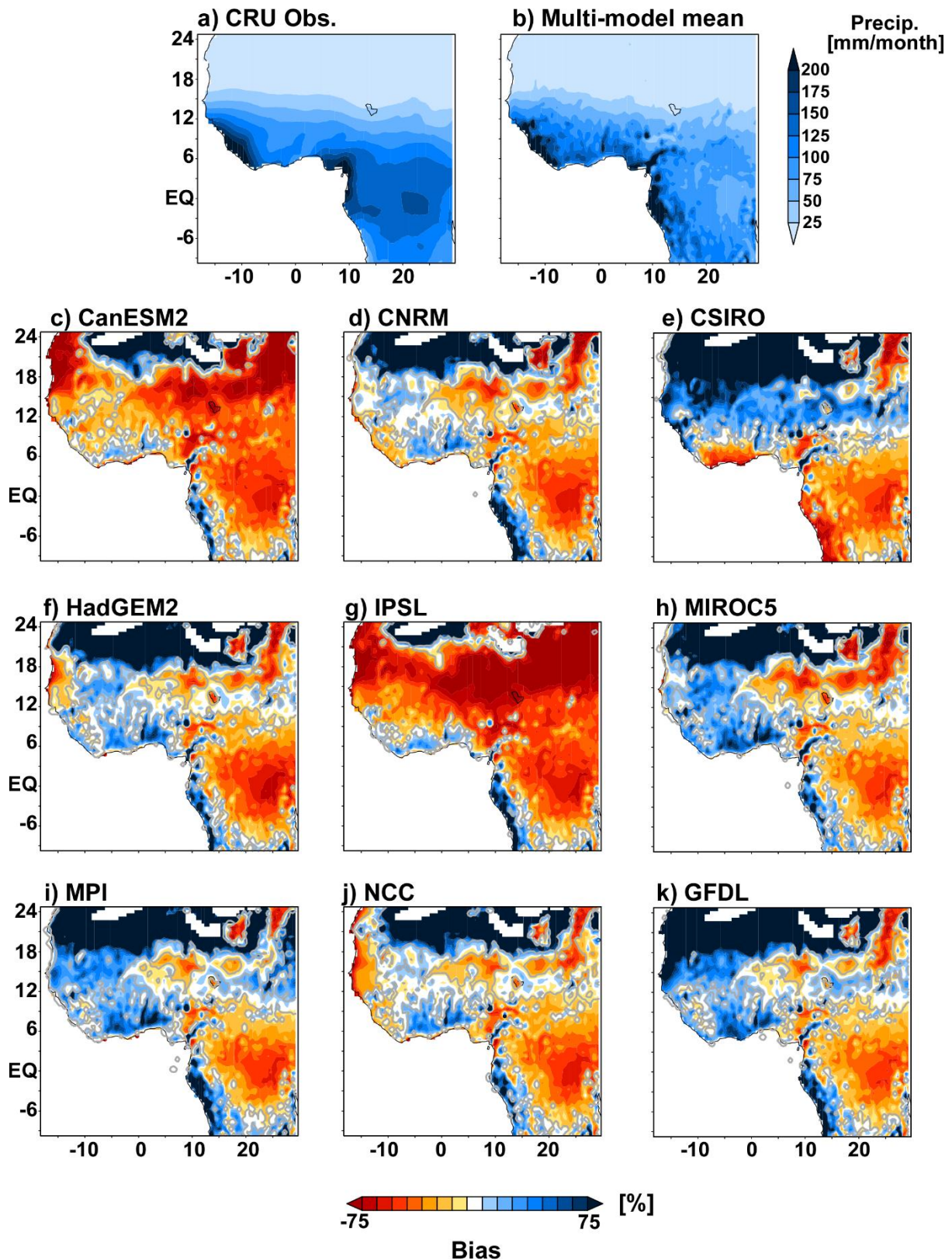


Figure 4.2: Long-term mean monthly historical precipitation (1951-2005) in (a) CRU observation (b) Multi-model mean. Long-term historical percentage bias between models and CRU precipitation fields (1951-2005) (c) CanESM2 (d) CNRM (e) CSIRO (f) HadGEM2 (g) IPSL (h) MIROC5 (i) MPI (j) NCC (k) GFDL. Grey contours highlight regions of significant difference between observations and simulations at $p \leq 0.1$ based on a t test.

The deviations between simulations and observations result in bias in the CDFs. As determined using KS-tests most of the study area is characterized by high dissimilarity between statistical distributions of observations and simulations (Figure 4.3a). Highest differences (dissimilarity statistics > 0.5) can be observed in Central Equatorial Africa (Figure 4.3a). At $p \leq 0.1$, multi-model agreement indicates that less than 5% of the study area presents significantly similar statistical distributions (Figure 4.3b). The dissimilarity is however smaller between 12°N and 18°N for most models (except CSIRO and IPSL), confirming a good representation of rainfall distributions over the Sahel (Figure 4.3a). For each model, the ability to reproduce the seasonal cycle is also investigated (cf. Figure S4.2). For all models, the critical value ($D = 0.1645$) at $p \leq 0.1$ is in general exceeded for each month. The lowest values are observed between December and February, albeit with the highest inter-quartile range (Figure S4.2). Highest dissimilarities occur from May to October (Figure S4.2), suggesting that uncertainties mainly arise from the representation of the West African Monsoon (WAM) meridional migrations, as described by Sultan and Janicot (2000).

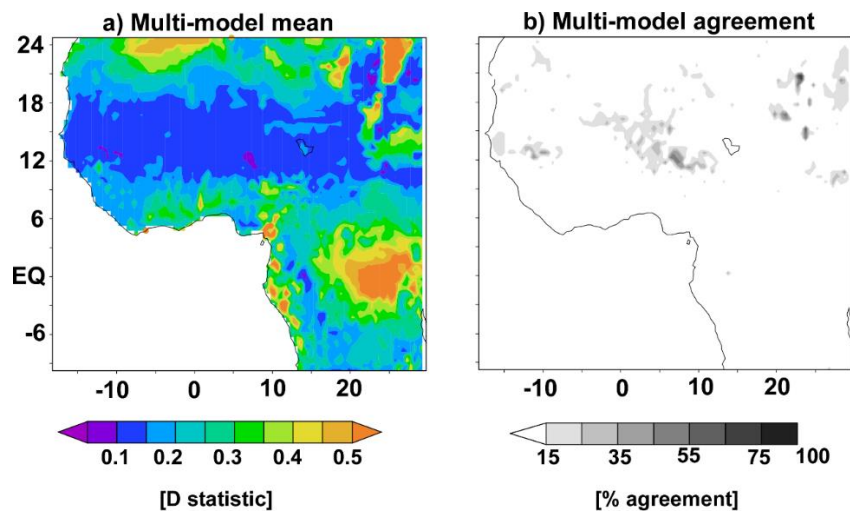


Figure 4.3: Distributional biases between models and CRU precipitation fields (1951-2005) (a) Multi-model mean dissimilarity statistic (b) Models agreement on CDFs similarity at $p \leq 0.1$ significance level based on the KS-test: darker colours correspond to higher model agreement on the similarity in CDFs.

4.3.1.1.2. Minimum and Maximum temperatures

Similar to long-term precipitation, maximum temperatures over the study area are characterized by a strong meridional gradient with highest temperatures reported along the Sahelian band ($>35^{\circ}\text{C}$) and lowest maximum temperatures in western Central Africa ($20\text{-}25^{\circ}\text{C}$) (Figure 4.4a). This meridional pattern is relatively well represented by most models except CNRM, CSIRO and GFDL (not shown). The median absolute bias over the study area suggests that majority of the models present a cold bias ranging from -0.37°C in HadGEM2 to -1.30°C in GFDL (Figure 4.4c-k). This cold bias is predominantly located in Sudanian and Sahelian regions (Figure 4.4c-k), as already reported by Sarr (2017). From the Gulf of Guinea to Central Africa, most models present warm biases, ranging from $+0.84^{\circ}\text{C}$ in GFDL to $+2.7^{\circ}\text{C}$ in IPSL.

For minimum temperatures, the long-term climatology highlights a zonal gradient, where most of West Africa (up to 21°N) is warmer ($20^{\circ}\text{C}\text{-}25^{\circ}\text{C}$) than eastern and Central Africa ($15^{\circ}\text{C}\text{-}20^{\circ}\text{C}$; Figure 4.5a). This zonal pattern is best reproduced by CSIRO (median absolute bias -0.13°C), MIROC5 (median absolute bias of -0.17°C) and IPSL (median absolute bias of 0.18°C), showing the lowest biases over the region (Figure 4.5e, h, g). All models are characterized by a cold bias ranging from -0.74°C in MIROC5 to -3.18°C in CNRM (Figure 4.5c-k), which similarly to maximum temperatures is located along the Sahelian band (Figure 4.4c-k). Moreover, the amplitude of the warm bias detected for maximum temperatures over the Gulf of Guinea and Central Africa is dampened: from $+0.42^{\circ}\text{C}$ in MIROC5 to $+1.68^{\circ}\text{C}$ in IPSL (Figure 4.5h, g).

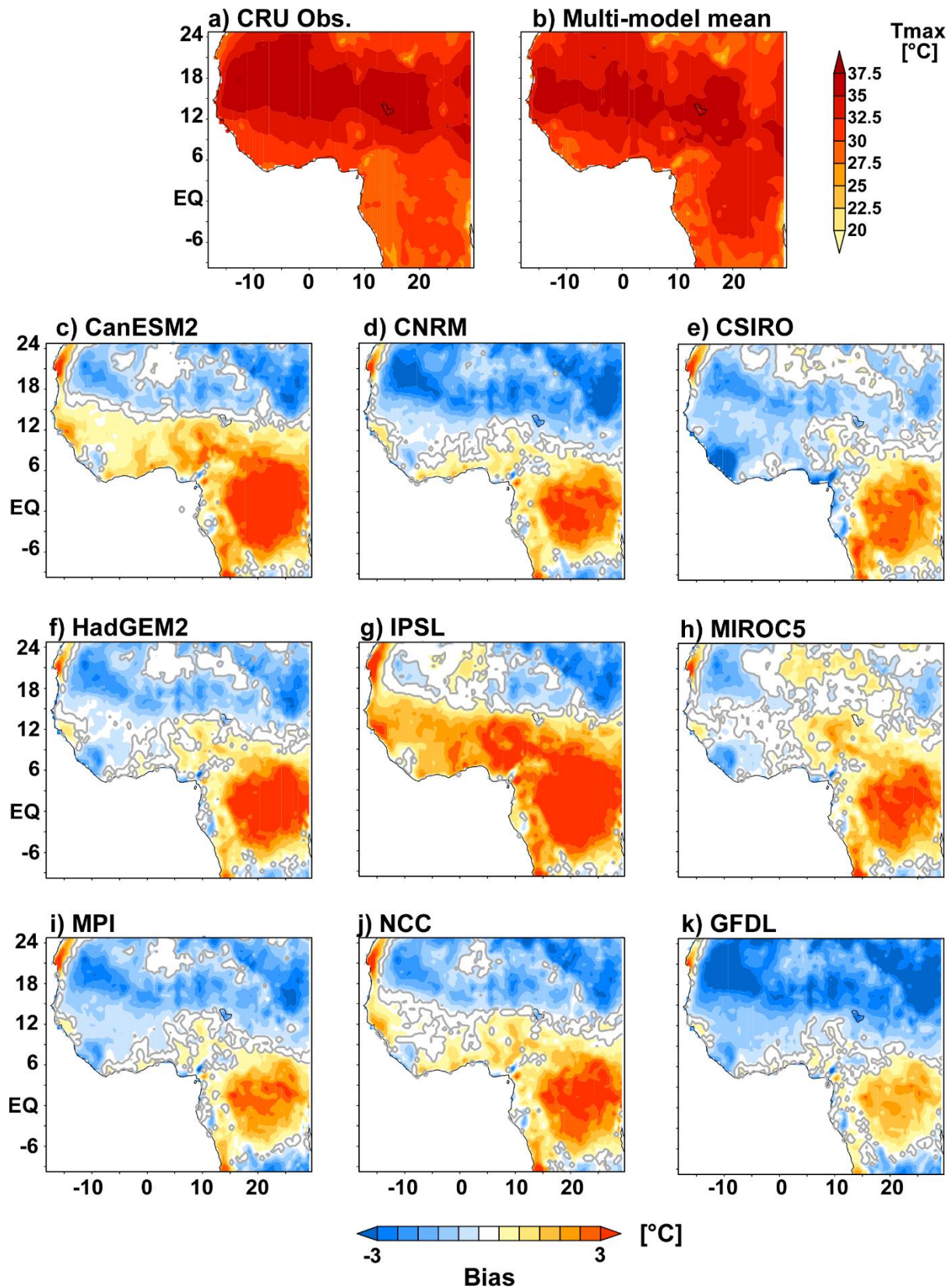


Figure 4.4: Long-term mean monthly historical maximum temperatures (1951-2005) (a) CRU observation (b) Multi-model mean. Long-term historical absolute bias between models and CRU maximum temperature (c) CanESM2 (d) CNRM (e) CSIRO (f) HadGEM2 (g) IPSL (h) MIROC5 (i) MPI (j) NCC (k) GFDL. Grey contours highlight regions of significant difference between observations and simulations ($p \leq 0.1$) based on a t test.

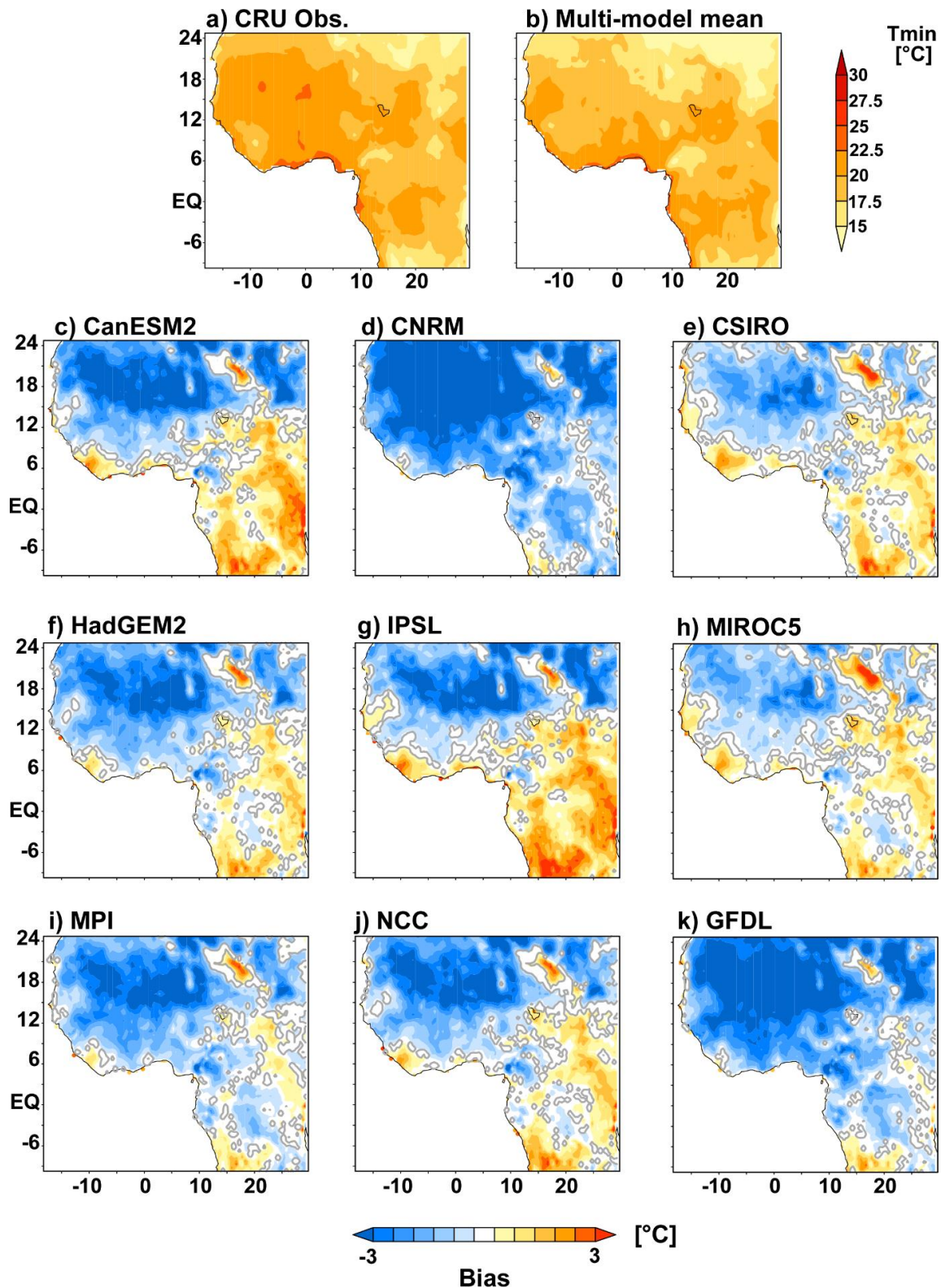


Figure 4.5: Long-term mean monthly historical minimum temperatures (1951-2005) (a) CRU observation (b) Multi-model mean. Long-term historical absolute bias between models and CRU minimum temperature (c) CanESM2 (d) CNRM (e) CSIRO (f) HadGEM2 (g) IPSL (h) MIROC5 (i) MPI (j) NCC (k) GFDL. Grey contours highlight regions of significant difference between observations and simulations ($p \leq 0.1$) based on a t test.

Biases in CDFs are also found in historical simulations for temperature, with the highest dissimilarity statistics observed in Central Equatorial Africa (Figure 4.6a, c). We note that distributional biases in minimum temperatures are higher than those observed for maximum temperatures (Figure 4.6c). In addition, multi-model agreement highlights that less than 2% of the study region present significantly similar CDFs at $p \leq 0.1$ (Figure 4.6b, d).

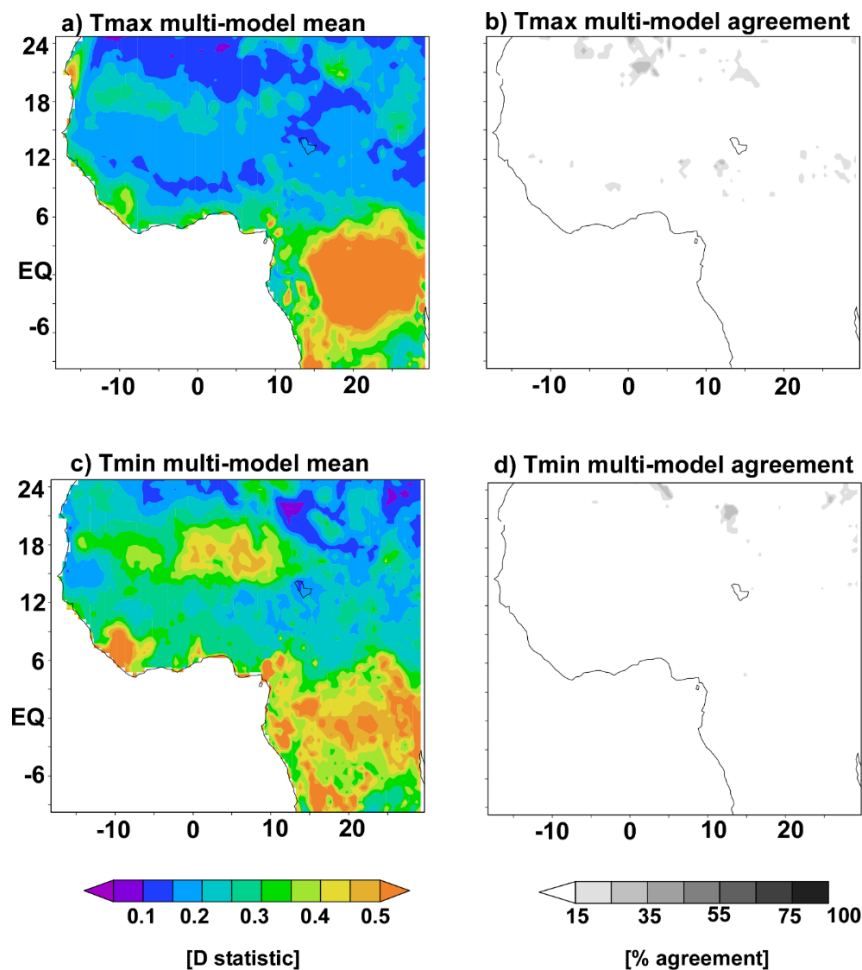


Figure 4.6: Distributional biases between models and CRU observations (1951-2005) (a-b) Maximum temperatures: (a) Maximum temperature multi-model mean dissimilarity statistic (b) Models agreement on CDFs similarity at $p \leq 0.1$ significance level based on the KS-test: darker colours correspond to higher model agreement on the similarity in CDFs (c-d) Minimum temperatures: (c) minimum temperature multi-model mean dissimilarity statistic (d) Models agreement on CDFs similarity at $p \leq 0.1$ significance level based on the KS-test: darker colours correspond to higher model agreement on the similarity in CDFs.

Seasonal cycles of distributional biases in T_{\max} and T_{\min} underline high discrepancies (median dissimilarity statistic ranging from 0.4 and 0.8; Figure S4.3-4.4). While distributional biases in maximum temperature are more important between May and October (Figure S4.3), those

observed in minimum temperature are homogenous throughout the year with no marked seasonality (cf. Figure S4.4).

According to Sarr (2017), the predominant cold bias observed for the different temperature fields over the study area is mainly due to the misrepresentation of climatic processes in GCMs. Other factors, such as excess cloudiness, surface albedo, and aerosols could play an important role (e.g. Giannini *et al.*, 2003; Nicholson, 2013).

4.3.1.2. Bias correction and cross validation

Model evaluation highlighted important biases in precipitation and temperatures. The bias-correction algorithms were thus applied to all hydroclimatic variables. Cross-validation results highlight the ability of the QDM algorithms to satisfactorily reduce these biases (Figure 4.7). In fact, median PBIAS over the study area is now within the range $\pm 1.1\%$ for precipitation fields (not shown). More importantly, higher order moments are also improved in precipitation: median ratio of standard deviation over the study area is around 1.05 for all models (not shown). In precipitation, the distributional biases are thus significantly reduced for more than 55% of the study area (Figure 4.7a-c). Distributional biases in the seasonal cycle are also significantly corrected with median dissimilarity statistic below 0.2 at $p \leq 0.1$ (cf. Figure S4.2).

In general, bias correction algorithms yielded better results for temperatures compared to precipitation, with median absolute bias of $\pm 0.05^\circ\text{C}$ (standard deviation ratio of 1.02; Figure 4.7d-i). In maximum temperatures, distributional biases are corrected (at $p \leq 0.1$) for more than 80% of the study area (Figure 4.7d-f). Significant biases however remain over parts of Central Africa, where multi-model agreement is low (Figure 4.7e). Similar patterns are identified for minimum temperatures (Figure 4.7g-i), with however residual significant distributional biases extending to the Gulf of Guinea coastal regions (Figure 4.7h). Seasonal distributional dissimilarities in maximum and minimum temperature are also satisfactorily corrected (cf. Figure S4.3-4.4).

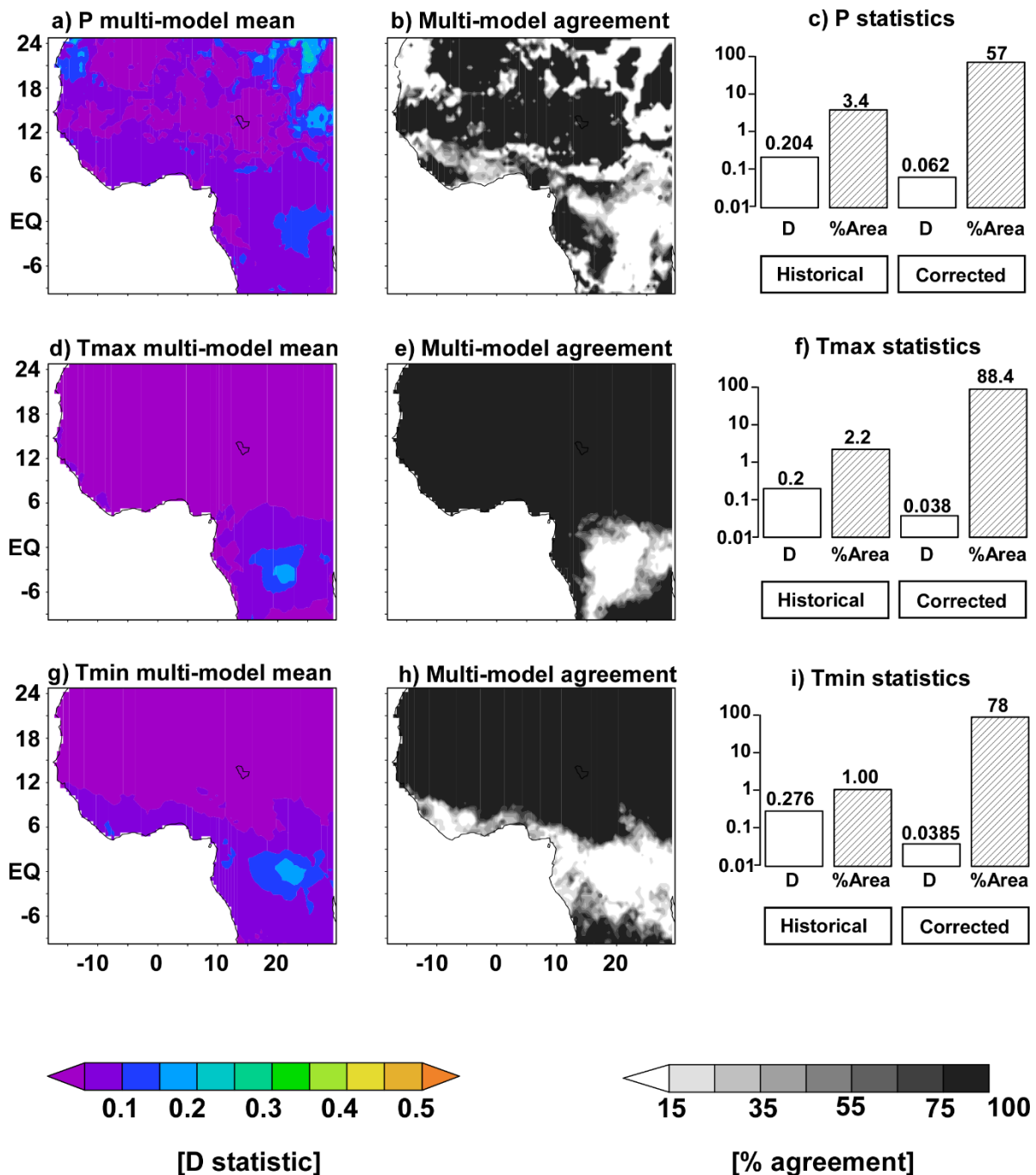


Figure 4.7: Distributional biases between bias-corrected model simulations and CRU observations (a-c) Precipitation fields: (a) Precipitation multi-model mean dissimilarity static (b) Models agreement on CDFs similarity at $p \leq 0.1$ significance level based on the KS-test: darker colours correspond to higher model agreement on the similarity in CDFs (c) Summary of bias correction performances: white histograms refer to the average dissimilarity statistics (D); Grey histograms refer to the percentage of area with significantly similar CDFs (%Area) (d-f) Maximum temperature fields: (d) Maximum temperature multi-model mean dissimilarity static (e) Models agreement on CDFs similarity at $p \leq 0.1$ significance level based on the KS-test: darker colours correspond to higher model agreement on the similarity in CDFs (f) Summary of bias correction performances: white histograms refer to the average dissimilarity statistics (D); Grey histograms refer to the percentage of area with significantly similar CDFs (%Area) (g-i) Minimum temperature fields: (g) Minimum temperature multi-model mean dissimilarity static (h) Models agreement on CDFs similarity at $p \leq 0.1$ significance level based on the KS-test: darker colours correspond to higher model agreement on the similarity in CDFs (i) Summary of bias correction performances: white histograms refer to the average dissimilarity statistics (D); Grey histograms refer to the percentage of area with significantly similar CDFs (%Area).

Despite overall good skills, the bias correction algorithms presented limited skill in Central Equatorial Africa, where distributional biases remain significant. This can be attributed partly to the lack of observed gauge data over the region (New *et al.*, 2000; Nikulin *et al.*, 2012), resulting in a limited representation of the regional climatic processes, and therefore difficulties in model evaluation and bias correction. In addition, several GCMs present the so-called “double ITCZ problem” (Lin, 2007), characterized by precipitation overestimation off the equator, and underestimation along the equator, over Central Africa, as a result of poor representation of environmental processes controlling the formation and propagation of Mesoscale Convective Systems (MCSs) (Aloysius *et al.*, 2016). Disentangling the part of uncertainties related to the quality of observation gridded-data and to climate models is however difficult. Further details about model parametrization, performances and potential inadequacies in tropical regions are provided in Monerie *et al.* (2012), Washington *et al.* (2013) among others.

4.3.2. Hydrological modelling: calibration and validation

According to Sidibe *et al.* (2018), missing information in discharge time series over the region mainly occur in the early 1950s and 2000s. To reduce the uncertainty associated with the reconstructed streamflow datasets, the 1960-1999 period has thus been selected to quantify hydrological model parameters. Models are calibrated using automated calibration algorithms on a decade and validated on the next, with a warm-up period of 5 years. Calibration intervals are also used for validation to assess model robustness. Two different performance criteria are used to assess model efficiency: the Nash-Sutcliffe efficiency criterion (NSE; Nash and Sutcliffe, 1970) and the modified Kling-Gupta criterion (Kling *et al.*, 2012). Both models are calibrated through sampling the parameter space: uniform grid screening for GR2M (Michel, 1989) and Latin hypercube sampling (McKay *et al.*, 1979) for IHACRES-CWI.

Even though simple in their parametrization, the hydrological models were able to capture to some extent the complexity of hydrological processes occurring over the study area. Both models perform well over most of the region, with median KGE higher than 0.7 (median NSE above 0.75) (Figure 4.8). GR2M however, seems to perform slightly better than IHACRES-CWI, which present higher inter-quartile ranges. For GR2M, we also note that performances tend to be better when models are calibrated on relatively drier periods (*i.e.* 1970s and 1980s), as suggested by Dezetter *et al.* (2008) for 49 river basins over the same region.

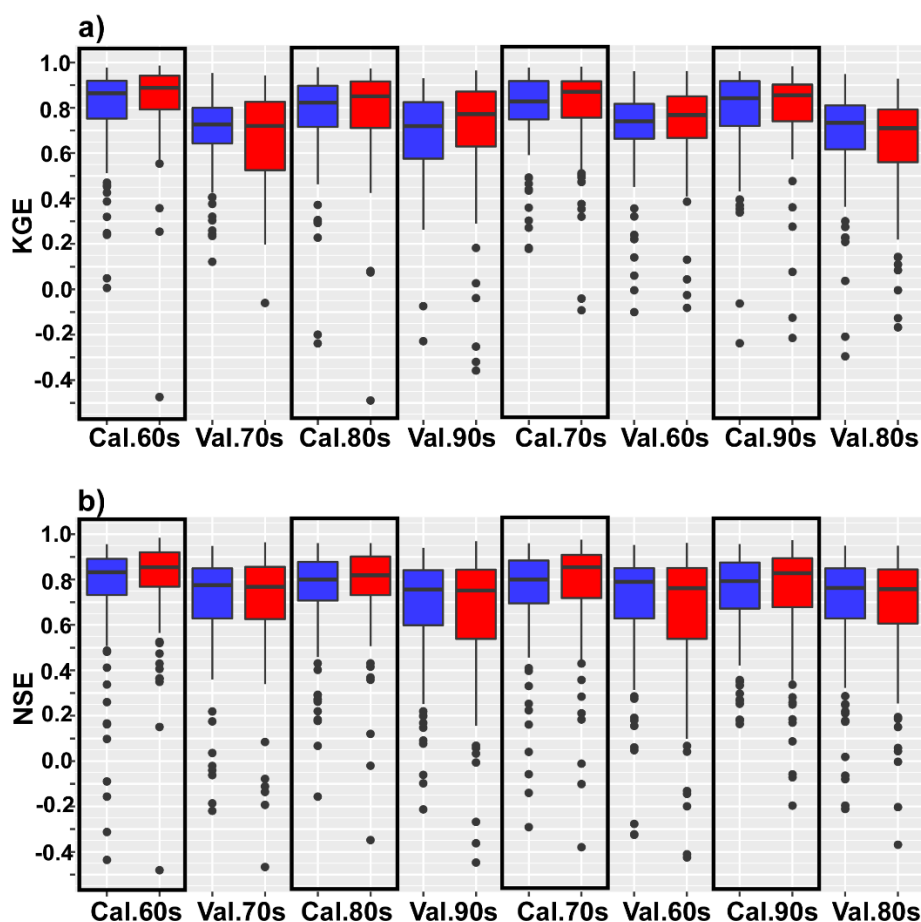


Figure 4.8: Hydrological model performances for different calibration and validation periods. a) Kling-Gupta Efficiency; b) Nash-Sutcliffe Efficiency. Blue refers to GR2M and red to IHACRES-CWI.

Despite overall good performances, the implemented hydrological models showed limited skill regionally. For instance, GR2M performs poorly ($KGE < 0.4$) over the Niger River middle reach (*e.g.* at Tossaye [MLQ0036] and Niamey [NEQ2000]; Figure 4.9). This may be due to the impact of the Inner Niger Delta (flooded area $\sim 40,000$ km² resulting in annual water losses

of ~40%), which significantly modifies downstream rainfall-runoff relationships (Mahé *et al.*, 2009; Zaré *et al.*, 2017). Low performances are also observed in GR2M for basins in the northeastern part of the study region (*e.g.* at Logone Gana [TDQ5006]) and the northern fringe of the Congo basin (*e.g.* at M'bata [CFQ0034], Bwembe [CGQ0013] and Gamboma [CGQ0017]; Figure 4.9a, b). This could be explained through changes in runoff coefficients after 1970, as described by Mahé *et al.* (2005) and Mahé & Paturel (2009), and/or to the quality of gridded observational data over Central Africa, where few stations were assimilated to build the CRU dataset (New *et al.*, 2000; Nikulin *et al.*, 2012; Aloysius *et al.*, 2016).

Interestingly, we note that IHACRES-CWI capture to some extent the hydrological conditions downstream the Inner Niger Delta (Figure 4.9c, d). This results from the linear routing function, which accounts for a lag-time between input and simulated outflow. However, this model presents limited efficiency in parts of Central Africa (*e.g.* at Bwembe [CGQ0013] and Gamboma [CGQ0017]), and over humid regions of West Africa (*e.g.* Hetin Sota [BJQ0036]), where Mahé *et al.* (2005) found significant changes in groundwater levels. This might thus highlight limitations in IHACRES-CWI, which does not account for groundwater interactions.

As illustrated in Figure S4.5, model parameters could slightly change from one period to another due to changes in climate variability and land-use (Niel *et al.*, 2003; Dezetter *et al.*, 2008; Ibrahim *et al.*, 2015). To better account for non-stationarity in model parametrization, future streamflow scenarios presented in Section 4.3.4.3 were thus derived using model parameters estimated for the 1970-1999 period, which roughly corresponds to an average response of the system (Figure S4.5).

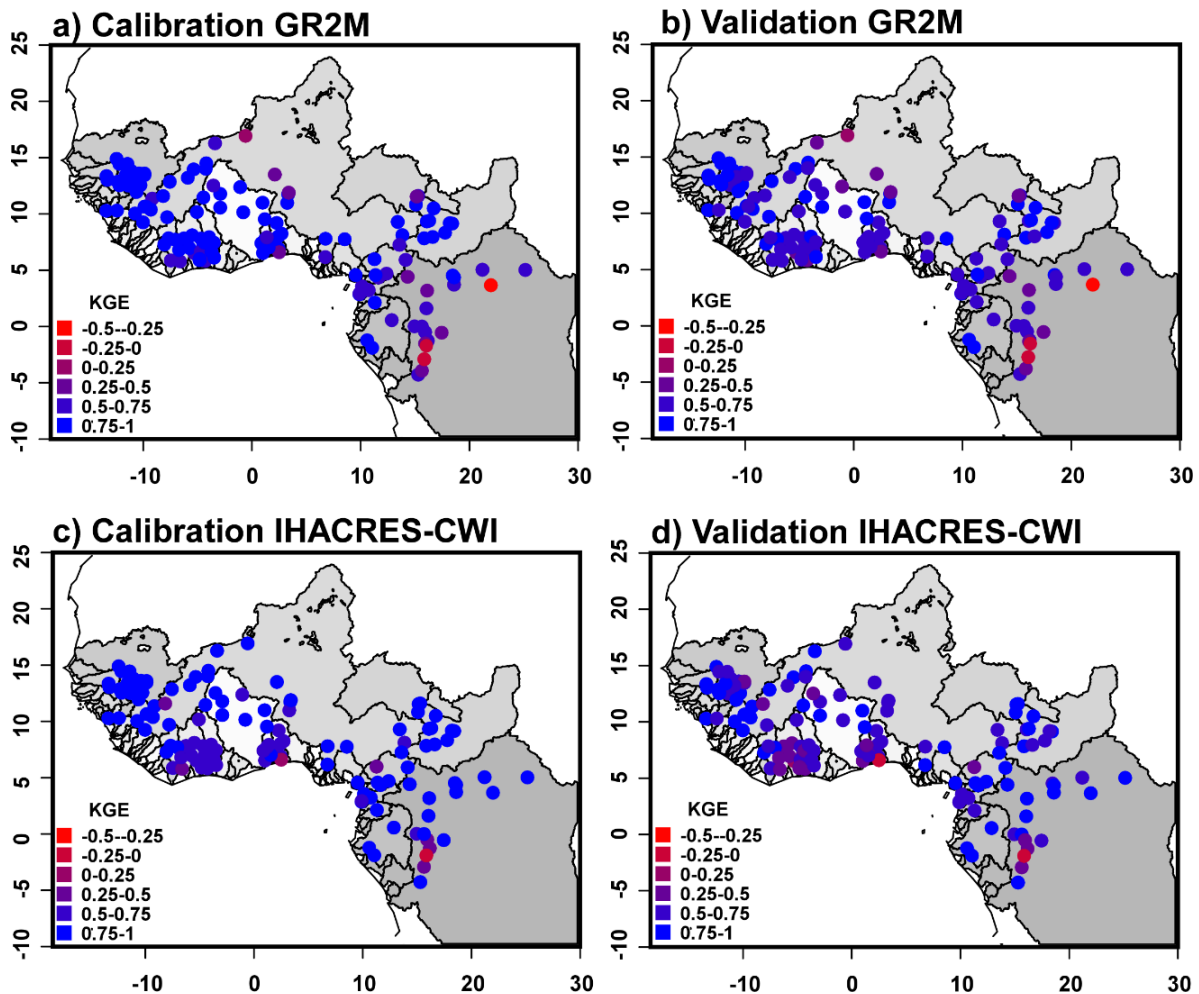


Figure 4.9: Spatial distribution of hydrological model performances (KGE average for all periods) for calibration and validation periods. Overall average performances for GR2M calibration (a) validation (b). Overall average performances for IHACRES-CWI calibration (c) validation (d). Blue values indicate good performances, while red values indicate poor performances. Grey polygons display the geographic boundaries of the major river basins.

4.3.3. Linear regression-based streamflow SST model

Previous studies seeking to link local climatic variables with large-scale SST anomalies, indicated the importance of predictor domain size on linear model skills (*e.g.* Benestad, 2002; Mtongori *et al.*, 2016). In this study, we found that a domain comprising the Atlantic and Pacific basins results in higher cross-validation performances (median KGE ~ 0.4). The spatial distribution of model efficiency highlights good skills for most catchments (Figure 4.10). However, the results contrast slightly with the hydrological models presented in the previous sections. In fact, poor performances (KGE < 0.4) are now mainly observed on the upper Niger River reach, *i.e.* from the Guinean highlands to southern Mali (Figure 4.10). Similar results

also are observed in parts of the Volta basin and in some regions of northern and western Central Africa (Gabon; Figure 4.10). These results might stem from weak predictor-predictand relationships and human-induced catchment modifications. Interestingly, we observe that some catchments in Central Africa, where hydrological models were performing poorly now present better results (see Appendix A). For instance, over parts of Central Africa (*e.g.* the N’Keni basin at Gamboma [CGQ0017]), the regression model outperformed ($KGE > 0.8$) the hydrological models ($KGE < 0.2$), which were mainly impacted by the quality of observed gridded precipitation and temperature datasets. This highlights the potential added-value of regression-based models in data-scarce environments, where gridded observational datasets quality is likely to be poor, for improved predictions.

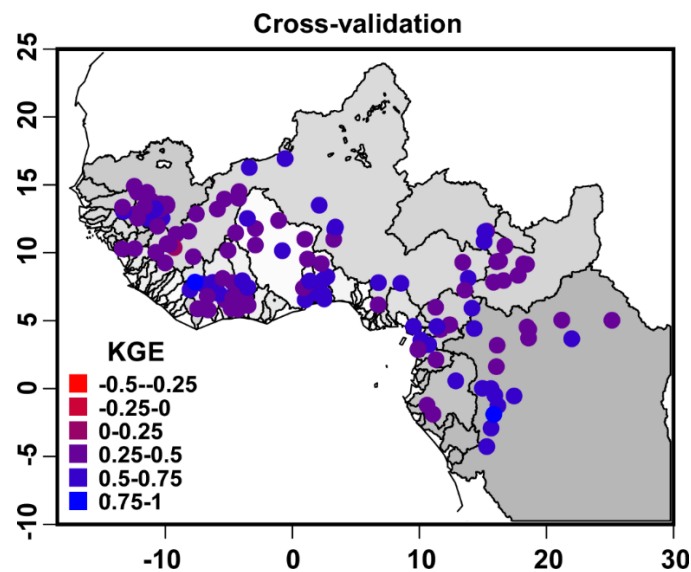


Figure 4.10: Performance of multi-timescale linear regression models based on K-fold cross-validation, as determined using KGE criterion. Blue values indicate good performances, while red values indicate poor performances. Grey polygons display the geographic boundaries of the major river basins.

4.3.4. Future hydroclimatic variability in West and Central Africa by mid-21st century

4.3.4.1. Changes in near-term precipitation

In Figure 4.11, near-term (2020-2050) projected precipitation changes relative to the historical period are explored under the RCP4.5 emission scenario. Most models (except CSIRO [-2.2%] and MPI [-2.1%]) show slight positive relative changes over the study area (from 2 to 12%;

Figure 4.11). Good agreement is observed between uncorrected simulations and bias-corrected data (not shown).

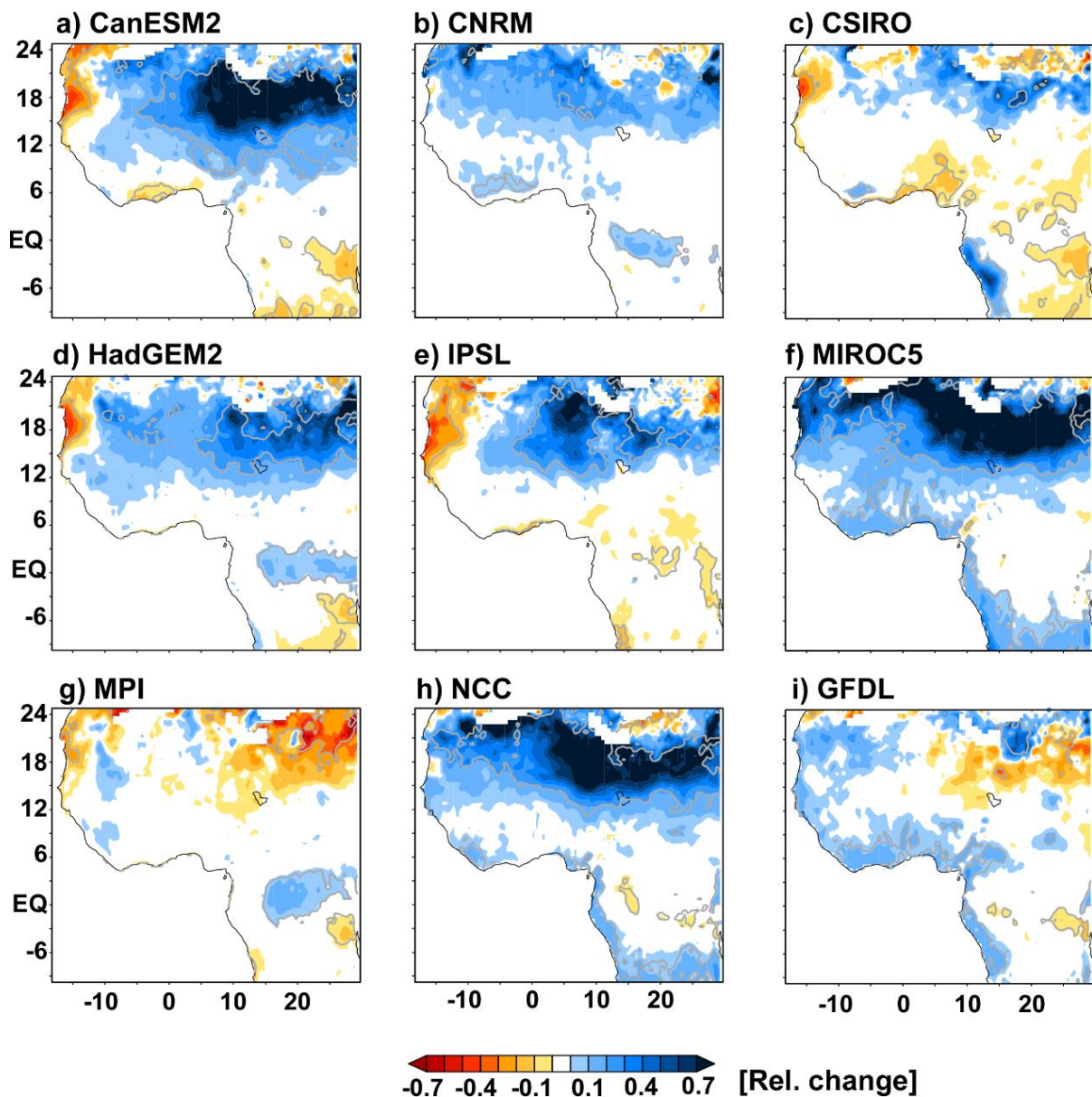


Figure 4.11: Near-term (2020-2050) relative change in precipitation under RCP4.5 emission scenario (a) CanESM2 (b) CNRM (c) CSIRO (d) HadGEM2 (e) IPSL (f) MIROC5 (g) MPI (h) NCC (i) GFDL. White colour corresponds to relative changes of ± 0.05 . Grey contours highlight regions of significant changes ($p \leq 0.1$) based on a t test.

In Central Africa, the mid-21st century will be characterized by slight changes ($\pm 4\%$) with a trend towards wetter conditions, within the range predicted by Aloysius *et al.* (2016) using the same emission scenario. A similar pattern is identified along the Gulf of Guinea coastal regions, where GFDL and MIROC5 both predict higher relative changes in precipitation of around

+8.5% and +6.7%, respectively (Figure 4.11i, f). Further North, along the Sahelian strip, relative changes are more significant, with highest changes predicted by CanESM2 (+17%), MIROC5 (+16.4%), NCC (+15.8%) and HadGEM2 (+12%).

In addition, the Sahelian band presents a zonal contrast, with its westernmost part drier than central and eastern regions (except for CNRM, MIROC5, NCC and GFDL). This pattern is consistent with previous investigation of future rainfall in the Sahel (*e.g.* Monerie *et al.*, 2012; Sylla *et al.*, 2016). Over the westernmost part of the Sahel, precipitation decrease of up to -22% is reported in IPSL (Figure 4.11e). In the central and eastern regions, most models (except CSIRO, MPI and GFDL) predict significant positive changes: CanESM2 (+28%), NCC (+28%), MIROC5 (+23%), HadGEM2 (+18.6%) IPSL (+16%) and CNRM (+8.7%).

4.3.4.2.Changes in near-term temperatures

Absolute changes in temperature by the mid-21st century over West and Central Africa show significant warming trends, with an overall good agreement between models (Figure 4.12).

Changes in maximum temperatures are expected to range between +1.2°C and +1.9°C (Figure 4.12). Spatial patterns, however, suggest regional contrasts (Figure 4.12). For instance, greater warming tends to be observed in Central Africa and over the northern fringe (Sahara) of the study area, while weaker warming tends to be identified along the Gulf of Guinea coastal regions (Figure 4.12).

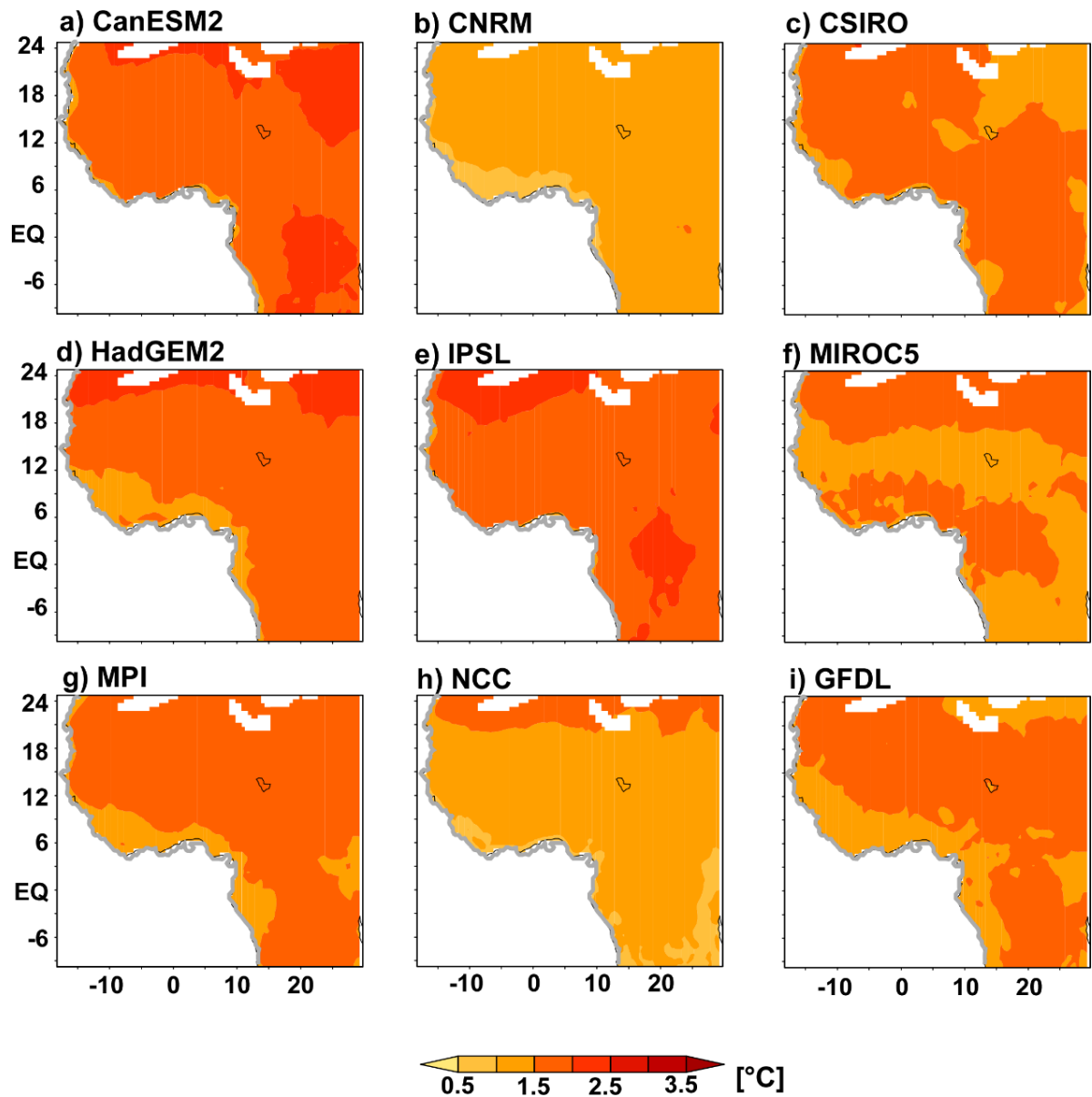


Figure 4.12: Near-term (2020-2050) absolute changes in maximum temperatures under RCP4.5 emission scenario (a) CanESM2 (b) CNRM (c) CSIRO (d) HadGEM2 (e) IPSL (f) MIROC5 (g) MPI (h) NCC (i) GFDL. Grey contours highlight regions of significant changes ($p < 0.1$) based on a t test.

According to Figure 4.13, over the study area minimum temperatures rise faster than maximum temperatures by the mid-21st century, consistently with previous findings (Funk *et al.*, 2012; Ringard *et al.*, 2016; Sarr, 2017). Median warming anomalies range between +1.4°C in CNRM and +2.2°C in IPSL (Figure 4.13b, e). By the mid-21st century, all models, but one (CNRM), predict minimum temperatures anomalies larger than +1.7°C.

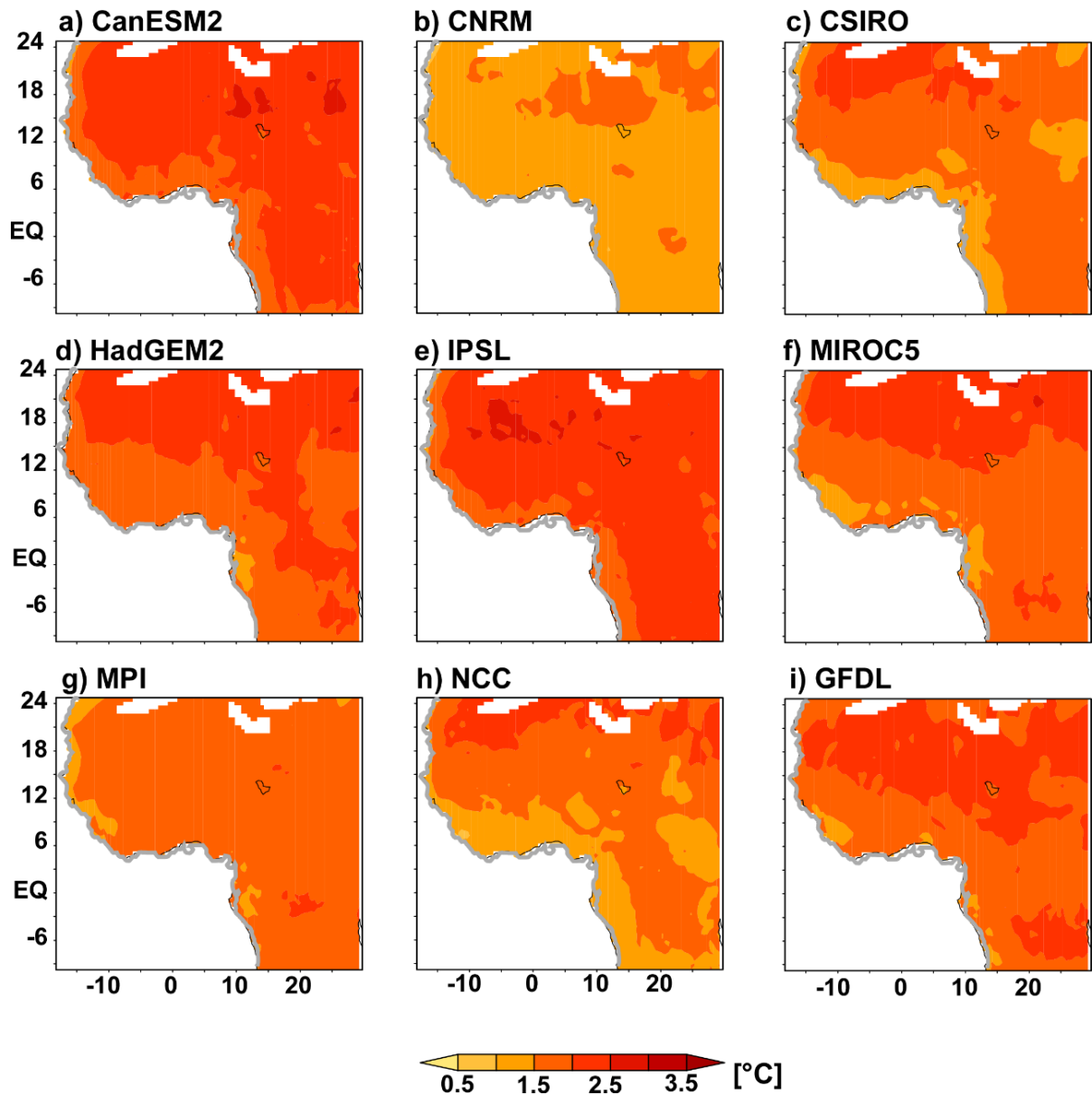


Figure 4.13: Near-term (2020-2050) absolute changes in minimum temperatures under RCP4.5 emission scenario (a) CanESM2 (b) CNRM (c) CSIRO (d) HadGEM2 (e) IPSL (f) MIROC5 (g) MPI (h) NCC (i) GFDL. Grey contours highlight regions of significant changes ($p < 0.1$) based on a t test.

Temperature trends presented in this study corroborate previous findings describing Sahelian and tropical West African regions as hotspots of climate change (IPCC, 2014; Niang *et al.*, 2014; Sylla *et al.*, 2016).

4.3.4.3. Discharge evolution by the mid-21st century in West and Central Africa

Changes in river discharge are explored relatively to the historical period using two conceptual hydrological models in Figure 4.14-4.15, and a multi-timescale regression-based model in

Figure 4.16. Projections are compared to historical streamflow generated with calibrated model parameters and bias-corrected hydroclimatic variables rather than observed streamflow to limit the uncertainty related to residual biases in the mean of bias-corrected climate inputs.

Despite differences in their ability to capture some hydrological processes, hydrological models generally predicted consistent changes in streamflow over the region and show slight changes in river discharge by the mid-21st century. Depending on the driving GCMs, we observe differences in the proportion of area with significant streamflow changes at $p \leq 0.1$: CanESM2 (38.2%), CNRM (20%), CSIRO (36%), HadGEM2 (33.6%), IPSL (14.5%), MIROC5 (59.5%), MPI (10%), NCC (36.6%) and GFDL (42.7%).

Using the GR2M model, projected climate variables result in positive changes in streamflow for most models, except one (CSIRO [-9.4%]), with changes ranging from +1.4% to +19.4% on average over the entire region (Figure 4.14). More specifically, most parts of Central Africa present slight changes $\pm 5\%$ (with most models predicting wetter conditions; Figure 4.14). Along the Gulf of Guinea up to 11°N, where hydrological regimes are bimodal (Descroix *et al.*, 2009; Roudier *et al.*, 2014), changes are mostly positive, reaching +23.5% in MIROC5 (Figure 4.14). Changes in the Gambia River basin are uncertain, with some models predicting negative changes mainly in the headwater (CNRM, CSIRO, IPSL, MIROC5 and MPI), and others slightly positive changes (CanESM2, HadGEM2, NCC and GFDL). Further North, in the Sahelian regions, changes in river discharge are even stronger (Figure 4.14). Over this region, which comprises the Senegal and the upper reach of the Niger River, the highest relative changes in streamflow are predicted by HadGEM2 (+22.5%), MIROC5 (+21%), CanESM2 (+18.7%) and NCC (+18.4%). Although positive trends in river discharge are consistent with predicted rainfall, they could appear counterintuitive considering the expected increase in temperatures and evapotranspiration. This is nonetheless consistent with a recent assessment

of future water availability by Sylla *et al.* (2018), suggesting that increased precipitation overcompensates the increased evapotranspiration.

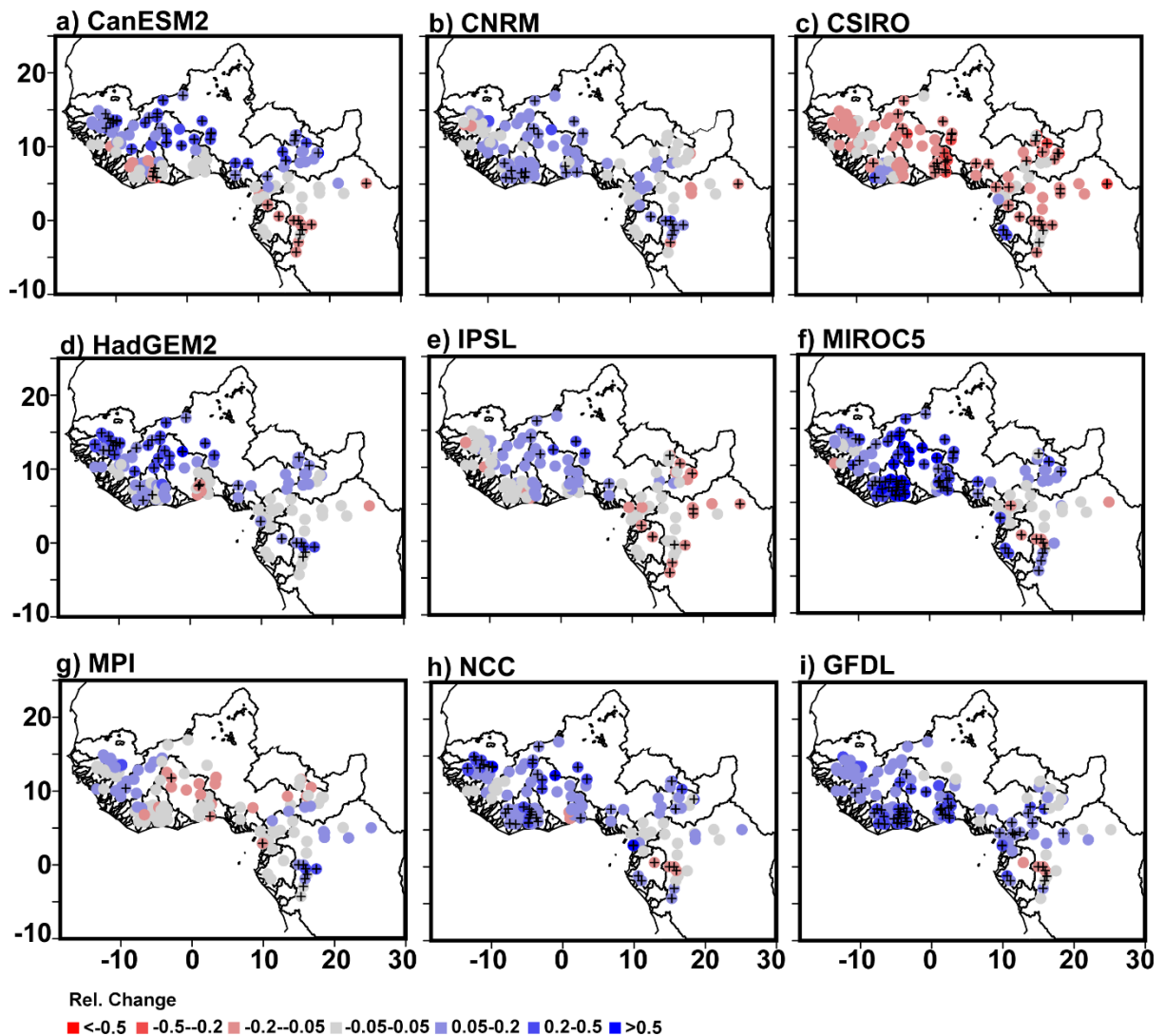


Figure 4.14: Near-term (2020-2050) relative change in discharge for the GR2M model under RCP4.5 emission scenario (a) CanESM2 (b) CNRM (c) CSIRO (d) HadGEM2 (e) IPSL (f) MIROC5 (g) MPI (h) NCC (i) GFDL. Black crosses highlight regions of significant changes ($p \leq 0.1$) based on a t test.

In general, similar patterns are observed using IHACRES-CWI model (Figure 4.15). Except CSIRO, IPSL and MPI, which show negative changes in river discharge, West Africa is mostly characterized by positive trends using IHACRES-CWI (Figure 4.15), consistently with GR2M predictions. Median changes over the study area are also relatively smaller in IHACRES-CWI compared to GR2M (Figure S4.6). This is probably inherent to the structure of IHACRES-CWI, which accounts for catchment moisture levels. In Central Africa, projected changes are

uncertain with most models predicting relatively small positive changes ranging from +0.1% to +6.8%, while the rest of the models present negative changes ranging from -5% to -8% (CanESM2, CSIRO, IPSL; Figure 4.15). In addition, at the catchment scale, we note positive changes for catchments in the Gulf of Guinea region (*e.g.* Sassandra [+11%], Bandama [+11%]), except for the Cavally basin, where changes are of opposite signs for GR2M (+5%) and IHACRES-CWI (-1.2%).

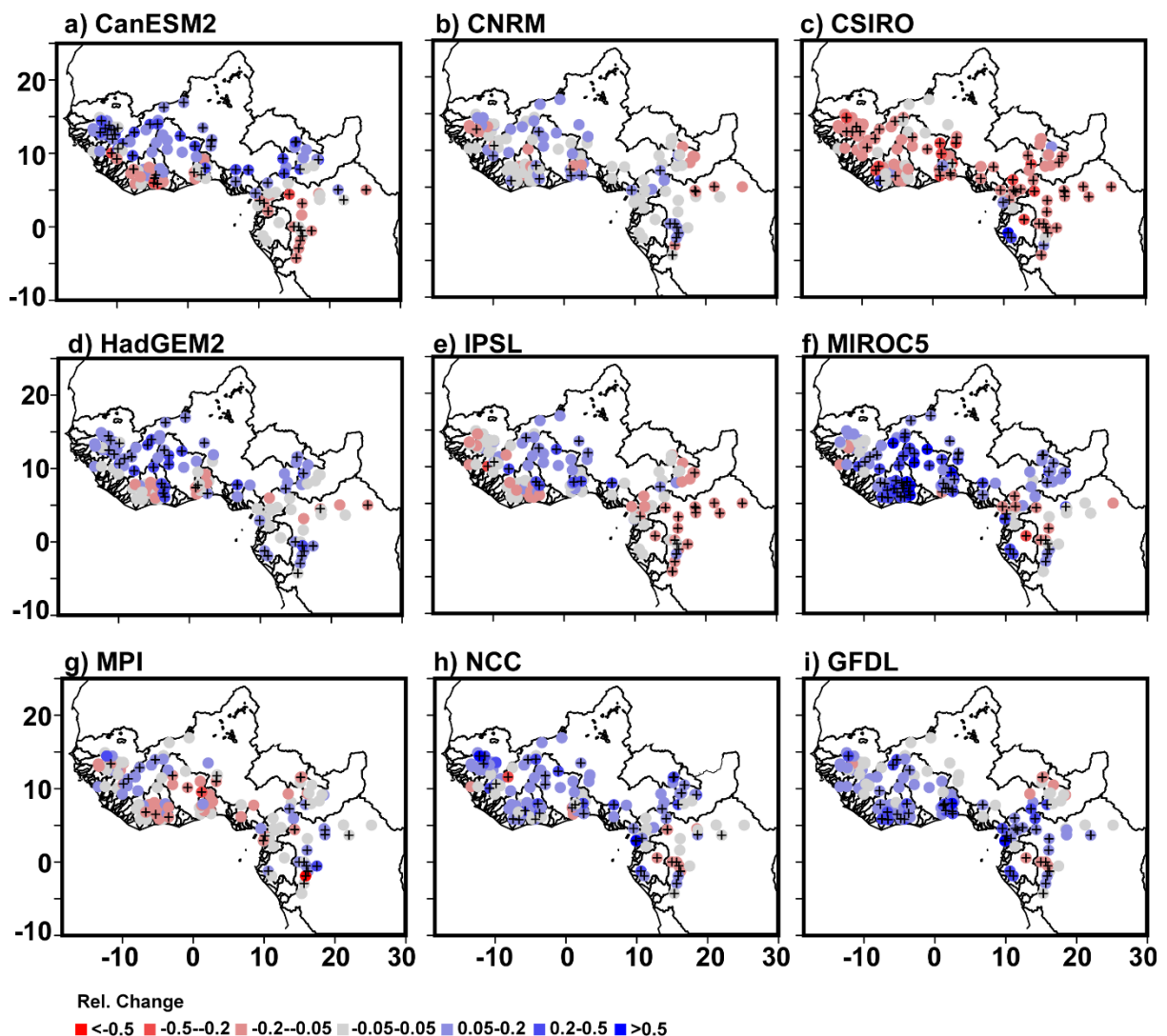


Figure 4.15: Near-term (2020-2050) relative change in discharge for the IHACRES model under RCP4.5 emission scenario (a) CanESM2 (b) CNRM (c) CSIRO (d) HadGEM2 (e) IPSL (f) MIROC5 (g) MPI (h) NCC (i) GFDL. Black crosses highlight regions of significant changes ($p \leq 0.1$) based on a t test.

Using the multi-timescale regression-based model, discharges in West and Central Africa by mid-21st also present slight positive changes (from +2% to +27%) for most models (Figure

4.16), except in CNRM (-1.1%), CSIRO (-20%) and MPI (-15%), at the regional scale. In Central Africa, in particular, where the linear-regression model presents sometimes higher prediction skills compared to hydrological models, streamflow changes range from -8% (NCC) to +2.5% (GFDL) and can even reach +15% using HadGEM2 (Figure 4.16). Over the Gulf of Guinea and Sudano-sahelian regions, predicted changes are more important, yet more uncertain. In these regions, most models present changes in the range of +5%, approximately, and +25% using HadGEM2 (Figure 4.16d). Reversely, negative changes are found using CSIRO, and reach up to -40% using MPI (Figure 4.16c, g). Median changes in streamflow over the study area are summarized in Figure S4.7. In addition, at the catchment scale, the Bandama catchment shows contrasting results for the linear regression model regardless of the driving GCM (median change \sim -12%). This could have resulted from complex predictor-predictand relationships, which are not fully captured by the regression-based model.

These results suggest that for some regions in Central Africa, where strong SST-streamflow teleconnections exist, regression models can serve as an alternative to hydrological models that require more input data. However, the higher spread of predictions observed over the Gulf of Guinea and Sudano-sahelian regions underline the need for larger multi-model ensembles for a better representation of predictor (SST) fields. In their evaluation of SST patterns from CMIP5 models (22 models), Wang *et al.* (2014) highlighted important biases (too low values in the Northern Hemisphere and too high values in the Southern Hemisphere) mainly resulting from model misrepresentation of physical processes and feedback mechanisms. For example, the amplitude of Global SST biases is significantly associated with model capacity to characterize the Atlantic Meridional Overturning Circulation (AMOC): biases increase as the AMOC circulation weakens. Dieppois *et al.* (2015, 2019) also highlighted important biases in the representation of the El-Nino-Southern Oscillation (ENSO) patterns, as well as of decadal models of global SST variability, which significantly impact the study region.

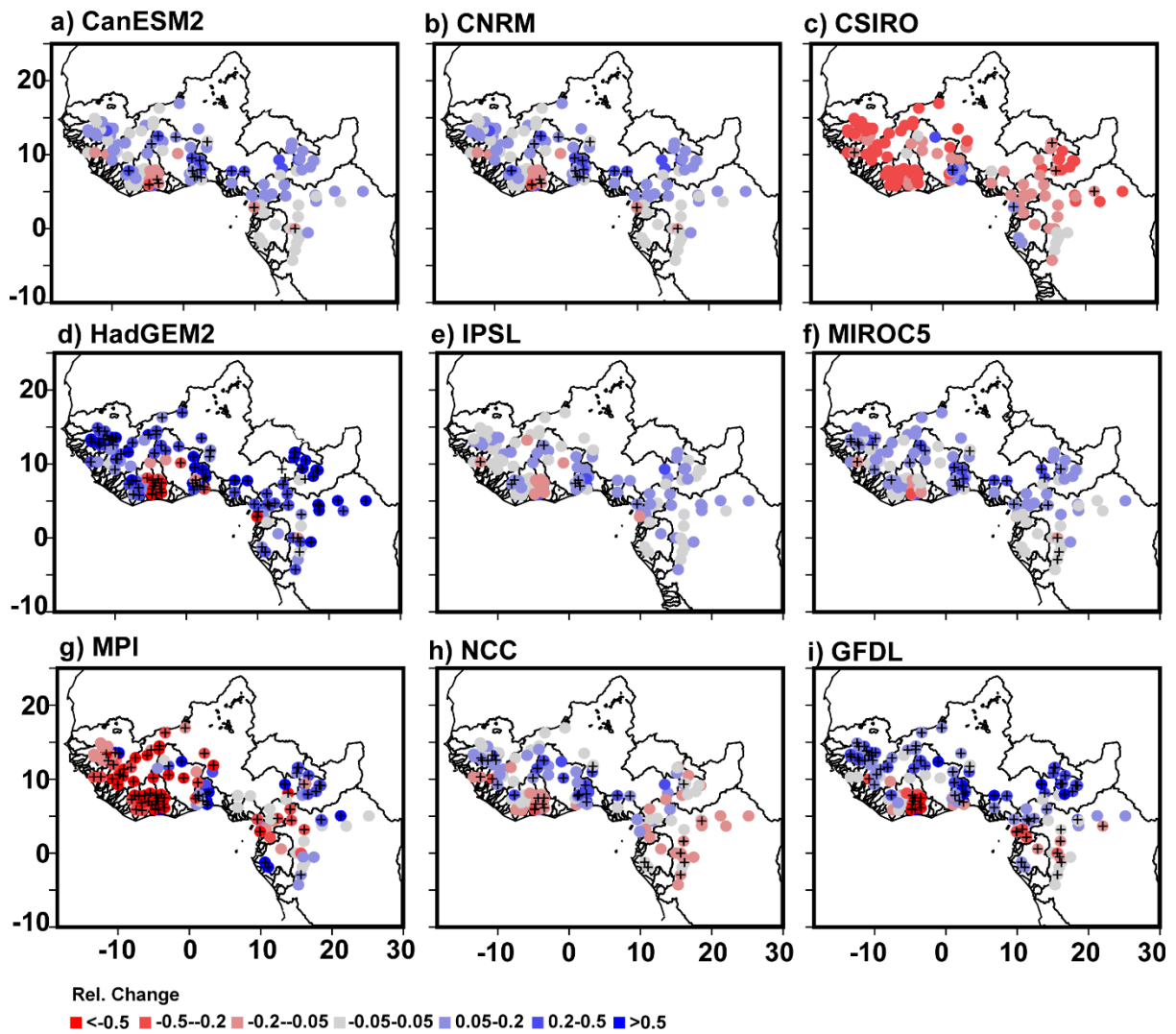


Figure 4.16: Near-term (2020-2050) relative changes in discharge for the teleconnections-based linear regression model under RCP4.5 emission scenario (a) CanESM2 (b) CNRM (c) CSIRO (d) HadGEM2 (e) IPSL (f) MIROC5 (g) MPI (h) NCC (i) GFDL. Black crosses highlight regions of significant changes ($p \leq 0.1$) based on a t test.

The findings presented in this section are consistent with previous investigation of near-term river flow evolution in West Africa under similar emission scenario (Ardoin-Bardin *et al.*, 2009; Roudier *et al.*, 2014; Aich *et al.*, 2014; Mbaye *et al.*, 2015; Yira *et al.*, 2017; Stanzel *et al.*, 2018), except for the Gambia River basin where most studies predict significant negative trends. For instance, Bodian *et al.* (2018) found a decrease of up to -22% for the near-term future using a set of six GCMs (statistically downscaled with the delta change method) and the GR4J hydrological model. However, different results could have resulted from the use of the

RCA4-RCM, which has a tendency towards wetter projections over West Africa compared to other RCMs (Stanzel *et al.*, 2018).

4.4. CONCLUSIONS

In this study, we investigated the impact of near-term (2020-2050) climate change on hydrological systems over West and Central Africa using a regional multi-model ensemble, bias-correction algorithms and different runoff modelling strategies.

Evaluation of climate model outputs highlighted different levels of accuracy in the representation of key WAM features, which sometimes result in important dissimilarities. For instance, biases in precipitation are often associated with model representation of the ITCZ intensity and northward propagation (Nikulin *et al.*, 2012). Over Central Equatorial Africa, however, these biases were more important regardless of the driving GCM. This can be attributed to the quality of gridded observational datasets over this region and other factors such as representation of topography and environmental processes controlling the formation and propagation of MCSs (Aloysius *et al.*, 2016).

Two different approaches were adopted to assess future streamflow fluctuations in the region. Firstly, bias correction algorithms were applied to climatic variables (precipitation, maximum and minimum temperatures) prior to their use in two conceptual hydrological models. These bias correction algorithms satisfactorily reduced discrepancies between model simulations and observations, and importantly preserved the climate change signal predicted by climate models. However, the bias correction presented limited skill over Central Equatorial Africa, stemming mainly from the quality of observational datasets (New *et al.*, 2000; Nikulin *et al.*, 2012). Input data quality in this region might have also impacted hydrological models, which performed poorly. Elsewhere, hydrological models presented higher skill, and more importantly, their different structures satisfactorily characterized different important hydrological processes: while GR2M provided insights for regions with important groundwater interactions,

IHACRES-CWI satisfactorily captured complex hydrological processes occurring downstream the Inner Niger Delta and the Benue River.

Secondly, streamflow projections were derived based on large-scale SST teleconnections using multi-timescale linear regression models (Massei *et al.*, 2017). This latter procedure, applied here for the first time across West and Central Africa, appeared as a reliable alternative to hydrological models for impact studies in data-scarce regions with robust streamflow-SST teleconnections. For instance, over parts of Central Africa (*e.g.* the N'Keni basin at Gamboma [CGQ0017]), the regression model outperformed ($KGE > 0.8$) both hydrological models ($KGE < 0.2$), which were mainly impacted by the quality of observation datasets. This regression model nevertheless presented limited skills over the upper reach of the Niger River in the Guinean and Sudanian regions, where complex SST teleconnections were highlighted in previous studies (Wotling *et al.*, 1995; Nicholson, 2008; Sidibe *et al.*, 2019).

West and Central Africa are found to be characterized by slightly wetter conditions by the mid-21st century under RCP4.5 scenario, and, according to previous studies (Hawkins and Sutton, 2009; IPCC, 2013; Sylla *et al.*, 2016), these results are expected to be consistent using more pessimistic or optimistic scenarios (*e.g.* RCP8.5 and 2.6). Overall, precipitation is likely to increase within a range of +2 to +12%, with however important spatial variability from Central Africa ($\pm 4\%$) to the Sahel (-22 to +28%), where a zonal contrast (drier western and wetter eastern) is apparent in some models. Temperatures present a sustained increasing rate (higher for minimum temperatures) between +1.2°C and +2.2°C, with highest absolute changes occurring mainly along the Sahelian band.

These fluctuations in climatic variables are therefore likely to result in slight positive streamflow changes ($\sim +5\%$), which are consistent across the different modelling strategies, despite local differences. The pattern closely mimics the change in rainfall, with smaller

(higher) changes in Central Africa (further North). Despite agreements in streamflow projected changes over the entire study area, a higher interquartile range ($\pm 40\%$) is observed for the linear regression-based model, due to uncertainties in SST simulations. This is especially true for the different future trajectories of main modes of variability in the Atlantic and Pacific Oceans (*e.g.* ENSO, AMO) predicted by CMIP5 models (Wang *et al.*, 2014; Dieppois *et al.*, 2019). Further investigations with larger multi-model ensembles will shed light on uncertainties associated with SST projections, streamflow large-scale climate teleconnections, and help assess the full spectrum of future streamflow fluctuations.

In addition, river flow projections presented in this study account only for climate change and variability. It should not be forgotten that an expected population increase in Sub-Saharan Africa by 2050 (population expected to approach 2 billion people) will result in rising demand posing substantial threats to water security (quantity and quality; Serdeczny *et al.*, 2017), and greatly modifying hydrological regimes (Mahé *et al.*, 2013). Detailed investigations must be conducted to integrate the influence of three other key aspects significantly impacting river flow (Sterling *et al.*, 2013): land use, water consumption/withdrawal and carbon effect on plant water use. This will require an integrated approach with different modelling strategies but most importantly a joint effort for data collection and sharing across key actors (*e.g.* national water offices, water practitioners, stakeholders) in sub-Saharan Africa.

Acknowledgements

Moussa gratefully acknowledges the funding received towards his PhD studies from Coventry University, UK, and resources provided by the Centre for Agroecology Water and Resilience (CAWR). The authors are also grateful to the developers and maintainers of R packages (**airGR**, **esd**, **Hydromad**, **MBC** and **wmtsa**) used in this study. Authors also thank the National hydrological services in Africa which collected discharges data used in this study.

4.5. Appendix A: List of selected stations with model performances and multi-model ensemble relative change in streamflow under RCP4.5 emission scenario

Station Metadata						Model calibration (KGE)			Relative Change (MME)		
ID	Basin	Station	Area(km2)	LAT	LON	GR2M	IHACRES	SST-Q	GR2M	IHACRES	SST-Q
BFQ0010	LERABA	YENDERE au pont	6288	10.167	-5.068	0.85	0.7	0.46	0.157	0.107	-0.02
BFQ0060	VOLTA	WAYEN	20241	12.379	-1.08	0.83	0.7	0.26	0.287	0.233	0.295
BFQ0064	VOLTA	BOROMO	54499	11.783	-2.917	0.74	0.72	0.47	0.202	0.1	0.126
BFQ0065	VOLTA	DAPOLA	86566	10.567	-2.917	0.91	0.91	0.39	0.212	0.132	-0.07
BFQ0072	VOLTA	NWOKUY	15463.75	12.528	-3.55	0.75	0.81	0.64	0.144	0.123	0.174
BFQ0074	VOLTA	SAMANDENI	4454	11.467	-4.467	0.91	0.87	0.43	0.157	0.094	0.142
BJQ0009	SOTA	COUBERI	25974	11.74	3.333	0.89	0.77	0.54	0.115	0.063	0.127
BJQ0022	COUFFO	LANHOUNTA - LANTA	1701.517	7.1	1.883	0.8	0.7	0.4	0.08	0.003	0.315
BJQ0033	OUEME	BONOU	48816	6.9	2.45	0.9	0.66	0.61	0.097	0.023	0.419
BJQ0036	OUEME	HETIN SOTA	49907.33	6.6	2.5	0.7	0.61	0.61	0.042	0.09	0.09
BJQ0047	OKPARA	KABOUA	10430	8.25	2.717	0.79	0.44	0.55	0.08	0.005	0.338
BJQ0050	SOTA	RTE KANDI-SEGBANA AMONT	8426	10.983	3.25	0.86	0.69	0.49	0.101	0.015	0.146
BJQ1000	PENDJARI	PORGA	22920	10.994	0.977	0.84	0.8	0.42	0.163	0.063	0.077
BJQ2000	NIGER	MALANVILLE	719331	11.888	3.383	0.53	0.82	0.5	0.15	0.059	-0.07
BJQ2004	OUEME	PONT DE BETEROU	10491	9.199	2.268	0.84	0.83	0.49	0.087	0.044	0.314
BJQ2005	OUEME	PONT DE SAVE	23476	8	2.417	0.82	0.86	0.55	0.1	0.139	0.442
CFQ0025	OUBANGUI	ZINGA TRANSIT	526113	3.714	18.587	0.85	0.93	0.49	-0.03	0.001	0.069
CFQ0027	MBOMOU	ZEMIO	27952	5.029	25.147	0.76	0.81	0.47	-0.07	-0.068	0.091
CFQ0028	BANGUI-KETTE	ALINDAO	4551	5.045	21.202	0.58	0.85	0.45	-0	-0.04	0.155
CFQ0034	LOBAYE	M'BATA	31346	3.666	21.981	-0.21	0.88	0.52	0.006	-0.03	-0.02
CFQ0040	M'POKO	BOSSELE-BALI	10573.43	4.531	18.469	0.84	0.83	0.47	0.014	-0.056	0.148
CFQ0057	SANGHA	SALO	72416	3.182	16.114	0.44	0.89	0.44	0.002	-0.047	-0.01
CFQ2000	OUBANGUI	BANGUI	499000	4.364	18.595	0.85	0.92	0.46	-0.03	-0.017	0.068

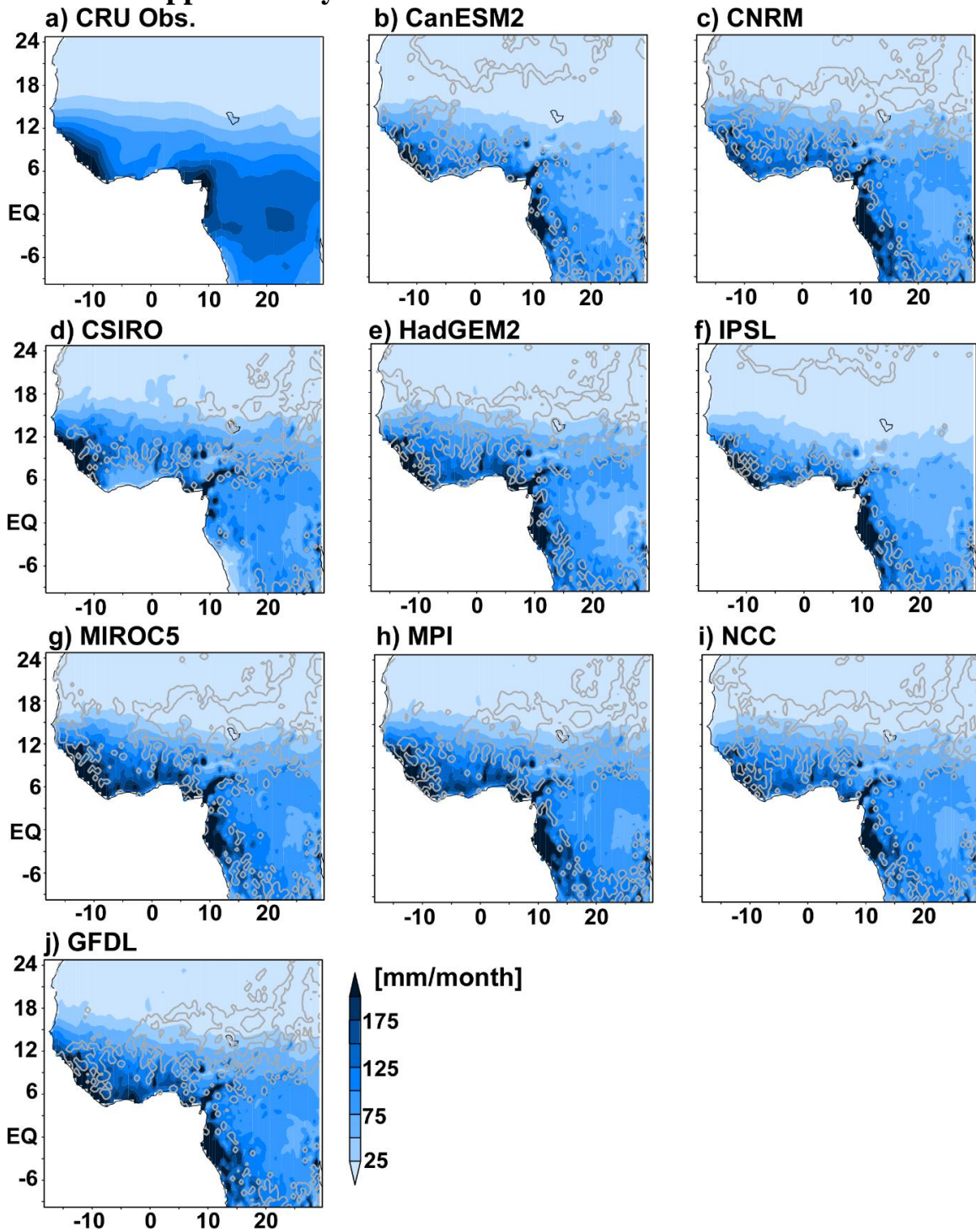
CGQ0003	ALIMA	TCHIKAPIKA	20067	-1.264	16.169	0.66	0.04	0.73	0.005	0.023	0.004
CGQ0013	LEFINI	BWEMBE	13589	-2.917	15.631	0.1	0.18	0.57	0.005	0.016	0.008
CGQ0014	LIKOUALA	ETOUMBI	4647.94	0.017	14.95	0.71	0.58	0.59	-0.01	-0.035	0.043
CGQ0015	LIKOUALA	MAKOUA	15037.86	0.002	15.633	0.73	0.75	0.62	-0.02	-0.061	-0.13
CGQ0017	N'KENI	GAMBOMA	6202	-1.9	15.85	-0.57	0.14	0.84	0.018	-0.035	0.013
CGQ0020	KOUYOU	LINNEGUE	6890.2	-0.5	15.933	0.49	0.49	0.55	0.002	0.016	0.021
CGQ0026	LIKOUALA	BOTOUALI	19223	-0.55	17.45	0.47	0.87	0.66	0.046	-0.003	0.113
CGQ2000	CONGO	BEACH - V.N. Brazzaville	3700000	-4.273	15.294	0.65	0.85	0.62	-0.03	-0.057	0.05
CGQ2001	SANGHA	OUESSO	159016	1.617	16.05	0.44	0.95	0.45	-0	-0.034	-0.02
CIQ0013	BANDAMA	KIMOUKRO BALISE 10201	56364.5	6.506	-5.305	0.72	0.6	0.41	0.114	0.004	-0.09
CIQ0032	MARAOUÉ	RTE BEOUMI-SEQUELA - KONGASSO 10145	12905	7.832	-6.254	0.85	0.85	0.52	0.125	0.022	-0.15
CIQ0033	MARAOUÉ	BOUAFLE 10147	21267	6.98	-5.754	0.84	0.53	0.53	0.124	0.104	-0.1
CIQ0058	NZI	BOCANDA	20880	7.044	-4.52	0.83	0.83	0.5	0.134	-0.006	-0.35
CIQ0061	NZI	DIMBOKRO 10141	24100	6.636	-4.71	0.76	0.72	0.46	0.141	-0.015	-0.29
CIQ0154	KOUROUKELE	IRADOUGOU	1820	9.707	-7.803	0.91	0.74	0.45	0.124	0.177	-0.15
CIQ0292	KAVI	MBESSE	975	5.839	-4.296	0.65	0.4	0.39	0.095	0.06	0.675
CIQ0312	CAVALLY	FLAMPLEU	2508	7.283	-8.058	0.81	0.89	0.52	0.057	-0.012	-0
CIQ0314	CAVALLY	TAI	12719	5.86	-7.45	0.89	0.84	0.56	0.149	0.136	-0.05
CIQ0319	NSE	TAI 1 (TAI PONT)	1424.36	5.875	-7.458	0.75	0.81	0.44	0.16	0.117	-0.07
CIQ4020	BANDAMA	BADA	23809	8.107	-5.497	0.79	0.71	0.46	0.103	-0.015	-0.23
CIQ4022	BANDAMA	TIASSALE 10144	61850	5.895	-4.818	0.78	0.53	0.45	0.113	0.023	-0.33
CIQ4025	NZI	FETEKRO	10175	7.811	-4.688	0.88	0.82	0.49	0.122	-0.031	-0.35
CIQ4026	NZI	MBAHIKRO 10133	15368	7.446	-4.356	0.84	0.8	0.49	0.124	-0.03	-0.38
CIQ4027	NZI	NZIENOA 10136	35340	5.996	-4.813	0.77	0.74	0.47	0.154	-0.045	-0.44
CIQ4028	COMOE	ANIASSUE PONT 10138	70636	6.638	-3.713	0.81	0.56	0.46	0.155	0.212	-0.34
CIQ4029	COMOE	MBASSO	70500	6.125	-3.48	0.79	0.54	0.49	0.152	0.09	-0.38
CIQ4030	COMOE	SEREBOU	50587	7.938	-3.942	0.84	0.7	0.51	0.162	0.253	-0.27

CIQ4031	SASSANDRA	SEMIEN 10130	29900	7.708	-7.067	0.96	0.87	0.57	0.105	0.053	-0.11
CIQ4032	SASSANDRA	SOUBRE	62173	5.783	-6.613	0.61	0.26	0.41	0.115	0.06	-0.07
CIQ4033	BAFING	BAFINGDALA BIANKOUMA 10162	6049	7.842	-7.667	0.94	0.9	0.79	0.064	-0.007	0.099
CIQ4034	LOBO	NIBEHIBE	6233.53	6.8	-6.7	0.77	0.79	0.37	0.147	0.005	-0.1
CIQ4035	COMOE	AKAKOMOEKRO 10149	57803	7.447	-3.509	0.78	0.6	0.51	0.158	0.151	-0.37
CMQ0029	SANAGA	NACHTIGAL	78625.04	4.35	11.633	0.62	0.86	0.43	0.027	0.009	0.072
CMQ0030	SANAGA	NANGA EBOKO	67600.32	4.7	12.383	0.64	0.88	0.41	0.029	0.017	0.021
CMQ0038	MBAM	BAC DE GOURA	42240.11	4.567	11.367	0.94	0.93	0.53	0.001	-0.015	0.069
CMQ0071	NYONG	DEHANE	26398.84	3.567	10.117	0.55	0.9	0.51	0.001	-0.039	0.061
CMQ5006	BENOUE	BUFFLE NOIR	3309	8.117	13.833	0.91	0.88	0.59	0.096	0.04	0.114
CMQ5007	BENOUE	GAROUA	46940	9.294	13.404	0.89	0.8	0.49	0.061	0.02	0.481
CMQ5015	MAPE	AU PONT DE MAGBA AMONT	4260	5.983	11.267	0.75	0.94	0.42	0.034	-0.011	0.07
CMQ5016	VINA DU SUD	LAHORE	1680	7.25	13.567	0.69	0.92	0.5	0.061	0.125	0.017
CMQ5018	LOBE	BAC KRIBI-CAMPO	3403	2.867	9.883	0.8	0.82	0.35	0.111	0.134	-0.07
CMQ5019	LOKOUNDJE	LOLODORF	1051	3.233	10.733	0.65	0.78	0.54	0.007	-0.032	-0.04
CMQ5038	MUNGO	MUNDAME	2730	4.567	9.533	0.78	0.89	0.63	-0	0.039	0.035
CMQ5040	NTEM	BAC DE NGOAZIK	18100	2.133	11.3	0.83	0.87	0.5	-0.02	-0.008	-0.07
CMQ5044	LOM	BETARE OYA	6931	5.917	14.133	0.7	0.91	0.62	0.027	0.044	0.014
CMQ5047	KIENKE	KRIBI SCIERIE	1533	2.933	9.9	0.73	0.71	0.48	0.145	0.217	-0.17
CMQ5050	KADEI	BATOURI	8974.88	4.417	14.317	0.47	0.87	0.51	-0.01	-0.092	-0.01
GAQ0028	IVINDO	MAKOKOU (LMNG)	35800	0.569	12.861	0.72	0.85	0.56	-0.03	-0.091	-0.02
GAQ0041	NGOUNIE	FOUGAMOU S H O (LMNG)	21620	-1.216	10.591	0.87	0.9	0.32	0.115	0.176	0.088
GAQ0046	NGOUNIE	MOUILA VAL MARIE	14908	-1.887	11.056	0.86	0.85	0.36	0.097	0.144	0.125
GHQ0045	NASIA	NASIA	4968.985	10.15	-0.8	0.84	0.7	0.5	0.125	0.066	-0.27
GNQ0015	NIGER	FARANAH	3171	10.037	-10.749	0.9	0.88	0.45	0.044	0.001	-0.24
GNQ0016	NIGER	KOUROUSSA	17164	10.652	-9.871	0.91	0.89	0.34	0.082	0.124	-0
GNQ0018	NIGER	TIGUIBERY (Siguiiri)	6974	11.354	-9.165	0.7	0.93	0.41	0.044	0.115	0.001

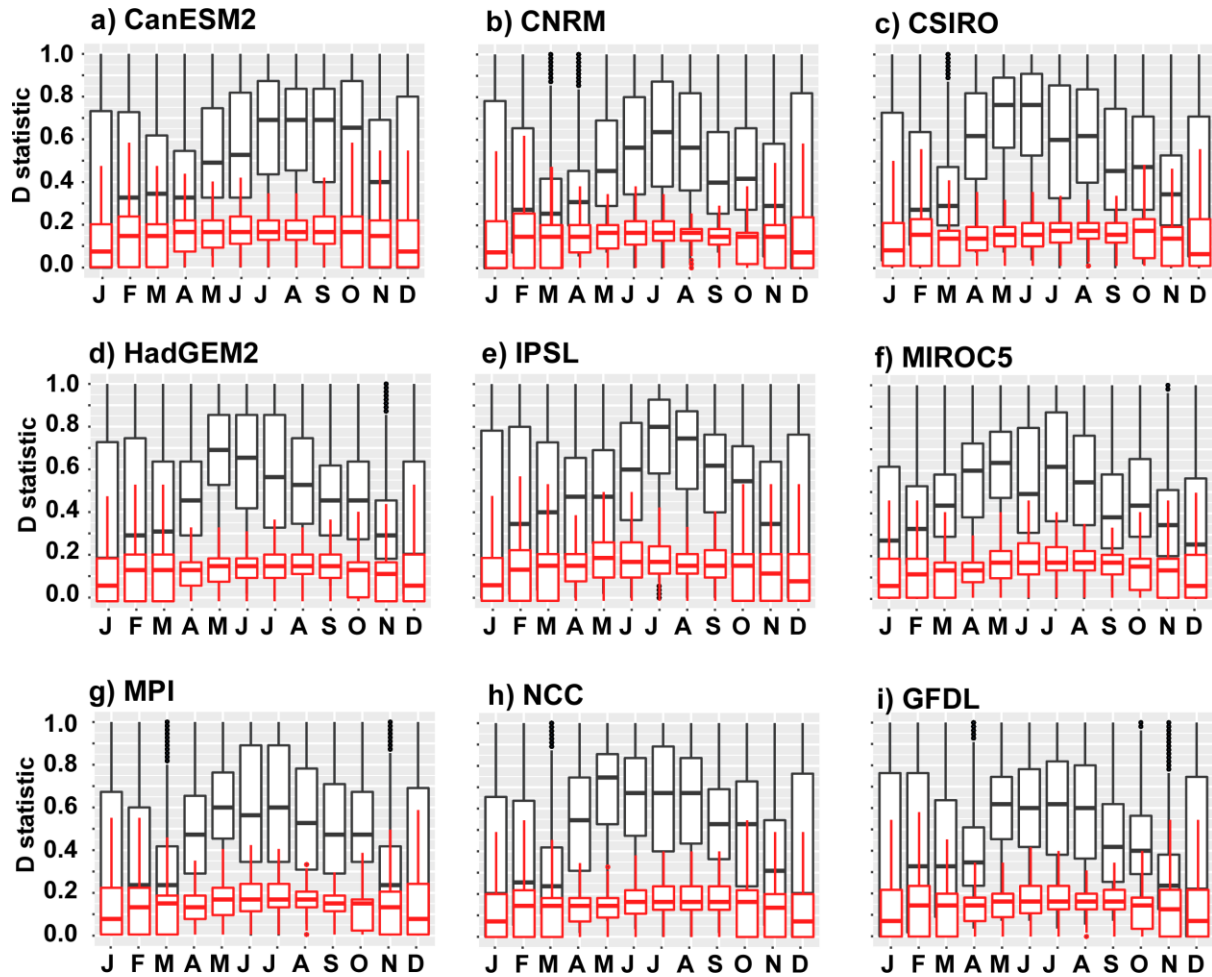
GNQ0026	MILO	KANKAN	10047	10.383	-9.3	0.96	0.92	0.25	0.069	0.034	-0.11
GNQ0030	NIANDAN	BARO	1307	10.617	-9.7	0.77	0.95	0.48	0.04	0.029	-0.01
GNQ0034	NIANDAN	KISSIDOUGOU (NIANDAN SCIERIE)	1398	9.25	-10.017	0.76	0.92	0.49	0.045	-0.006	-0.03
GNQ0200	BADI	BAC DE BADI	3095.6	10.283	-13.4	0.86	0.79	0.39	0.014	0.007	-0.05
GNQ0204	KONKOURE	PONT DE LINSAN	1278.69	10.3	-12.417	0.88	0.8	0.35	0.019	0.016	-0.08
MLQ0009	NIGER	DIRE	341047	16.276	-3.395	0.58	0.9	0.52	0.141	0.075	-0.05
MLQ0012	NIGER	KE MACINA	160848	13.958	-5.359	0.93	0.89	0.39	0.108	0.139	0.022
MLQ0019	NIGER	KOULIKORO	120315	12.857	-7.558	0.93	0.92	0.34	0.089	0.072	-0.03
MLQ0022	NIGER	MOPTI	301898	14.496	-4.201	0.85	0.94	0.46	0.142	0.036	-0.06
MLQ0036	NIGER	TOSSAYE	35195	16.933	-0.583	0.27	0.9	0.55	0.076	0.073	0.027
MLQ0091	BANI	SOFARA	130331	14.014	-4.243	0.84	0.93	0.44	0.188	0.135	-0.06
MLQ0123	SENEGAL	GALOUGO	120821	13.833	-11.133	0.92	0.91	0.48	0.142	0.109	0.053
MLQ0130	SENEGAL	BAFING MAKANA	20529	12.55	-10.267	0.84	0.95	0.51	0.057	0.031	0.042
MLQ0131	SENEGAL	SOUKOUTALI	26614	13.2	-10.417	0.96	0.96	0.47	0.078	0.059	0.02
MLQ0134	BAKOYE	OUALIA	78154.91	13.6	-10.383	0.9	0.77	0.38	0.213	0.017	0.171
MLQ0135	BAKOYE	TOUKOTO	16860	13.45	-9.883	0.92	0.75	0.45	0.146	0.075	-0.11
MLQ0137	FALEME	FADOUGOU	8200	12.517	-11.383	0.95	0.92	0.51	0.096	0.074	-0.03
MLQ0145	BAOULE	SIRAMAKANA (Balenda)	51029	13.583	-9.883	0.86	0.76	0.43	0.269	0.018	0.216
MLQ2007	SANKARANI	SELINGUE	6084	11.583	-8.167	0.72	0.72	0.4	0.058	0.004	0.067
MLQ2008	BANI	DOUNA	101225	13.214	-5.903	0.85	0.81	0.42	0.182	0.2	-0.19
MLQ2064	SENEGAL	DAKA SAIDOU	15660	11.95	-10.617	0.97	0.91	0.46	0.061	0.033	-0.03
MLQ2066	SENEGAL	DIBIA	32453	13.233	-10.8	0.9	0.81	0.57	0.083	0.028	0.171
MLQ2069	FALEME	GOURBASSY	16315	13.4	-11.633	0.96	0.73	0.42	0.097	0.052	-0.1
MLQ2070	SENEGAL	KAYES	160835	14.45	-11.45	0.88	0.9	0.5	0.152	0.1	0.07
NEQ2000	NIGER	NIAMEY	631549	13.502	2.105	0.43	0.86	0.54	0.169	0.098	-0.01
NGQ0001	BENUE	MAKURDI	289983	7.75	8.533	0.88	0.92	0.51	0.036	0.036	0.191
NGQ0002	NIGER	ONITSHA	124794	6.167	6.75	0.7	0.91	0.44	0.059	0.047	0.078
NGQ2000	NIGER	LOKOJA	1023616	7.8	6.767	0.91	0.93	0.72	0.117	0.137	0.221

SNQ2039	GAMBIE	KEDOUGOU	8127	12.55	-12.183	0.96	0.95	0.42	0.059	-0.01	0.081
SNQ2045	GAMBIE	MAKO	11007	12.867	-12.35	0.96	0.91	0.46	0.062	0.017	0.121
SNQ2055	GAMBIE	SIMENTI	20936	13.033	-13.3	0.96	0.83	0.51	0.07	0.01	0.118
SNQ2060	GAMBIE	WASSADOU-AMONT	21767	13.35	-13.367	0.95	0.82	0.48	0.069	-0.008	0.1
SNQ2062	GAMBIE	WASSADOU-AVAL	33392	13.35	-13.383	0.93	0.83	0.41	0.085	0.009	0.089
SNQ2063	SENEGAL	BAKEL	220818	14.9	-12.45	0.9	0.91	0.42	0.151	0.026	0.024
SNQ2065	FALEME	KIDIRA UHEA	28703.4	14.455	-12.205	0.96	0.75	0.46	0.112	0.16	-0.01
TDQ0004	CHARI	SARH (EX.FORT-ARCHAMBAULT)	192042.6	9.15	18.417	0.77	0.87	0.4	0.058	0.068	0.084
TDQ0009	CHARI	MAILAO	590607	11.6	15.283	0.76	0.94	0.46	0.066	0.038	0.141
TDQ0013	BAHR-SARA	MANDA	79176.06	9.183	18.2	0.92	0.9	0.44	0.008	-0.011	0.13
TDQ0014	BAHR-SARA	MOISSALA	66467.04	8.333	17.767	0.94	0.89	0.46	0.009	-0.017	0.102
TDQ0036	LIM	OULI BANGALA	4231.94	7.833	15.833	0.9	0.86	0.36	0.128	0.141	-0.04
TDQ0041	PENDE	GORE	11508.84	7.95	16.617	0.86	0.85	0.42	0.053	-0.01	0.244
TDQ0043	TANDJILE	TCHOA	6669.972	9.333	16.083	0.75	0.7	0.39	-0	0.068	0.374
TDQ2011	CHARI	BOUSSO	461854	10.5	16.717	0.84	0.93	0.44	0.07	0.061	0.103
TDQ5004	LOGONE	KATOA	77557	10.833	15.083	0.95	0.96	0.54	0.042	0.034	0.163
TDQ5005	LOGONE	LAI (MISSION)	61010	9.4	16.3	0.95	0.92	0.46	0.053	0.052	0.102
TDQ5006	LOGONE	LOGONE-GANA	3396	11.55	15.15	0.33	0.93	0.53	0.031	0.075	0.159
TOQ0006	KARA	LAMA KARA 1	1502	9.533	1.183	0.88	0.81	0.47	0.062	-0.007	0.132
TOQ0037	SIO	KPEDJI	1824	6.532	1.008	0.85	0.64	0.53	0.002	-0.035	0.075
TOQ0042	MONO	CORREKOPE	9859	7.8	1.3	0.86	0.59	0.59	0.073	0.095	0.143
TOQ0043	MONO	DOTAIKOPE	5797	7.817	1.267	0.85	0.87	0.57	0.068	-0.008	0.123
TOQ0046	MONO	TETETOU	20492	7.017	1.533	0.89	0.72	0.54	0.063	0.071	0.149
TOQ0048	AMOU	AMOU OBLO	197.2919	7.4	0.867	0.8	0.73	0.3	-0	-0.035	0.053
TOQ0053	ANIE	PONT C F T	3688.05	7.733	1.2	0.79	0.72	0.5	0.077	0.019	-0.06
TOQ0059	OGOUE	SIRKA	3745	7.917	1.367	0.7	0.7	0.66	0.083	0.124	0.126

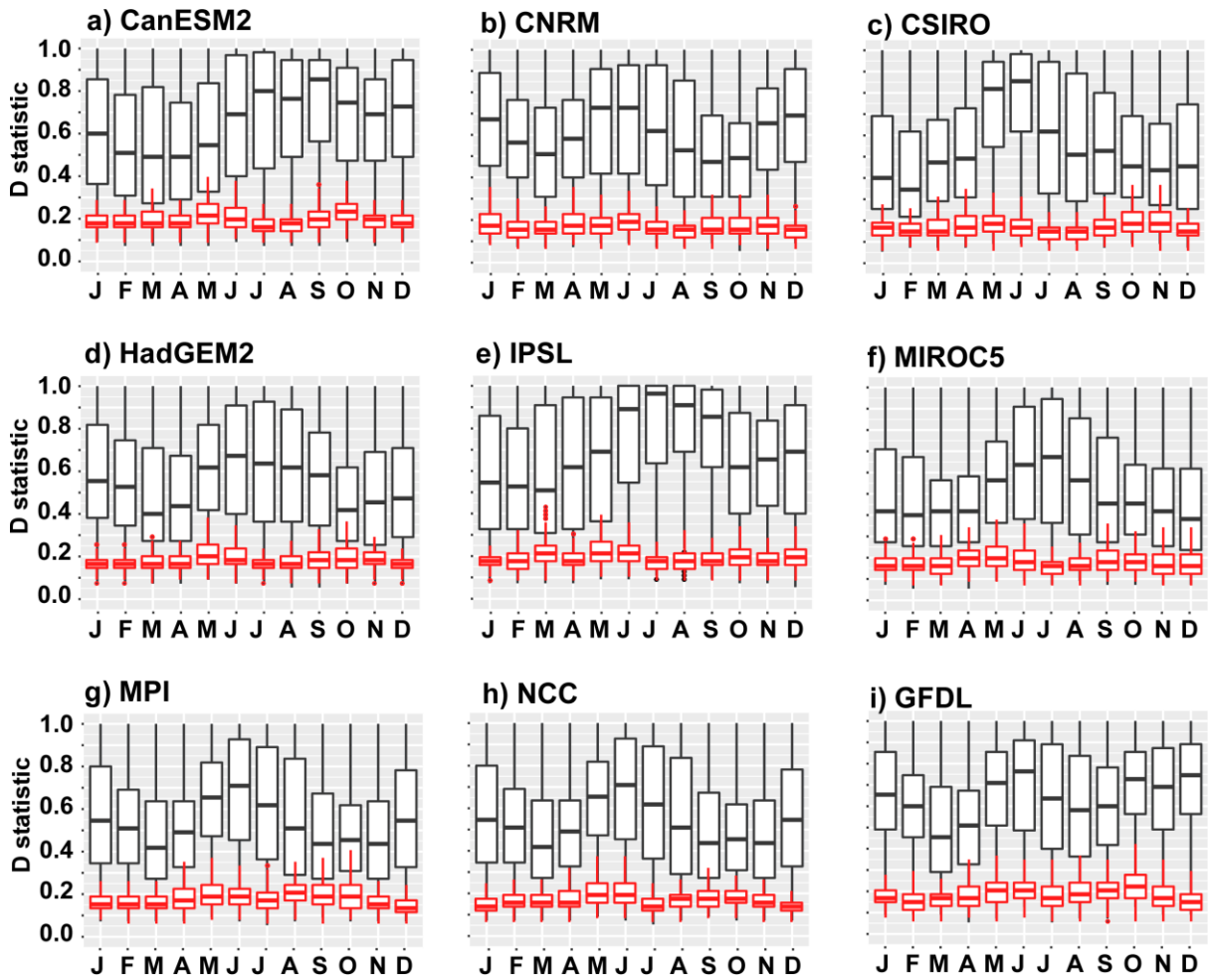
4.6. Supplementary materials



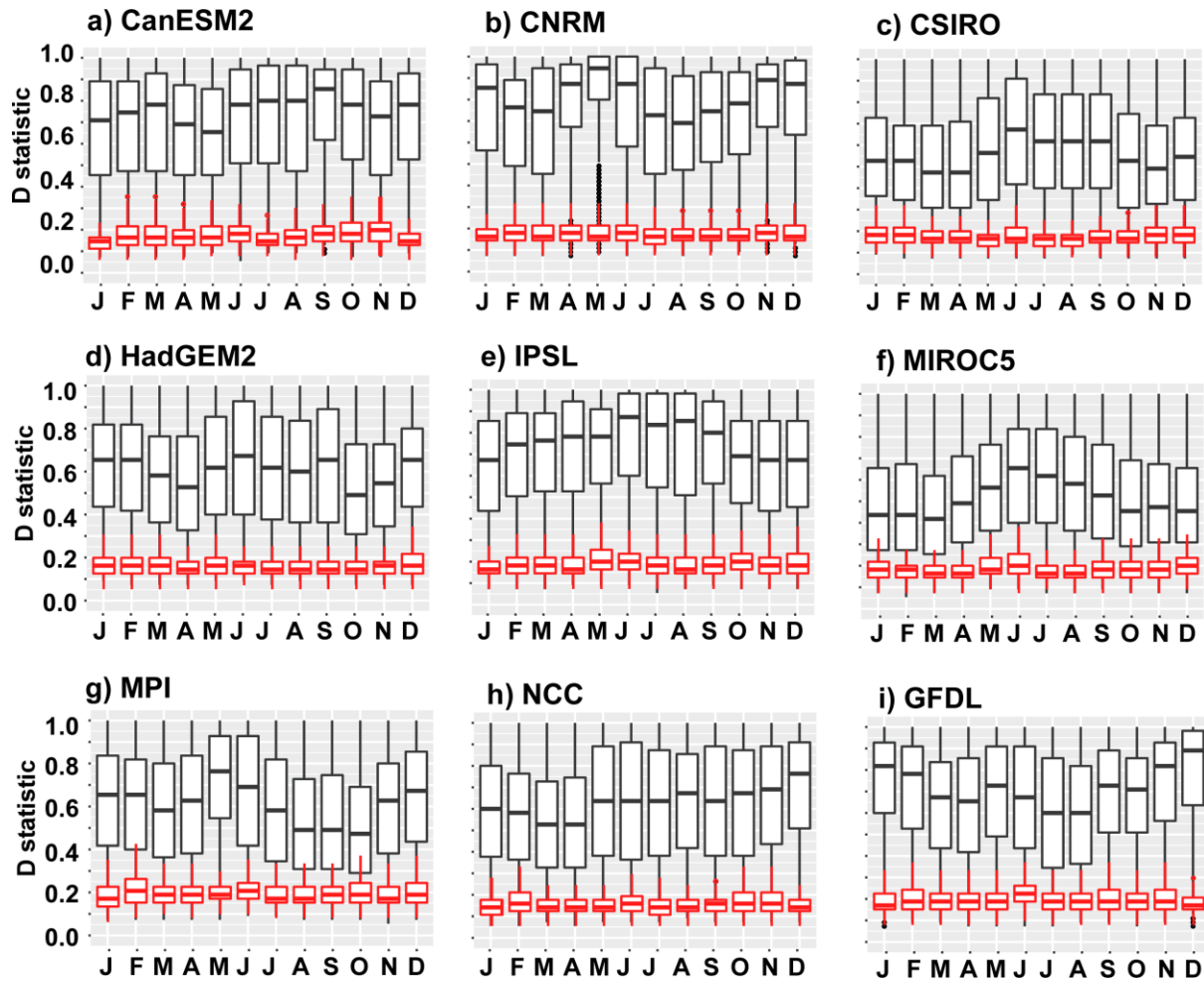
S4.1: Long-term mean monthly historical precipitation (1951-2005) (a) CRU observations (b) CanESM2 (c) CNRM (d) CSIRO (e) HadGEM2 (f) IPSL (g) MIROC5 (h) MPI (i) NCC (j) GFDL. Grey contours highlight regions of significant difference between observations and simulations ($p < 0.1$) based on a t test.



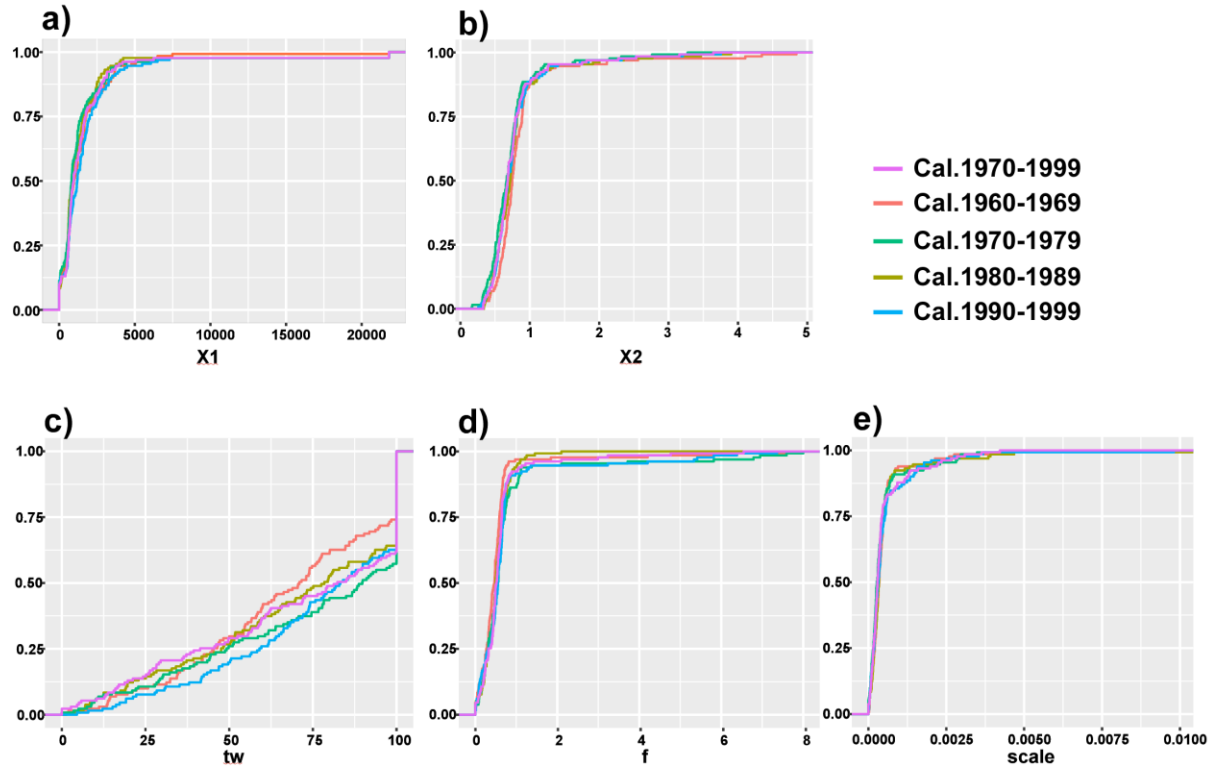
S4.2: Seasonal distributional biases (KS-test dissimilarity statistics) in historical precipitation between observation and climate model simulations for the period 1951-2005. White boxplots correspond to historical simulations and red boxplot correspond to bias-corrected simulations. (a) CanESM2 (b) CNRM (c) CSIRO (d) HadGEM2 (e) IPSL (f) MIROC5 (g) MPI (h) NCC (i) GFDL. At $p=0.1$ the critical value is 0.1645.



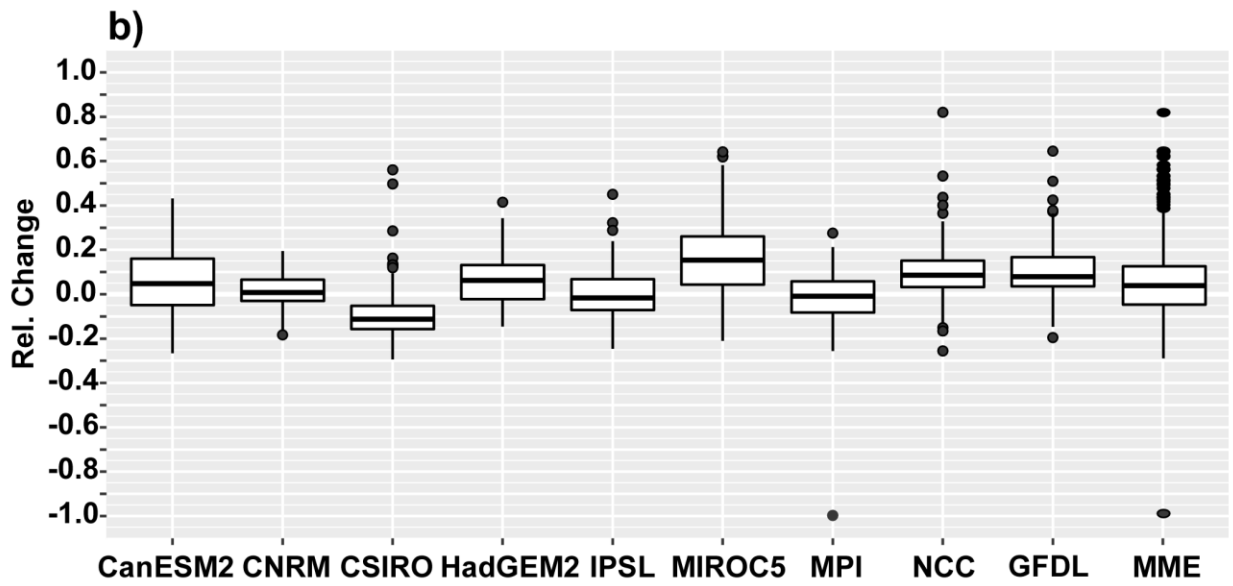
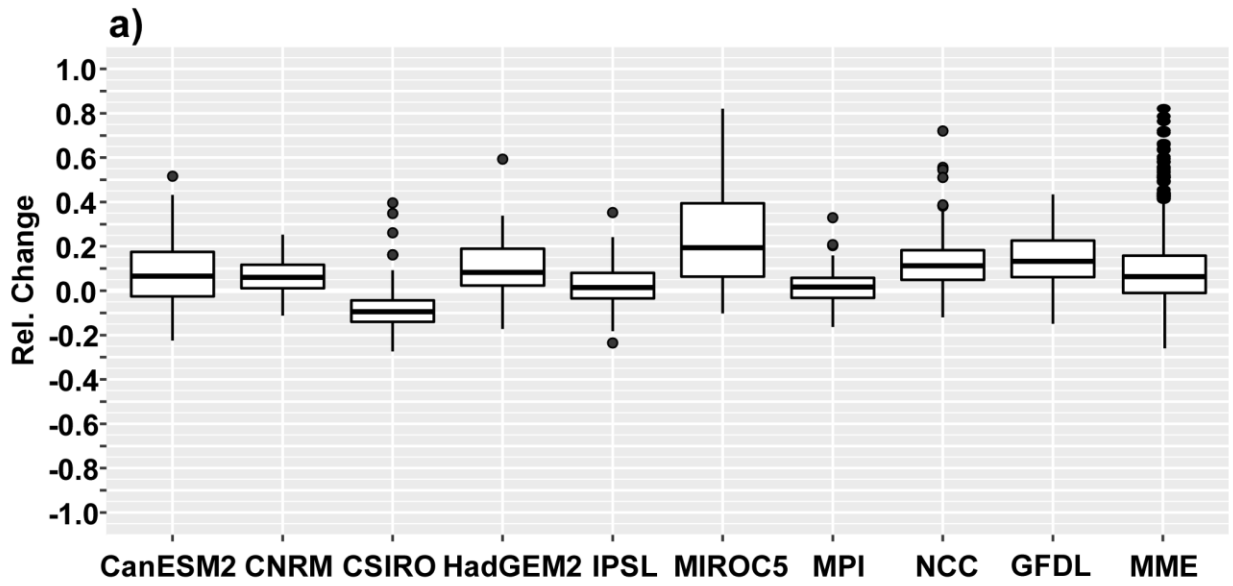
S4.3: Seasonal distributional biases (KS-test dissimilarity statistics) in historical maximum temperatures between observation and climate model simulations for the period 1951-2005. White boxplots correspond to historical simulations and red boxplot correspond to bias-corrected simulations. (a) CanESM2 (b) CNRM (c) CSIRO (d) HadGEM2 (e) IPSL (f) MIROC5 (g) MPI (h) NCC (i) GFDL. At $p=0.1$ the critical value is 0.1645.



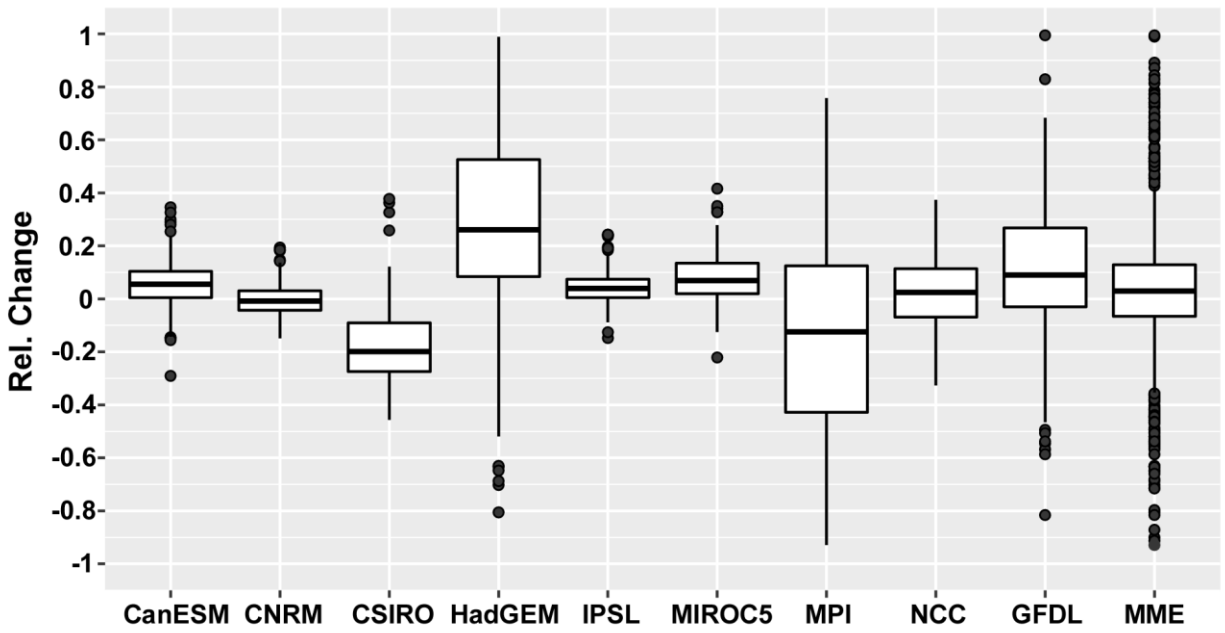
S4.4: Seasonal distributional biases (KS-test dissimilarity statistics) in historical minimum temperatures between observation and climate model simulations for the period 1951-2005. White boxplots correspond to historical simulations and red boxplot correspond to bias-corrected simulations. (a) CanESM2 (b) CNRM (c) CSIRO (d) HadGEM2 (e) IPSL (f) MIROC5 (g) MPI (h) NCC (i) GFDL. At $p=0.1$ the critical value is 0.1645.



S4.5: Cumulated distribution functions of Hydrological model parameters for different calibration periods over the entire study area (a) GR2M $X1$ parameter (b) GR2M $X2$ parameter (c) IHACRES-CWI tw parameter (d) IHACRES-CWI f parameter (e) IHACRES-CWI $scale$ parameter.



S4.6: Relative change in streamflow by mid-21st simulated by both hydrological models (a) GR2M (b) IHACRES-CWI.



S4.7: Relative change in streamflow by mid-21st simulated by the multi-timescale teleconnections-based regression model.

CHAPTER 5: GENERAL DISCUSSIONS

5. General Discussions

The overall aim of this thesis was to provide better understanding of past and future hydroclimatic variability across West and Central Africa and their teleconnections.

The results documented here shed light on past hydroclimatic variability across West and Central Africa and interactions with both catchment properties and large-scale climate variability. In addition, new robust approaches were presented to predict the impact of near-term climate change on hydrological systems. The key findings of this thesis will be discussed in turn, highlighting their significance and identifying areas requiring further research and recommendations to advance the understanding of hydrological processes in Sub-Saharan Africa.

5.1. Past hydroclimatic variability in West and Central Africa

Since the 1950s, significant unprecedented changes in climate conditions occurred across Sub-Saharan Africa, triggering several important studies (*e.g.* Dai *et al.*, 2004; Held *et al.*, 2005; Ali and Lebel, 2009; Mahé *et al.*, 2013; Nicholson, 2013; Panthou *et al.*, 2014, 2018). Important advances were made in terms of understanding hydroclimatic trends, but difficulties inherent to data-scarcity tend to limit investigations to local scales. These issues are addressed within the first objective of the thesis: *“To assemble a new, robust reconstructed streamflow dataset for West and Central Africa and examine hydroclimatic trends and variability over the region between 1950 and 2005”*.

To address the gap of data-scarcity in the study area, state-of-the-art data imputation techniques (**MICE**: Van Buuren and Oudshoorn, 1999; **Random Forest**: Stekhoven and Bühlmann, 2012) were implemented to construct a complete monthly streamflow dataset (1950-2005) for river basins in West and Central Africa (cf. Chapter 2). Both methods yielded satisfactory results providing high confidence about the quality of the reconstructed dataset. Nonetheless, analyses

were performed using the Random Forest reconstruction outputs, which appear to better capture the complex changes in streamflow (cf. Chapter 2).

Often, changes (whether natural or artificial) in hydroclimatic time series occur abruptly (step change) or gradually (trend) or in more complex forms (Machiwal and Jha, 2006). In Chapter 2, applying step-change algorithms, two main change-points were detected at the regional scale in 1970 and 1993, respectively. Trend analysis indicated that the period 1950–1970 was characterized by negative streamflow trends in Sahelian and Sudanian regions of West Africa, while positive streamflow trends were observed in Central Africa. The following period (1970–1993) was characterized mostly by negative trends due to dryer conditions. This pattern is reversed during the most recent period 1993–2005, with mainly positive trends resulting from increased rainfall and changes in land use in Sahelian regions. In general, findings indicate good agreement between streamflow and precipitation trends, with an offsetting effect of potential evapotranspiration observed in some regions (*e.g.* Niger, Chad and northern Nigeria). These results confirmed previous findings (*e.g.* Mahé *et al.*, 2001, 2005; Conway *et al.*, 2009; Nicholson, 2013; Roudier *et al.*, 2014), but more importantly elucidated the impact of internal variability on long-term trends through multi-temporal trend analyses. In fact, the results highlighted important interannual to decadal fluctuations in both annual precipitation and streamflow, which significantly influence long-term trends. Chapter 2 thus provided a different perspective on hydroclimatic variability over West and Central Africa. For instance, the so-called “Sahelian paradox” (Albergel, 1987; Mahé *et al.*, 2005; Descroix *et al.*, 2013, 2018) presented as a paradoxical increase in streamflow despite decreasing annual rainfall can be viewed as hydrological responses of degraded land surfaces: amplifying (damping) high (low) frequency fluctuations and surface runoff (baseflow). Furthermore, the weak amplitude of long-term trends in Central Africa could be attributed to the

importance of interannual and decadal fluctuations. While time-scale dependent fluctuations in hydroclimatic variables were highlighted in Chapter 2, the main drivers of these fluctuations remained an open research question which was investigated in Chapter 3 of the thesis.

5.2. Drivers of streamflow variability: from catchment properties to large-scale climate patterns

At the regional scale, few studies have investigated streamflow variability and its drivers (Roudier *et al.*, 2014). Building upon the findings presented in Chapter 2, analyses were performed as a further step towards unravelling processes associated with streamflow variability (Chapter 3) and therefore answer the questions associated with the second research objective: *“To unravel the complex processes associated with streamflow variability beyond the catchment scale perspective in data scarce environments”*.

Applying spectral analysis and clustering techniques, three homogenous regions of streamflow variability were defined. Over parts of Central Africa and the lower Niger River (Clusters 1-2), streamflow variability is mainly related to interannual and quasi-decadal fluctuations. In most regions of West Africa, however, interannual and quasi-decadal fluctuations are also combined with multi-decadal fluctuations. The difference observed in streamflow variability over West Africa and parts of Central Africa is consistent with the findings of Mahé *et al.* (2001), reporting a contrast between West Africa and Central Africa in terms of rainfall variability for the 1951-1989 period. In addition, Dieppois *et al.* (2015) documented important interannual to multi-decadal fluctuations in the Sahel rainfall, which explain to some extent the observed modes of streamflow variability. This suggests that regional scale streamflow variability is mainly driven by rainfall fluctuations. Nonetheless, differences observed in terms of explained total variance between modes of rainfall and streamflow suggest that catchment properties serve as a proxy for shaping rainfall-runoff relationships. PCA indicated that high interannual variability is generally observed

in steep, round catchments with shallow groundwater systems, whereas a greater contribution of multi-decadal timescales is more likely to occur in large elongated catchments with deep groundwater. At the same time, decadal fluctuations are mainly positively related to vegetation cover and water holding capacity. It is also worth mentioning that catchment properties interact in a complex way as Hortonian runoff can be observed in Sudanian regions, and inversely “Hewlett-type” runoff processes are observable in the Sahelian regions (Descroix *et al.*, 2009).

Beyond the catchment scale drivers, the interactions between streamflow variability and the key processes driving the WAM were also investigated. The results indicated significant teleconnections from interannual to multi-decadal timescales. For instance, positive streamflow phases at interannual timescales are associated with a southerly position of the ITCZ for Clusters 1 and 2 (parts of Central Africa and the lower Niger River), and a northward position for Cluster 3 (mostly West Africa). These teleconnections are different for multi-decadal timescales with a northeastward shift of the ITCZ over the entire study area: this suggests that low frequency fluctuations in streamflow (*e.g.* baseflow) are driven by the same climatic processes at the regional scale. In the mid to upper-troposphere, significant teleconnections were also detected for the leading circulation features (AEJ and TEJ). Despite spatial discrepancies, it appears that positive streamflow anomalies over the study area are associated with a stronger TEJ and weaker AEJ. Modes of streamflow variability also presented significant multi-timescale teleconnections with SST. For instance, interannual streamflow variability is associated with warm (Clusters 1 and 2) and cold (Cluster 3) anomalies in the global tropical oceans, namely the Atlantic Niño, Indian Ocean dipole and ENSO-like patterns in the Pacific Ocean. Meanwhile decadal timescales seem to be dominated by the combined effect of inter-hemispheric SST gradient in the Atlantic and Pacific Ocean: AMO and PDO. The different zonal gradients driven by ENSO at the interannual

timescale (*e.g.* Giannini *et al.*, 2005; Rodriguez-Fonseca *et al.*, 2015), and the PDO at decadal timescales (*e.g.* Wang *et al.*, 2014), contribute in triggering shifts in the Walker circulations detected in the OLR anomalies. Interestingly, the multi-resolution analysis also indicated divergences at interannual timescales (*e.g.* components 1 and 2) pointing out the unstable nature of detected teleconnections, as observed in some studies of rainfall-SST teleconnections (*e.g.* Rodriguez-Fonseca *et al.*, 2015; Suárez-Moreno *et al.*, 2018). The teleconnections highlighted herein, present great similarities with those detected for rainfall, and therefore open-up the potential for robust multi-timescale climate-streamflow prediction in data-scarce environments. The streamflow predictability skills provided by these teleconnections were tested in Chapter 4.

5.3. Impact of near-term climate change on hydrological systems in West and Central Africa

Streamflow projections are impacted by uncertainties in both input data and modelling steps. In addition, existing studies mainly focus on individual basins with climate change scenarios often provided by coarse spatial scale GCMs or early versions of RCMs (Roudier *et al.*, 2014; Stanzel *et al.*, 2018). In Chapter 4, a novel strategy for streamflow prediction, based on the recommendations by Clark *et al.* (2016) and streamflow-SST teleconnections detected in Chapter 3, is implemented to answer the scientific questions associated with the third research objective: ***“To provide further insights into the response of hydrological systems to a changing climate across West and Central Africa by the mid-21st century”.***

The first approach inspired from the framework provided by Clark *et al.* (2016) aimed to reduce uncertainties through adequate methods, models selection. This led to the selection of the near future (2020-2050) as a temporal window combined with a single emission scenario (RCP4.5) to mitigate to some extent the scenario uncertainty in future climate projections. State-of-the-art bias-

correction algorithms were applied to climatic variables (P , T_{\max} and T_{\min}) prior to their use in two conceptual hydrological models. These bias-correction algorithms satisfactorily reduced discrepancies between model simulations and observations, and importantly preserved the climate change signal predicted by climate models. However, the bias-correction presented limited skill over Central Equatorial Africa, stemming mainly from the quality of observational datasets (New *et al.*, 2000; Nikulin *et al.*, 2012), which also impacted the performance of hydrological models. Nonetheless, the hydrological modelling strategy favouring different model structures provided useful insights into the different hydrological processes occurring at the regional scale: while important groundwater interactions occurring mostly in Sudanian and Guinean regions were captured by GR2M, IHACRES-CWI satisfactorily represented the complex processes occurring downstream the Inner Niger Delta and the Benue River.

The second approach was built upon streamflow-large scale climate teleconnections. Streamflow projections were derived based on large-scale SST teleconnections using multi-timescale linear regression models (Massei *et al.*, 2017). The main hypothesis was that reducing the steps in the traditional streamflow prediction chain could provide better results in data-scarce regions. This hypothesis is confirmed mostly in Central Africa. In fact, despite limited skill over the upper reach of the Niger River in the Guinean and Sudanian regions, the results suggest that this approach can serve as a reliable alternative to hydrological models for impact studies in data-scarce regions with robust streamflow-SST teleconnections.

Under a mitigation scenario (RCP4.5), West and Central Africa, will be characterized by slightly wetter conditions (from 2 to 12% increase) by mid-21st century. The future rainfall pattern is however characterized by a high spatial variability with lower changes expected in Central Africa ($\pm 4\%$) and more important changes along the Sahelian strip (-22 to 28%), where a zonal contrast

(drier western and wetter eastern) is apparent in some models. Temperatures present a sustained increasing rate (higher for minimum temperatures) between +1.2°C and +2.2°C, with highest absolute changes occurring mainly along the Sahelian band. These fluctuations in climatic variables will result in slight positive streamflow changes (~ +5%), which are consistent across the different modelling strategies despite local differences. The pattern closely mimics the change in rainfall, with smaller (higher) changes in Central Africa (further North). Despite agreements in streamflow projected change over the entire study area, a higher interquartile range ($\pm 40\%$) is observed for the teleconnections-based regression model, due to uncertainties in SST simulations. This is especially true for the different future trajectories of main modes of variability in the Atlantic and Pacific Oceans (*e.g.* ENSO, AMO) predicted by CMIP5 models. Further investigations with large ensembles and larger multi-model ensembles will shed the light on uncertainties associated with SST projections, streamflow large-scale climate teleconnections and help assess the full spectrum of future streamflow fluctuations.

5.4. Conclusions and envisaged future work

From the investigation of past and future hydroclimatic variability in West and Central Africa, as well as their teleconnections with large-scale climate variability, the following conclusions can be made:

- Data imputation algorithms yield satisfactory results in the reconstruction of streamflow time series in West and Central Africa. However, due to significant changes and the intensification of the hydrological system, non-parametric methods appear to be more appropriate.
- Hydroclimatic records in West and Central Africa are highly non-stationary, with marked interannual to multi-decadal fluctuations.

- Modes of streamflow variability are mainly driven by fluctuations in precipitation modulated by catchment properties. These modes of variability thus present significant teleconnections with the key large-scale drivers of the WAM (ITCZ, global/regional SST, AEJ and TEJ).
- It is essential to consider different hydrological model structures for a better representation of hydrological processes across West and Central Africa. For instance, the findings highlighted that GR2M performed better in regions with important groundwater interactions, while IHACRES successfully captured complex rainfall-runoff relationships downstream of the Niger River inner delta and parts of Central Africa.
- In data-scarce regions, where bias-correction algorithms and hydrological models are substantially impacted by the quality of gridded observational datasets, simple regression models built upon streamflow-SST teleconnections can serve as an alternative to the traditional modelling chain.
- At the regional scale, near-term climate change will result in slight positive changes ($\sim +5\%$) in streamflow across West and Central Africa.

The present research on hydroclimatic variability over West and Central Africa point out to further research topics. Further improvements could be undertaken to advance the understanding of hydrological processes in a changing climate across Sub-Saharan Africa.

- Due to the overall decline in meteorological stations since the 2000s, which was associated with changes in data sharing policies, analyses in this study are limited to the 1950-2005 period. Extending the streamflow dataset to the recent conditions through national water offices would be an important improvement. A joint effort involving organisations such as the African Union (AU) and the World Meteorological Organization (WMO) is necessary

to improve observation networks and data sharing policies among national meteorological offices.

- The focus here was on monthly and annual averages, but with the intensification of the hydrological system reported in West Africa (*e.g.* Taylor *et al.*, 2017; Panthou *et al.*, 2018; Wilcox *et al.*, 2018), a shift to extreme events and daily time steps, will improve understanding of hydrological processes and inform natural hazard mitigation plans.
- Identifying the most appropriate model structure for the characterisation of hydrological processes and quantifying associated uncertainties are the main challenges facing the hydrological community (Clark *et al.*, 2008). In future studies, the focus will be on investigating the dominant hydrological processes over West and Central Africa, and providing a global map of hydrological model suitability. In addition, the large spread observed in linear regression-based streamflow predictions point out the need for larger multi-model ensembles to systematically assess the spectrum of uncertainties.
- River flow projections presented in this study account only for climate change and variability. By the mid-21st century, the growing population in Sub-Saharan Africa (~ 2 billion people by 2050), and associated increases in water demand, will pose substantial threats to water security (quantity and quality; Serdeczny *et al.*, 2017), with detrimental impacts on hydrological regimes (Mahé *et al.*, 2013). Detailed investigations must be undertaken to integrate the societal dimension of climate change, and to understand the connections between climate change and the water-energy-food nexus, as advocated by the Sustainable Development Goals (Stockholm Environment Institute, 2014). More specifically three other key aspects significantly impacting river flow (Sterling *et al.*, 2013): land use, water consumption/withdrawal and carbon effect on plant water use need

to be accounted for. Advances in climate modelling and water accounting techniques will serve as serious assets to answer those questions, but most importantly an integrated approach involving both impact modellers and social scientists will be necessary.

The results presented in this thesis, shed light on past and future hydroclimatic variability in West and Central Africa and their teleconnections with large scale climate variability. It is our hope that the findings presented here will foster research activity in view of developing sound climate change adaptation strategies in this part of the world.

Bibliography

- Adeaga, O., Mahé, G., Dieulin, C., Elbaz-Poulichet, F., Rouche, N., Seide, J. L., Servat, E. (2012) 'Rainfall-Runoff Simulation in Part of Lower Niger Basin'. *Journal of Environmental Science and Engineering*, 1(6B), 812.
- Aich, V., Liersch, S., Vetter, T., Huang, S., Tecklenburg, J., Hoffmann, P., Koch, H., Fournet, S., Krysanova, V., Müller, E.N., Hattermann, F.F. (2014) 'Comparing impacts of climate change on streamflow in four large African river basins'. *Hydrology and Earth System Sciences*, 18(4), 1305-1321.
- Akinsanola, A.A., Ajayi, V.O., Adejare, A.T., Adeyeri, O.E., Gbode, I.E., Ogunjobi, K.O., Nikulin, G., Abolude, A.T. (2018) 'Evaluation of rainfall simulations over West Africa in dynamically downscaled CMIP5 global circulation models'. *Theoretical and applied climatology*, 132(1-2), 437-450.
- Albergel, J. (1987) 'Sécheresse, désertification et ressources en eau de surface : application aux petits bassins du Burkina Faso'. *The influence of climate change and climatic variability on the hydrologic regime and water resources*, 168, 355-365.
- Ali, A., Lebel, T. (2009) 'The Sahelian standardized rainfall index revisited'. *International Journal of Climatology*, 29(12), 1705-1714.
- Allen, R.G., Luis, S.P., RAES, D., Smith, M. (1998) 'Crop evapotranspiration-Guidelines for computing crop water requirements-FAO Irrigation and drainage paper 56'. *FAO, Rome*, 300(9), D05109.
- Aloysius, N.R., Sheffield, J., Sainers, J.E., Li, H., Wood, E.F. (2016) 'Evaluation of historical and future simulations of precipitation and temperature in central Africa from CMIP5 climate models'. *Journal of Geophysical Research: Atmospheres*, 121(1), 130-152.
- Alsdorf, D., Beighley, E., Laraque, A., Lee, H., Tshimanga, R., O'Loughlin, F., Mahé, G., Dinga, B., Moukandi, G., Spencer, R.G.M. (2016) 'Opportunities for hydrologic research in the Congo Basin'. *Reviews of Geophysics*, 54(2), 378-409.
- Amogu, O., Descroix, L., Yéro, K.S., Le Breton, E., Mamadou, I., Ali, A., Vischel, T., Bader, J.-C., Moussa, I.B., Gautier, E., Boubkraoui, S., Belleudy, P. (2010) 'Increasing River Flows in the Sahel?'. *Water*, 2(2), 170-199.
- Amoussou, E. (2010). *Variabilité pluviométrique et dynamique hydro-sédimentaire du bassin versant du complexe fluvio-lagunaire Mono-Ahémé-Couffo (Afrique de l'ouest)* (Doctoral dissertation, Dijon).
- Ardoin-Bardin, S., Dezetter, A., Servat, E., Paturel, J.E., Mahé, G., Niel, H., Dieulin, C. (2009) 'Using general circulation model outputs to assess impacts of climate change on runoff for large hydrological catchments in West Africa'. *Hydrological Sciences Journal*, 54(1), 77-89.
- Asefi-Najafabady, S., Saatchi, S. (2013) 'Response of African humid tropical forests to recent rainfall anomalies'. *Philosophical Transactions of the Royal Society B: Biological Sciences*, 368(1625), 20120306.
- Auger, I.E., Lawrence, C.E. (1989) 'Algorithms for the optimal identification of segment neighborhoods'. *Bulletin of mathematical biology*, 51(1), 39-54.
- Ault, T.R., Cole, J.E., Overpeck, J.T., Pederson, G.T., George, S.S., Otto-Bliesner, B., Woodhouse, C.A., Deser, C. (2013) 'The Continuum of hydroclimate variability in Western North America during the last millennium'. *Journal of Climate*, 26(16), 5863-5878.
- Badr, H.S., Dezfouli, A.K., Zaitchik, B.F., Peters-Lidard, C.D. (2016) 'Regionalizing Africa: Patterns of precipitation variability in observations and global climate models'. *Journal of Climate*, 29(24), 9027-9043.

- Balas, N., Nicholson, S.E., Klotter, D. (2007) 'The relationship of rainfall variability in West Central Africa to sea-surface temperature fluctuations'. *International Journal of Climatology: A Journal of the Royal Meteorological Society*, 27(10), 1335-1349.
- Benestad, R.E. (2001) 'A comparison between two empirical downscaling strategies'. *International Journal of Climatology: A Journal of the Royal Meteorological Society*, 21(13), 1645-1668.
- Benestad, R.E. (2002) 'Empirically downscaled multimodel ensemble temperature and precipitation scenarios for Norway'. *Journal of Climate*, 15(21), 3008-3027.
- Biasutti, M. (2013) 'Forced Sahel rainfall trends in the CMIP5 archive'. *Journal of Geophysical Research: Atmospheres*, 118(4), 1613-1623.
- Biasutti, M., Held, I.M., Sobel, A.H., Giannini, A. (2008) 'SST forcings and Sahel rainfall variability in simulations of the twentieth and twenty-first centuries'. *Journal of Climate*, 21(14), 3471-3486.
- Biasutti, M., Sobel, A.H., Camargo, S.J. (2009) 'The role of the Sahara low in summertime Sahel rainfall variability and change in the CMIP3 models'. *Journal of Climate*, 22(21), 5755-5771.
- Bodian, A., Dezetter, A., Diop, L., Deme, A., Djaman, K., Diop, A. (2018) 'Future climate change impacts on streamflows of Two Main West Africa River Basins: Senegal and Gambia'. *Hydrology*, 5(1), 21.
- Boyer, J. F., Dieulin, C., Rouche, N., Cres, A., Servat, E., Paturel, J. E., Mahé, G. (2006) 'SIEREM: An environmental information system for water resources'. *IAHS publication*, 308, 19.
- Breiman, L. (2001). Random Forests. Vol. 45. *Mach Learn*, 1.
- Burpee, W. R. (1972) 'Origin and structure of easterly waves in lower troposphere of North Africa'. *Journal of the Atmospheric Sciences*, 29(1), 77-90.
- Camberlin, P., Janicot, S., Pocard, I. (2001) 'Seasonality and atmospheric dynamics of the teleconnection between African rainfall and tropical sea-surface temperature: Atlantic vs. ENSO'. *International Journal of Climatology*, 21(8), 973-1005.
- Cannon, A.J., Sobie, S.R., Murdock, T.Q. (2015) 'Bias correction of GCM precipitation by quantile mapping: How well do methods preserve changes in quantiles and extremes?'. *Journal of Climate*, 28(17), 6938-6959.
- Cappelaere, B., Descroix, L., Lebel, T., Boulain, N., Ramier, D., Laurent, J.P., Favreau, G., Boubkraoui, S., Boucher, M., Bouzou Moussa, I., Chaffard, V., Hiernaux, P., Issoufou, H.B.A., Le Breton, E., Mamadou, I., Nazoumou, Y., Oi, M., Otlé, C., Quantin, G. (2009) 'The AMMA-CATCH experiment in the cultivated Sahelian area of south-west Niger - Investigating water cycle response to a fluctuating climate and changing environment'. *Journal of Hydrology*, 375(1-2), 34-51.
- Charrad, M., Ghazzali, N., Boiteau, V., Niknafs, A. (2014) '**NbClust** : An R Package for Determining the Relevant Number of Clusters in a Dataset'. *Recuperado de: <https://cran.rproject.org/web/packages/NbClust/NbClust.pdf>*.
- Chiang, J.C.H., Friedman, A.R. (2012) 'Extratropical Cooling, Interhemispheric Thermal Gradients, and Tropical Climate Change'. *Annual Review of Earth and Planetary Sciences*, 40, 383-412.
- Chiew, F.H.S., McMahon, T.A. (2002) 'Global ENSO-streamflow teleconnection, streamflow forecasting and interannual variability'. *Hydrological Sciences Journal*, 47(3), 505-522.
- Chiew, F.H.S., Piechota, T.C., Dracup, J.A., McMahon, T.A. (1998) 'El Niño /Southern Oscillation and Australian rainfall, streamflow and drought: Links and potential for forecasting'. *Journal of Hydrology*, 204(1-4), 138-149.

Citeau, J., Bergès, J.C., Demarcq, H., Mahé, G. (1988) 'The watch of ITCZ migrations over the tropical atlantic oceanas an indicator in drought forecast over Sahelian areas'. *Tropical Ocean-Atmosphere Newsletter*, (45), 1-3.

Clark, M.P., Slater, A.G., Rupp, D.E., Woods, R.A., Vrugt, J.A., Gupta, H. V., Wagener, T., Hay, L.E. (2008) 'Framework for Understanding Structural Errors (FUSE): A modular framework to diagnose differences between hydrological models'. *Water Resources Research*, 44(12).

Clark, M.P., Wilby, R.L., Gutmann, E.D., Vano, J.A., Gangopadhyay, S., Wood, A.W., Fowler, H.J., Prudhomme, C., Arnold, J.R., Brekke, L.D. (2016) 'Characterizing Uncertainty of the Hydrologic Impacts of Climate Change'. *Current Climate Change Reports*, 2(2), 55-64.

Compo, G.P., Whitaker, J.S., Sardeshmukh, P.D., Matsui, N., Allan, R.J., Yin, X., Gleason, B.E., Vose, R.S., Rutledge, G., Bessemoulin, P., BroNnimann, S., Brunet, M., Crouthamel, R.I., Grant, A.N., Groisman, P.Y., Jones, P.D., Kruk, M.C., Kruger, A.C., Marshall, G.J., Maugeri, M., Mok, H.Y., Nordli, O., Ross, T.F., Trigo, R.M., Wang, X.L., Woodruff, S.D., Worley, S.J. (2011) 'The Twentieth Century Reanalysis Project'. *Quart. J. Roy. Meteor. Soc.*, 137, 1-28.

Conway, D. (2002) 'Extreme rainfall events and lake level changes in East Africa: Recent events and historical precedents'. *The East African great lakes: limnology, palaeolimnology and biodiversity* (pp. 63-92). Springer, Dordrecht.

Conway, D., Persechino, A., Ardoin-Bardin, S., Hamandawana, H., Dieulin, C., Mahé, G. (2009) 'Rainfall and Water Resources Variability in Sub-Saharan Africa during the Twentieth Century'. *Journal of Hydrometeorology*, 10(1), 41-59.

Cook, K.H., Vizi, E.K. (2012) 'Impact of climate change on mid-twenty-first century growing seasons in Africa'. *Climate Dynamics*, 39(12), 2937-2955.

Cornish, C.R., Bretherton, C.S., Percival, D.B. (2006) 'Maximal overlap wavelet statistical analysis with application to atmospheric turbulence'. *Boundary-Layer Meteorology*, 119(2), 339-374.

Croke, B.F.W., Jakeman, A.J. (2004) 'A catchment moisture deficit module for the IHACRES rainfall-runoff model'. *Environmental Modelling & Software*, 19(1), 1-5.

D'amato, N., Lebel, T. (1998) 'On the characteristics of the rainfall events in the Sahel with a view to the analysis of climatic variability'. *International Journal of Climatology*, 18(9), 955-974.

Dai, A., Lamb, P.J., Trenberth, K.E., Hulme, M., Jones, P.D., Xie, P. (2004) 'The recent Sahel drought is real'. *International Journal of Climatology: A Journal of the Royal Meteorological Society*, 24(11), 1323-1331.

Dardel, C., Kergoat, L., Hiernaux, P., Mougin, E., Grippa, M., Tucker, C.J. (2014) 'Re-greening Sahel: 30 years of remote sensing data and field observations (Mali, Niger)'. *Remote Sensing of Environment*, 140, 350-364.

Déqué, M., Rowell, D.P., Lüthi, D., Giorgi, F., Christensen, J.H., Rockel, B., Jacob, D., Kjellström, E., De Castro, M., Van Den Hurk, B. (2007) 'An intercomparison of regional climate simulations for Europe: Assessing uncertainties in model projections'. *Climatic Change*, 81(1), 53-70.

Descroix, L., Guichard, F., Grippa, M., Lambert, L., Panthou, G., Mahé, G., Gal, L., Dardel, C., Quantin, G., Kergoat, L., Bouaïta, Y., Hiernaux, P., Vichel, T., Pellarin, T., Faty, B., Wilcox, C., Malam Abdou, M., Mamadou, I., Vandervaere, J-P, Diongue-Niang, A., Ndiaye, O., Sané, Y., Dacosta, H., Gosset, M., Cassé, C., Sultan, B., Barry, A., Amogu, O., NkaNnomo, B., Barry, A., and Patuere, J.-E. (2018) 'Evolution of Surface Hydrology in the Sahelo-Sudanian Strip: An Updated Review'. *Water*, 10(6), 748.

Descroix, L., Mahé, G., Lebel, T., Favreau, G., Galle, S., Gautier, E., Olivry, J.C., Albergel, J., Amogu, O., Cappelaere, B., Dessouassi, R., Diedhiou, A., Le Breton, E., Mamadou, I., Sighomnou, D. (2009) 'Spatio-temporal variability of hydrological regimes around the boundaries between Sahelian and Sudanian areas of West Africa: A synthesis'. *Journal of Hydrology*, 375(1-2), 90-102.

Descroix, L., Moussa, I. B., Genthon, P., Sighomnou, D., Mahé, G., Mamadou, I., Vandervaere, J.-P., Gautier, E., Maiga, O. F., Rajot, J.-L., Abdou, M. M., Dessay, N., Ingatan, A., Noma, I., Yéro, K.S., Karambiri, H., Fensholt, R., Albergel, J., and Olivry, J.-C. (2013) 'Impact of Drought and Land – Use Changes on Surface – Water Quality and Quantity: The Sahelian Paradox'. *Current perspectives in contaminant hydrology and water resources sustainability*, 10, 243–271.

Deser, C., Phillips, A., Bourdette, V., Teng, H. (2012) 'Uncertainty in climate change projections: the role of internal variability'. *Climate dynamics*, 38(3-4), 527-546.

Dezetter, A., Girard, S., Paturel, J.E., Mahé, G., Ardoin-Bardin, S., Servat, E. (2008) 'Simulation of runoff in West Africa: Is there a single data-model combination that produces the best simulation results?'. *Journal of Hydrology*, 354(1-4), 203-212.

Dezfuli, A. K. (2017). *Climate of western and central equatorial Africa*.

Dezfuli, A.K., Nicholson, S.E. (2013) 'The relationship of rainfall variability in western equatorial africa to the tropical oceans and atmospheric circulation. Part II: The boreal autumn'. *Journal of Climate*, 26, 66–84.

Diem, J.E., Ryan, S.J., Hartter, J., Palace, M.W. (2014) 'Satellite-based rainfall data reveal a recent drying trend in central equatorial Africa'. *Climatic Change*, 126(1-2), 263-272.

Dieppois, B., Diedhiou, A., Durand, A., Fournier, M., Massei, N., Sebag, D., Xue, Y., Fontaine, B. (2013) 'Quasi-decadal signals of Sahel rainfall and West African monsoon since the mid-twentieth century'. *Journal of Geophysical Research: Atmospheres*, 118(22), 12-587.

Dieppois, B., Durand, A., Fournier, M., Diedhiou, A., Fontaine, B., Massei, N., Nouaceur, Z., Sebag, D. (2015) 'Low-frequency variability and zonal contrast in Sahel rainfall and Atlantic sea surface temperature teleconnections during the last century'. *Theoretical and applied climatology*, 121(1-2), 139-155.

Dieppois, B., Pohl, B., Cretat, J., Eden, J., Sidibe, M., New, M., Rouault, M., Lawler, D. (2019) 'Southern African summer-rainfall variability, and its teleconnections, on interannual to interdecadal timescales in CMIP5 models'. *Climate Dynamics*, 1-23.

Dieppois, B., Pohl, B., Rouault, M., New, M., Lawler, D., Keenlyside, N. (2016) 'Interannual to Interdecadal variability of winter and summer southern African rainfall, and their teleconnections'. *Journal of Geophysical Research: Atmospheres*, 121(11), 6215-6239.

Dieulin, C., Mahé, G., Paturel, J. E., Ejjiyar, S., Trambly, Y., Rouché, N., EL Mansouri, B. (2019) 'A New 60-Year 1940/1999 Monthly-Gridded Rainfall Data Set for Africa'. *Water*, 11(2), 387.

Drobinski, P., Sultan, B., Janicot, S. (2005) 'Role of the Hoggar massif in the West African monsoon onset'. *Geophysical research letters*, 32(1).

Droogers, P., Allen, R.G. (2002) 'Estimating reference evapotranspiration under inaccurate data conditions'. *Irrigation and drainage systems*, 16(1), 33-45.

Druyan, L.M., Feng, J., Cook, K.H., Xue, Y., Fulakeza, M., Hagos, S.M., Konaré, A., Moufouma-Okia, W., Rowell, D.P., Vizy, E.K., Ibrah, S.S. (2010) 'The WAMME regional model intercomparison study'. *Climate Dynamics*, 35(1), 175-192.

Eden, J.M., Widmann, M., Grawe, D., Rast, S. (2012) 'Skill, correction, and downscaling of GCM-simulated precipitation'. *Journal of Climate*, 25(11), 3970-3984.

Ekström, M., Jones, P.D., Fowler, H.J., Lenderink, G., Buishand, T. a., Conway, D. (2007) 'Regional climate model data used within the SWURVE project – 1: projected changes in seasonal patterns and estimation of PET'. *Hydrology and Earth System Sciences Discussions*, 11(3), 1069-1083.

Eltahir, E. A., Gong, C. (1996) 'Dynamics of wet and dry years in West Africa'. *Journal of Climate*, 9(5), 1030-1042.

FAO: Sahel: situation météorologique et état des cultures, Rapport du 11 juin 2004, <http://www.fao.org/docrep/006/j2517f/j2517f00.HTM> (last access: October 2016), 2004.

Favreau, G., Nazoumou, Y., Leblanc, M., Guéro, A., Baba Goni, I. (2012) 'Groundwater resources increase in the Iullemeden Basin, west Africa'. *Climate Change Effects on Groundwater Resources: A Global Synthesis of Findings and Recommendations. CRC Press/Balkema/Taylor & Francis. IAH Blue Book Series Publi*, 27, 113-128.

Fontaine, B., Gaetani, M., Ullmann, A., Roucou, P. (2011) 'Time evolution of observed July–September sea surface temperature-Sahel climate teleconnection with removed quasi-global effect (1900–2008)'. *Journal of Geophysical Research: Atmospheres*, 116(D4).

Fontaine B, Philippon N. (2000) 'Seasonal evolution of boundary layer heat content in the West African monsoon from the NCEP/NCAR reanalysis (1968-1998)'. *International journal of climatology*, 20(14), 1777-1790.

Fontaine, B., Trzaska, S., Janicot, S. (1998) 'Evolution of the relationship between near global and Atlantic SST modes and the rainy season in West Africa: statistical analyses and sensitivity experiments'. *Climate Dynamics*, 14(5), 353-368.

Funk, C., Michaelsen, J., Marshall, M.T. (2012) 'Mapping recent decadal climate variations in precipitation and temperature across eastern Africa'. *Remote sensing of drought: innovative monitoring approaches*, 331.

Gaetani, M., Fontaine, B., Roucou, P., Baldi, M. (2010) 'Influence of the Mediterranean Sea on the West African monsoon: Intraseasonal variability in numerical simulations'. *Journal of Geophysical Research: Atmospheres*, 115(D24).

Gal, L., Grippa, M., Hiernaux, P., Pons, L., Kergoat, L. (2017) 'The paradoxical evolution of runoff in the pastoral Sahel: Analysis of the hydrological changes over the Agoufou watershed (Mali) using the KINEROS-2 model'. *Hydrology and Earth System Sciences*, 21(9), 4591-4613.

Geisser, S. (1975) 'The predictive sample reuse method with applications'. *Journal of the American statistical Association*, 70(350), 320-328.

Gerbaux, M., Hall, N., Dessay, N., Zin, I. (2009) 'The sensitivity of Sahelian runoff to climate change'. *Hydrological Sciences Journal*, 54(1), 5-16.

Giannini, A., Biasutti, M., Held, I.M., Sobel, A.H. (2008) 'A global perspective on African climate'. *Climatic Change*, 90(4), 359-383.

Giannini, A., Saravanan, R., Chang, P. (2003) 'Oceanic Forcing of Sahel Rainfall on Interannual to Interdecadal Time Scales'. *Science*, 302(5647), 1027-1030.

Giannini, A., Saravanan, R., Chang, P. (2005) 'Dynamics of the boreal summer African monsoon in the NSIPP1 atmospheric model'. *Climate Dynamics*, 25(5), 517-535.

Giorgi, F., Jones, C., Asrar, G.R. (2009) 'Addressing climate information needs at the regional level: The CORDEX framework'. *World Meteorological Organization (WMO) Bulletin*, 58(3), 175.

Giorgi, F., Mearns, L.O. (1991) 'Approaches to the simulation of regional climate change: A review'. *Reviews of Geophysics*, 29(2), 191-216.

Giuntoli, I., Villarini, G., Prudhomme, C., Hannah, D. M. (2018) 'Uncertainties in projected runoff over the conterminous United States'. *Climatic change*, 150(3-4), 149-162.

Goulden, M., Conway, D., Persechino, A. (2009) 'Adaptation to climate change in international river basins in Africa: a review'. *Hydrological Sciences Journal*, 54(5), 805-828.

Grist, J.P., Nicholson, E. (2001) 'A study of the dynamic factors influencing the rainfall variability in the West African Sahel'. *Journal of climate*, 14(7), 1337-1359.

Gudmundsson, L., Bremnes, J.B., Haugen, J.E., Engen-Skaugen, T. (2012) 'Technical Note: Downscaling RCM precipitation to the station scale using statistical transformations: A comparison of methods'. *Hydrology and Earth System Sciences*, 16(9), 3383-3390.

Gyau-Boakye, P., Schultz, G.A. (1994) 'Filling gaps in runoff time series in west africa'. *Hydrological sciences journal*, 39(6), 621-636.

Hargreaves, G.H., Samani, Z. (1985) 'Reference crop evapotranspiration from temperature'. *Applied engineering in agriculture*, 1(2), 96-99.

Harris, I., Jones, P. D. (2017) 'CRU TS4. 00: Climatic Research Unit (CRU) Time-Series (TS) version 4.00 of high-resolution gridded data of month-by-month variation in climate (Jan. 1901–Dec. 2015)'. *Centre for Environmental Data Analysis*, 25.

Harris, I., Jones, P.D., Osborn, T.J., Lister, D.H. (2014) 'Updated high-resolution grids of monthly climatic observations - the CRU TS3.10 Dataset'. *International journal of climatology*, 34(3), 623-642.

Hattermann, F.F., Vetter, T., Breuer, L., Su, B., Daggupati, P., Donnelly, C., Fekete, B., Florke, F., Gosling, S.N., Hoffmann, P., Liersch, S., Masaki, Y., Motovilov, Y., Muller, C., Samaniego, L., Stacke, T., Wada, Y., Yang, T., Krysnova, V. (2018) 'Sources of uncertainty in hydrological climate impact assessment: A cross-scale study'. *Environmental Research Letters*, 13(1), 015006.

Hawkins, E., Sutton, R. (2009) 'The potential to narrow uncertainty in regional climate predictions'. *Bulletin of the American Meteorological Society*, 90(8), 1095-1108.

He, Y.C., Drange, H., Gao, Y., Bentsen, M. (2016) 'Simulated Atlantic Meridional Overturning Circulation in the 20th century with an ocean model forced by reanalysis-based atmospheric data sets'. *Ocean Modelling*, 100, 31-48.

Held, I. M., Delworth, T. L., Lu, J., Findell, K. U., Knutson, T. R. (2005) 'Simulation of Sahel drought in the 20th and 21st centuries'. *Proceedings of the National Academy of Sciences*, 102(50), 17891-17896.

Hempel, S., Frieler, K., Warszawski, L., Schewe, J., Piontek, F. (2013) 'A trend-preserving bias correction – the ISI-MIP approach'. *Earth System Dynamics*, 4(2), 219-236.

Hewlett, J.D. (1974) 'Comments on letters relating to 'Role of subsurface flow in generating surface runoff: 2, Upstream source areas' by R. Allan Freeze'. *Water resources research*, 10(3), 605-607.

Hingray, B., Saïd, M. (2014) 'Partitioning internal variability and model uncertainty components in a multimember multi-model ensemble of climate projections'. *Journal of Climate*, 27(17), 6779-6798

Horton, R. E. (1933) 'The role of infiltration in the hydrologic cycle'. *Transactions of the American Geophysical Union*, 445–460.

Hua, W., Zhou, L., Chen, H., Nicholson, S.E., Raghavendra, A., Jiang, Y. (2016) 'Possible causes of the Central Equatorial African long-term drought'. *Environmental Research Letters*, 11(12), 124002.

Huang, B., Thorne, P.W., Banzon, V.F., Boyer, T., Chepurin, G., Lawrimore, J.H., Menne, M.J., Smith, T.M., Vose, R.S., Zhang, H.M. (2017) 'Extended reconstructed Sea surface temperature, Version 5 (ERSSTv5): Upgrades, validations, and intercomparisons'. *Journal of Climate*, 30(20), 8179-8205.

Hubert, P., Carbonnel, J.P., Chaouche, A. (1989) 'Segmentation des séries hydrométéorologiques - application à des séries de précipitations et de débits de l'Afrique de l'ouest'. *Journal of hydrology*, 110(3-4), 349-367.

Hulme, M., Doherty, R., Ngara, T., New, M., Lister, D. (2001) 'African climate change: 1900-2100'. *Climate research*, 17(2), 145-168.

Hulme, M., Osborn, T.J., Johns, T.C. (1998) 'Precipitation sensitivity to global warming: Comparison of observations with HadCM2 simulations'. *Geophysical research letters*, 25(17), 3379-3382.

Ibrahim, B., Karambiri, H., Polcher, J. (2015) 'Hydrological Impacts of the Changes in Simulated Rainfall Fields on Nakanbe Basin in Burkina Faso'. *Climate*, 3(3), 442-458.

Intergovernmental Panel on Climate Change, IPCC (2013) *Climate Change 2013: The Physical Science Basis*. Contribution of Working Group I to the Fifth Assessment Report of the Intergovernmental Panel on Climate Change [Stocker, T.F., D. Qin, G.-K. Plattner, M. Tignor, S.K. Allen, J. Boschung, A. Nauels, Y. Xia, V. Bex and P.M. Midgley (eds.)]. Cambridge University Press, Cambridge, United Kingdom and New York, NY, USA.

Intergovernmental Panel on Climate Change, IPCC (2014) *Climate Change 2014: Synthesis Report*. Contribution of Working Groups I, II and III to the Fifth Assessment Report of the Intergovernmental Panel on Climate Change, Core Writing Team, R.K. Pachauri and L.A. Meyer.

Jakeman, A.J., Hornberger, G.M. (1993) 'How much complexity is warranted in a rainfall-runoff model?'. *Water resources research*, 29(8), 2637-2649.

Jakeman, A.J., Littlewood, I.G., Whitehead, P.G. (1990) 'Computation of the instantaneous unit hydrograph and identifiable component flows with application to two small upland catchments'. *Journal of hydrology*, 117(1-4), 275-300.

Janicot, S. (1992) 'Spatiotemporal variability of West African rainfall. Part I: Regionalizations and Typings'. *Journal of Climate*, 5(5), 489-497.

Janicot, S., Lafore, J. P., and Thorncroft, C. (2011) 'The West African Monsoon'. *The Global Monsoon System: Research and Forecast*, 111-135.

Joly, M., Voldoire, A., Douville, H., Terray, P., Royer, J.F. (2007) 'African monsoon teleconnections with tropical SSTs: Validation and evolution in a set of IPCC4 simulations'. *Climate Dynamics*, 29(1), 1-20.

Jones, P.D. (1994) 'Hemispheric surface air temperature variations: a reanalysis and an update to 1993'. *Journal of Climate*, 7(11), 1794-1802.

Jones, P.D., Moberg, A. (2003) 'Hemispheric and large-scale surface air temperature variations: An extensive revision and an update to 2001'. *Journal of climate*, 16(2), 206-223.

Jury, M.R. (2013) 'A return to wet conditions over Africa: 1995-2010'. *Theoretical and applied climatology*, 111(3-4), 471-481.

Kalteh, A.M., Hjorth, P. (2009). 'Imputation of missing values in a precipitation-runoff process database'. *Hydrology Research*, 40(4), 420-432.

Kauffeldt, A., Wetterhall, F., Pappenberger, F., Salamon, P., Thielen, J. (2016) 'Technical review of large-scale hydrological models for implementation in operational flood forecasting schemes on

continental level'. *Environmental Modelling & Software*, 75, 68-76.

Kendall, M. (1975). *Multivariate analysis*. Charles Griffin.

Killick, R., Eckley, I. (2014) 'changepoint: An R package for changepoint analysis'. *Journal of statistical software*, 58(3), 1-19.

Kim, J.W., Pachepsky, Y.A. (2010) 'Reconstructing missing daily precipitation data using regression trees and artificial neural networks for SWAT streamflow simulation'. *Journal of hydrology*, 394(3-4), 305-314.

Kingston, D.G., Fleig, A.K., Tallaksen, L.M., Hannah, D.M. (2013) 'Ocean–Atmosphere Forcing of Summer Streamflow Drought in Great Britain'. *Journal of Hydrometeorology*, 14(1), 331-344.

Kling, H., Fuchs, M., Paulin, M. (2012) 'Runoff conditions in the upper Danube basin under an ensemble of climate change scenarios'. *Journal of Hydrology*, 424, 264-277.

Kundzewicz, Z.W., Mata, L.J., Arnell, N.W., Döll, P., Kabat, P., Jimenez, B., Miller, K.A., Oki, T., Sen, Z., Shiklomanov, I.A. (2007). Freshwater resources and their management. In *Climate Change 2007: Impacts, Adaptation and Vulnerability*. Contribution of Working Group II to the Fourth Assessment Report of the Intergovernmental Panel on Climate Change.

Kundzewicz Z.W., Radziejewski M. (2006) 'Methodologies for trend detection'. *Climate Variability and Change-Hydrological Impacts (FRIEND)*, IAHS Publ. 308, 538-550.

L'Hôte, Y., Mahé, G., Somé, B., Triboulet, J.P. (2002) 'Analysis of a Sahelian annual rainfall index from 1896 to 2000; the drought continues'. *Hydrological Sciences Journal*, 47(4), 563-572.

Lambergeon, D., Dzierżara, S., Janicot, S. (1981) 'Comportement du champ de vent sur l'Afrique occidentale'. *La Météorologie*, 25, 69-82.

Lavaysse, C., Flamant, C., Janicot, S. (2010) 'Regional-scale convection patterns during strong and weak phases of the Saharan heat low'. *Atmospheric Science Letters*, 11(4), 255-264.

Lawrence, D., Vandecar, K. (2015) 'Effects of tropical deforestation on climate and agriculture'. *Nature Climate Change*, 5(1), 27.

Le Barbé, L., Lebel, T. (1997) 'Rainfall climatology of the HAPEX-Sahel region during the years 1950-1990'. *Journal of Hydrology*, 188, 43-73.

Le Barbé, L., Lebel, T., Tapsoba, D. (2002) 'Rainfall variability in West Africa during the years 1950-90'. *Journal of climate*, 15(2), 187-202.

Lebel, T., Diedhiou, A., Laurent, H. (2003) 'Seasonal cycle and interannual variability of the Sahelian rainfall at hydrological scales'. *Journal of Geophysical Research: Atmospheres*, 108(D8).

Lebel, T., Ali, A. (2009) 'Recent trends in the Central and Western Sahel rainfall regime (1990-2007)'. *Journal of Hydrology*, 375(1-2), 52-64.

Leblanc, M.J., Favreau, G., Massuel, S., Tweed, S.O., Loireau, M., Cappelaere, B. (2008) 'Land clearance and hydrological change in the Sahel: SW Niger'. *Global and Planetary Change*, 61(3-4), 135-150.

Lehner, B., Liermann, C.R., Revenga, C., Vörösmarty, C., Fekete, B., Crouzet, P., Döll, P., Endejan, M., Frenken, K., Magome, J., Nilsson, C., Robertson, J.C., Rödel, R., Sindorf, N., Wisser, D. (2011) 'High-resolution mapping of the world's reservoirs and dams for sustainable river-flow management'. *Front Ecol Environ*, 9, 494-502.

L'Hôte, Y., Dubreuil, P., Lericque, J. (1996) 'Carte des types de climats "en Afrique Noire à l'ouest du Congo". Rappels et extension aux régimes hydrologiques. In: *L'hydrologie Tropicale: Geoscience et*

Outil Pour le Développement (Mélanges à la mémoire de Jean Rodier. Paris, mai 1995)'. *IAHS Publ.* 238, 55-65

Liebmann, B., Dole, R.M., Jones, C., Bladé, I., Allured, D. (2010) 'Influence of choice of time period on global surface temperature trends estimates'. *Bulletin of the American Meteorological Society*, 91(11), 1485-1492.

Lienou, G., Mahe, G., Paturel, J.E., Servat, E., Sighomnou, D., Ekodeck, G.E., Dezetter, A., Dieulin, C. (2008) 'Evolution des régimes hydrologiques en région équatoriale camerounaise: Un impact de la variabilité climatique en Afrique équatoriale?'. *Hydrological Sciences Journal*, 53(4), 789-801.

Lin, J.L. (2007) 'The double-ITCZ problem in IPCC AR4 coupled GCMs: Ocean-atmosphere feedback analysis'. *Journal of Climate*, 20(18), 4497-4525.

Losada, T., Rodríguez-Fonseca, B., Polo, I., Janicot, S., Gervois, S., Chauvin, F., Ruti, P. (2010) 'Tropical response to the Atlantic Equatorial mode: AGCM multimodel approach'. *Climate Dynamics*, 35(1), 45-52.

Louvet, S., Fontaine, B., Roucou, P. (2003) 'Active phases and pauses during the installation of the West African monsoon through 5-day CMAP rainfall data (1979-2001)'. *Geophysical Research Letters*, 30(24).

Lu, J., Delworth, T.L. (2005) 'Oceanic forcing of the late 20th century Sahel drought'. *Geophysical Research Letters*, 32(22).

MacDonald, A.M., Bonsor, H.C., Dochartaigh, B.É.Ó., Taylor, R.G. (2012) 'Quantitative maps of groundwater resources in Africa'. *Environmental Research Letters*, 7(2), 024009.

Machiwal, D., Jha, M.K. (2006) 'Time series analysis of hydrologic data for water resources planning and management: a review'. *Journal of Hydrology and Hydromechanics*, 54(3), 237-257.

Mahé, G., Bamba, F., Soumaguel, A., Orange, D., Olivry, J.C. (2009) 'Water losses in the inner delta of the River Niger: Water balance and flooded area'. *Hydrological Processes: An International Journal*, 23(22), 3157-3160.

Mahé, G., Citeau, J. (1993) 'Interactions between the ocean, atmosphere and continent in Africa, related to the Atlantic monsoon flow. General pattern and the 1984 case study'. *Veille Climatique Satellitaire Ed. ORSTOM-METEO FRANCE*, 44, 34-54.

Mahé, G., L'Hôte, Y., Olivry, J.C., Wotling, G. (2001) 'Trends and discontinuities in regional rainfall of West and Central Africa: 1951–1989'. *Hydrological Sciences Journal*, 46(2), 211-226.

Mahé, G., Lienou, G., Descroix, L., Bamba, F., Paturel, J.E., Laraque, A., Meddi, M., Habaieb, H., Adeaga, O., Dieulin, C., Chahnez Kotti, F., Khomsi, K. (2013) 'The rivers of Africa: Witness of climate change and human impact on the environment'. *Hydrological Processes*, 27(15), 2105-2114.

Mahé, G., Olivry, J. C. (1999) 'Assessment of freshwater yields to the ocean along the intertropical Atlantic coast of Africa (1951–1989)'. *Comptes Rendus de l'Académie des Sciences-Series IIA-Earth and Planetary Science*, 328(9), 621-626.

Mahé, G., Paturel, J.E. (2009) '1896-2006 Sahelian annual rainfall variability and runoff increase of Sahelian Rivers'. *Comptes Rendus Geoscience*, 341(7), 538-546.

Mahé, G., Paturel, J.E., Servat, E., Conway, D., Dezetter, A. (2005) 'The impact of land use change on soil water holding capacity and river flow modelling in the Nakambe River, Burkina-Faso'. *Journal of Hydrology*, 300(1-4), 33-43.

Maidment, R.I., Allan, R.P., Black, E. (2015) 'Recent observed and simulated changes in

precipitation over Africa'. *Geophysical Research Letters*, 42(19), 8155-8164.

Mann, H.B. (1945) 'Nonparametric Tests Against Trend'. *Econometrica: Journal of the Econometric Society*, 245-259.

Mantua, N.J., Hare, S.R. (2002) 'The Pacific Decadal Oscillation'. *Journal of Oceanography*, 58(1), 35-44.

Maraun, D. (2012) 'Nonstationarities of regional climate model biases in European seasonal mean temperature and precipitation sums'. *Geophysical Research Letters*, 39(6).

Maraun, D., Wetterhall, F., Ireson, A.M., Chandler, R.E., Kendon, E.J., Widmann, M., Brienen, S., Rust, H.W., Sauter, T., Themel, M., Venema, V.K.C., Chun, K.P., Goodess, C.M., Jones, R.G., Onof, C., Vrac, M., Thiele-Eich, I. (2010) 'Precipitation downscaling under climate change: Recent developments to bridge the gap between dynamical models and the end user'. *Rev. Geophys*, 48(3), 1-34.

Martin, E.R., Thorncroft, C., Booth, B.B.B. (2014) 'The multi-decadal atlantic SST-sahel rainfall teleconnection in CMIP5 simulations'. *Journal of Climate*, 27(2), 784-806.

Mascaro, G., White, D.D., Westerhoff, P., Bliss, N. (2015) 'Performance of the CORDEX-Africa regional climate simulations in representing the hydrological cycle of the Niger river basin'. *Journal of Geophysical Research: Atmospheres*, 120(24), 12425-12444.

Masih, I., Maskey, S., Mussá, F.E.F., Trambauer, P. (2014) 'A review of droughts on the African continent: A geospatial and long-term perspective'. *Hydrology and Earth System Sciences*, 18(9), 3635-3649.

Massei, N., Dieppois, B., Hannah, D.M., Lavers, D.A., Fossa, M., Laignel, B., Debret, M. (2017) 'Multi-time-scale hydroclimate dynamics of a regional watershed and links to large-scale atmospheric circulation: Application to the Seine river catchment, France'. *Journal of Hydrology*, 546, 262-275.

Mba, W.P., Longandjo, G.N.T., Moufouma-Okia, W., Bell, J.P., James, R., Vondou, D.A., Haensler, A., Fotso-Nguemo, T.C., Guenang, G.M., Tchotchou, A.L.D., Kamsu-Tamo, P.H., Takong, R.R., Nikulin, G., Lennard, C.J., Dosio, A. (2018) 'Consequences of 1.5 °c and 2 °c global warming levels for temperature and precipitation changes over Central Africa'. *Environmental Research Letters*, 13(5), 055011.

Mbaye, M.L., Hagemann, S., Haensler, A., Stacke, T., Gaye, A.T., Afouda, A. (2015) 'Assessment of Climate Change Impact on Water Resources in the Upper Senegal Basin (West Africa)'. *American Journal of Climate Change*, 4(01), 77.

McCabe, G.J., Wolock, D.M. (2002) 'A step increase in streamflow in the conterminous United States'. *Geophysical Research Letters*, 29(24), 38-1.

McCartney, M., Forkuor, G., Sood, A., Amisigo, B., Hattermann, F., Muthuwatta, L. (2012). *The water resource implications of changing climate in the Volta River Basin*, IWMI Research Report (Vol.146).

McGregor, G. (2017) 'Hydroclimatology, modes of climatic variability and stream flow, lake and groundwater level variability: A progress report'. *Progress in Physical Geography*, 41(4), 496-512.

Michel, C. (1989) 'Hydrologie appliquée aux petits bassins versants ruraux'. *Cemagref, Antony*.

Mitchell, T.D., Jones, P.D. (2005) 'An improved method of constructing a database of monthly climate observations and associated high-resolution grids'. *International journal of climatology*, 25(6), 693-712.

Moalafhi, D.B., Sharma, A., Evans, J.P. (2017) 'Reconstructing hydro-climatological data using dynamical downscaling of reanalysis products in data-sparse regions – Application to the Limpopo

catchment in southern Africa'. *Journal of Hydrology: Regional Studies*, 12, 378-395.

Mohino, E., Janicot, S., Bader, J. (2011) 'Sahel rainfall and decadal to multi-decadal sea surface temperature variability'. *Climate dynamics*, 37(3-4), 419-440.

Mohino, E., Losada, T. (2015) 'Impacts of the Atlantic Equatorial Mode in a warmer climate'. *Climate Dynamics*, 45(7-8), 2255-2271.

Monerie, P.A., Fontaine, B., Roucou, P. (2012) 'Expected future changes in the African monsoon between 2030 and 2070 using some CMIP3 and CMIP5 models under a medium-low RCP scenario'. *Journal of Geophysical Research: Atmospheres*, 117(D16).

Monerie, P. A., Sanchez-Gomez, E., Boé, J. (2016) 'On the range of future Sahel precipitation projections and the selection of a sub-sample of CMIP5 models for impact studies'. *Climate Dynamics*, 7(48), 2751-2770.

Mortimore, M. (2010) 'Adapting to drought in the Sahel: lessons for climate change'. *Wiley interdisciplinary reviews: climate change*, 1(1), 134-143.

Moss, R.H., Edmonds, J.A., Hibbard, K.A., Manning, M.R., Rose, S.K., Van Vuuren, D.P., Carter, T.R., Emori, S., Kainuma, M., Kram, T., Meehl, G.A., Mitchell, J.F.B., Nakicenovic, N., Riahi, K., Smith, S.J., Stouffer, R.J., Thomson, A.M., Weyant, J.P., Wilbanks, T.J. (2010) 'The next generation of scenarios for climate change research and assessment'. *Nature*, 463(7282), 747.

Mouelhi, S., Michel, C., Perrin, C., Andréassian, V. (2006) 'Stepwise development of a two-parameter monthly water balance model'. *Journal of Hydrology*, 318(1-4), 200-214.

Mtongori, H.I., Stordal, F., Benestad, R.E. (2016) 'Evaluation of empirical statistical downscaling models' skill in predicting Tanzanian rainfall and their application in providing future downscaled scenarios'. *Journal of Climate*, 29(9), 3231-3252.

Nalley, D., Adamowski, J., Khalil, B., Biswas, A. (2016) 'Inter-annual to inter-decadal streamflow variability in Quebec and Ontario in relation to dominant large-scale climate indices'. *Journal of hydrology*, 536, 426-446.

Nash, J.E., Sutcliffe, J. V. (1970) 'River Flow Forecasting Through Conceptual Models Part I-a Discussion of Principles*'. *Journal of hydrology*, 10, 282-290

New, M., Hulme, M., Jones, P. (2000) 'Representing twentieth-century space-time climate variability. Part II: Development of 1901-96 monthly grids of terrestrial surface climate'. *Journal of climate*, 13(13), 2217-2238.

Niang, I., Ruppel, O.C., Abdrabo, M.A., Esse, I A., Lennard, C., Padgham, J., Urquhart, P. (2014) *In Climate change 2014: impacts, adaptation and vulnerability*. Contribution of Working Group II to the Fifth Assessment Report of the Intergovernmental Panel on Climate Change. Cambridge, UK: Cambridge University Press, Cambridge

Nicholson, S. E. (2009) 'A revised picture of the structure of the "monsoon" and land ITCZ over West Africa'. *Climate Dynamics*, 32(7-8), 1155-1171.

Nicholson, S.E. (2005) 'On the question of the "recovery" of the rains in the West African Sahel'. *Journal of arid environments*, 63(3), 615-641.

Nicholson, S.E. (2000) 'The nature of rainfall variability over Africa on time scales of decades to millenia'. *Global and planetary change*, 26(1-3), 137-158.

Nicholson, S.E. (2008) 'The intensity, location and structure of the tropical rainbelt over west Africa as factors in interannual variability'. *International Journal of Climatology: A Journal of the Royal*

Meteorological Society, 28(13), 1775-1785.

Nicholson, S.E. (2009) 'A revised picture of the structure of the "monsoon" and land ITCZ over West Africa'. *Climate Dynamics*, 32(7-8), 1155-1171.

Nicholson, S.E. (2013) 'The West African Sahel: A Review of Recent Studies on the Rainfall Regime and Its Interannual Variability'. *ISRN Meteorology*, 2013., 1–32.

Nicholson, S.E., Grist, J.P. (2001) 'A conceptual model for understanding rainfall variability in the West African Sahel on interannual and interdecadal timescales'. *International Journal of Climatology: A Journal of the Royal Meteorological Society*, 21(14), 1733-1757.

Nicholson, S.E., Grist, J.P. (2003) 'The seasonal evolution of the atmospheric circulation over West Africa and equatorial Africa'. *Journal of climate*, 16(7), 1013-1030.

Nicholson, S.E., Some, B. and Kone, B. (2000) 'An Analysis of Recent Rainfall Conditions in West Africa, Including the Rainy Seasons of the 1997 El Niño and the 1998 La Niña Years'. *Journal of climate*, 13(14), 2628-2640.

Niel, H., Paturel, J.E., Servat, E. (2003) 'Study of parameter stability of a lumped hydrologic model in a context of climatic variability'. *Journal of Hydrology*, 278(1-4), 213-230.

Nikulin, G., Jones, C., Giorgi, F., Asrar, G., Büchner, M., Cerezo-Mota, R., Christensen, O.B., Déqué, M., Fernandez, J., Hänsler, A., van Meijgaard, E., Samuelsson, P., Sylla, M.B., Sushama, L. (2012) 'Precipitation climatology in an ensemble of CORDEX-Africa regional climate simulations'. *Journal of Climate*, 25(18), 6057-6078.

Nka, B.N., Oudin, L., Karambiri, H., Paturel, J.E., Ribstein, P. (2015) 'Trends in floods in West Africa: Analysis based on 11 catchments in the region'. *Hydrology and Earth System Sciences*, 19(11), 4707-4719.

Ogungbenro, S.B., Morakinyo, T.E. (2014) 'Rainfall distribution and change detection across climatic zones in Nigeria'. *Weather and Climate Extremes*, 5, 1-6.

Okumura, Y., Xie, S.P. (2006) 'Some overlooked features of tropical atlantic climate leading to a new Niño-like phenomenon'. *Journal of climate*, 19(22), 5859-5874.

Oyerinde, G., Wisser, D., Hountondji, F., Odofoin, A., Lawin, A., Afouda, A., Diekkrüger, B. (2016) 'Quantifying Uncertainties in Modeling Climate Change Impacts on Hydropower Production'. *Climate*, 4(3), 34.

Ozer, P., Erpicum, M., Demarée, G., Vandiepenbeeck, M. (2003) 'The Sahelian drought may have ended during the 1990s'. *Hydrological Sciences Journal*, 48(3), 489-492.

Page, E.S. (1954) 'Continuous Inspection Schemes'. *Biometrika*, 41(1/2), 100-115.

Panthou, G, Lebel, T, Vischel, T, Quantin, G, Sane, Y, Ba, A, Ndiaye, O, Diongue-Niang, A, and Diopkane, M. (2018) 'Rainfall intensification in tropical semi-arid regions: the Sahelian case'. *Environmental Research Letters*, 13(6), 064013.

Panthou, G., Vischel, T., Lebel, T. (2014) 'Recent trends in the regime of extreme rainfall in the Central Sahel'. *Journal of Climatology*, 34(15), 3998-4006.

Parker, D.J., Burton, R.R., Diongue-Niang, A., Ellis, R.J., Felton, M., Taylor, C.M., Thorncroft, C.D., Bessemoulin, P., Tompkins, A.M. (2005). 'The diurnal cycle of the West African monsoon circulation'. *Quarterly Journal of the Royal Meteorological Society*, 131(611), 2839-2860.

Paturel, J. E., Ouedraogo, M., Mahé, G., Servat, E., Dezetter, A., Ardoin, S. (2003) 'The influence of distributed input data on the hydrological modelling of monthly river flow regimes in West Africa'. *Hydrological sciences journal*, 48(6), 881-890.

Paturel, J.E., Servat, E., Vassiliadis, A. (1995) 'Sensitivity of conceptual rainfall-runoff algorithms to errors in input data - case of the GR2M model'. *Journal of hydrology*, 168(1-4), 111-125.

Patricola, C. M., Li, M., Xu, Z., Chang, P., Saravanan, R., Hsieh, J. S. (2012) 'An investigation of tropical Atlantic bias in a high-resolution coupled regional climate model'. *Climate dynamics*, 39(9-10), 2443-2463.

Percival, D.B., Walden, A.T. (2000) *Wavelet Methods for Time Series Analysis* (Vol. 4). Cambridge, UK: Cambridge University Press.

Peterson, T.C., Vose, R.S. (1997) 'An Overview of the Global Historical Climatology Network Temperature Database'. *Bulletin of the American Meteorological Society*, 78(12), 2837-2850.

Peyrillé P. (2006). *Etude idéalisée de la mousson ouest-africaine à partir d'un modèle numérique bi-dimensionnel*. Thèse de Doctorat, Université Paul Sabatier Toulouse III. 206p.

Poccard, I., Janicot, S., Camberlin, P. (2000) 'Comparison of rainfall structures between NCEP/NCAR reanalyses and observed data over tropical Africa'. *Climate Dynamics*, 16(12), 897-915.

Pohl, B., Dieppois, B., Crédat, J., Lawler, D., Rouault, M. (2018) 'From synoptic to interdecadal variability in Southern African rainfall: toward a unified view across time scales'. *Journal of Climate*, 31(15), 5845-5872.

Polo, I., Rodríguez-Fonseca, B., Losada, T., García-Serrano, J. (2008) 'Tropical atlantic variability modes (1979-2002). Part I: Time-evolving SST modes related to West African rainfall'. *Journal of Climate*, 21(24), 6457-6475.

Reynolds, R. W., Rayner, N. A., Smith, T. M., Stokes, D. C., Wang, W. (2002) 'An improved in situ and satellite SST analysis for climate'. *Journal of climate*, 15(13), 1609-1625.

Richter, I., Xie, S. P. (2008) 'On the origin of equatorial Atlantic biases in coupled general circulation models'. *Climate Dynamics*, 31(5), 587-598.

Ringard, J., Dieppois, B., Rome, S., Diedhiou, A., Pellarin, T., Konaré, A., Diawara, A., Konaté, D., Dje, B.K., Katiellou, G.L., Seidou Sanda, I., Hassane, B., Vischel, T., Garuma, G.F., Mengistu, G., Camara, M., Diongue, A., Gaye, A.T., Descroix, L. (2016) 'The intensification of thermal extremes in west Africa'. *Global and Planetary Change*, 139, 66-77.

Rodríguez-Fonseca, B., Janicot, S., Mohino, E., Losada, T., Bader, J., Caminade, C., Chauvin, F., Fontaine, B., García-Serrano, J., Gervois, S., Joly, M., Polo, I., Ruti, P., Roucou, P., Voldoire, A. (2011) 'Interannual and decadal SST-forced responses of the West African monsoon'. *Atmospheric Science Letters*, 12(1), 67-74.

Rodríguez-Fonseca, B., Mohino, E., Mechoso, C.R., Caminade, C., Biasutti, M., Gaetani, M., Garcia-Serrano, J., Vizy, E.K., Cook, K., Xue, Y., Polo, I., Losada, T., Druryan, L., Fontaine, B., Bader, J., Doblaz-Reyes, F.J., Goddard, L., Janicot, S., Arribas, A., Lau, W., Colman, A., Vellinga, M., Rowell, D.P., Kucharski, F., Voldoire, A. (2015) 'Variability and predictability of west African droughts: A review on the role of sea surface temperature anomalies'. *Journal of Climate*, 28(10), 4034-4060.

Rodríguez-Fonseca, B., Polo, I., García-Serrano, J., Losada, T., Mohino, E., Mechoso, C.R., Kucharski, F. (2009) 'Are Atlantic Niños enhancing Pacific ENSO events in recent decades?'. *Geophysical Research Letters*, 36(20).

Roehrig, R., Bouniol, D., Guichard, F., Hourdin, F. d'eric, Redelsperger, J.L. (2013) 'The present and future of the west african monsoon: A process-oriented assessment of CMIP5 simulations along the AMMA transect'. *Journal of Climate*, 26(17), 6471-6505.

Roudier, P., Ducharne, A., Feyen, L. (2014) 'Climate change impacts on runoff in West Africa: A review'. *Hydrology and Earth System Sciences*, 18, 2789-2801.

Roudier, P., Sultan, B., Quirion, P., Berg, A. (2011) 'The impact of future climate change on West African crop yields: what does the recent literature say?'. *Global Environmental Change*, 21(3), 1073-1083.

Rowell, D. P., Folland, C. K., Maskell, K., Ward, M. N. (1995) 'Variability of summer rainfall over tropical North Africa (1906–92): Observations and modelling'. *Quarterly Journal of the Royal Meteorological Society*, 121(523), 669-704.

Rowell, D.P. (2001) 'Teleconnections between the tropical Pacific and the Sahel'. *Quarterly Journal of the Royal Meteorological Society*, 127(575), 1683-1706.

Rowell, D. P. (2003) 'The impact of Mediterranean SSTs on the Sahelian rainfall season'. *Journal of Climate*, 16(5), 849-862.

Rubin, D.B. (1987) 'Introduction'. In *Multiple Imputation for Nonresponse in Surveys* (pp. 1–26). New York: Wiley.

Salack, S., Sarr, B., Sangare, S.K., Ly, M., Sanda, I.S., Kunstmann, H. (2015) 'Crop-climate ensemble scenarios to improve risk assessment and resilience in the semi-arid regions of West Africa'. *Climate Research*, 65, 107-121.

Sarr, A. (2017) 'Multi-Scale Characteristics of Precipitation and Temperature over West Africa Using SMHI-RCA Driven by GCMs under RCP8.5'. *American Journal of Climate Change*, 6(03), 455.

Schönbrodt, F.D., Perugini, M. (2013) 'At what sample size do correlations stabilize?'. *Journal of Research in Personality*, 47(5), 609-612.

Sen, A.K. (2012) 'Streamflow variability in the Southern Appalachians and atmospheric teleconnections'. *River research and applications*, 28(5), 630-636.

Serdeczny, O., Adams, S., Baarsch, F., Coumou, D., Robinson, A., Hare, W., Schaeffer, M., Perrette, M., Reinhardt, J. (2017) 'Climate change impacts in Sub-Saharan Africa: from physical changes to their social repercussions'. *Regional Environmental Change*, 17(6), 1585-1600.

Servat, É., Paturel, J. E., Lubes-Niel, H., Kouame, B., Travaglio, M., Marieu, B. (1997) 'Regarding the reduction of flow in Western and Central Africa'. *Comptes Rendus de l'Academie des Sciences Series IIA Earth and Planetary Science*, 9(325), 679-682.

Sheen, K., Smith, D., Dunstone, N., Eade, R., Rowell, D., Vellinga, M. (2017). 'Skilful prediction of Sahel summer rainfall on inter-annual and multi-year timescales'. *Nature Communications*, 8, 14966.

Sidibe, M., Dieppois, B., Mahé, G., Paturel, J.E., Amoussou, E., Anifowose, B., Lawler, D. (2018) 'Trend and variability in a new, reconstructed streamflow dataset for West and Central Africa, and climatic interactions, 1950–2005'. *Journal of hydrology*, 561, 478-493.

Sidibe, M., Dieppois, B., Eden, J., Mahé, G., Paturel, J. E., Amoussou, E., Anifowose, B., Lawler, D. (2019) 'Interannual to Multi-decadal streamflow variability in West and Central Africa: Interactions with catchment properties and large-scale climate variability'. *Global and Planetary Change*, 177, 141-156.

Stanzel, P., Kling, H., Bauer, H. (2018) 'Climate change impact on West African rivers under an ensemble of CORDEX climate projections'. *Climate Services*, 11, 36-48.

Steinschneider, S., Wi, S., Brown, C. (2015) 'The integrated effects of climate and hydrologic

uncertainty on future flood risk assessments'. *Hydrological Processes*, 29(12), 2823-2839.

Stekhoven, D.J., Bühlmann, P. (2012) 'Missforest-Non-parametric missing value imputation for mixed-type data'. *Bioinformatics*, 28, 112–118.

Sterling, S.M., Ducharne, A., Polcher, J. (2013) 'The impact of global land-cover change on the terrestrial water cycle'. *Nature Climate Change*, 3(4), 385.

Stockholm Environment Institute (2014) *Cross-sectoral integration in the sustainable development goals: A nexus approach*. Stockholm: Stockholm Environment Institute

Stott, P.A., Gillett, N.P., Hegerl, G.C., Karoly, D.J., Stone, D.A., Zhang, X., Zwiers, F. (2010) 'Detection and attribution of climate change: A regional perspective'. *Wiley Interdisciplinary Reviews: Climate Change*, 1(2), 192-211.

Suárez-Moreno, R., Rodríguez-Fonseca, B., Barroso, J.A., Fink, A.H. (2018) 'Interdecadal changes in the leading ocean forcing of Sahelian rainfall interannual variability: Atmospheric dynamics and role of multi-decadal SST background'. *Journal of Climate*, 31(17), 6687-6710.

Sultan, B., Janicot, S. (2000) 'Abrupt shift of the ITCZ over West Africa and intra-seasonal variability'. *Geophysical Research Letters*, 27(20), 3353-3356.

Sultan, B., Janicot, S. (2003) 'The West African monsoon dynamics. Part II: The "preonset" and "onset" of the summer monsoon'. *Journal of climate*, 16(21), 3407-3427.

Suzuki, R., Shimodaira, H. (2006) 'Pvclust: An R package for assessing the uncertainty in hierarchical clustering'. *Bioinformatics*, 22(12), 1540–1542.

Sylla, M.B., Nikiema, P.M., Gibba, P., Kebe, I., Klutse, N.A.B. (2016) 'Climate change over West Africa: Recent trends and future projections'. In *Adaptation to climate change and variability in rural West Africa* (pp. 25-40). Springer, Cham.

Sylla, M.B., Pal, J.S., Faye, A., Dimobe, K., Kunstmann, H. (2018) 'Climate change to severely impact West African basin scale irrigation in 2 °C and 1.5 °C global warming scenarios'. *Scientific reports*, 8(1), 14395.

Taylor, C.M., Belusic, D., Guichard, F., Parker, D.J., Vischel, T., Bock, O., Harris, P.P., Janicot, S., Klein, C., and Panthou, G. (2017) 'Frequency of extreme Sahelian storms tripled since 1982 in satellite observations'. *Nature*, 544(7651), 475.

Taylor, C.M., Lambin, E.F., Stephenne, N., Harding, R.J., Essery, R.L.H. (2002) 'The influence of land use change on climate in the Sahel'. *Journal of Climate*, 15(24), 3615-3629.

Taylor, K.E., Stouffer, R.J., Meehl, G.A. (2012) 'An overview of CMIP5 and the experiment design'. *Bulletin of the American Meteorological Society*, 93(4), 485-498.

Teutschbein, C., Seibert, J. (2012) 'Bias correction of regional climate model simulations for hydrological climate-change impact studies: Review and evaluation of different methods'. *Journal of Hydrology*, 456, 12-29.

Thorncroft, C. D., Blackburn, M. (1999) 'Maintenance of the African easterly jet'. *Quarterly Journal of the Royal Meteorological Society*, 125(555), 763-786.

Torrence, C., Compo, G.P. (1998) 'A Practical Guide to Wavelet Analysis'. *Bulletin of the American Meteorological society*, 79(1), 61-78.

- Trichon, V., Hiernaux, P., Walcker, R., and Mougin, E. (2018) 'The persistent decline of patterned woody vegetation: The tiger bush in the context of the regional Sahel greening trend'. *Global change biology*, 24(6), 2633-2648.
- Troyanskaya, O., Cantor, M., Sherlock, G., Brown, P., Hastie, T., Tibshirani, R., Botstein, D., Altman, R.B. (2001) 'Missing value estimation methods for DNA microarrays'. *Bioinformatics*, 17(6), 520-525.
- Tshimanga, R.M., Tshitenge, J.M., Kabuya, P., Alsdorf, D., Mahe, G., Kibukusa, G., Lukanda, V. (2016) 'A Regional Perceptive of Flood Forecasting and Disaster Management Systems for the Congo River Basin'. In *Flood Forecasting* (pp. 87-124). Academic Press.
- Van Buuren, S., Oudshoorn, K. (1999) *Flexible multivariate imputation by MICE*. Leiden: TNO.
- Vicente-Serrano, S.M., Beguería, S., Gimeno, L., Eklundh, L., Giuliani, G., Weston, D., El Kenawy, A., López-Moreno, J.I., Nieto, R., Ayenew, T., Konte, D., Ardö, J., Pegram, G.G.S. (2012) 'Challenges for drought mitigation in Africa: The potential use of geospatial data and drought information systems'. *Applied Geography*, 34, 471-486.
- Villamayor, J., Mohino, E. (2015) 'Robust Sahel drought due to the Interdecadal Pacific Oscillation in CMIP5 simulations'. *Geophysical Research Letters*, 42(4), 1214-1222.
- Von Storch, H. (1995) 'Misuses of Statistical Analysis in Climate'. *Anal. Clim. Var. Appl. Stat. Tech.* 11–26.
- Von Storch, H., Zwiers, F.W. (1999) 'Statistical Analysis in Climate Research'. *J. Am. Stat. Assoc.* 95, 1375.
- Wang, C., Zhang, L., Lee, S.K., Wu, L., Mechoso, C.R. (2014) 'A global perspective on CMIP5 climate model biases'. *Nature Climate Change*, 4(3), 201.
- Wang, G., Eltahir, E. A. (2000) 'Ecosystem dynamics and the Sahel drought'. *Geophysical Research Letters*, 27(6), 795-798.
- Wang, S., Huang, J., He, Y., Guan, Y. (2014) 'Combined effects of the Pacific Decadal Oscillation and El Niño -Southern Oscillation on Global Land Dry-Wet Changes'. *Scientific reports*, 4, 6651.
- Ward, M.N. (1998) 'Diagnosis and short-lead time prediction of summer rainfall in tropical North Africa at interannual and multi-decadal timescales'. *Journal of Climate*, 11(12), 3167-3191.
- Washington, R., James, R., Pearce, H., Pokam, W.M., Moufouma-Okia, W. (2013) 'Congo basin rainfall climatology: Can we believe the climate models?' *Philosophical Transactions of the Royal Society B: Biological Sciences*, 368(1625), 20120296.
- Webster, P.J., Magaña, V.O., Palmer, T.N., Shukla, J., Tomas, R.A., Yanai, M., Yasunari, T. (1998) 'Monsoons: Processes, predictability, and the prospects for prediction'. *Journal of Geophysical Research: Oceans*, 103(C7), 14451-14510.
- Webster, P.J., Moore, A.M., Loschnigg, J.P., Leben, R.R. (1999) 'Coupled ocean-atmosphere dynamics in the Indian Ocean during 1997-98'. *Nature*, 401(6751), 356.
- Wilby, R.L., Wigley, T.M.L. (1997) 'Downscaling general circulation model output: A review of methods and limitations'. *Progress in physical geography*, 21(4), 530-548.
- Wilcox, C., Vischel, T., Panthou, G., Bodian, A., Blanchet, J., Descroix, L., Quantin, G., Cassé, C., Tanimoun, B., and Kone, S. (2018) 'Trends in hydrological extremes in the Senegal and Niger Rivers'. *Journal of hydrology*, 566, 531-545.

World Bank (2010). *Report on the Status of Disaster Risk Reduction in Sub-Saharan Africa*.
<http://www.gfdr.org/sites/gfdr/files/publication/AFR.pdf>.

World Bank (2015b) *Regional dashboard: poverty and equity, Sub-Saharan Africa*.
<http://povertydata.worldbank.org/poverty/region/SSA>. Accessed 13 Jan 2015

Yarnal B. (1993) *Synoptic Climatology in Environmental Analysis: a primer*. Belhaven Press.

Yin, X., Gruber, A. (2010) 'Validation of the abrupt change in GPCP precipitation in the Congo River Basin'. *International Journal of Climatology: A Journal of the Royal Meteorological Society*, 30(1), 110-119.

Yira, Y., Diekkrüger, B., Steup, G., Yaovi Bossa, A. (2017) 'Impact of climate change on hydrological conditions in a tropical West African catchment using an ensemble of climate simulations'. *Hydrology and Earth System Sciences*, 21(4), 2143.

Yue, S., Pilon, P., Phinney, B., Cavadias, G. (2002) 'The influence of autocorrelation on the ability to detect trend in hydrological series'. *Hydrological processes*, 16(9), 1807-1829.

Yue, S., Wang, C.Y. (2004) 'The Mann-Kendall test modified by effective sample size to detect trend in serially correlated hydrological series'. *Water resources management*, 18(3), 201-218.

Zaré, A., Mahé, G., Paturel, J.E., Barbier, B. (2017) 'Influence du Bani sur la variabilité saisonnière et interannuelle de la crue du fleuve Niger dans le delta intérieur au Mali'. *Hydrological sciences journal*, 62(16), 2737-2752.

Co-authors declaration

Content removed due to data protection considerations.

Content removed due to data protection considerations.

Content removed due to data protection considerations.